



BDPA radicals with improved persistence for dynamic nuclear polarization

Sucharita Mandal



**Faculty of Physical Science
School of Engineering and Natural Sciences
University of Iceland
2020**

BDPA radicals with improved persistence for dynamic nuclear polarization

Sucharita Mandal

Dissertation submitted in partial fulfillment of a
Philosophiae Doctor degree in Chemistry

Advisor

Prof. Snorri Þór Sigurðsson

PhD Committee

Prof. Guðmundur G. Haraldsson

Prof. Már Másson

Opponents

Dr. Stefán Jónsson

Dr. Bela E. Bode

Faculty of Physical Science
School of Engineering and Natural Sciences
University of Iceland
Reykjavik, December 2020

BDPA radicals with improved persistence for dynamic nuclear polarization

BDPA radicals with improved persistence

Dissertation submitted in partial fulfillment of a *Philosophiae Doctor* degree in Chemistry

Copyright © 2020 Sucharita Mandal

All rights reserved

Faculty of Physical Science
School of Engineering and Natural Sciences
University of Iceland
Dunhagi 3
107 Reykjavik
Iceland

Telephone: 525 4000

Bibliographic information:

Sucharita Mandal, 2020, *BDPA radicals with improved persistence for dynamic nuclear polarization*, PhD dissertation, Faculty of Physical Science, University of Iceland, 137 pp.

ISBN 978-9935-9564-0-8

Printing: Háskólaprent ehf.
Reykjavik, Iceland, December 2020

Abstract

Dynamic nuclear polarization (DNP) has emerged as an important technique to enhance the signal intensity of nuclear magnetic resonance (NMR) spectroscopy by transferring spin polarization from unpaired electrons to nuclei of interest. Persistent organic radicals are a common source of unpaired electrons for DNP. Carbon-based radicals, such as trityl and 1,3-bisdiphenylene-2-phenylallyl (BDPA), are very promising polarizing agents at high magnetic fields. BDPA has the advantage that it is easier to synthesize than trityl, but its lack of solubility in aqueous media limits its application for structural studies of biomolecules by DNP NMR. This PhD thesis describes the design and synthesis of BDPA radicals that are soluble in aqueous media and have improved persistence.

The first part revolves around the syntheses of phosphoester-derived BDPA radicals. Unexpectedly, these BDPA radicals, and BDPA radicals in general, were found to have limited persistence. Therefore, the effects of various factors on the persistence were investigated. Decomposition in the solid state was found to be due to oxidation while dimer formation was discovered to be a significant pathway of degradation in solution.

In the second part, a new class of BDPA radicals is described, their synthesis and characterization. The radicals contain four alkyl/aryl-ammonium groups and are soluble in aqueous solution. More importantly, they are highly persistent in polar solvents due to reduced decomposition via dimerization.

The third part describes the synthesis of three water-soluble BDPA-nitroxide biradicals. Different linkers were used to optimize the spin-spin interaction between the two radical centers. These biradicals are being investigated by our collaborators, as polarizing agents for DNP-NMR spectroscopy at high magnetic fields.

Útdráttur

Mögnun á kjarnskautun (e. dynamic nuclear polarization, DNP) er mikilvæg aðferð til að auka styrkleika merkja í kjarnsegulgreiningu (e. nuclear magnetic resonance (NMR) spectroscopy) með því að flytja skautun óparaðra rafeinda yfir í þá kjarna sem mæla skal. Algengt er að nota stöðugar lífrænar stakeindir fyrir DNP. Kolefnisstakeindir, til að mynda trítýl eða 1,3-bistvífenýlen-2-fenýllallýl (BDPA), eru slík skautunarefni sem lofa góðu í sterku segulsviði. Það sem BDPA hefur fram yfir trítýl er auðveldari efnasmíð, en lág leysni í vatni kemur í veg fyrir notkun þess fyrir rannsóknir á byggingum lífefna með DNP NMR. Þessi doktorsritgerð lýsir hönnun og efnasmíði BDPA stakeinda sem eru leysanlegar í vatnslausnum og bjóða upp á aukinn stöðugleika.

Fyrsti hluti ritgerðarinnar lýsir efnasmíðum á fosfóester afleiðum BDPA stakeinda. Það kom á óvart að þessar nýju BDPA stakeindir, og BDPA stakeindir almennt, virtust vera óstöðugar. Því voru rannsókuð áhrif mismunandi þátta á stöðugleika BDPA stakeindanna. Niðurbrot stakeindanna á föstu formi var rakið til súrefnis, en sýnt var fram á að meginniðurbrot í lausn væri vegna myndunar á BDPA tvíliðum.

Í öðrum hluta ritgerðarinnar er greint frá nýjum flokki BDPA stakeinda, efnasmíði þeirra og eiginleikum. Þessar stakeindir innihalda fjóra alkýl/aryl ammóníum hópa og eru leysanlegar í vatnslausnum. Þar að auki eru þessar BDPA stakeindir töluvert stöðugri vegna takmörkunar á myndun tvíliða.

Þriðji huti ritgerðarinnar lýsir smíði þriggja vatnleysanlegra BDPA-nítroxíð tvístakeinda. Notast var við tengla af mismunandi lengd á milli stakeindanna sem leiðir til breytileika í spuna-spuna víxlverkun og þar með mismunandi DNP eiginleika. Samstarfsaðilar okkar eru að rannsaka þessar stakeindir sem skautunarefni fyrir DNP NMR í sterku segulsviði.

Dedicated to my parents,

without whom I would not be wherever I am today

Table of Contents

List of Figures	xi
List of Schemes	xiii
Abbreviations	xiv
Acknowledgements	xvii
1 Objective and scope of the PhD thesis	1
2 Introduction.....	3
2.1 Nuclear Magnetic Resonance Spectroscopy	4
2.1.1 Solid-state NMR using magic-angle spinning (MAS).....	5
2.1.2 Low sensitivity of NMR	6
2.2 Dynamic Nuclear Polarization	7
2.2.1 Theory of DNP.....	7
2.2.2 Polarization transfer mechanisms and pathways	9
2.2.3 Instrumentation	15
2.2.4 Solvents for DNP experiments.....	17
2.2.5 Polarizing agents.....	18
2.3 Contribution of this PhD dissertation.....	24
3 Limited persistence of BDPA radicals	27
3.1 Synthesis of the radicals	27
3.2 Quantification of BDPA radicals	29
3.3 Persistence of BDPA under different conditions	31
3.3.1 Persistence in absence of oxygen.....	32
3.3.2 Solvent-dependence	33
3.3.3 Concentration-dependence.....	34
3.3.4 Analysis of BDPA-decomposition products.....	34
3.3.5 Persistence at lower temperatures.....	36
3.3.6 Persistence in solid state	36
3.4 Conclusions	37
4 Water-soluble BDPA radicals with improved persistence.....	39
4.1 Synthetic strategy	39
4.2 Synthesis of tetraalkyl/aryl-ammonium BDPAs.....	40
4.3 Persistence of the tetraalkylammonium BDPA radical.....	43
4.3.1 Solvent-dependent persistence.....	44
4.3.2 Evidence for dimerization in water.....	45
4.4 Conclusions	47
5 Water-soluble BDPA-nitroxide biradicals.....	49
5.1 Synthesis of the biradicals.....	49

5.2 Spin–spin coupling interaction in the biradicals.....	51
5.3 Conclusions.....	53
6 Conclusions	55
References	57
Publications.....	69

List of Figures

Figure 2.1 Energy-level diagram of a nucleus with a spin quantum number $\frac{1}{2}$ in a magnetic field	5
Figure 2.2 Solid state ^{13}C -NMR spectra of polycrystalline glycine in absence and presence of magic-angle spinning	6
Figure 2.3 Spin polarization of protons and electrons as a function of temperature	8
Figure 2.4 Energy level diagram of a coupled electron–nuclear spin pair	9
Figure 2.5 Energy level diagram of an electron–nuclear spin pair demonstrating the Overhauser Effect (OE)	11
Figure 2.6 Energy level diagram of a coupled electron–nuclear spin pair illustrating the solid effect (SE) DNP	12
Figure 2.7 Energy level diagram for three spin cross-effect (CE) mechanism	13
Figure 2.8 A visual representation of polarization transfer from electrons to nuclei	15
Figure 2.9 A schematic representation of a solid-state DNP NMR setup	16
Figure 2.10 The polarizing agents commonly used in DNP experiments	18
Figure 2.11 The initial design of nitroxide biradicals.....	19
Figure 2.12 Rigid nitroxide biradicals.	20
Figure 2.13 Water-soluble nitroxide biradicals.	20
Figure 2.14 Open and closed nitroxide biradicals.	21
Figure 2.15 Efficient nitroxide biradicals at high magnetic field (≥ 18.8 T).....	21
Figure 2.16 The heterobiradicals TEMTriPol-1 and HyTEK2	22
Figure 2.17 Initially designed BDPA-nitroxide biradicals.	23
Figure 2.18 One of the most efficient biradicals at high magnetic field (≥ 18.8 T).....	23
Figure 2.19 Reported water-soluble BDPA radicals.	24
Figure 3.1 EPR spectra of three different radicals.....	30
Figure 3.2 The rate of degradation of biradical 3 determined by both UV-vis and EPR spectroscopy	31
Figure 3.3 Persistence of three different BDPA radicals in DMSO	32

Figure 3.4 The degradation of the biradical 3 under air vs. argon in MeOH	32
Figure 3.5 Rate of degradation of different BDPA radicals in various solvents.....	33
Figure 3.6 Concentration-dependent initial rates of biradical 3 in DMSO at 23 °C.	34
Figure 3.7 The HRMS (ESI) spectrum of the decomposition products of the BDPA radical 10	35
Figure 3.8 The rate of decomposition of biradical 3 at lower temperatures	36
Figure 3.9 The persistence of BDPA radicals at 23 °C in the solid state.....	37
Figure 4.1 The improved persistence of tetraalkylammonium BDPA radical 30a compared to the unsubstituted BDPA (9) in DMSO.....	44
Figure 4.2 Persistence of the water-soluble BDPA radical 30a in solution	45
Figure 4.3 Concentration-dependent initial rates of BDPA radical 30a in water	45
Figure 4.4 The HRMS (ESI) spectrum of radical 30a in water	46
Figure 4.5 The persistence of radical 30a in water (5 mM) with a varying concentration of NaCl at 23 °C.	47
Figure 5.1 EPR spectra of a mixture of BDPA and nitroxide radicals (5:5), and the BDPA-nitroxide biradicals in DMSO	53

List of Schemes

Scheme 3.1 Strategy for preparation of phosphoester-derived BDPA radicals.....	27
Scheme 3.2 Synthesis of BDPA-phosphate radical 2	28
Scheme 3.3 Synthesis of BDPA-TEMPO biradical 3 containing a phosphodiester linker	29
Scheme 4.1 Synthetic strategy to increase the water solubility of BDPA.	40
Scheme 4.2 Synthesis of the dihydroxy fluorene derivative 12	40
Scheme 4.3 Condensation of 12 with 4-formyl benzoic acid followed by bromination.	41
Scheme 4.4 Unsuccessful model reaction of 11 and its silyl ether derivative 21 with bromo-compound 22 to construct the BDPA unit.	41
Scheme 4.5 Synthesis of BDPA derivative 27	42
Scheme 4.6 Deprotection of methoxy ethers of BDPA 27	42
Scheme 4.7 Synthesis of tetraalkyl/aryl-ammonium BDPA derivatives.	43
Scheme 5.1 Synthesis of water-soluble BDPA-nitroxide biradicals from the BDPA derivative 28	49
Scheme 5.2 The coupling of the carboxylic acid of 28 to 4-amino TEMPO.....	50
Scheme 5.3 Synthesis of the water-soluble BDPA-TEMPO biradical 32	50
Scheme 5.4 Synthesis of BDPA-nitroxide biradical 34 with a glycine linker.	51
Scheme 5.5 Synthesis of BDPA-nitroxide biradical 37 with a piperazine linker.	51

Abbreviations

BCDP	Bis(2-cyanoethyl)- <i>N,N</i> -diisopropylphosphoramidite
BDPA	1,3-Bisdiphenylene-2-phenylallyl
bTbk	Bis-TEMPO-bis-ketal
BT n E	Bis-TEMPO- <i>n</i> -ethylene glycol
CE	Cross effect
CMPI	2-Chloro-1-methylpyridinium iodide
CP	Cross-polarization
Cryo-EM	Cryogenic electron microscopy
DCE	1,2-Dichloroethane
DMF	Dimethylformamide
DMSO	Dimethyl sulfoxide
DNP	Dynamic nuclear polarization
DOTA	Dodecane tetraacetic acid
DQ	Double quantum
EM	Electron microscopy
EPR	Electron paramagnetic resonance
ESI	Electrospray ionization
FRET	Fluorescence resonance energy transfer
HPLC	High-performance liquid chromatography
HRMS	High resolution mass spectrometry
MAS	Magic angle spinning
NMIT	<i>N</i> -Methylimidazolium triflate
NMR	Nuclear magnetic resonance
OE	Overhauser effect
OTP	<i>ortho</i> -Terphenyl
PBS	Phosphate-buffered saline
PHIP	Parahydrogen induced polarization
PRE	Paramagnetic relaxation enhancement
SANS	Small-angle neutron scattering
SAXS	Small-angle X-ray scattering
SD	Spin diffusion

SE	Solid effect
SQ	Solid quantum
TBDMS	<i>tert</i> -Butyldimethylsilyl
TCE	1,1,2,2-Tetrachloroethane
TEMPO	2,2,6,6-Tetramethylpiperidine-1-oxyl
TEMPOL	4-Hydroxy-2,2,6,6-tetramethylpiperidin-1-oxyl
TFA	Trifluoroacetic acid
TLC	Thin layer chromatography
TM	Thermal mixing
ZQ	Zero quantum

Acknowledgements

The first person I would like to express my gratitude is my doctoral advisor, Prof. Snorri Th. Sigurdsson. This work would not have been possible without his constant guidance, support, and encouragements throughout this PhD journey. I thank him wholeheartedly for shaping me to be a better version of myself, both professionally and personally.

My sincere thanks go to my PhD committee members, Prof. Guðmundur G. Haraldsson and Prof. Már Mátsson for their insightful comments and encouragements. I would also like to thank the opponents, Dr. Stefán Jónsson and Dr. Bela E. Bode for taking time out of their busy schedule to review my work.

My earnest appreciation goes to present and past members of our research group, especially Anna-Lena Johanna Segler, Dr. Thomas Halbritter, Dr. Haraldur Y. Júlíusson, Svava Dögg Hreinsdóttir, Dr. Subham Saha and Dr. Marco Körner for their friendship and supports along the way. I am extremely grateful to Anna-Lena and Thomas for their immense help during my study and for all the fun we have had together.

I am thankful to the Icelandic Research Fund (163393-052) for the PhD fellowship.

Finally, I would like to thank my family for their love and supports. My deepest gratitude goes to my parents for always believing in me and to my sisters, the best in the world and my cheerleaders. I owe a million thanks to my dearest Sveinn who is my biggest pillar of support. I am grateful for his love, patience and for always uplifting my spirit whenever I am a little down. I am also thankful to his wonderful family who showered me with love from the day that I met them and stood by me since then.

1 Objective and scope of the PhD thesis

Nuclear magnetic resonance (NMR) spectroscopy is a widely used technique to determine structure and dynamics of biomacromolecules at atomic-scale resolution. However, the sensitivity of NMR is inherently low due to a small difference in populations between the nuclear spins aligned parallel or antiparallel to an external magnetic field. The population difference, also termed as spin polarization, can however, be significantly enhanced using dynamic nuclear polarization (DNP). DNP transfers the spin polarization of unpaired electrons to the nuclei of interest. Since the electronic spin polarization is several hundred-fold higher than that of nuclei, it can lead to a large enhancement in signal-to-noise ratio. The unpaired electrons required for DNP experiments are mainly provided in the form of persistent organic radicals. Thus, design of efficient radicals for DNP is of considerable interest. 1,3-Bisdiphenylene-2-phenylallyl (BDPA) radicals are very promising polarizing agents for DNP at high magnetic field. However, the lack of solubility of BDPA radicals in aqueous media limits their application for structural studies of biomolecules. This doctoral dissertation is based on the design and synthesis of BDPA radicals that are soluble in aqueous media and have improved persistence.

A brief introduction into DNP is given in **Chapter 2**. It covers the theory of DNP, the primary mechanisms for polarization transfer from electrons to nuclei and the instruments used for DNP-NMR experiments. Furthermore, the design and development of radicals over the years have been described outlining the key structural parameters that contributed to the efficiency of the radicals. The evolution of polarizing agents, from nitroxide biradicals to heteromeric trityl-nitroxide or BDPA-nitroxide biradicals has also been delineated.

In **Chapter 3**, the syntheses of a phosphomonoester-derived BDPA radical and a BDPA-nitroxide biradical, employing a phosphodiester linkage, are described. However, we unexpectedly encountered limited persistence of the BDPA radicals during our work, both in solution and in solid state. Consequently, we focused on investigating the cause of the limited persistence. Decomposition in the solid state was found to be due to oxidation while the limited persistence in solution was primarily due to dimerization. This is the first report of dimerization being a major pathway of degradation for BDPA radicals. Our findings offer

the first comprehensive description of the persistence of BDPA radicals and provide guidelines on how to handle BDPA radicals that are prepared for DNP-NMR experiments.

The strategy to improve the persistence of BDPA radicals has been described in **Chapter 4**. We have synthesized a tetrabromo-BDPA intermediate, where the bromides can be readily substituted with nucleophiles and thus, can be used to prepare a wide variety of BDPA radicals with tailor-made properties. To demonstrate, we prepared four tetraalkyl/aryl-ammonium BDPA radicals which are soluble in polar solvents and are highly persistent due to a reduced tendency for dimerization. Our approach will be very useful for future design of BDPA radicals with high persistence.

Finally, one of these highly persistent tetraalkyl/aryl-ammonium BDPAs was utilized to synthesize the first series of water-soluble BDPA-nitroxide biradicals, described in **Chapter 5**. The linkers between the two radical centers varied in length and flexibility, which resulted in different exchange interactions between the two radical centers. Thus, these biradicals are promising candidates for DNP-NMR experiments for biomolecules. Moreover, the DNP performance of these biradicals will guide further development of BDPA-nitroxide biradicals with improved properties.

2 Introduction

Biomacromolecules, such as nucleic acids, carbohydrates, lipids and proteins are the building blocks of living organisms. These biomolecules are essential for the sustenance of life as they regulate most of the cellular processes, for example the storage and transfer of the genetic code, metabolism, cell-division, transport of nutrients into and out of the cell, and catalysis of most chemical reactions that take place in organisms. Consequently, malfunctions of these biomolecules can lead to diseases. Therefore, understanding of the structures of the biomolecules is of great importance to comprehend their functions. Several techniques have been developed over the years to study the structure and dynamics of biomolecules. One of the most powerful techniques is X-ray crystallography, which provides three-dimensional structures of biomolecules at an atomic scale.¹ This is accomplished by passing X-rays through a crystalline sample, which causes diffraction of the rays. The angles and intensities of diffracted X-rays are measured, from which the density of electrons within the crystal are mapped out providing positions of the atoms. Although, this technique provides comprehensive structural information, it is not without limitations. For instance, X-ray crystallography requires a high-quality crystal, which can be a tedious or unfeasible task as some biomolecules do not crystallize. The crystal structure of a molecule might not represent the biologically relevant conformation. Furthermore, flexible region of a biomolecule which lacks a particular structure cannot be resolved by X-ray crystallography.

Small-angle scattering techniques, such as small-angle X-ray scattering (SAXS) and small-angle neutron scattering (SANS), on the other hand, provide structural information of macromolecules under physiologically relevant conditions.^{2,3} This is achieved by analyzing the scattered X-ray (SAXS) or neutrons (SANS) after it passes through a sample, which provides information about the size and shape of the biomacromolecule. The deflection of the scattered radiation is typically small ($0.1-10^\circ$) hence, it is called small-angle scattering. The disadvantage of these techniques is low resolution ($\sim 10 \text{ \AA}$). Thus, it cannot provide the positions of the atoms within a molecule but an overall shape of the molecule.

Fluorescence resonance energy transfer (FRET)⁴⁻⁶ and electron paramagnetic resonance (EPR) spectroscopy⁷⁻¹⁰ are also used to study structure and dynamics of biomolecules under biologically relevant conditions by measuring distances in the range of 10-100 Å between fluorescent dyes or paramagnetic centers, respectively. Although, these techniques are highly sensitive, they provide lower resolution and often require incorporation of fluorescent or paramagnetic labels to the biomolecule of interest.

Electron microscopy (EM), particularly cryogenic EM (cryo-EM) is drawing widespread attention as an alternative to X-ray crystallography. This technique does not require the biomacromolecules to be crystallized and, therefore, the structure and dynamics can be determined in their native state.¹¹⁻¹³ Using cryo-EM, the structures of a wide variety of complexes, such as viruses,^{14, 15} protein filaments in bacteria¹⁶ and several other proteins¹⁷⁻¹⁹ have been determined. In cryo-EM, a beam of electrons is passed through a sample to produce a magnified image of the sample. It is carried out at cryogenic temperatures to protect the sample from radiation damage. Although, the resolution provided by cryo-EM is still low (4-6 Å) in comparison to X-ray crystallography, it is rapidly transforming into a powerful tool in combination with other techniques, especially solid-state nuclear magnetic resonance (NMR) spectroscopy.^{20, 21} The structures of enzyme complexes,²² nucleic acids,²³ amyloid fibrils^{24, 25} and a variety of proteins²⁶⁻²⁹ have been uncovered with a combination of these techniques.

NMR spectroscopy is possibly the near-perfect technique in structural biology.^{30, 31} It has several advantages over the other techniques. For example, NMR is a non-invasive method, i.e., it does not cause damage to the sample. It can be carried out under physiological conditions and provides three-dimensional structural information of biomacromolecules at atomic resolution. It can also monitor molecular interactions and conformational dynamics. The following section describes this technique in detail, both the advantages and the shortcomings.

2.1 Nuclear Magnetic Resonance Spectroscopy

NMR spectroscopy investigates the local environments of nuclear spins utilizing nuclear magnetic moments. When placed into an external magnetic field, nuclear spins align themselves either parallel or anti-parallel to the magnetic field as shown in **Figure 2.1**. When

radio frequency is applied, transitions between these two energy levels take place giving rise to NMR signals.

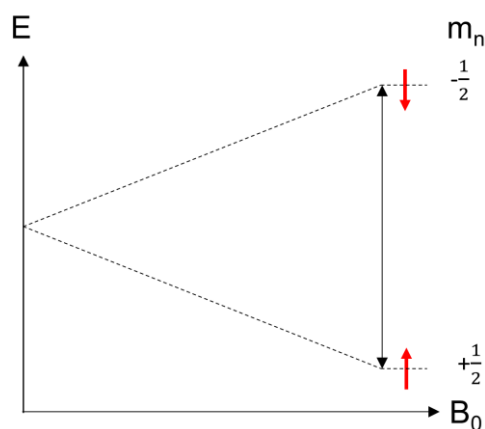


Figure 2.1 Energy-level diagram of a nucleus with a spin quantum number $\frac{1}{2}$ in a magnetic field (B_0).

NMR spectroscopy is commonly performed on samples either in solution or in solid state. Most experiments are carried out in the solution state, where the sample is dissolved in an appropriate solvent. However, solution-state NMR generally requires a sample concentration above 100 μM and it is also limited to biomolecules with molecular weights less than *ca.* 40 kD.³² Thus, molecules with insufficient solubility and larger size cannot be studied by solution-state NMR. These samples can be studied by solid-state NMR.

2.1.1 Solid-state NMR using magic-angle spinning (MAS)

In solid state, molecules take on all possible orientations, unlike in the case of solution-state, where orientational distributions of molecules get averaged out due to rapid tumbling. This leads to broadened lines in the NMR spectrum, known as “powder patterns”.³³⁻³⁵ For example, **Figure 2.2a** shows a solid state ^{13}C -NMR spectrum of polycrystalline glycine (approximately 5% ^{13}C enrichment at the carboxyl site) and a broad line-shape can be observed for the carboxyl carbon spanning between 100–250 ppm.³² Although, these broad lines contain valuable information of the local geometry and electronic structure of the molecules, it leads to significant reduction in resolution and sensitivity. Therefore, to obtain sharp lines, a technique referred to as magic angle spinning (MAS) is used where the sample is rotated rapidly at approx. 54.74° to the external magnetic field. This leads to averaging out of orientational distributions of the molecules.³⁵⁻³⁷ **Figure 2.2b-d** show the solid state ^{13}C -NMR spectra of the polycrystalline glycine using MAS at different spinning frequencies.

When the MAS rotation frequency (ν_R) exceeds the linewidth of the powder pattern, a sharper line arises at the isotropic chemical shift frequency, such as at 177 ppm for the carboxyl carbon and 43 ppm for the α -carbon. Lines whose frequencies vary with ν_R are known as spinning sidebands and contain similar information as the powder pattern.

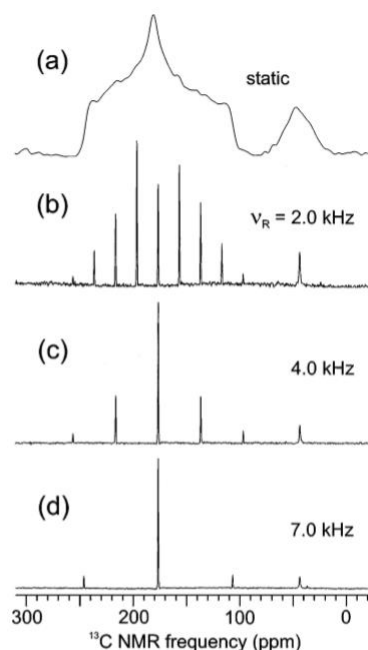


Figure 2.2 Solid state ¹³C-NMR spectra of polycrystalline glycine in absence and presence of magic-angle spinning at the indicated spinning frequencies (ν_R). This figure has been printed with permission from *Annu. Rev. Phys. Chem.* **2001**, 52 (1), 575-606.

High-resolution structural information of complex systems, such as amyloid fibrils,³⁸⁻⁴⁰ membrane proteins,^{40, 41} heterogeneous catalysts,^{42, 43} and polymorphic pharmaceuticals⁴⁴ has been acquired through solid-state MAS-NMR.

2.1.2 Low sensitivity of NMR

Even though NMR spectroscopy is very useful, it suffers from a major limitation, namely its intrinsically low sensitivity. The NMR signal arises from transitions between nuclear states under an applied magnetic field, as mentioned earlier (**Figure 2.1**). The intensity of the signals is proportional to the population difference between the two nuclear states, known as the Boltzmann spin polarization (P):

$$P = \frac{N_1 - N_2}{N_1 + N_2} = \tanh\left(\frac{\gamma \hbar B_0}{2K_B T}\right) \quad (\text{Eq. 1})$$

Here, N_1 and N_2 represent population of two nuclear spin states, γ is the gyromagnetic ratio of the nucleus, \hbar is the reduced Planck constant, B_0 is the magnetic field strength, K_B is the Boltzmann constant and T is the temperature in Kelvin.

The Boltzmann polarization (P) of nuclei is extremely low, leading to low sensitivity of NMR experiments. For example, the spin polarization is only $\sim 0.003\%$ for ^1H at 9.4 T (400 MHz) and 300 K. This scenario is exacerbated in case of low abundance NMR active nuclei, such as ^{13}C ($P \sim 0.0008\%$) or ^{15}N ($P \sim 0.0003\%$). As the Boltzmann polarization of nuclei depends upon the magnetic field strength and the temperature (**Eq. 1**), technological developments, such as higher magnetic fields⁴⁵⁻⁴⁷ and cryogenically cooled probes⁴⁸ have been implemented to increase the spin polarization of nuclei. However, even at 18.8 T (800 MHz) and 10 K, the polarization for ^1H is only $\sim 0.2\%$.

Hyperpolarization techniques, such as para-hydrogen induced polarization (PHIP),⁴⁹⁻⁵¹ optical pumping,^{52,53} dynamic nuclear polarization (DNP)^{54,55} and photochemically-induced DNP⁵⁶⁻⁵⁸ can produce much larger spin polarization. Among these, DNP offers significantly broader applicability from material sciences to structural biology. DNP-NMR is nowadays routinely performed under MAS conditions to study solid samples, such as polymers,⁵⁹⁻⁶² porous materials,⁶³⁻⁶⁹ nanoparticles,⁷⁰⁻⁷² heterogeneous catalysts,⁷³⁻⁷⁹ zeolites,^{80, 81} pharmaceuticals,⁸²⁻⁸⁴ and biomolecules,⁸⁵⁻⁹¹ which would have been challenging or unfeasible otherwise. The work for this PhD thesis is based on this technique and will be discussed in detail in the following sections.

2.2 Dynamic Nuclear Polarization

2.2.1 Theory of DNP

The concept of DNP was first introduced by Albert Overhauser in 1953.⁹² He proposed that spin polarization of electron spins which is several hundred-fold higher than that of the nuclear spins (**Figure 2.3**),⁹³ can be transferred to nuclear spins. In practice, the sample under study is mixed with a source of unpaired electrons, which are commonly persistent organic radicals and microwave irradiation is applied to saturate the electron spin transitions.

Subsequently, an exchange of polarization takes place between electron spins and nuclear spins and the nuclear spins reach a significantly higher polarization, above the Boltzmann limit. This leads to enhanced NMR signals.

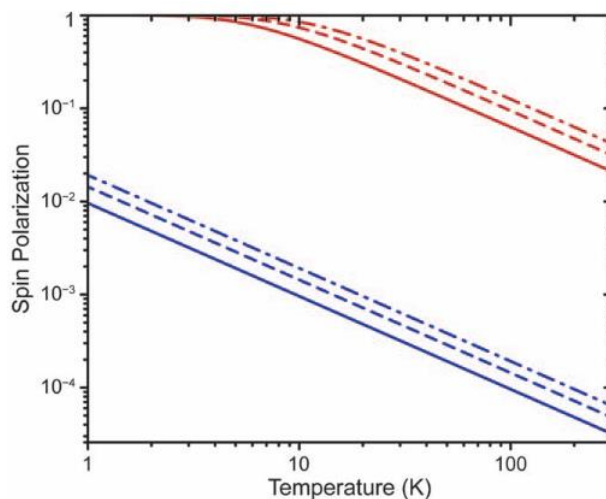


Figure 2.3 Spin polarization of protons and electrons as a function of temperature (blue and red lines respectively) at 9.4 T (solid line), 14.1 T (dashed line), and 18.8 T (dash-dotted line). This figure has been printed with permission from *Paramagnetism in Experimental Biomolecular NMR*, **2018**, 219-257.

The Boltzmann polarization of electrons is higher than nuclear spins, since the gyromagnetic ratio of electrons is higher than that of nuclei:

$$\frac{P_e}{P_n} = \frac{\tanh\left(\frac{\gamma_e \hbar B_0}{2k_B T}\right)}{\tanh\left(\frac{\gamma_n \hbar B_0}{2k_B T}\right)} \approx \frac{\gamma_e}{\gamma_n} \quad (\text{Eq. 2})$$

This ratio also indicates the highest level of polarization transfer that can be achieved through DNP and consequently, the maximum NMR signal enhancement (ϵ) that can be obtained ($\epsilon_{\text{max}} = \gamma_e/\gamma_n$). The theoretical signal enhancement value is ~ 660 for ^1H and even larger for nuclei with smaller gyromagnetic ratios, for example it is ~ 2600 for ^{13}C and ~ 6600 for ^{15}N . In practice, enhancements up to 330 (^1H) has been observed for DNP-NMR experiments performed at 9.4 T.⁹⁴ At higher magnetic fields, the enhancement gets even smaller due to inefficient polarization transfer from electrons to nuclei.

The polarization transfer in DNP takes place through different mechanisms as discussed below.

2.2.2 Polarization transfer mechanisms and pathways

The polarization transfer from electrons to nuclei in DNP occurs through the interactions between the electronic and the nuclear spin states. The energy level diagram of a coupled electron-nuclear pair with spin quantum numbers $S = \frac{1}{2}$ and $I = \frac{1}{2}$ is shown in **Figure 2.4**. The spin population at thermal equilibrium is governed by the Boltzmann distribution which is represented by the size of the grey balls. There are six possible transitions among the four energy levels. Among these, EPR (blue) and NMR (red) transitions are allowed single-quantum (SQ) transitions involving one spin flip. The remaining two transitions (green) involve a simultaneous spin flip of an electron spin and a nuclear spin and are thus referred to as the forbidden zero-quantum (ZQ) and double-quantum (DQ) transitions. DNP mechanisms rely on excitation of these forbidden transitions with microwave irradiation.

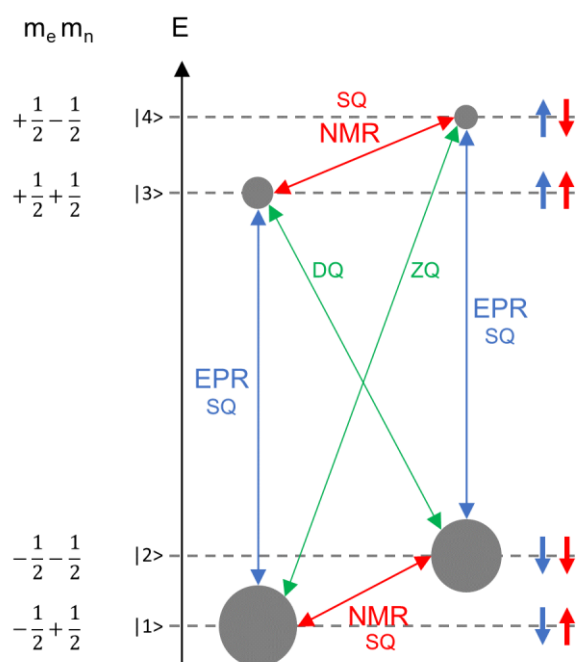


Figure 2.4 Energy level diagram of a coupled electron–nuclear spin pair. The population at thermal equilibrium is governed by the Boltzmann distribution and represented by the size of the grey balls. The arrows show different transitions: electronic or EPR transitions (blue), nuclear or NMR transitions (red) and mixed electronic-nuclear transitions (green). The EPR and NMR transitions are allowed single-quantum (SQ) transitions, whereas the electronic-nuclear transitions are forbidden zero-quantum (ZQ) or double-quantum transitions.

The primary polarization transfer mechanisms are the Overhauser effect (OE),⁹⁵ the solid effect (SE),⁹⁶⁻⁹⁸ the cross effect (CE)⁹⁶⁻⁹⁹ and the thermal mixing (TM).¹⁰⁰⁻¹⁰² These mechanisms mainly differ by the number of electron spins involved for the process. The SE is the simplest mechanism involving a single electron and a nuclear spin, whereas the CE is a three-spin process between two electrons and a nucleus. The TM occurs between a strongly coupled network of electron spins and a nuclear spin. The OE is a two-spin process similar to SE, however, OE relies on cross relaxation processes between states $|2\rangle$ and $|3\rangle$ or $|1\rangle$ and $|4\rangle$ (DQ or ZQ, **Figure 2.4**), whereas SE depends on transition probabilities among the same states.

The DNP mechanisms are usually not active simultaneously during a DNP-NMR experiment. The polarization mechanism which dominates during a DNP experiment is dependent on the experimental parameters, for example the frequency of the microwave, temperature and EPR properties of the radical. For instance, if the EPR linewidth of the radical (δ) is narrower than the Larmor frequency of the nuclei (ω_n) being polarized (i.e., $\delta < \omega_n$), the SE dominates, whereas the CE and TM are dominant when $\delta > \omega_n$. The CE and TM are further differentiated by whether the EPR spectrum is broadened by homogeneous or inhomogeneous interactions, respectively.¹⁰³

The Overhauser Effect

The mechanism proposed by Overhauser is known as the OE.⁹² It was first experimentally demonstrated by Carver and Slichter in powdered Li samples.¹⁰⁴ It was initially thought to occur only in systems with mobile electrons, such as conducting solids and liquids,^{105, 106} however, OE has also been observed in dielectric solids doped with radicals with narrow EPR linewidths.^{95, 107, 108}

The OE relies on the microwave irradiation (μw) of the EPR transitions of the electrons followed by electron-nuclear cross-relaxation as illustrated in **Figure 2.5**. After the microwave irradiation, states $|1\rangle$ and $|3\rangle$ reach equal population. Similarly, the populations of states $|2\rangle$ and $|4\rangle$ are also equalized. Subsequently, if one of the cross-relaxation pathways (DQ or ZQ, **Figure 2.5**) is dominant over the other, it leads to the hyperpolarized nuclear spin states. For example, a dominant DQ cross-relaxation increases the population of states $|2\rangle$ and $|4\rangle$ over the other two states, leading to a negative NMR signal enhancement. On

the other hand, when ZQ cross-relaxation is prevalent, states $|1\rangle$ and $|3\rangle$ reach higher population and a positive NMR signal enhancement is achieved.

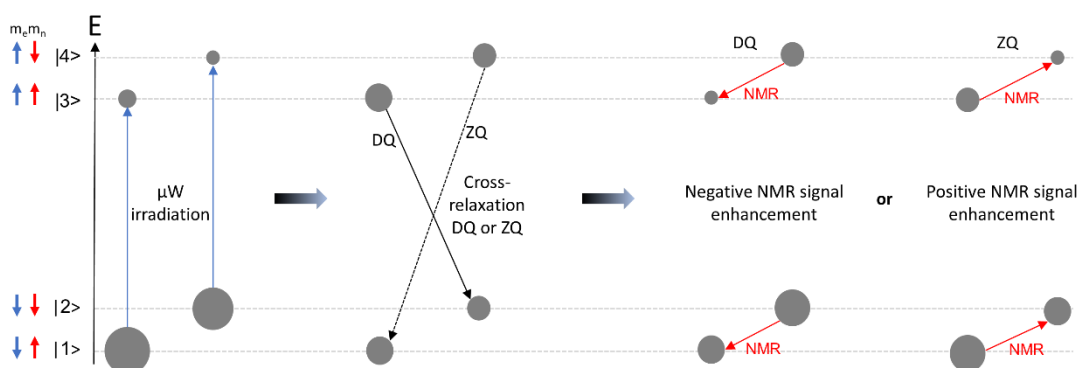


Figure 2.5 Energy level diagram of an electron–nuclear spin pair demonstrating the Overhauser Effect (OE). Microwave irradiation followed by electron–nuclear cross-relaxation (either DQ or ZQ) leads to hyperpolarized nuclear spin states.

The Solid Effect

The SE is a two-spin process between a single electron and a nuclear spin and relies on the microwave irradiation of forbidden ZQ or DQ transitions where an electron and nuclear spins are simultaneously flipped (left, **Figure 2.6**). Excitation of one of these forbidden transitions increases the population difference between the NMR transitions; DQ excitation leads to hyperpolarized states $|1\rangle$ and $|3\rangle$ and a positive signal enhancement is obtained (middle, **Figure 2.6**) where as ZQ excitation increases the population of states $|2\rangle$ and $|4\rangle$ leading to a negative enhancement (right, **Figure 2.6**).

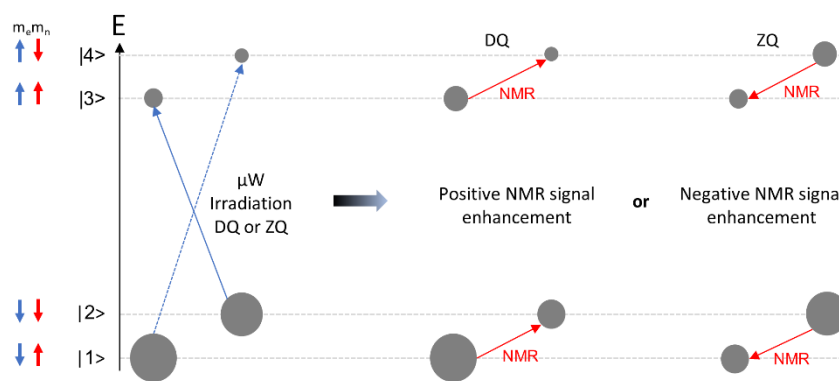


Figure 2.6 Energy level diagram of a coupled electron–nuclear spin pair illustrating the solid effect (SE) DNP. Microwave irradiation of forbidden ZQ or DQ transitions increases the population difference between the nuclear spin states.

Simultaneous excitation of the DQ transition and SQ transition causes partial or complete cancellation of nuclear hyperpolarization. This can be avoided by using a polarizing agent with a narrow EPR linewidth. Carbon-centered radicals, such as trityl,¹⁰⁹ 1,3-bisdiphenylene-2-phenylallyl (BDPA)¹¹⁰ radicals and paramagnetic metal ions^{111, 112} are often used for SE due to their narrow EPR linewidths. However, the efficiency of SE is limited as the excitation of the forbidden ZQ or DQ transitions is required, which is less favorable.

The Cross Effect

The CE is currently the most efficient DNP mechanism.¹¹³ It is a three-spin process involving two electrons and a nucleus. An energy level diagram for a three-spin system is shown in **Figure 2.7**. The conditions of CE are that the two electrons must be dipolar coupled and their electron spin resonance frequencies should be separated by the nuclear Larmor frequency, $|\omega_{e1} - \omega_{e2}| = \omega_n$. Fulfillment of this condition leads to two degenerate energy levels, $|4\rangle$ and $|5\rangle$ (middle, **Figure 2.7**) or $|3\rangle$ and $|6\rangle$. Due to this degeneracy, microwave irradiation at the EPR transition of one of the two electrons, e_2 (blue spin, the transitions are shown by the solid blue arrows) leads to equalized populations of four connected levels, $|2\rangle$, $|4\rangle$, $|5\rangle$ and $|7\rangle$. The microwave irradiation also equalizes the population of $|1\rangle$ and $|3\rangle$ due to the EPR transitions of e_2 (dashed blue arrows) between the levels $|1\rangle \leftrightarrow |3\rangle$. Similarly, the populations of states $|6\rangle$ and $|8\rangle$ are also equalized. Subsequently, the populations between the levels get redistributed as shown in **Figure 2.7** (right) and lead to a positive

NMR enhancement. Excitation of e_1 (green spin), on the other hand, will lead to negative NMR enhancement.

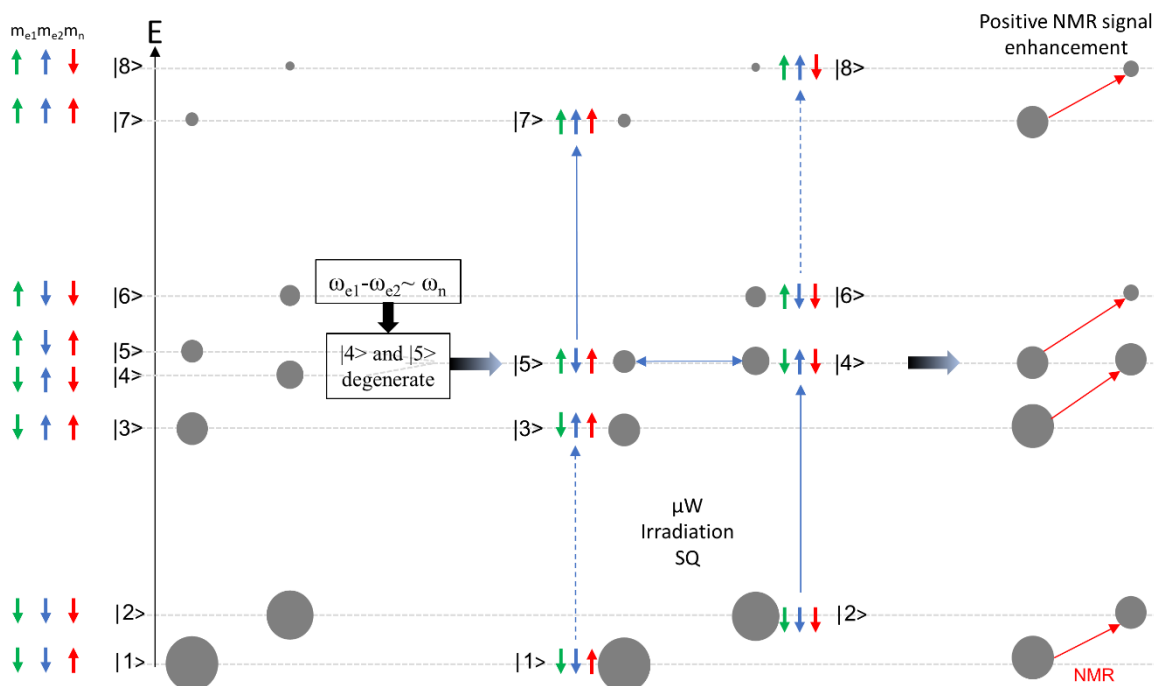


Figure 2.7 Energy level diagram for three spin cross-effect (CE) mechanism. When the frequency difference of the two electron spins is equal to the nuclear Larmor frequency, energy levels $|4\rangle$ and $|5\rangle$ become degenerate and irradiation with microwaves at the EPR transition of one of the electrons builds up the nuclear polarization. Excitation of the EPR transition of only e_2 (blue) is shown here which leads to a positive NMR enhancement.

The scenario depicted above is, however, for a static sample case i.e., without MAS. The CE mechanism gets significantly more complex under MAS. In this case, the polarization transfer between the electrons and nuclear spins takes place through a series of energy levels crossing/anti-crossing (rotor events).⁹⁷⁻⁹⁹ The first crossing occurs when the microwave frequency matches the EPR frequency of one of the electrons ($\omega_{\mu W} \sim \omega_{e1}$ or ω_{e2}) and reduces the polarization of that particular electron from its thermal equilibrium value. This leads to a polarization difference between the two electrons. The second crossing takes place when the difference of the EPR frequencies of the two electrons equals the NMR frequency of the nucleus ($\omega_{e1} - \omega_{e2} \sim \omega_n$) and leads to a transfer of some of the polarization difference between the two electrons to the nucleus.

Depolarization by CE during MAS

The polarization transfer through CE under MAS does not require microwave irradiation. In other words, the nuclear polarization can be altered even without microwave irradiation by spinning the sample. This process can result in a reduction of the nuclear polarization, relative to the Boltzmann polarization. This effect is known as nuclear depolarization and should be taken into account when calculating the enhancement factor. The reason for this is that the DNP enhancement factor ($\epsilon_{\text{on/off}}$) has been conventionally calculated as the ratio of NMR signal intensities obtained with and without microwave irradiation. However, the NMR signal intensity could be significantly less under ‘microwave off’ condition due to the depolarization effect. Thus, the $\epsilon_{\text{on/off}}$ might be larger than the actual signal enhancement in a DNP experiment.

Thermal mixing

The TM is a multi-spin process between many electron spins and a nuclear spin. The mechanism of TM is similar to the cross effect. However, it requires a strongly coupled network of electrons with homogeneously broadened EPR spectrum larger than the nuclear Larmor frequency ($\delta > \omega_n$). It takes place under very low temperatures ($< 10 \text{ K}$)^{100, 101} and is not prevalent for MAS DNP.

Spin diffusion

The concentration of the unpaired electrons in DNP-NMR is kept diluted (typically 5-20 mM) to reduce paramagnetic broadening of NMR spectra caused by the unpaired electrons. Therefore, the polarization transfer through the DNP mechanisms discussed above takes place with a small number of nuclei at close proximity to the polarizing agent, as shown in **Figure 2.8** (middle). However, the polarization can be propagated from these nuclei to the bulk nuclei (far away from the polarizing agent) by a mechanism called spin diffusion (SD) (**Figure 2.8**, right). SD is a process by which polarization can be exchanged spontaneously between homonuclear spins. This exchange is mediated by the dipole-dipole interactions between the homonuclear spins. Thus, SD is an essential process in DNP-NMR to obtain a uniformly polarized sample.

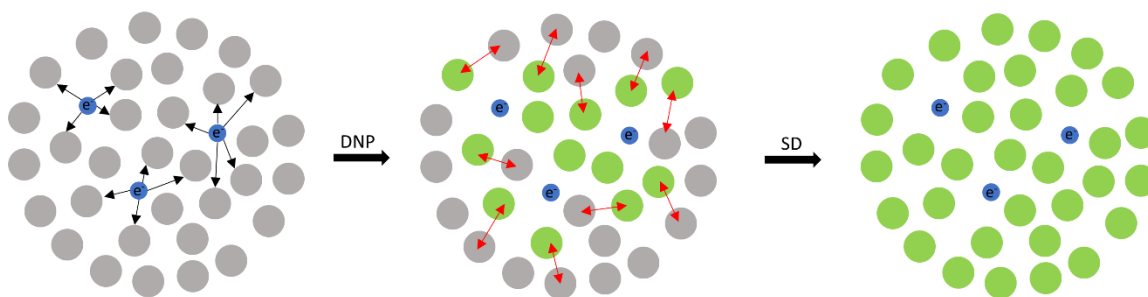


Figure 2.8 A visual representation of polarization transfer from electrons to nuclei. First the polarization from electrons (blue) is transferred to the nuclei (grey) at proximity through DNP (black arrows) leading to hyperpolarized nuclei (green). Spin diffusion (SD) (red arrows) exchanges polarization between nuclear spins.

Cross-polarization

In DNP, polarization is transferred from electrons to nuclei. On the other hand, cross-polarization (CP) is a technique in which polarization can be transferred from one type of nucleus to a different type. CP is a common technique in solid-state NMR and is quite often combined with DNP to enhance the sensitivity of low- γ nuclei, such as ^{13}C , ^{15}N , ^{17}O and ^{29}Si . In this approach, the protons of a sample are initially hyperpolarized by DNP, since protons have a high abundance and a large γ and, therefore, an efficient hyperpolarization can be achieved throughout the sample. This enhanced polarization of ^1H is then further transferred to less-sensitive low- γ nuclei by CP for detection.

2.2.3 Instrumentation

State-of-the-art solid-state NMR instruments use magnetic fields up to 28 T (1.2 GHz)⁴⁷ and MAS probes that can spin samples up to 126 kHz at 20 °C,¹¹⁴ which significantly improve the spectral resolution. However, combining these techniques with DNP is extremely challenging, since DNP additionally requires high-frequency microwaves and sample spinning at cryogenic temperatures as typical experiments are performed at 100 K or below. Therefore, solid-state DNP-NMR instrumentation involves significant modifications to an existing MAS-NMR setup. A schematic representation of a MAS-DNP NMR instrument is shown in **Figure 2.9**.¹¹⁵ The additional components beside the MAS NMR instrumentation, include a high-frequency microwave source (commonly a gyrotron), a transmission line to propagate microwaves from the gyrotron to the NMR sample and a cryogenic MAS unit. A brief description of the components is given below.

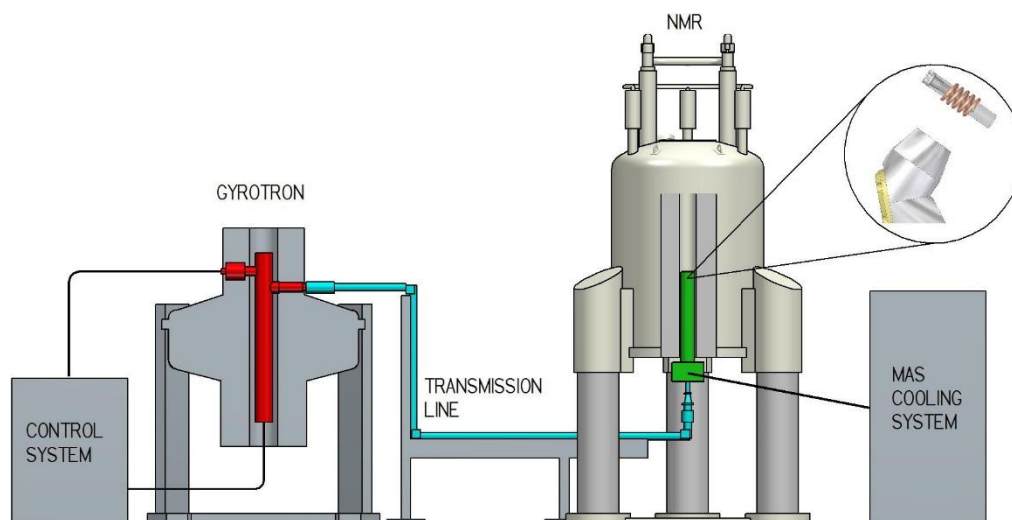


Figure 2.9 A schematic representation of a solid-state DNP NMR setup with a microwave source (gyrotron tube, red), the microwave transmission line (blue), the NMR spectrometer with a MAS probe (green) attached to a cooling system. This figure has been printed with permission from *J. Magn. Reson.* **2016**, 264, 88-98.

The microwave source

DNP-NMR experiments performed at higher fields require a source of high-frequency microwaves. For example, NMR experiments performed at 200–1000 MHz frequencies (^1H) require a microwave source with frequency range 130–660 GHz,¹¹⁶ whereas routine EPR measurements are performed at 9.4 GHz. Until recently, such high-frequency microwaves were not available due to technical difficulties. A major breakthrough came with the development of gyrotrons.¹¹⁷⁻¹¹⁹ A gyrotron is a class of vacuum electronic devices, where an electron beam is accelerated through a strong magnetic field, generated by a superconducting magnet. This causes a gyration (rotation) of the electrons and consequently microwaves are produced. The most advanced gyrotrons can now generate microwaves with a frequency of 593 GHz which enables the DNP-NMR experiments to be performed at an external magnetic field of 21.1 T (900 MHz ^1H).¹²⁰

The waveguide

Current technology demands that the gyrotron magnet to be placed at a distance from the NMR magnet.¹²¹ Therefore, the microwaves must be delivered from the gyrotron to the NMR sample through a transmission line of few meters with minimum power losses (**Figure 2.9**). This is accomplished using corrugated waveguide, which are more efficient than fundamental rectangular waveguides.¹²¹

Cryogenic MAS: Cooling gases, rotors

DNP-NMR experiments are often performed at cryogenic temperatures as the relaxation times of both the electrons and nuclei are more favorable at ~100 K for an efficient polarization transfer.¹¹⁶ Temperatures down to 100 K can be achieved with a cooling system employing N₂ as the cryogen. For lower temperatures, He is used instead. However, the viscosity of the cryogenic gas increases as the temperature gets closer to the liquefaction point, which reduces the spinning frequency of the MAS significantly as compared to conventional MAS-NMR experiments performed at higher temperatures. Spinning frequencies up to 15 kHz can be achieved with the most common MAS rotors that have a diameter of 3.2 mm.¹²² In 2016, MAS frequency has been extended up to 40 kHz using 1.3 mm rotors.¹²³ Most recently, 65 kHz MAS rates have been attained with a 0.7 mm rotor.¹²⁴

2.2.4 Solvents for DNP experiments

In most DNP experiments, the polarizing agent is dissolved in a solvent along with the sample and subsequently frozen, since DNP-NMR experiments are commonly performed at cryogenic temperatures, as mentioned earlier. In order to achieve an optimal DNP efficiency, the solvent must fulfill three major conditions. First, the solvent must produce a glassy matrix once frozen to prevent crystallization of the solvent which causes aggregation of the polarizing agents. This leads to inhomogeneous radical distribution in the sample and consequently the DNP efficiency reduces significantly.¹²⁵ Second, the solvent needs to be a cryoprotectant. In other words, it needs to protect the cold-sensitive molecules, such as proteins from possible denaturation upon freezing.⁵⁴ Third, the solvent should be partially deuterated. Deuteration of the solvent matrix has been observed to increase the polarization of nuclei.¹²⁶ However, a complete deuteration is avoided so that spin diffusion (¹H-¹H) remains effective during the DNP experiment to distribute polarization across the sample. Thus, d₈-glycerol/D₂O/H₂O (60:30:10), commonly referred to as “DNP juice”¹¹⁸ or d₆-DMSO/D₂O/H₂O mixtures are often used as the glass-forming matrix. Glycerol/water is the most preferred choice as it forms a glassy matrix regardless of the rate of cooling.¹²⁷ For hydrophobic compounds, glass-forming organic solvents, such as 1,1,2,2-tetrachloroethane (TCE) or *ortho*-terphenyl (OTP) have been used.^{128, 129}

2.2.5 Polarizing agents

The electrons, from which the large polarization gets transferred to nuclei during DNP experiments, come from compounds (polarizing agents) containing unpaired electrons. Typically, persistent organic radicals are introduced in the samples as the polarizing agent. **Figure 2.10** shows common radicals used in DNP experiments, such as the nitroxide, 2,2,6,6-tetramethylpiperidine 1-oxyl (**TEMPO**) and the carbon-centered radicals, **Finland trityl** and **BDPA**. These radicals have different EPR properties, such as their EPR linewidths and relaxation times, which can invoke different DNP mechanisms. The following section describes these radicals in detail. Apart from these radicals, complexes of paramagnetic metal ions, such as **Gd-DOTA** and **Mn-DOTA** (**Figure 2.10**), have also been used as polarizing agents in DNP experiments.^{111, 112}

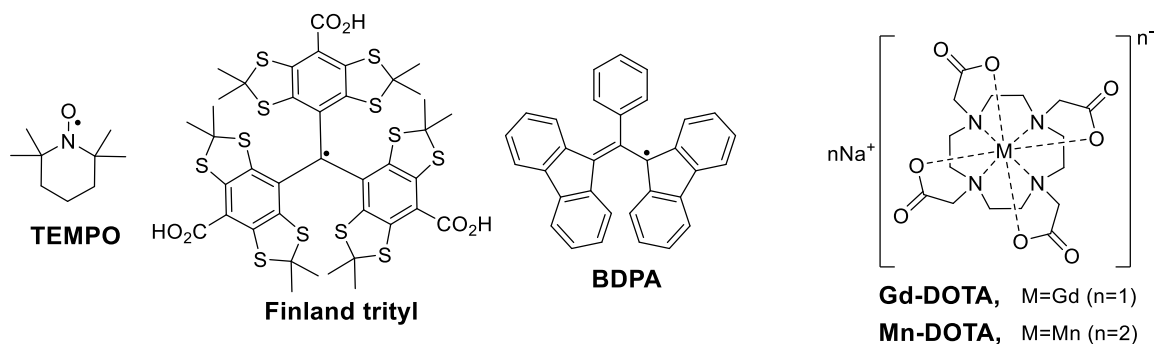


Figure 2.10 The polarizing agents commonly used in DNP experiments, **TEMPO**, **Finland trityl**, **BDPA**, **Gd-** and **Mn-DOTA**.

Nitroxides

Aminoxyl radicals, commonly called nitroxides are often the preferred choice of polarizing agent due to their high persistence and relative ease of synthesis. Furthermore, their broad EPR linewidth enables them to satisfy the frequency matching condition for the CE. The CE involves two dipolar coupled electrons, as described before, hence it is more efficient when biradicals are used as the polarizing agents instead of monoradicals. Another advantage of using biradicals is that efficient DNP can be achieved with far lower radical concentrations (5-10 mM), compared to experiments with monoradicals (~40 mM).¹³⁰ This reduces the NMR line-broadening due to paramagnetic relaxation enhancement (PRE) that is caused by

the radicals.¹³¹ Thus, nitroxide biradicals with improved DNP performance have been prepared over the last years, mostly by trial and error, as discussed below.

The efficiency of biradicals as polarizing agents for DNP depends on the dipolar coupling and *J*-coupling between two radical centers.^{97, 98} To optimize the coupling, Hu *et al.* synthesized the first nitroxide biradical series, bis-TEMPO-*n*-ethylene glycols (**BT_nE**) (*n* = 2-4 ethylene glycol unit) by tethering two TEMPO radicals with a poly-ethylene glycol chain as shown in **Figure 2.11**.¹³¹ **BT2E** (two ethylene glycol units) was the most efficient among the series and yielded ~4 times larger signal enhancement ($\epsilon \sim 175$, 5 T) over the monomeric TEMPO.¹³¹ After the success of **BT2E**, **TOTAPOL** was synthesized soon thereafter as a water-soluble variant which yielded similar enhancement as **BT2E** (**Figure 2.11**).¹³²

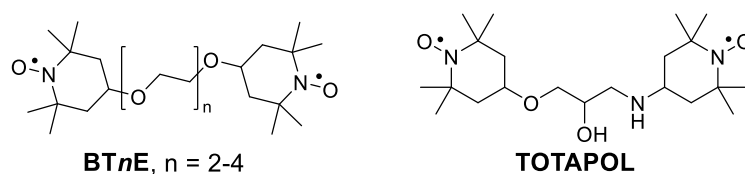


Figure 2.11 The initial design of nitroxide biradicals.

The flexibility of the linker between the two nitroxides in **TOTAPOL** was found to be a limiting factor in its DNP performance.^{122, 133} Consequently, **bTbk** was synthesized where the two TEMPO radicals were tethered by a rigid linker at an orthogonal orientation (**Figure 2.12**), resulting in 1.4-fold improved DNP performance ($\epsilon \sim 250$, 5 T) relative to **TOTAPOL**.¹³⁴ The **bTbk** was further modified by replacing the geminal methyl groups next to the nitroxide with cyclohexyl groups (**bCTbk**, **Figure 2.12**).¹³⁵ This modification was introduced to increase the relaxation times of the unpaired electrons, which facilitates the saturation of the electronic transitions. Indeed, **bCTbk** yielded a higher signal enhancement ($\epsilon \sim 100$, 9.4 T) compared to **bTbk** ($\epsilon \sim 26$, 9.4 T).¹³⁵ Following the success of **bCTbk**, **TEKPol** (**Figure 2.12**) was prepared to lengthen the relaxation time of electrons even further by increasing the molecular weight of the biradical ($\epsilon \sim 200$, 9.4 T).¹²⁸ Bulkier radicals lead to slower relaxation times due to reduced molecular motion/tumbling in the glassy matrix.¹³⁶

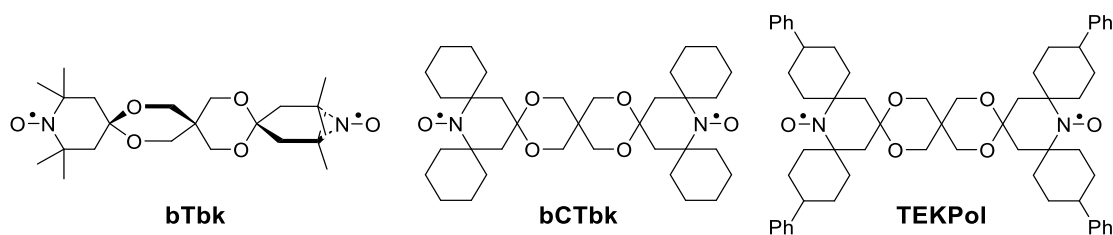


Figure 2.12 Rigid nitroxide biradicals.

The solubility of the **bTbk** series in aqueous media was severely limited. Subsequently, water-soluble nitroxide biradicals, **PyPol**¹³³ and **AMUPol**¹³³ (**Figure 2.13**) were synthesized, both of which gave excellent DNP performance (**AMUPol**: $\epsilon \sim 230$, 9.4 T) due to their rigid structure, optimal dipolar coupling between the two electrons and longer electron relaxation times. The solubility and performance were further improved with introduction of **bcTol**¹³⁷ ($\epsilon \sim 230$, 9.4 T) and **bcTol-M**¹³⁸ ($\epsilon \sim 240$, 9.4 T) (**Figure 2.13**).

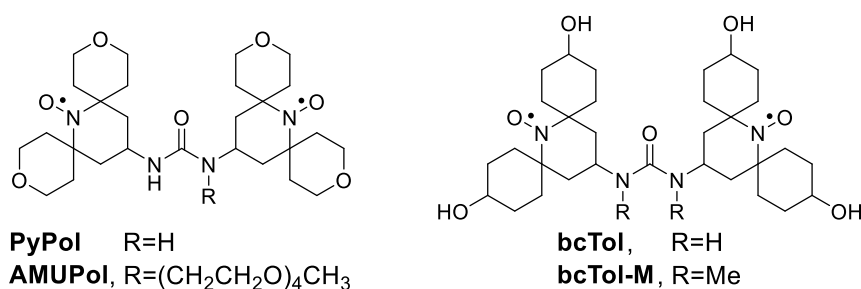


Figure 2.13 Water-soluble nitroxide biradicals.

Recently, another parameter has been identified which influences the performance of nitroxides. It has been reported that the local geometry around the unpaired electron governs the DNP efficiency.⁹⁴ For example, **HydrOPol** ($\epsilon \sim 330$, 9.4 T), where the two spiro-tetrahydropyran rings at the α -position of the nitroxide were placed away from the radical, was considerably more efficient than **C-HydrOPol** ($\epsilon \sim 30$, 9.4 T) where the rings were pointed towards the radical (**Figure 2.14**). It was postulated that the greater solvent accessibility to the electron spin in the case of **HydrOPol** leads to a higher extent of polarization transfer. Under the same experimental conditions, the DNP efficiency of **HydrOPol** was found to be 2-fold higher than **AMUPol**, which can exist as both in an open and closed conformation.

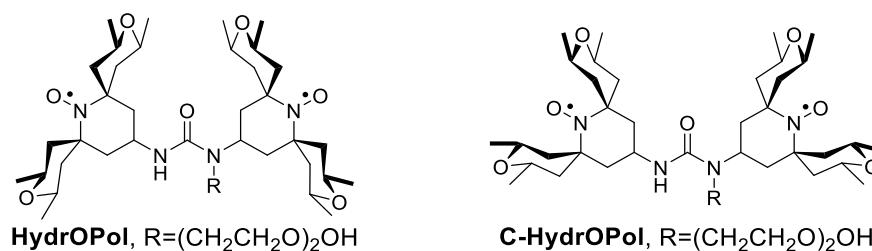


Figure 2.14 Open and closed nitroxide biradicals.

The biradicals discussed above, however, have two major limitations. First, the DNP efficiency decreases significantly with increasing magnetic field. Second, they produce considerable depolarization effect under MAS, a process that decreases the effective gain in signal enhancement (**Section 2.2.2**).^{139, 140} For instance, the actual enhancement gain for **AMUPol** has been reported to be ~ 90 (9.4 T) rather than ~ 200 ($\epsilon_{\text{on/off}}$) when depolarization effect is considered.⁷⁴ Therefore, significant efforts have been placed lately to overcome these issues. A family of asymmetric biradicals, the **AsymPols** composed of a piperidine- and a pyrrolidine-based nitroxides were designed for this purpose, employing advanced simulations.¹⁴¹ **AsymPolPOK** (**Figure 2.15**) was substantially more efficient ($\epsilon \sim 83$, 9.4 T) than **AMUPol** ($\epsilon \sim 43$, 9.4 T) under similar experimental conditions and showed negligible depolarization. Even at 18.8 T and with MAS frequencies of up to 40 kHz, **AsymPolPOK** yielded 2 times higher NMR sensitivity ($\epsilon \sim 30$, 3.2 mm rotor) relative to **AMUPol**. More recently, another biradical, **M-TinyPol** (**Figure 2.15**) has been reported to be highly efficient at high magnetic field with reduced depolarization ($\epsilon \sim 90$, 18.8 T, 1.3 mm rotor).¹⁴²

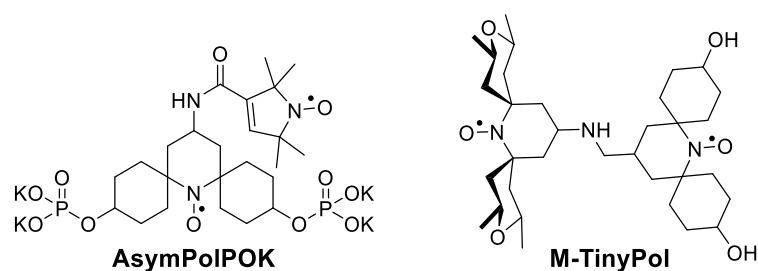


Figure 2.15 Efficient nitroxide biradicals at high magnetic field (≥ 18.8 T).

Trityl/BDPA-nitroxide heterobiradicals

The ideal polarizing agent for CE-DNP experiments should have an EPR spectrum consisting of two sharp lines separated by the Larmor frequency of the nucleus to be

polarized, $\omega_{e1}-\omega_{e2} = \omega_n$.^{98, 103} However, no radical or radical pair is known to possess such an EPR spectrum that rigorously satisfies this condition. Narrow-line radicals, such as the Finland trityl or BDPA (**Figure 2.10**) attached to a nitroxide serve as a reasonable approximation for this approach as the separation between the maxima in their EPR spectra closely matches the ^1H Larmor frequency. This was first experimentally demonstrated by Hu *et al.* with an equimolar mixture of trityl and TEMPO radicals, where the signal enhancement was 4-fold compared to TEMPO alone.¹⁰³

The efficiency of these radical mixtures can be further improved by connecting the two radicals with linkers, which leads to larger electron-electron coupling between the radicals. **TEMTriPol-1** and **HyTEK2** (**Figure 2.16**) were developed for this purpose and yielded excellent results, especially at high fields ($\epsilon \sim 65$, 18.8 T, 3.2 mm rotor), compared to nitroxide biradicals.^{120, 143} The superior performance of these heteromeric biradicals was attributed to the different EPR spectral- and relaxation-properties of the two radical components, in addition to the efficient CE matching described above. Specifically, the EPR transition of the slow-relaxing narrow-line carbon radical requires lower microwave power and can be saturated efficiently while the fast-relaxing nitroxide ensures multiple polarization transfer to the nuclei.⁵⁴ Another advantage of such biradicals, compared to most nitroxide biradicals, is that they produce less depolarization under MAS-DNP conditions.¹³⁹⁻

141

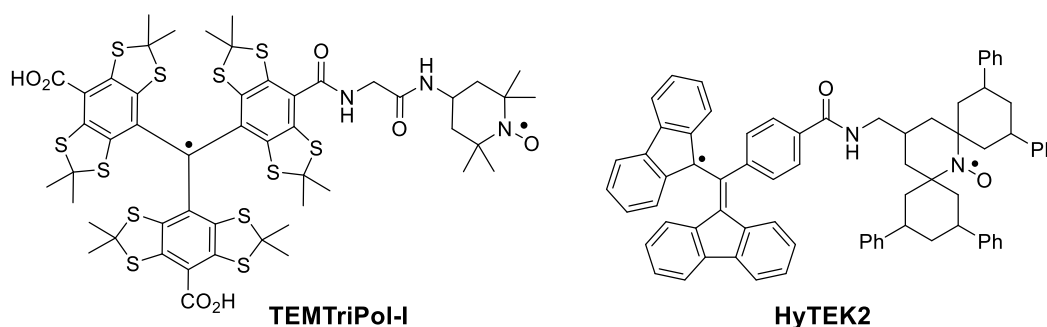


Figure 2.16 The heterobiradicals **TEMTriPol-1** and **HyTEK2**.

BDPA radicals

An advantage of the carbon-based BDPA radical over the Finland trityl is its relative ease of synthesis.^{144, 145} Several BDPA-nitroxide biradicals have been prepared,^{120, 146, 147} such as

BDPA-TEMPO (Figure 2.17) where the two radicals were attached through an amide linkage. However, no DNP measurements have been reported.¹⁴⁶ **BDPAesterTEMPO** (Figure 2.17) was prepared by linking the two radicals with an ester group and excellent DNP results were obtained in fast dissolution DNP.¹⁴⁷

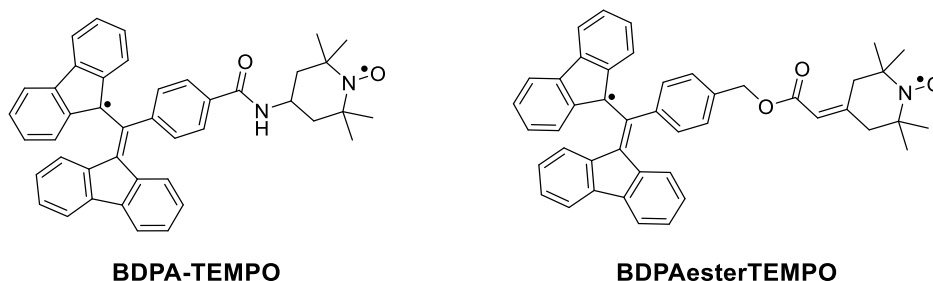


Figure 2.17 Initially designed BDPA-nitroxide biradicals.

More recently, a series of BDPA-nitroxide biradicals has been prepared by varying the length and rigidity of the linker and also the nitroxide center.¹²⁰ Among these, **HyTEK2** (Figure 2.18) has been reported to be most efficient due to two factors, the short methylene linker that results in an optimal electron–electron interaction and the lengthened spin relaxation time of the nitroxide owing to the phenyl-spirocyclohexyl groups at the α -positions. An enhancement of 185 at 18.8 T (1.3 mm rotor) was obtained for **HyTEK2**.¹²⁰ At higher field (21.1 T), the enhancement was even higher ($\epsilon \sim 200$, 0.7 mm rotor) according to a recent report.¹²⁴

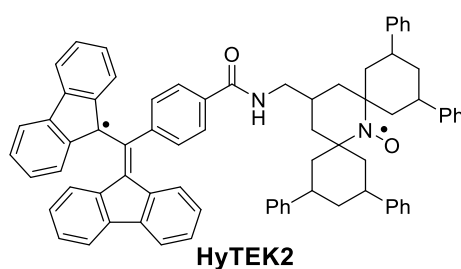


Figure 2.18 One of the most efficient biradicals at high magnetic field (≥ 18.8 T).

Although BDPA radicals, described above have been shown to be excellent polarizing agents, they suffer from a major limitation. The lack of solubility of BDPA radicals in aqueous media limits their applications for DNP experiments with biomolecules. Only two water-soluble BDPA derivatives have been reported thus far.^{110, 148} Dane *et al.* reported

WS-BDPA (Figure 2.19), however, the solubility of the radical was extremely limited (1 mM, PBS buffer, pH 8). The solubility of **WS-BDPA** was higher in DNP juice (10 mM) after adjusting the pH to 8 with NaHCO_3 .¹⁴⁸ DNP experiments with **WS-BDPA** have not been reported. The same research group has also synthesized sulfonated BDPA radicals (**Figure 2.19**), which is a mixture of radicals with different degrees of substitution (**SA-BDPA**), and another derivative with selective substitutions at the meta positions of the fluorene rings (**SA-BDPA-2**).¹¹⁰ Nonetheless, these sulfonated BDPA radicals cannot be readily conjugated to nitroxides for the preparation of biradicals.

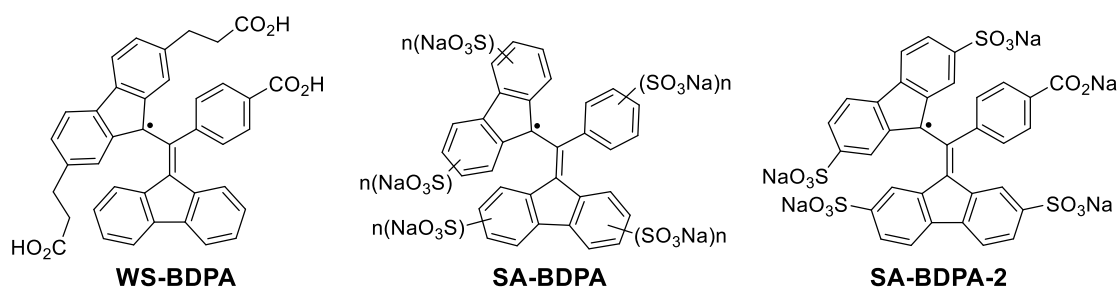


Figure 2.19 Reported water-soluble BDPA radicals.

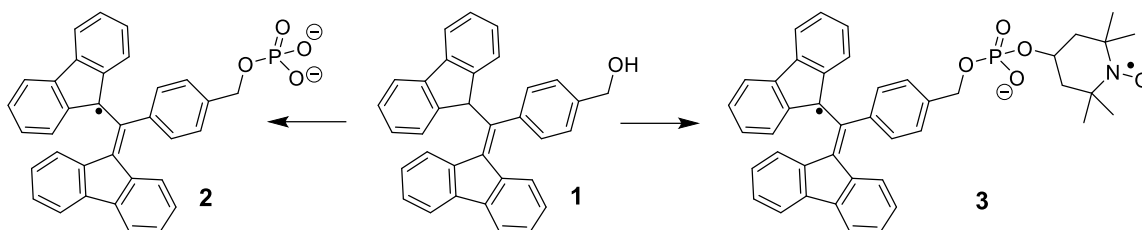
2.3 Contribution of this PhD dissertation

The goal of this PhD work was to synthesize new BDPA radicals, especially water-soluble radicals with increased efficiency for DNP. For this purpose, a phosphomonoester-derived BDPA radical and a BDPA-nitroxide biradical, employing a phosphodiester linkage, were prepared (**Chapter 3**). However, during their syntheses, an unforeseen challenge was encountered. A rapid degradation of the BDPA radicals was observed, which made handling of these radicals extremely challenging. Surprisingly, no detailed description of this limited persistence was found in the literature. In contrast, BDPA radicals had been referred to as stable radicals. As a result, the goal of the project shifted towards finding the cause of this limited persistence. Extensive studies were carried out to assess the persistence of BDPA radicals under various conditions. The investigation revealed dimerization of BDPA radicals as the major cause of this limited persistence. The detailed investigation and the results are described in **Chapter 3**.

The second part of the thesis focuses on the synthesis of a new class of BDPA radicals that addresses the two shortcomings of BDPA radicals, namely the lack of solubility in aqueous media and the limited persistence. **Chapter 4** describes the synthesis of four tetraalkyl/aryl-ammonium derivatives with solubility in aqueous media and high persistence due to reduced tendency for dimerization. Synthesis of a series of water-soluble BDPA-nitroxide biradicals is described in **Chapter 5**. These biradicals are being evaluated by our collaborators as polarizing agents for DNP-NMR.

3 Limited persistence of BDPA radicals

The goal of this doctoral work was to develop efficient BDPA radicals with an emphasis on water-solubility, as discussed earlier. The first strategy was to attach a hydrophilic functional group at the *para*-position on the benzene ring of the BDPA (**Scheme 3.1**), since this position can be readily functionalized.^{146, 149-151} We chose to incorporate a phosphate group to prepare a phosphomonoester-derived BDPA radical (**2**) as phosphate-derived radicals have excellent solubility in aqueous solutions.¹⁴¹ We also decided to prepare a BDPA-nitroxide biradical (**3**), employing a phosphodiester linkage, as shown in **Scheme 3.1**. The solubility of **3** in aqueous solutions is expected to be limited, however, it might be useful for DNP experiments in organic solvents.^{120, 147}



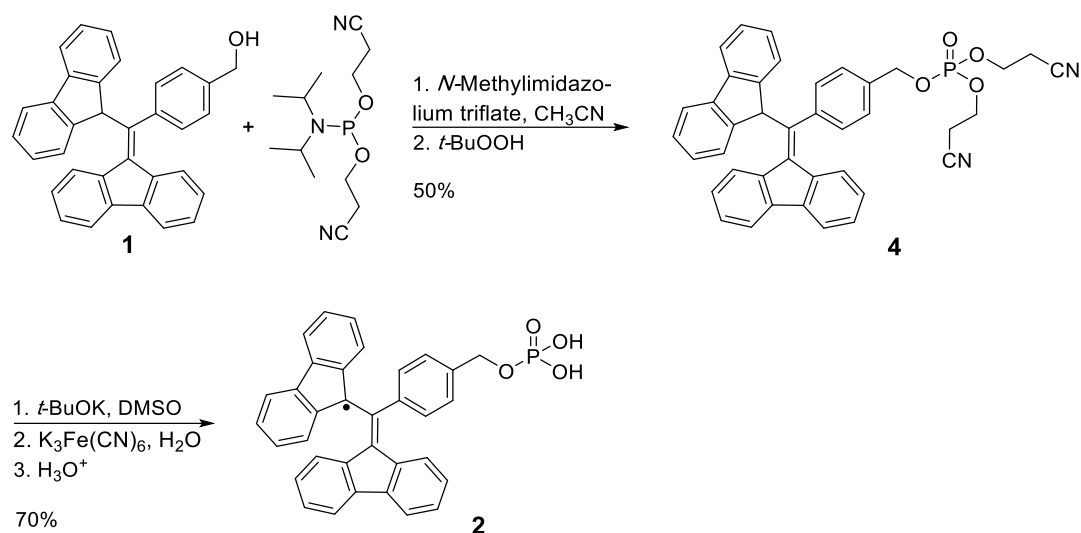
Scheme 3.1 Strategy for preparation of phosphoester-derived BDPA radicals.

The syntheses of **2** and **3** are described in the following section. During the synthetic process, it was observed that BDPA radicals have limited persistence, which was unexpected, since these radicals have been described as stable in the literature.^{145, 149} Therefore, the project took a different turn from there as we decided to focus on finding the cause of this limited persistence. Consequently, we have carried out a systematic investigation of the stability of BDPA radicals under various conditions which is discussed in the following sections.

3.1 Synthesis of the radicals

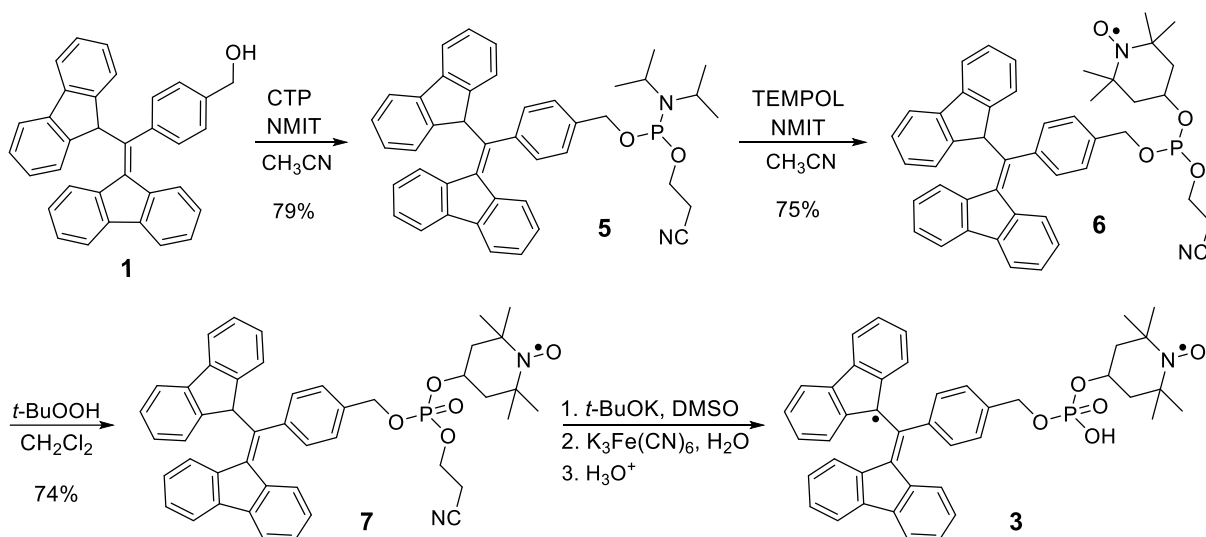
The benzyl alcohol derivative of BDPA (**1**) was synthesized following a reported protocol.^{146, 150} The hydroxyl group of BDPA **1** was phosphitylated, followed by oxidation of the phosphorous to give compound **4** (**Scheme 3.2**) in moderate yields. A methanolic

solution of ammonia was used to remove the cyanoethyl groups of **4**, but this procedure also generated a significant amount of radical, which was difficult to quantify. Since *t*-BuOK can be used to remove the cyanoethyl protecting groups, the deprotection and radical generation were carried out using a two-step, one-pot procedure to yield **2**.



Scheme 3.2 Synthesis of BDPA-phosphate radical **2**.

To prepare the BDPA-nitroxide biradical, employing the phosphate group as a linker, BDPA alcohol **1** was phosphitylated to give phosphoramidite **5** with good yields (**Scheme 3.3**). Subsequent reaction of **5** with 4-hydroxy-2,2,6,6-tetramethylpiperidin-1-oxyl (TEMPO) resulted in compound **6**. Oxidation of the phosphorous of **6** gave phosphodiester **7** in good yields. Compound **7** was sequentially treated with *t*-BuOK and K₃Fe(CN)₆, to deprotect the cyanoethyl protecting group and to generate BDPA-nitroxide biradical **3**.



Scheme 3.3 Synthesis of BDPA-TEMPO biradical **3** containing a phosphodiester linker. CTP: 2-Cyanoethyl *N,N,N',N'*-tetraisopropylphosphorodiamidite, NMIT: *N*-Methylimidazolium triflate.

During the synthesis of the BDPA radicals, it became clear that they had limited persistence, both in solution and as a solid. Although BDPA radicals have been reported to be stable in the solid state,¹⁴⁵ they have been described to react with oxygen in solution in presence of light.¹⁴⁹ Therefore, the rapid decomposition of the synthesized radicals in solution, even in absence of oxygen (**Section 3.3.1**), was surprising and we decided to investigate it further. The EPR spectrum of biradical **3** allowed quantification of the BDPA radical center rather easily and is further described in the next section.

3.2 Quantification of BDPA radicals

Figure 3.1 shows the EPR spectra of three different radicals **2**, **7** and **3**. A single peak (**Figure 3.1**, top) was observed for the carbon-centered BDPA monoradical (**2**), whereas nitroxide monoradical **7** showed the characteristic three peaks of a nitroxide (**Figure 3.1**, middle).

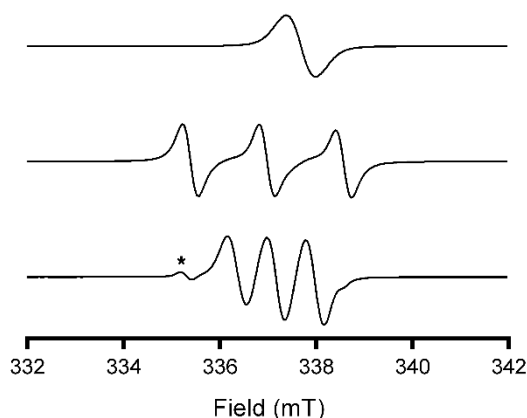


Figure 3.1 EPR spectra of three different radicals; BDPA radical **2** (top), nitroxide **7** (middle) and BDPA-nitroxide biradical **3** (bottom). The peak marked by asterisk in the biradical spectrum originated from a nitroxide monoradical that is present in the sample of the biradical. Experimental parameters: 9.43 GHz, microwave power 1 mW, sweep width 12 mT, modulation 0.2 mT, 23 °C.

For biradical **3**, three peaks with narrower spectral width than a nitroxide, are expected due to the strong J -coupling (~ 100 MHz) between the nitroxide and the BDPA radical.^{146, 147} However, more than three peaks were observed in the EPR spectrum of biradical **3** as shown in **Figure 3.1** (bottom). This was due to presence of two components, the biradical itself (the central three peaks) and a nitroxide monoradical derived from **3**, where one of its three peaks is well separated from the spectrum of **3** (**Figure 3.1**, bottom, asterisk). It is to be noted that the presence of two components have also been reported for previously synthesized BDPA-nitroxide biradicals.^{146, 147} Nevertheless, due to this well separated peak, the ratio of these two spectral components representing the biradical and the nitroxide monoradical, can be quantified by double integration of the spectrum as described by Dane *et al.*,¹⁴⁶ which was determined to be *ca.* 90% for biradical **3** (**Figure 3.1**). Thus, EPR spectroscopy can be readily used to quantify the amount of biradical **3** relative to the nitroxide present in the sample at any given time and we used this method primarily to investigate the persistence of BDPA radicals.

The persistence of BDPA radicals can also be investigated by UV-vis spectroscopy, as they absorb strongly in the visible region.¹⁴⁹ **Figure 3.2A** shows the UV-vis spectra of biradical **3** in DCE at various times. The peak between 400 – 550 nm arises from the absorption of the BDPA radical and decreases when the radical decomposes. **Figure 3.2B** shows the plots of absorbance at 490 nm (left y-axis) and the percentage of the biradical relative to the

nitroxide monoradical determined by EPR spectroscopy (right y-axis) as a function of time. Both techniques give similar results.

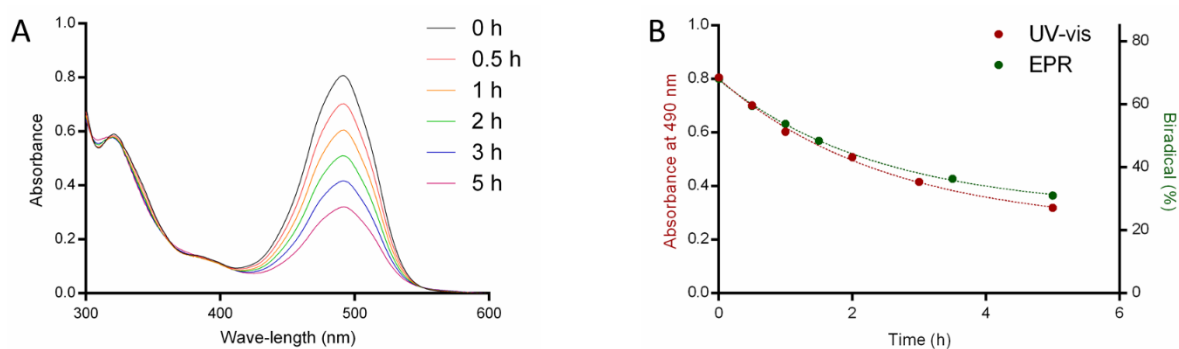


Figure 3.2 The rate of degradation of biradical **3** determined by both UV-vis and EPR spectroscopy in DCE (5 mM) at 23 °C. **A.** The UV-vis absorbance spectra of biradical **3** at different times. **B.** The absorbance of the BDPA radical at 490 nm (left y-axis) and the percentage of the biradical relative to the nitroxide monoradical as determined by EPR spectroscopy (right y-axis), were plotted as a function of time.

The next section describes our systematic investigation of the persistence of biradical **3** under various conditions, such as solvents, temperature, oxygen etc. Chromatographic purification of biradical **3** was carried out prior to these studies to obtain a pure biradical sample by removing traces of any reagents, impurities and degradation products present in the sample. However, since the BDPA radicals decomposed continuously through the purification process, it yielded only *ca.* 70% biradical relative to the nitroxide monoradical, even if *ca.* 90% biradical was formed during the reaction.¹⁵² Therefore, the experiments were performed with samples containing 70% biradical.

3.3 Persistence of BDPA under different conditions

To start our investigation, we wanted to understand whether BDPA radicals have intrinsically limited persistence or if this issue is only present for biradical **3**. Therefore, we decided to compare the persistence of **3** with two previously reported BDPA radicals (**Figure 3.3**), a BDPA-nitroxide biradical (**8**)¹⁴⁶ and a BDPA monoradical (**9**)¹⁴⁵ in solution. The normalized EPR areas for the radicals were plotted as a function of time as shown in **Figure 3.3**. A similar rate of degradation was observed for all the radicals indicating that in general BDPA radicals have limited persistence.

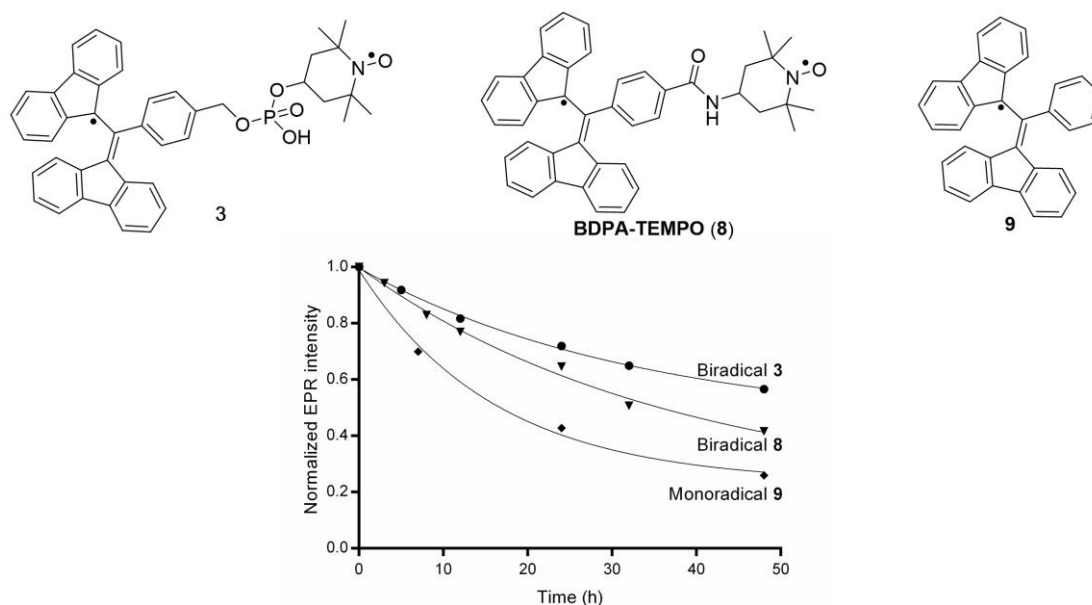


Figure 3.3 Persistence of three different BDPA radicals in DMSO (5 mM) at 23 °C.

3.3.1 Persistence in absence of oxygen

The next step was to find the cause of this limited persistence. First, we investigated the effect of oxygen on the persistence of **3**, since reactions of BDPA radicals with oxygen have been reported.¹⁴⁹ The persistence of **3** in the presence of air was compared with its persistence under a reduced atmosphere of O₂, accomplished by bubbling a solution of **3** with Ar and keeping the solution under a positive pressure of Ar. EPR spectra were recorded at various time intervals and the amount of the biradical was plotted as a function of time, as shown in **Figure 3.4**. Only a small difference in persistence was observed in presence and absence of oxygen, indicating that oxidation was not the only pathway of degradation for BDPA radicals.

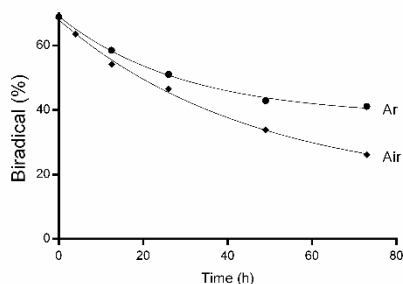


Figure 3.4 The degradation of the biradical **3** under air vs. argon in MeOH (5 mM) at 23 °C.

3.3.2 Solvent-dependence

To explore other possible reasons for degradation for BDPA radicals, we investigated the persistence in different solvents. **Figure 3.5** (left) shows a plot of the percentage of biradical **3** as a function of time in three solvents, DMSO, MeOH and 1,2-dichloroethane (DCE), that vary significantly in polarity. The initial rates of degradation were determined from the plots¹⁵² and observed to decrease with increasing polarity of the solvent. The highest persistence was observed in DMSO, and the lowest in DCE, with initial rates of degradation $(1.50 \pm 0.09) \cdot 10^{-8} \text{ Ms}^{-1}$ and $(1.79 \pm 0.35) \cdot 10^{-7} \text{ Ms}^{-1}$, respectively. The persistence in MeOH was slightly lower than in DMSO ($(1.79 \pm 0.03) \cdot 10^{-8} \text{ Ms}^{-1}$).

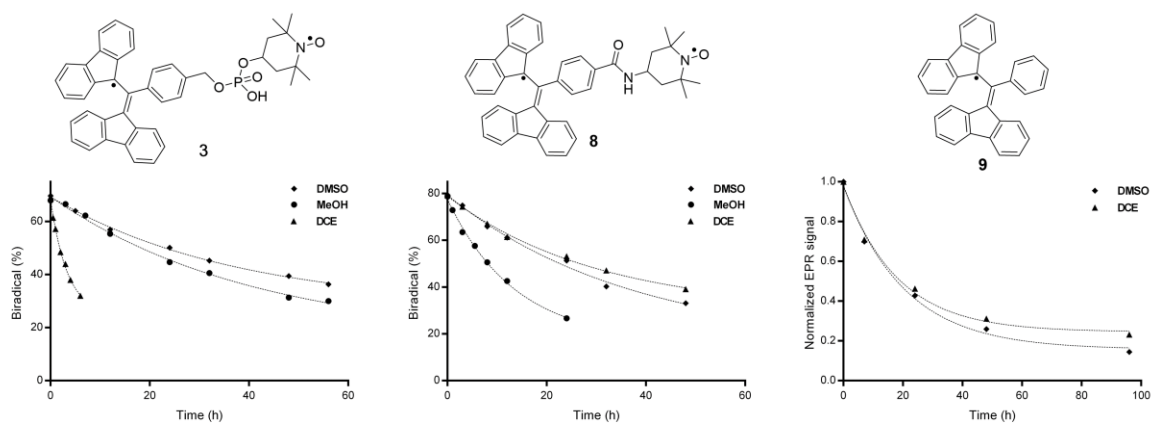


Figure 3.5 Rate of degradation of different BDPA radicals in various solvents (5 mM) at 23 °C. The percentage of each biradical relative to a nitroxide monoradical and the EPR area for monoradical **9** were determined by double integration of its EPR spectrum and plotted as a function of time.

To investigate the role of solvent polarity further, the solvent-dependency of biradical **8** and monoradical **9**, which are less polar than **3**, was determined. **Figure 3.5** (middle) shows the rate of degradation of biradical **8** in solution at 23 °C. The rate of decomposition was found to be similar to that of **3**, although the solvent-dependence on the rates of decomposition was different. Biradical **8** has a similar initial rate of degradation in DMSO ($(2.28 \pm 0.15) \cdot 10^{-8} \text{ Ms}^{-1}$) as biradical **3** but different rates in DCE and MeOH. In DCE, **8** was considerably more persistent than **3** with an initial rate of degradation $(2.24 \pm 0.23) \cdot 10^{-8} \text{ Ms}^{-1}$, whereas the opposite trend was observed in MeOH ($(7.18 \pm 0.64) \cdot 10^{-8} \text{ Ms}^{-1}$). BDPA monoradical **9** showed a similar rate of degradation in solution (**Figure 3.5**, middle) as the biradicals and the same solvent dependence as **8** ($(3.71 \pm 0.12) \cdot 10^{-8} \text{ Ms}^{-1}$ and $(4.64 \pm 0.18) \cdot 10^{-8} \text{ Ms}^{-1}$ for DCE and DMSO, respectively). One possible explanation for this compound-specific

solvent dependence is aggregation and subsequent dimerization, since the polar biradical **3** degrades faster in a non-polar solvent and non-polar **8** and **9** are more unstable in a polar solvent.

3.3.3 Concentration-dependence

To further investigate this putative aggregation-induced degradation, we determined the persistence of **3** at different radical concentrations. **Figure 3.6** shows the concentration-dependent initial rates of biradical **3** in DMSO for a series of solutions with varying concentration. A non-linear increase in rates was observed with increased radical concentration of **3**. A 2-fold increase in the concentration resulted in a 3-fold increase in the rate of degradation with a reaction order of *ca.* 1.6 with respect to biradical **3**. This is evidence for additional degradation pathways besides the oxidation of BDPA radicals, since the oxidation is presumably a first/pseudo-first order reaction with respect to the biradical. The likely explanation is dimerization, which follows second order kinetics. This would also explain the solvent-dependent persistence as increased aggregation would facilitate the dimerization process.

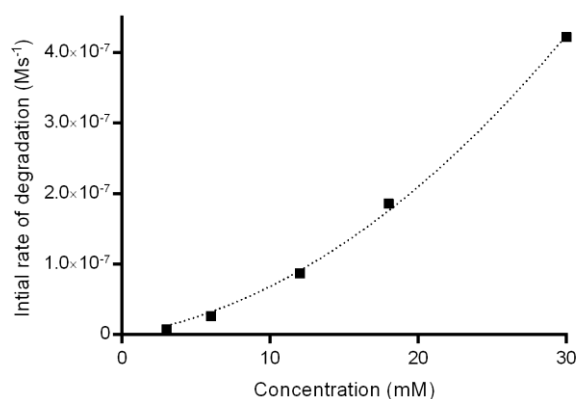


Figure 3.6 Concentration-dependent initial rates of biradical **3** in DMSO at 23 °C.

3.3.4 Analysis of BDPA-decomposition products

In an attempt to detect a BDPA dimer, the decomposed products of biradical **3** were analyzed by ESI mass spectrometry. Formation of multiple products including the oxygenated products as previously described by Breslin and Fox,¹⁴⁹ was observed but the dimer of **3** was

not found. However, masses approximately 1.8-fold the monomeric mass of **3** were observed, which might be formed from a short-lived dimer. We also investigated the decomposed products of BDPA radical **10**, a derivative of compound **1**, which we had on hand. Indeed, the dimer of **10** was found in the mass spectrum (**Figure 3.7**). This is the first reported evidence that dimerization of BDPA radicals could be a pathway of decomposition.

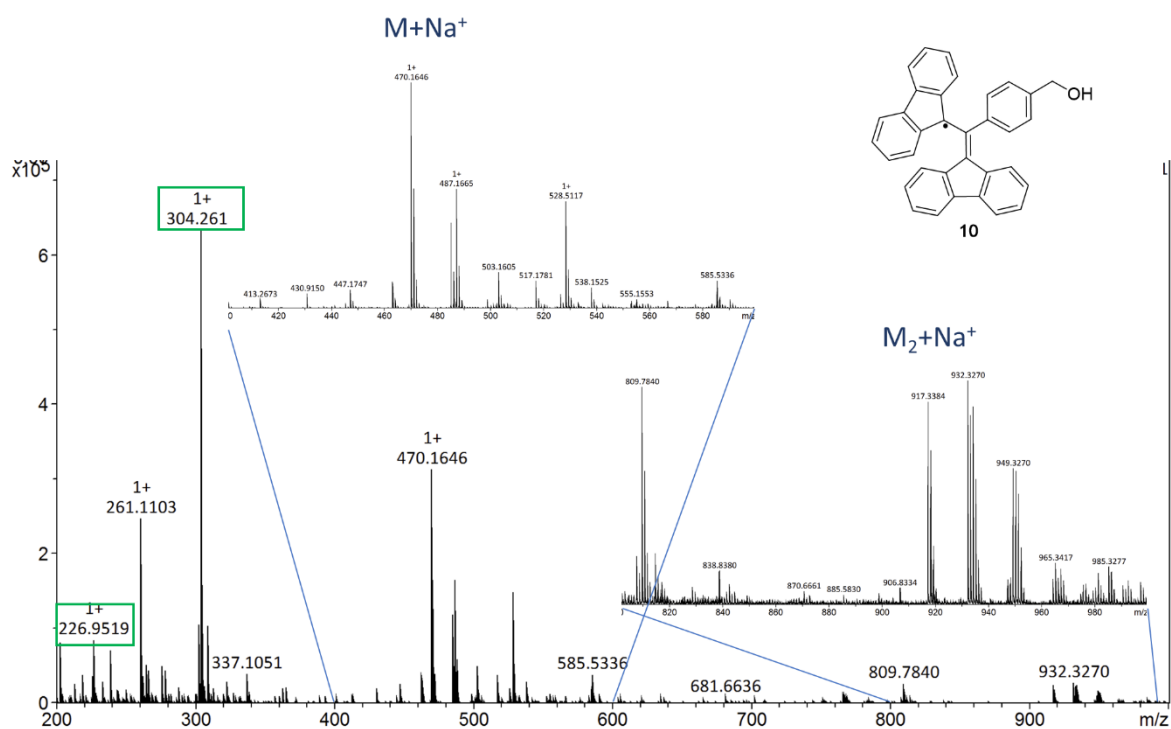


Figure 3.7 The HRMS (ESI) spectrum of the decomposition products of the BDPA radical **10** in MeOH (5 mM) at 23 °C, recorded in a positive-ion mode. The green boxes indicate the peaks of the reference compounds.

It is not surprising that BDPA radicals can dimerize, since dimerization of the carbon-centered Gomberg's radical¹⁵³ (triphenylmethyl/trityl) is well-known.¹⁵⁴ The dimerization of trityls has been prevented with introduction of substituents into the aromatic rings, for example the Finland trityl.¹⁴⁴

With a better understanding of the degradation pathways, we focused on optimizing the storage conditions for long term stability of the BDPA radicals. These conditions could then serve as guidelines on how to handle BDPA radicals.

3.3.5 Persistence at lower temperatures

First, we investigated the persistence of **3** at lower temperatures in solution. The persistence of **3** in MeOH, DMSO and DCE at $-18\text{ }^{\circ}\text{C}$ is shown in **Figure 3.8A**. *Ca.* 6-fold decrease in the rate of degradation was observed for MeOH and DCE compared to $23\text{ }^{\circ}\text{C}$. However, the rate in DMSO at $-18\text{ }^{\circ}\text{C}$ was unexpectedly found to be higher than at $23\text{ }^{\circ}\text{C}$. One possible explanation is that aggregation of the radicals occurs at the crystal boundaries of the frozen DMSO. Quick-freezing in liquid nitrogen followed by incubation at $-18\text{ }^{\circ}\text{C}$ was attempted to reduce the aggregation, but it yielded the same result. When the temperature of the DMSO solution was further lowered to $-80\text{ }^{\circ}\text{C}$, a significant increase in the persistence was observed; very little decomposition was observed after a month and after six months *ca.* 55% of the biradical remained intact (**Figure 3.8B**). Similar decomposition was observed in DCE after six months at $-80\text{ }^{\circ}\text{C}$ but *ca.* 40% biradical remained in MeOH under the same conditions.

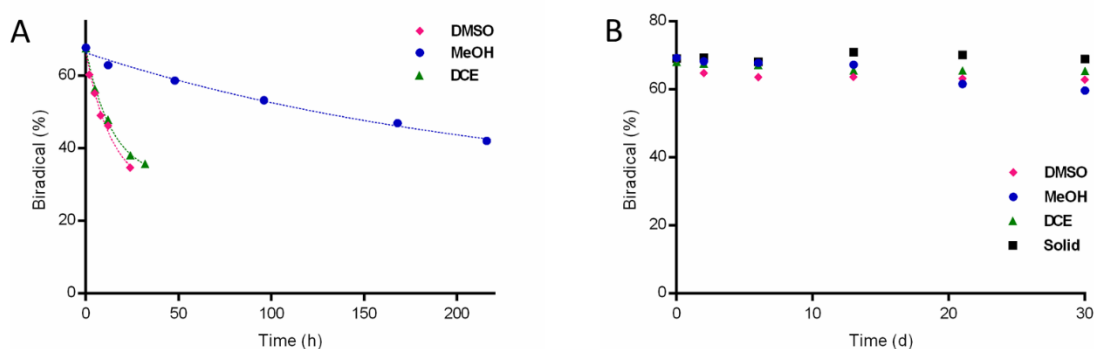


Figure 3.8 The rate of decomposition of biradical **3** at lower temperatures. **A.** The persistence at $-18\text{ }^{\circ}\text{C}$ in different solvents (5 mM). **B.** The degradation at $-80\text{ }^{\circ}\text{C}$ as a solid and after dissolution in different solvents (5 mM).

3.3.6 Persistence in solid state

Next, we investigated the persistence of biradical **3** as a solid. Considerable decomposition was observed at $23\text{ }^{\circ}\text{C}$ (**Figure 3.9A**). This decomposition was found to be due to oxidation, since no decomposition was observed when the solid samples were kept under vacuum for two weeks (**Figure 3.9B**). BDPA radicals were found to be stable at $-80\text{ }^{\circ}\text{C}$ as well. Negligible decomposition was observed for **3** in the solid state at $-80\text{ }^{\circ}\text{C}$ after six months

(Figure 3.8B). Therefore, BDPA radicals can be stored safely without significant decomposition at -80 °C.

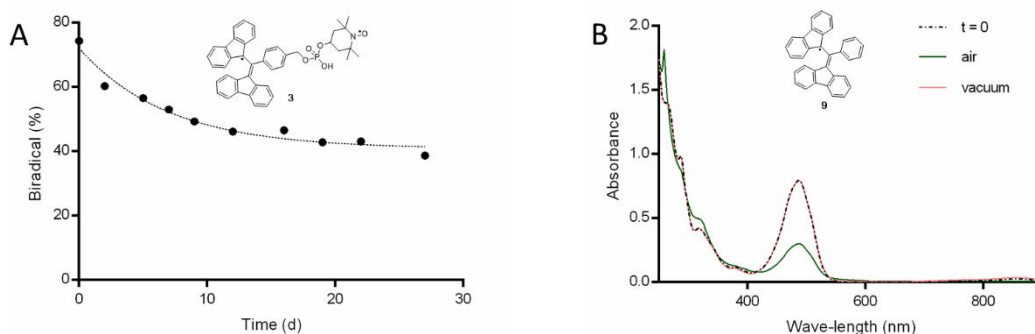


Figure 3.9 The persistence of BDPA radicals at 23 °C in the solid state. **A.** The rate of degradation for biradical **3** for a month. **B.** The UV-vis spectra of solid samples of the unsubstituted BDPA (**9**), kept under air and vacuum for 14 days. The spectra for t = 0 and vacuum (t = 14 days) are superimposable.

3.4 Conclusions

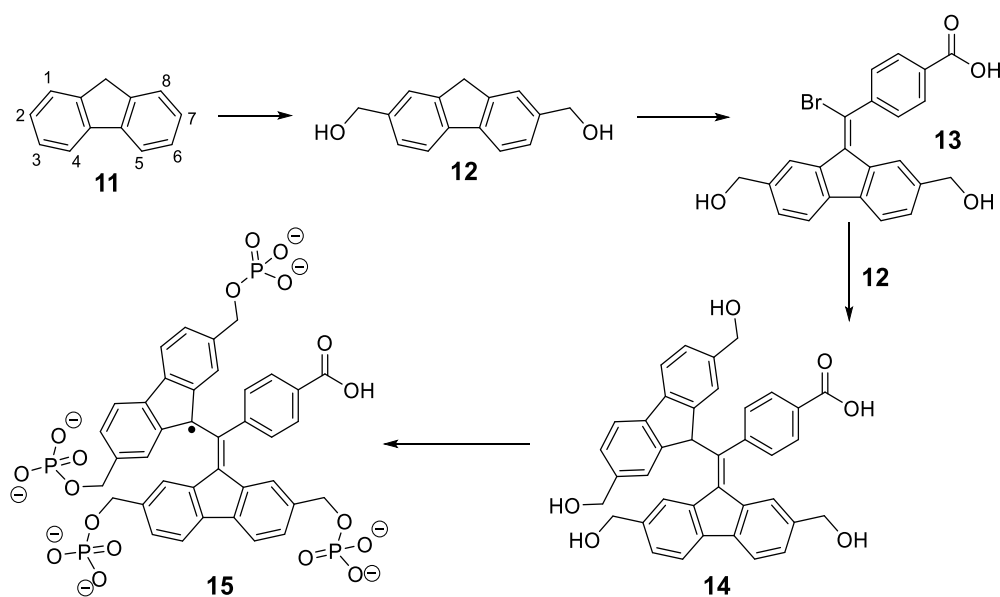
In conclusion, we have shed light on the instability of BDPA radicals, both in solution and the solid state. We have also provided guidelines on how to handle these radicals. The BDPA radicals were found to be stable as solids at -80 °C with no noticeable decomposition for six months, but we observed degradation in this time-frame under all other conditions that were tested. The radical concentration was found to significantly affect the rate of decomposition; a 2-fold increase in the concentration resulted in a 3-fold increase in the rate of decomposition. A dimer of a BDPA radical was detected by mass spectrometry, indicating that dimerization of BDPA radicals is one pathway of decomposition. The polarity of the solvent affected the rate of BDPA decomposition. A polar radical degraded faster in a non-polar solvent whereas a non-polar radical was less persistent in a polar solvent. This trend can be explained by increased aggregation of the radicals due to the mismatch in polarity with the solvent, polar radicals aggregate in non-polar solvents and non-polar radicals aggregate in polar solvents. Such aggregation would facilitate decomposition through dimer formation.

4 Water-soluble BDPA radicals with improved persistence

As discussed in **Chapter 3**, one of the major degradation pathways for BDPA radicals is dimerization. Therefore, we focused on synthesis of BDPA radicals that would be less susceptible towards dimerization. We decided to attach charged functional groups to BDPA that would limit dimerization and, therefore, increase the persistence of BDPA radicals. The charged groups would also render the radicals soluble in aqueous media.

4.1 Synthetic strategy

The aim was to functionalize the fluorenyl rings of BDPA. We selected positions 2 and 7 of fluorene (**11**) (**Scheme 4.1**), as these positions can be readily modified and enable incorporation of four charged groups to the BDPA. We chose to incorporate an isolating methylene linker between the fluorene ring and these functional groups to prevent their interaction with the BDPA radical, which is delocalized in the fluorene rings.¹⁵⁵ The plan was to incorporate hydroxyl groups to fluorene to afford the dihydroxy fluorene derivative **12** (**Scheme 4.1**). Subsequent reactions with **12** would provide bromo-compound **13**. Coupling of **13** with another unit of dihydroxy fluorene **12** would result in compound **14**. The hydroxyl groups of **14** can be further modified with phosphate groups by the phosphoramidite method to yield BDPA phosphate **15**. Additionally, the carboxylic acid group in the *para*-position of the benzene ring can be used to attach other radicals to BDPA, to give water-soluble BDPA-derived biradicals.

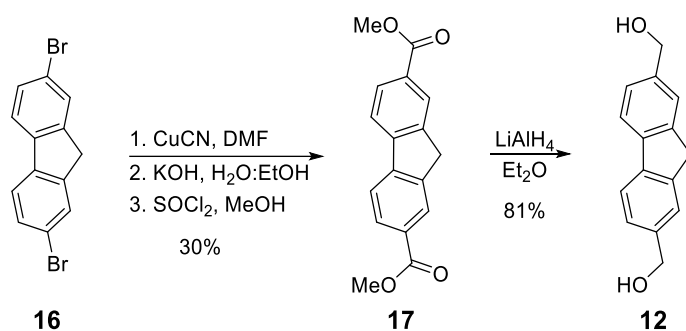


Scheme 4.1 Synthetic strategy to increase the water solubility of BDPA.

However, the synthesis shown above did not go as planned and we ended up modifying the synthetic scheme accordingly, as described below.

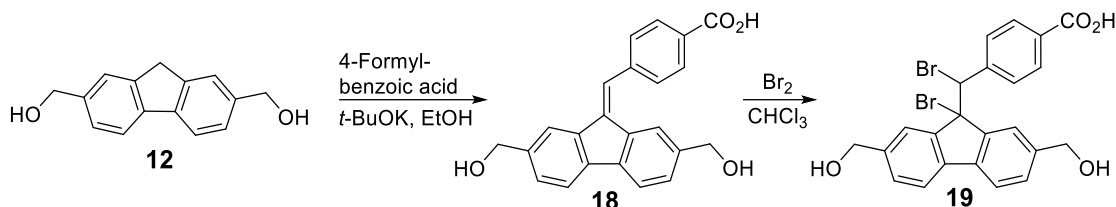
4.2 Synthesis of tetraalkyl/aryl-ammonium BDPAs

The synthesis started with incorporation of cyano groups by the Sandmeyer reaction of 2,7-dibromofluorene (**16**), followed by their hydrolysis (**Scheme 4.2**).¹⁵⁶ Purification of the resulting fluorene-2,7-dicarboxylic acid was not feasible due to its extremely limited solubility. Consequently, the carboxylates were converted to esters to yield fluorene derivative **17** and subsequently reduced to afford diol **12** in good yields.



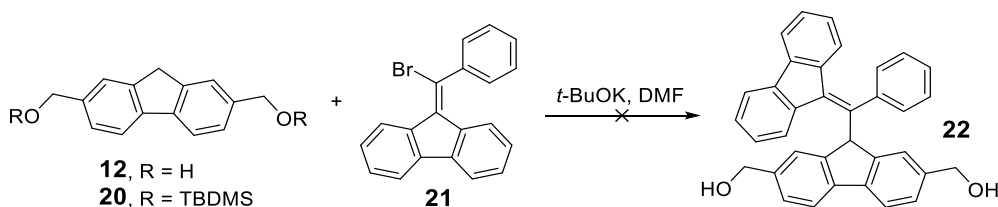
Scheme 4.2 Synthesis of the dihydroxy fluorene derivative **12**.

Compound **12** was condensed with 4-formylbenzoic acid to provide **18** (Scheme 4.3). Bromination of **18** was carried out next, which was found to be challenging. It led to a mixture of products with very low yields of **19**, possibly due to presence of the hydroxyl groups.



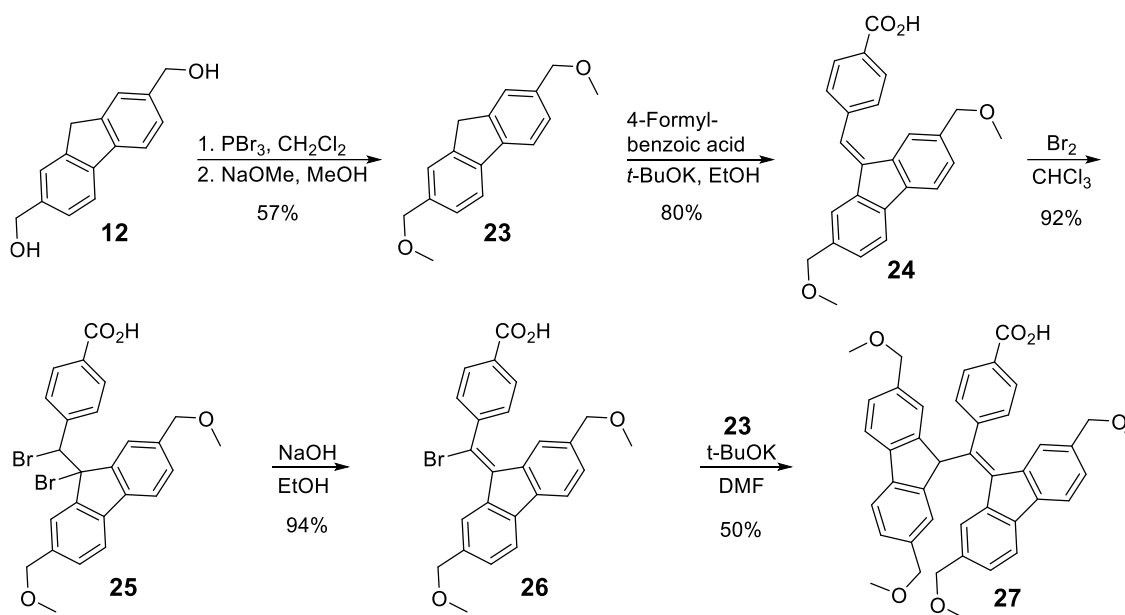
Scheme 4.3 Condensation of **12** with 4-formyl benzoic acid followed by bromination.

In parallel, we attempted to react **12** with bromo-compound **21**, a model reaction to construct the BDPA unit (Scheme 4.4). This reaction was not successful. Therefore, we decided to protect the hydroxyl groups of **12**. Initially, they were protected as silyl ethers (**20**). However, the coupling reaction of **20** with compound **21** did not work either. The TBDMS groups were found to be unstable under the reaction conditions for the coupling.



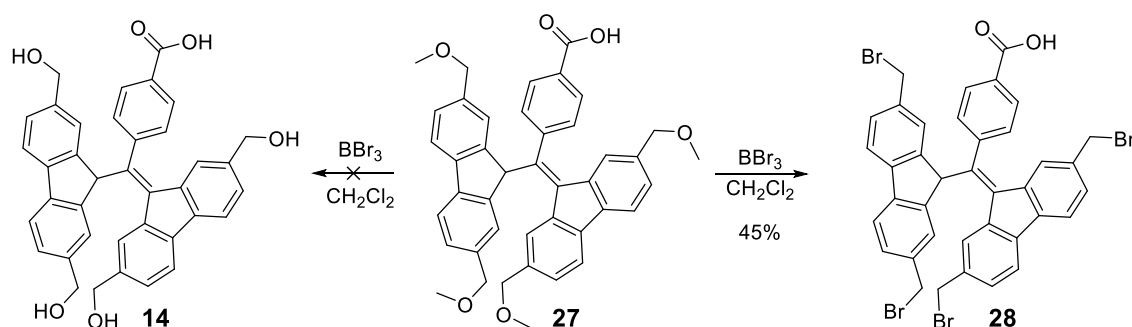
Scheme 4.4 Unsuccessful model reaction of **11** and its silyl ether derivative **21** with bromo-compound **22** to construct the BDPA unit.

As a result, we opted for a protecting group that would be stable under strong basic conditions and, therefore, the hydroxyl groups of **12** were protected as methoxy ethers to provide **23** (Scheme 4.5). Compound **23** was condensed with 4-formylbenzoic acid to afford **24**. Bromination, followed by elimination, gave **26** in excellent yields. Compound **26** was further coupled with another unit of 2,7-dimethoxymethylfluorene (**23**) to yield BDPA derivative **27**.



Scheme 4.5 Synthesis of BDPA derivative **27**.

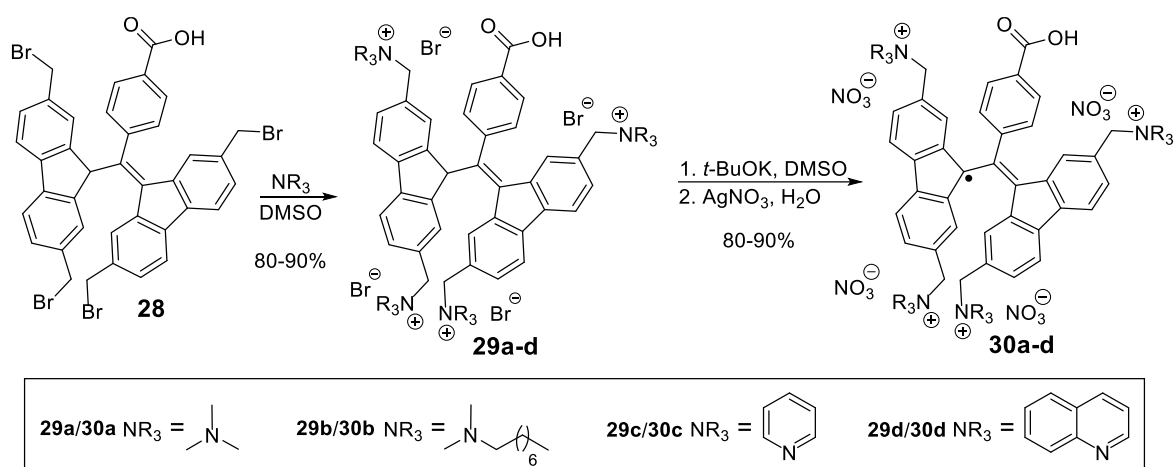
The deprotection of the methoxy ether groups of BDPA **27** was carried out with BBr_3 to obtain tetra-(hydroxymethyl)-BDPA **13**, which we had planned to phosphorylate to achieve water-soluble BDPA radicals (**Scheme 4.6**). However, the reaction yielded tetra-(bromomethyl)-BDPA **28** instead, since the substitution at the benzylic carbon is more favorable than at the methyl carbon.



Scheme 4.6 Deprotection of methoxy ethers of BDPA **27**.

The benzylic bromides of **28** can be readily substituted with nucleophiles. Hence, compound **28** was used as a building block to synthesize a series of BDPA radicals with different tetraalkylammonium groups, to prepare BDPA derivatives with custom-made solubilities (**Scheme 4.7**). In addition to trimethylamine, the more lipophilic *N,N*-dimethyloctylamine was selected, along with the aromatic amines pyridine and quinoline. Reaction of these

amines with **28** afforded compounds **29a-d** in good yields. The products were easily isolated from the reaction mixture by precipitation. These compounds had good solubility in DNP-juice and their relative variance in solubility reflected the nature of the substituents on the tetraalkylammonium groups; **29a** had the highest solubility (>150 mM) and **29b**, which is more lipophilic, the lowest (20 mM), while the pyridinium and the quinolinium derivatives had intermediate solubility (**29c**, 65 mM; **29d**, 45 mM). Sequential treatment of compounds **29a-d** with *t*-BuOK and AgNO₃ yielded BDPA radicals **30a-d**; again the products were isolated from the reaction mixture by precipitation. As is common for such reactions,¹⁵² *ca.* 85% of the products were radicals, as determined by spin-counting using EPR spectroscopy.



Scheme 4.7 Synthesis of tetraalkyl/aryl-ammonium BDPA derivatives.

4.3 Persistence of the tetraalkylammonium BDPA radical

Having demonstrated the advantages of the charged tetraalkyl/aryl-ammonium groups to improve the solubility of the BDPA radicals in aqueous media, we proceeded to investigate their persistence. Both EPR and UV-vis spectroscopy can be used for this study (**Section 3.2**). We chose to use UV-vis spectroscopy here due to the ease of the process (e.g., monitoring the persistence through EPR was time-consuming as it involved double-integration of the EPR spectrum for each data point separately). As expected, the persistence of the tetraalkyl/aryl-ammonium BDPA radicals was found to be remarkably higher than that of the unsubstituted BDPA (**Figure 4.1**).

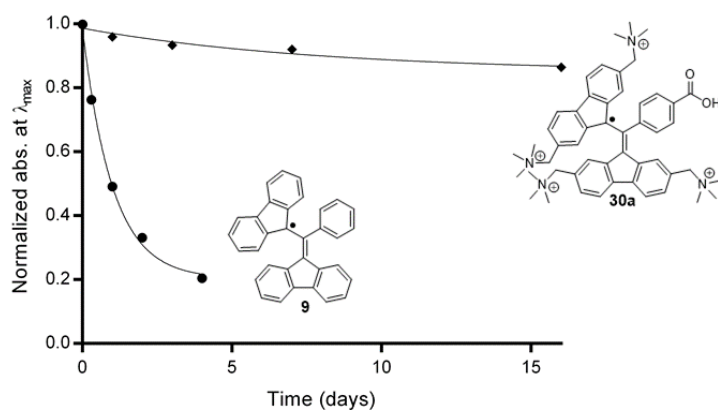


Figure 4.1 The improved persistence of tetraalkylammonium BDPA radical **30a** compared to the unsubstituted BDPA (**9**) in DMSO at 23 °C, monitored by UV-vis spectroscopy at 503 nm (**30a**) and 488 nm (**9**).

4.3.1 Solvent-dependent persistence

Since we observed a great extent of solvent-dependency on the persistence of BDPA radicals previously (**Chapter 3**), we decided to investigate the persistence of **30a** in different solvents. **Figure 4.2** shows a plot of the persistence of **30a** as a function of time in four different solvents: DMSO, DNP juice, MeOH and water. Again, a large variation in solvent-dependent persistence was observed. The persistence was highest in DMSO; only *ca.* 15% of the radical had degraded in DMSO after two weeks. The persistence was, however, markedly lower in polar protic solvents than it was in DMSO; *ca.* 50% and 60% of the radicals had degraded in DNP juice and MeOH, respectively after two weeks. However, the rate of degradation in MeOH was still at least 5-fold lower than what has been previously observed with BDPA radicals.¹⁵²

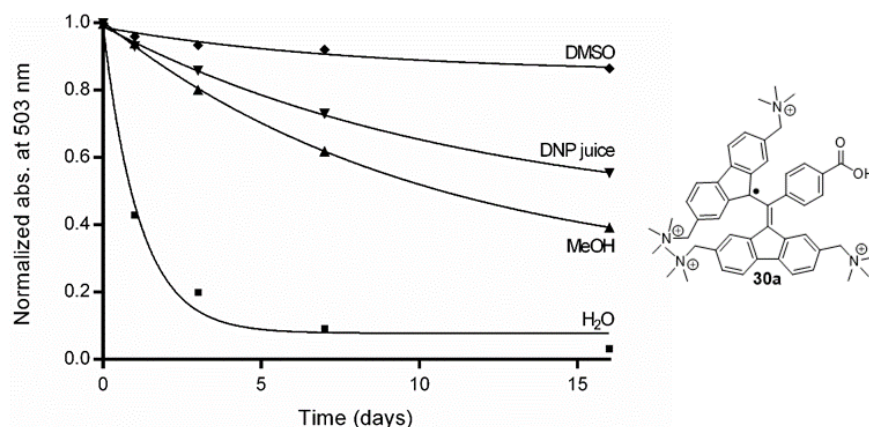


Figure 4.2 Persistence of the water-soluble BDPA radical **30a** in solution (10 mM) at 23 °C, monitored by UV-vis spectroscopy at 503 nm.

Surprisingly, the persistence of **30a** was much lower in water, with *ca.* 50% decomposition within 48 h. A likely explanation was dimerization. Therefore, we determined the concentration-dependent persistence of **30a** in water.

4.3.2 Evidence for dimerization in water

Figure 4.3 shows the concentration-dependent initial rates of degradation for a series of aqueous solutions of **30a**. Indeed, a non-linear concentration-dependency was observed, as in the case of phosphodiester-derived BDPA-nitroxide biradical **3**, described in **Chapter 3**. This data suggested that dimerization was taking place in water.

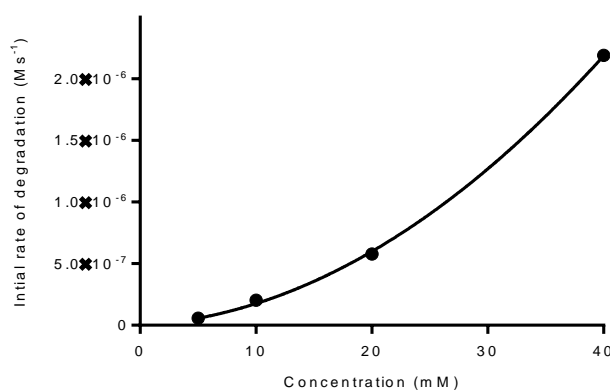


Figure 4.3 Concentration-dependent initial rates of BDPA radical **30a** in water at 23 °C.

We investigated the decomposed products of **30a** in water by HRMS (ESI). Formation of a major peak (m/z 560.6397) was observed in the mass spectrum which possibly originates from dimerization of **30a** (**Figure 4.4**). We speculate the dimer is formed in a similar fashion as the Gomberg radical through a σ -bond formation between two radicals, followed by oxidation/ H_2 elimination. A putative structure of the dimer ($C_{100}H_{118}N_{11}O_{13}^{3+}$; m/z 560.6309) is shown in **Figure 4.4**.

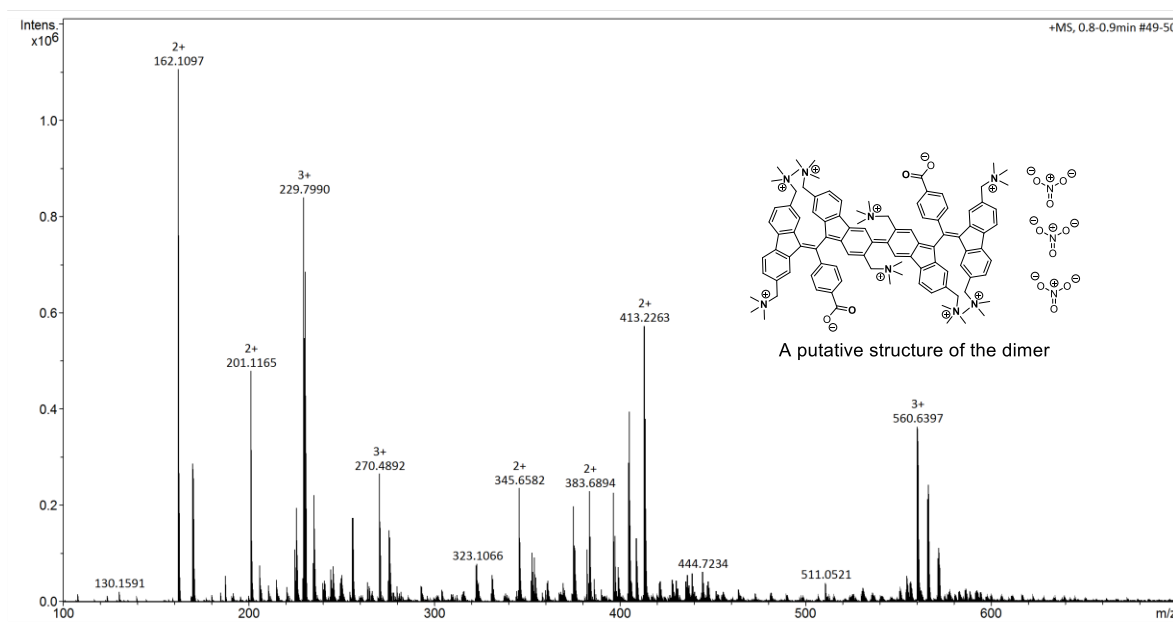


Figure 4.4 The HRMS (ESI) spectrum of radical **30a** in water (5 mM) kept for 48 h at 23 °C, recorded in a positive-ion mode. All the masses in the spectrum originate from the sample.

The most likely explanation for why **30a** dimerizes in water is aggregation. It may seem counterintuitive that such polar compounds aggregate in water, however, there have been reports of aggregation of tetraalkylammonium salts in water.¹⁵⁷⁻¹⁵⁹ It has been postulated that this may be due to the electrostatic attraction between the positively charged nitrogen and the counter anion, as well as hydrophobic interactions between the alkyl substituents.¹⁵⁷⁻¹⁵⁹ DMSO has also been shown to reduce aggregation of ammonium-functionalized polythiophene relative to water.¹⁶⁰ This is consistent with our results, since the highest persistence was observed in DMSO.

An attempt to reduce aggregation of **30a** in water by increasing the ionic strength, resulted in a decrease of its persistence (**Figure 4.5**). The initial rate of degradation increased *ca.* 2-

fold in presence of 100 mM NaCl. The persistence was even lower in presence of NaNO₃ and Na₃PO₄.

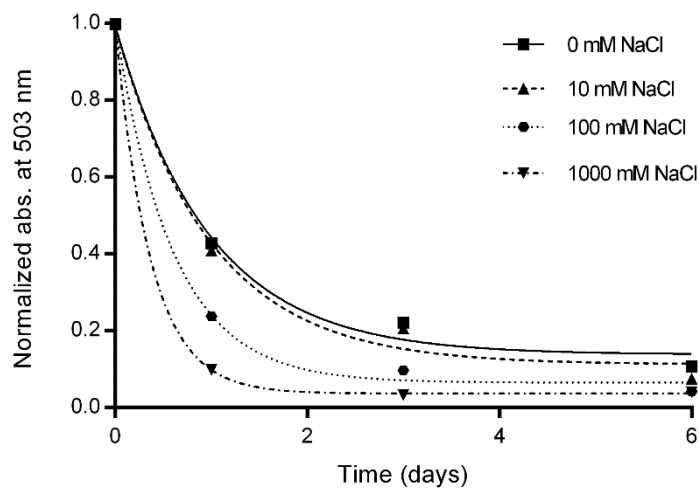


Figure 4.5 The persistence of radical **30a** in water (5 mM) with a varying concentration of NaCl at 23 °C.

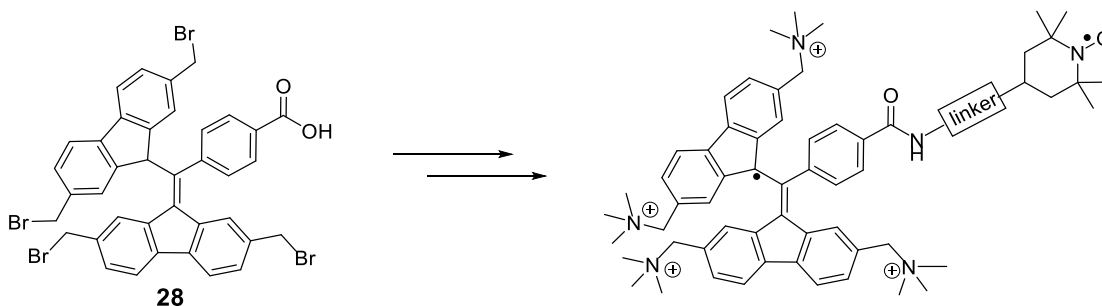
4.4 Conclusions

In summary, we have described the synthesis and characterization of a series of water-soluble tetraalkyl/aryl-ammonium BDPA radicals. These BDPA radicals can be readily used to prepare heterobiradicals as polarizing agents for investigation of biomolecules by MAS-DNP NMR spectroscopy at high magnetic fields. The radicals show significantly improved persistence in solution,¹⁵² presumably due to reduced tendency to aggregate. Although the persistence of these radicals in water was substantially less than in DMSO, tetrabromo intermediate **28** can be used to prepare a wide variety of derivatives with tailor-made properties, including limited aggregation in water.

5 Water-soluble BDPA-nitroxide biradicals

As discussed in **Chapter 4**, we designed a new class of BDPA radicals that have improved solubility and persistence in polar solvents. The next goal was to use these radicals to prepare heterobiradicals. The advantages of such biradicals is that they give significantly higher signal enhancements than nitroxide biradicals at high magnetic field, as described earlier (**Chapter 2**).^{103, 120, 143}

The carboxylic acid group at the *para*-position on the benzene ring of BDPA derivative **28**, can be coupled to nitroxides carrying an amine functionality (**Scheme 5.1**). We decided to synthesize a series of BDPA-nitroxide biradicals using different linkers to tune the *J*-coupling and dipolar interaction between the two radicals. The reason is that the efficiency of biradicals as polarizing agent for DNP is governed by the magnitude of the exchange coupling between two radical centers (**Chapter 2**).^{97, 98} A moderate *J*-coupling (30-70 MHz) has been observed to be optimal.^{120, 143}

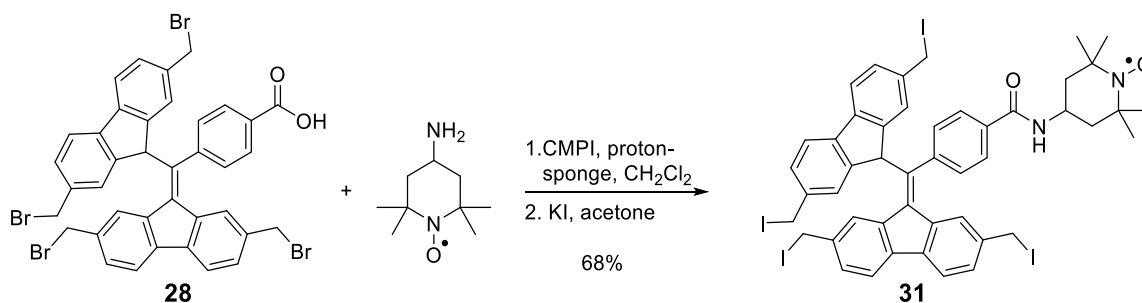


Scheme 5.1 Synthesis of water-soluble BDPA-nitroxide biradicals from the BDPA derivative **28**.

5.1 Synthesis of the biradicals

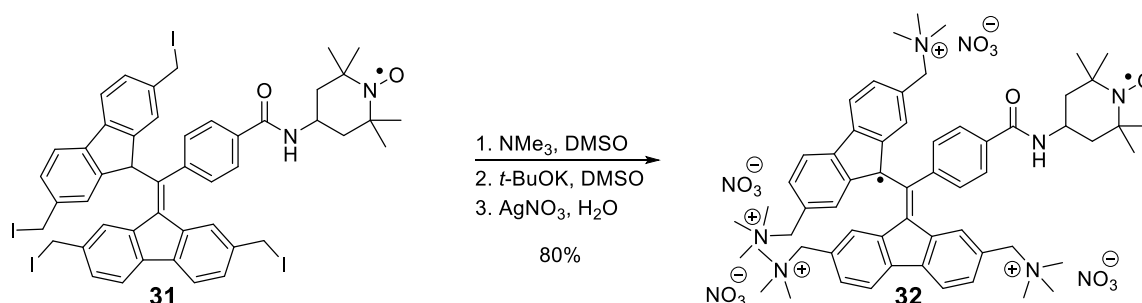
The syntheses of water-soluble BDPA-nitroxides began by coupling of BDPA **28** to 4-amino TEMPO (**Scheme 5.2**). The coupling reaction was found to be challenging due to presence of the highly substitutable benzyl bromides on **28**. Proton-sponge (1,8-bis(dimethylamino)naphthalene), a strong base but a weak nucleophile, was used for the

coupling reaction since bases, such as pyridine, triethylamine, DIPEA were found to substitute the bromides of **28**. The reaction with reagents, such as oxalyl chloride, DCC, EDC and HOBt gave low yields. The best conversion was obtained when 2-chloro-1-methylpyridinium iodide (CMPI) and proton-sponge were used (**Scheme 5.2**). This resulted in a coupled product containing a mixture of halides (-Cl, -Br and- I) in the benzylic positions, which were exchanged by iodides using KI to yield **31**.



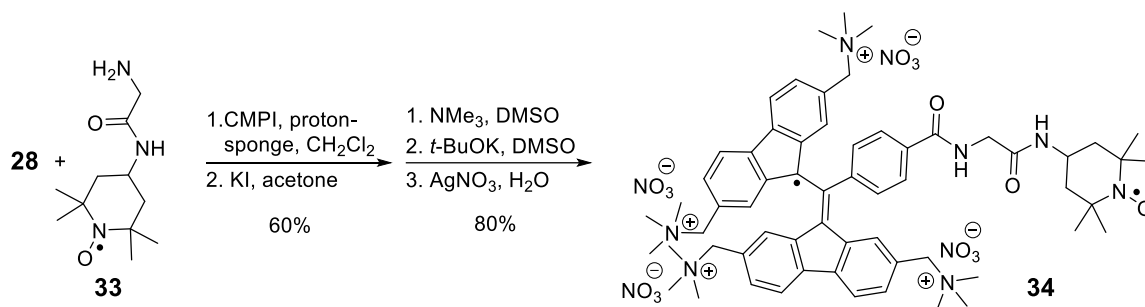
Scheme 5.2 The coupling of the carboxylic acid of **28** to 4-amino TEMPO.

Compound **31** was treated sequentially with trimethylamine, *t*-BuOK and AgNO₃ to give water-soluble BDPA-nitroxide biradical **32** (**Scheme 5.3**).



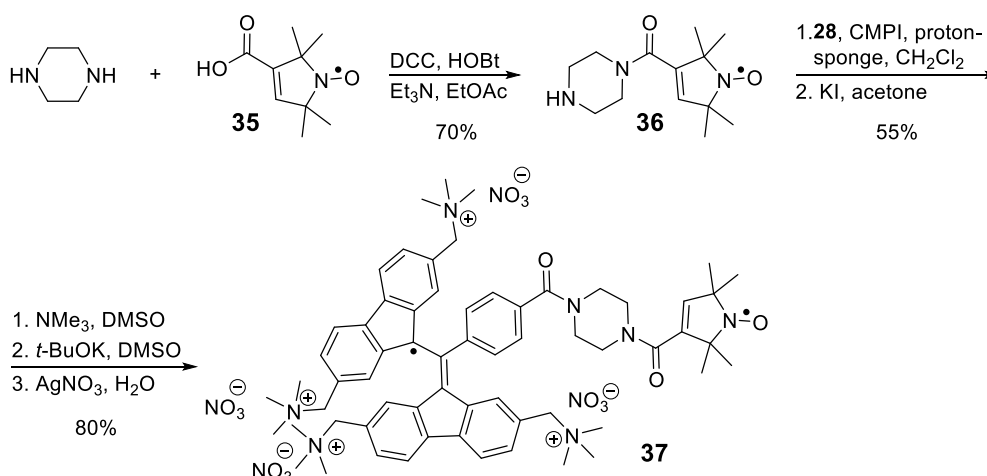
Scheme 5.3 Synthesis of the water-soluble BDPA-TEMPO biradical **32**.

Two additional BDPA-nitroxide biradicals have been prepared in a similar fashion, both of which have longer linkers between the two radical centers than **32**. The synthesis of biradical **34** with a glycine linker was achieved by coupling compound **28** with amino-nitroxide **33**¹⁶¹ and subsequent reactions with trimethylamine, *t*-BuOK and AgNO₃ (**Scheme 5.4**).



Scheme 5.4 Synthesis of BDPA-nitroxide biradical **34** with a glycine linker.

To synthesize biradical **37**, nitroxide **36** that contains a piperazine group, was prepared by reacting nitroxide **35**¹⁶² with piperazine (**Scheme 5.5**). Coupling of nitroxide **36** with BDPA derivative **28** followed by sequential reaction with trimethylamine, *t*-BuOK and AgNO₃ yielded biradical **37**.



Scheme 5.5 Synthesis of BDPA-nitroxide biradical **37** with a piperazine linker.

5.2 Spin–spin coupling interaction in the biradicals

We expected a large variation in the *J*-coupling between biradicals **32**, **34** and **37**. A strong coupling is expected for biradical **32** due to the short and direct linkage between the two radical centers.¹⁴⁶ On the other hand, a weaker *J*-coupling is expected for biradical **37**, which has a long and relatively rigid piperazine linker.¹⁶¹ For biradical **34**, a wide range of *J*-coupling is anticipated since the flexible glycine linker could lead to a variety of conformations. A similar observation has been made for **TEMTriPol-1** (**Figure 2.16**) that also has a glycine linker between the trityl and the TEMPO radical resulting in a *J*-coupling

varying from 70 MHz to 800 MHz.^{143, 161} The high DNP efficiency of **TEMTriPol-1** ($\epsilon \sim 65$ and ~ 87 at 18.8 T and 14.1 T, respectively) has been attributed to this distribution of J values.¹⁴³

Biradical **32** shows a triplet signal in its EPR spectrum (**Figure 5.1**) due to the strong spin–spin coupling. A J -coupling of 140 MHz has been determined for a BDPA–TEMPO biradical with the same core structure.¹⁴⁶ The EPR spectra of **34** and **37** look similar and closely resemble the spectrum of a mixture of BDPA and nitroxide radicals (5:5); the three EPR peaks of the nitroxide and one peak of the BDPA are clearly observed, indicating weak interaction between the two radicals. Similar spectral features have been reported for two BDPA-nitroxide biradicals, **Hy-3** and **HyPTEK**, recorded in trichloroethylene at 22 °C.¹²⁰ A J -coupling of ~ 5 MHz has been reported for both the radicals. However, viscosity of solvents has been stated to affect the J -coupling with higher viscosity leading to low J -coupling.¹⁶³ Therefore, the J -coupling of **34** and **37** (EPR spectra recorded in DMSO) might be higher in other solvents.

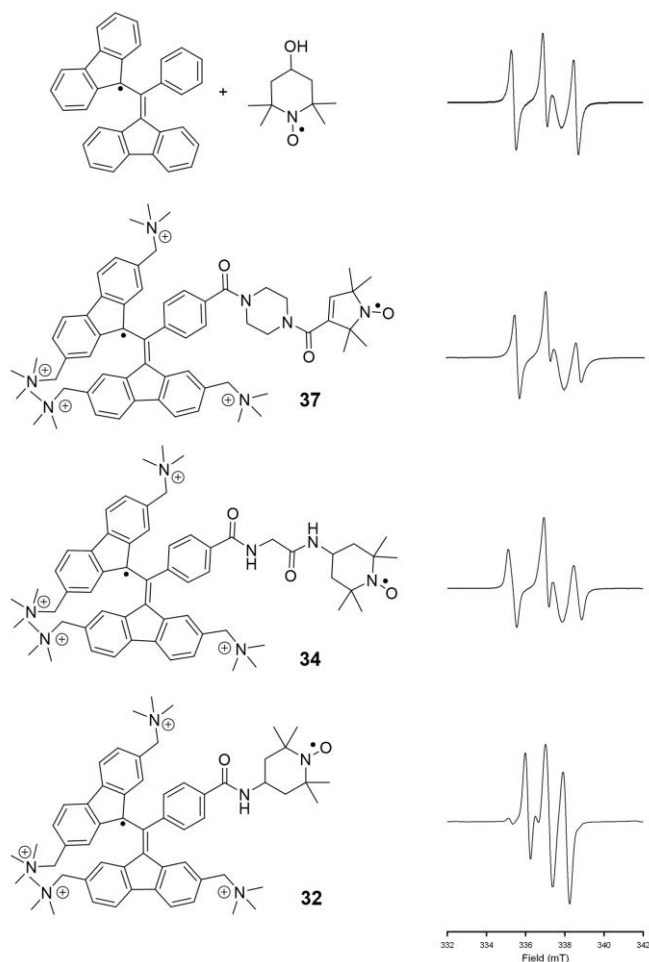


Figure 5.1 EPR spectra of a mixture of BDPA and nitroxide radicals (5:5), and the BDPA-nitroxide biradicals in DMSO. Experimental parameters: 9.43 GHz, microwave power 1 mW, sweep width 12 mT, modulation 0.2 mT, 23 °C.

DNP experiments using these biradicals as polarizing agents are being carried out in the research group of Dr. Gaël De Paëpe at Institute of Nanosciences and Cryogenics (CEA).

5.3 Conclusions

Three water-soluble BDPA-nitroxide biradicals have been prepared (unpublished), in which the length and the flexibility of the linker were varied. This resulted in different spin-spin interactions between the two paramagnetic centers, as manifested in their EPR spectra. The DNP performance of these biradicals will be a guiding factor for future design of biradicals with improved properties.

6 Conclusions

The work presented in this doctoral dissertation is based on the design and synthesis of water-soluble BDPA radicals as polarizing agents for DNP-NMR spectroscopy, for investigation of biomolecules. The syntheses of phosphoester-derived BDPA radicals are described in **Chapter 3**. Unexpectedly, these BDPA radicals were found to have limited persistence. Therefore, a detailed investigation of the persistence under different conditions was carried out. Various factors affected the stability of BDPA radicals in solution. Solvent polarity was found to play an important role; a polar radical was less persistent in a non-polar solvent whereas non-polar radicals degraded faster in polar solvents. A non-linear dependency on the radical concentration was observed with a reaction order of *ca.* 1.6 suggesting additional degradation pathways besides oxidation of BDPA radicals, since oxidation is a first-order reaction with respect to the radical. Dimerization is likely a major pathway of degradation; a dimer of a BDPA radical was observed in the mass spectrum of the decomposed products of the radical. Degradation in solid state was found to be due to oxidation. These findings shed light upon the limited persistence of BDPA radicals and provide detailed guidelines on how to handle these radicals.

To improve the persistence of BDPA radicals, we developed a new class of BDPA radicals, described in **Chapter 4**. These radicals have four tetraalkyl/aryl ammonium groups that reduce their tendency for dimerization. High persistence was observed for the radicals in polar organic solvents. In addition, this functionalization renders the radicals soluble in aqueous media. The tetraalkyl/aryl ammonium BDPA radicals were prepared from a common intermediate, a tetrabromo-BDPA derivative, which can be used to prepare a wide variety of BDPA radicals with tailor-made properties, including BDPA-nitroxide biradicals which are efficient polarizing agents for DNP-NMR experiments at high magnetic fields.

To demonstrate this approach, three water-soluble BDPA-nitroxide biradicals were synthesized, as described in **Chapter 5**. They are the first examples of water-soluble BDPA-nitroxide biradicals. The distance and orientation between the radical centers in the biradicals varied as different linkers were used for the synthesis resulting in a range of spin-spin interaction. Therefore, these biradicals are promising polarizing agents for investigation of

biomolecules by DNP-NMR spectroscopy at high magnetic fields. Furthermore, the DNP efficiency of these biradicals will provide guidance for the design of more efficient water-soluble BDPA-nitroxide biradicals.

References

1. Llamas-Saiz, A. L.; Raaij, M. J. v., X-Ray Crystallography of Biological Macromolecules: Fundamentals and Applications. In *Proteins in Solution and at Interfaces: Methods and Applications in Biotechnology and Materials Science*, 2013; pp 1-22.
2. Di Cola, E.; Grillo, I.; Ristori, S., Small Angle X-ray and Neutron Scattering: Powerful Tools for Studying the Structure of Drug-Loaded Liposomes. *Pharmaceutics* **2016**, *8* (2), 10.
3. Semeraro, E. F.; Marx, L.; Frewein, M. P. K.; Pabst, G., Increasing complexity in small-angle X-ray and neutron scattering experiments: from biological membrane mimics to live cells. *Soft Matter* **2020**.
4. Shrestha, D.; Jenei, A.; Nagy, P.; Vereb, G.; Szöllősi, J., Understanding FRET as a Research Tool for Cellular Studies. *Int. J. Mol. Sci.* **2015**, *16* (4), 6718-6756.
5. Roy, R.; Hohng, S.; Ha, T., A practical guide to single-molecule FRET. *Nat. Methods* **2008**, *5* (6), 507-516.
6. Padilla-Parra, S.; Tramier, M., FRET microscopy in the living cell: Different approaches, strengths and weaknesses. *BioEssays* **2012**, *34* (5), 369-376.
7. Bonucci, A.; Ouari, O.; Guigliarelli, B.; Belle, V.; Mileo, E., In-Cell EPR: Progress towards Structural Studies Inside Cells. *ChemBioChem* **2020**, *21* (4), 451-460.
8. Jeschke, G., The contribution of modern EPR to structural biology. *Emerging Topics in Life Sciences* **2018**, *2* (1), 9-18.
9. Möbius, K.; Lubitz, W.; Cox, N.; Savitsky, A., Biomolecular EPR Meets NMR at High Magnetic Fields. *Magnetochemistry* **2018**, *4* (4), 50.
10. Shelke, S. A.; Sigurdsson, S. T., Site-Directed Spin Labeling for EPR Studies of Nucleic Acids. In *Modified Nucleic Acids*, Nakatani, K.; Tor, Y., Eds. Springer International Publishing: Cham, 2016; pp 159-187.
11. Murata, K.; Wolf, M., Cryo-electron microscopy for structural analysis of dynamic biological macromolecules. *Biochim. Biophys. Acta, Gen. Subj.* **2018**, *1862* (2), 324-334.
12. Milne, J. L. S.; Borgnia, M. J.; Bartesaghi, A.; Tran, E. E. H.; Earl, L. A.; Schauder, D. M.; Lengyel, J.; Pierson, J.; Patwardhan, A.; Subramaniam, S., Cryo-electron microscopy – a primer for the non-microscopist. *The FEBS Journal* **2013**, *280* (1), 28-45.
13. Renaud, J.-P.; Chari, A.; Ciferri, C.; Liu, W.-t.; Rémy, H.-W.; Stark, H.; Wiesmann, C., Cryo-EM in drug discovery: achievements, limitations and prospects. *Nat. Rev. Drug Discovery* **2018**, *17* (7), 471-492.
14. Yu, X.; Veesler, D.; Campbell, M. G.; Barry, M. E.; Asturias, F. J.; Barry, M. A.; Reddy, V. S., Cryo-EM structure of human adenovirus D26 reveals the conservation of structural organization among human adenoviruses. *Sci. Adv.* **2017**, *3* (5), e1602670.
15. Luque, D.; Castón, J. R., Cryo-electron microscopy for the study of virus assembly. *Nat. Chem. Biol.* **2020**, *16* (3), 231-239.
16. Neuhaus, A.; Selvaraj, M.; Salzer, R.; Langer, J. D.; Kruse, K.; Kirchner, L.; Sanders, K.; Daum, B.; Averhoff, B.; Gold, V. A. M., Cryo-electron microscopy

- reveals two distinct type IV pili assembled by the same bacterium. *Nat. Commun.* **2020**, *11* (1), 2231.
17. Khoshouei, M.; Radjainia, M.; Baumeister, W.; Danev, R., Cryo-EM structure of haemoglobin at 3.2 Å determined with the Volta phase plate. *Nat. Commun.* **2017**, *8* (1), 16099.
 18. Merk, A.; Bartesaghi, A.; Banerjee, S.; Falconieri, V.; Rao, P.; Davis, M. I.; Pragani, R.; Boxer, M. B.; Earl, L. A.; Milne, J. L. S.; Subramaniam, S., Breaking Cryo-EM Resolution Barriers to Facilitate Drug Discovery. *Cell* **2016**, *165* (7), 1698-1707.
 19. Bonomi, M.; Pellarin, R.; Vendruscolo, M., Simultaneous Determination of Protein Structure and Dynamics Using Cryo-Electron Microscopy. *Biophys. J.* **2018**, *114* (7), 1604-1613.
 20. Geraets, J. A.; Pothula, K. R.; Schröder, G. F., Integrating cryo-EM and NMR data. *Curr. Opin. Struct. Biol.* **2020**, *61*, 173-181.
 21. Cuniasse, P.; Tavares, P.; Orlova, E. V.; Zinn-Justin, S., Structures of biomolecular complexes by combination of NMR and cryoEM methods. *Curr. Opin. Struct. Biol.* **2017**, *43*, 104-113.
 22. Gauto, D. F.; Estrozi, L. F.; Schwieters, C. D.; Effantin, G.; Macek, P.; Sounier, R.; Sivertsen, A. C.; Schmidt, E.; Kerfah, R.; Mas, G.; Colletier, J.-P.; Güntert, P.; Favier, A.; Schoehn, G.; Schanda, P.; Boisbouvier, J., Integrated NMR and cryo-EM atomic-resolution structure determination of a half-megadalton enzyme complex. *Nat. Commun.* **2019**, *10* (1), 2697.
 23. Zhang, K.; Keane, S. C.; Su, Z.; Irobalieva, R. N.; Chen, M.; Van, V.; Sciandra, C. A.; Marchant, J.; Heng, X.; Schmid, M. F.; Case, D. A.; Ludtke, S. J.; Summers, M. F.; Chiu, W., Structure of the 30 kDa HIV-1 RNA Dimerization Signal by a Hybrid Cryo-EM, NMR, and Molecular Dynamics Approach. *Structure* **2018**, *26* (3), 490-498.e3.
 24. Iadanza, M. G.; Silvers, R.; Boardman, J.; Smith, H. I.; Karamanos, T. K.; Debelouchina, G. T.; Su, Y.; Griffin, R. G.; Ranson, N. A.; Radford, S. E., The structure of a β 2-microglobulin fibril suggests a molecular basis for its amyloid polymorphism. *Nat. Commun.* **2018**, *9* (1), 4517.
 25. Gremer, L.; Schölzel, D.; Schenk, C.; Reinartz, E.; Labahn, J.; Ravelli, R. B. G.; Tusche, M.; Lopez-Iglesias, C.; Hoyer, W.; Heise, H.; Willbold, D.; Schröder, G. F., Fibril structure of amyloid- β (1-42) by cryo-electron microscopy. *Science* **2017**, *358* (6359), 116-119.
 26. Demers, J.-P.; Habenstein, B.; Loquet, A.; Kumar Vasa, S.; Giller, K.; Becker, S.; Baker, D.; Lange, A.; Sgourakis, N. G., High-resolution structure of the Shigella type-III secretion needle by solid-state NMR and cryo-electron microscopy. *Nat. Commun.* **2014**, *5* (1), 4976.
 27. Perilla, J. R.; Zhao, G.; Lu, M.; Ning, J.; Hou, G.; Byeon, I.-J. L.; Gronenborn, A. M.; Polenova, T.; Zhang, P., CryoEM Structure Refinement by Integrating NMR Chemical Shifts with Molecular Dynamics Simulations. *J. Chem. Phys. B* **2017**, *121* (15), 3853-3863.
 28. Frye, J. J.; Brown, N. G.; Petzold, G.; Watson, E. R.; Grace, C. R. R.; Nourse, A.; Jarvis, M. A.; Kriwacki, R. W.; Peters, J.-M.; Stark, H.; Schulman, B. A., Electron microscopy structure of human APC/CCDH1-EMII reveals multimodal mechanism of E3 ligase shutdown. *Nat. Struct. Mol. Biol.* **2013**, *20* (7), 827-835.
 29. Baker, L. A.; Sinnige, T.; Schellenberger, P.; de Keyzer, J.; Siebert, C. A.; Driessen, A. J. M.; Baldus, M.; Grünewald, K., Combined 1H-Detected Solid-State

- NMR Spectroscopy and Electron Cryotomography to Study Membrane Proteins across Resolutions in Native Environments. *Structure* **2018**, *26* (1), 161-170.e3.
30. Teng, Q., *Structural Biology - Practical NMR Applications*. Springer US: 2013.
 31. Delsuc, M. A.; Vitorino, M.; Kieffer, B., Determination of Protein Structure and Dynamics by NMR. In *Structural Biology in Drug Discovery*, Renaud, J. P., Ed. 2020; pp 295-323.
 32. Tycko, R., Biomolecular solid state NMR: Advances in Structural Methodology and Applications to Peptide and Protein Fibrils. *Annu. Rev. Phys. Chem.* **2001**, *52* (1), 575-606.
 33. Pake, G. E., Nuclear Resonance Absorption in Hydrated Crystals: Fine Structure of the Proton Line. *J. Chem. Phys.* **1948**, *16* (4), 327-336.
 34. Haeberlen, U., *High Resolution NMR in Solids Selective Averaging*. Academic Press: 1976; p 204.
 35. Mehring, M., *Principles of High Resolution NMR in Solids*. Springer-Verlag Berlin Heidelberg: 1983; p 344.
 36. Andrew, E. R.; Bradbury, A.; Eades, R. G., Nuclear Magnetic Resonance Spectra from a Crystal rotated at High Speed. *Nature* **1958**, *182* (4650), 1659-1659.
 37. Lowe, I. J., Free Induction Decays of Rotating Solids. *Phys. Rev. Lett.* **1959**, *2* (7), 285-287.
 38. Meier, B. H.; Riek, R.; Böckmann, A., Emerging Structural Understanding of Amyloid Fibrils by Solid-State NMR. *Trends Biochem. Sci* **2017**, *42* (10), 777-787.
 39. Tycko, R., Solid-State NMR Studies of Amyloid Fibril Structure. *Annu. Rev. Phys. Chem.* **2011**, *62* (1), 279-299.
 40. Renault, M.; Cukkemane, A.; Baldus, M., Solid-State NMR Spectroscopy on Complex Biomolecules. *Angew. Chem. Int. Ed.* **2010**, *49* (45), 8346-8357.
 41. Mandala, V. S.; Williams, J. K.; Hong, M., Structure and Dynamics of Membrane Proteins from Solid-State NMR. *Annu. Rev. Biophys.* **2018**, *47* (1), 201-222.
 42. Zhang, W.; Xu, S.; Han, X.; Bao, X., In situ solid-state NMR for heterogeneous catalysis: a joint experimental and theoretical approach. *Chem. Soc. Rev.* **2012**, *41* (1), 192-210.
 43. Lapina, O. B., Modern ssNMR for heterogeneous catalysis. *Catal. Today* **2017**, *285*, 179-193.
 44. Harris, R. K., Applications of solid-state NMR to pharmaceutical polymorphism and related matters. *J. Pharm. Pharmacol.* **2007**, *59* (2), 225-239.
 45. Fu, R.; Brey, W. W.; Shetty, K.; Gor'kov, P.; Saha, S.; Long, J. R.; Grant, S. C.; Chekmenev, E. Y.; Hu, J.; Gan, Z.; Sharma, M.; Zhang, F.; Logan, T. M.; Brüschweller, R.; Edison, A.; Blue, A.; Dixon, I. R.; Markiewicz, W. D.; Cross, T. A., Ultra-wide bore 900MHz high-resolution NMR at the National High Magnetic Field Laboratory. *J. Magn. Reson.* **2005**, *177* (1), 1-8.
 46. Gan, Z.; Hung, I.; Wang, X.; Paulino, J.; Wu, G.; Litvak, I. M.; Gor'kov, P. L.; Brey, W. W.; Lendi, P.; Schiano, J. L.; Bird, M. D.; Dixon, I. R.; Toth, J.; Boebinger, G. S.; Cross, T. A., NMR spectroscopy up to 35.2T using a series-connected hybrid magnet. *J. Magn. Reson.* **2017**, *284*, 125-136.
 47. Hashi, K.; Ohki, S.; Matsumoto, S.; Nishijima, G.; Goto, A.; Deguchi, K.; Yamada, K.; Noguchi, T.; Sakai, S.; Takahashi, M.; Yanagisawa, Y.; Iguchi, S.; Yamazaki, T.; Maeda, H.; Tanaka, R.; Nemoto, T.; Suematsu, H.; Miki, T.; Saito, K.; Shimizu, T., Achievement of 1020MHz NMR. *J. Magn. Reson.* **2015**, *256*, 30-33.

48. Kovacs, H.; Moskau, D.; Spraul, M., Cryogenically cooled probes—a leap in NMR technology. *Prog. Nucl. Magn. Reson. Spectrosc.* **2005**, *46* (2), 131-155.
49. Duckett, S. B.; Mewis, R. E., Application of Parahydrogen Induced Polarization Techniques in NMR Spectroscopy and Imaging. *Acc. Chem. Res.* **2012**, *45* (8), 1247-1257.
50. Henning, H.; Dyballa, M.; Scheibe, M.; Klemm, E.; Hunger, M., In situ CF MAS NMR study of the pairwise incorporation of parahydrogen into olefins on rhodium-containing zeolites Y. *Chem. Phys. Lett.* **2013**, *555*, 258-262.
51. Arzumanov, S. S.; Stepanov, A. G., Parahydrogen-Induced Polarization Detected with Continuous Flow Magic Angle Spinning NMR. *J. Phys. Chem. C* **2013**, *117* (6), 2888-2892.
52. Raftery, D.; MacNamara, E.; Fisher, G.; Rice, C. V.; Smith, J., Optical Pumping and Magic Angle Spinning: Sensitivity and Resolution Enhancement for Surface NMR Obtained with Laser-Polarized Xenon. *J. Am. Chem. Soc.* **1997**, *119* (37), 8746-8747.
53. Brunner, E.; Seydoux, R.; Haake, M.; Pines, A.; Reimer, J. A., Surface NMR Using Laser-Polarized ^{129}Xe under Magic Angle Spinning Conditions. *J. Magn. Reson.* **1998**, *130* (1), 145-148.
54. Lilly Thankamony, A. S.; Wittmann, J. J.; Kaushik, M.; Corzilius, B., Dynamic nuclear polarization for sensitivity enhancement in modern solid-state NMR. *Prog. Nucl. Magn. Reson. Spectrosc.* **2017**, *102-103*, 120-195.
55. Corzilius, B., High-Field Dynamic Nuclear Polarization. *Annu. Rev. Phys. Chem.* **2020**, *71* (1), 7.1-7.28.
56. Zysmilich, M. G.; McDermott, A., Photochemically Induced Dynamic Nuclear Polarization in the Solid-State ^{15}N Spectra of Reaction Centers from Photosynthetic Bacteria *Rhodospira rubra* R-26. *J. Am. Chem. Soc.* **1994**, *116* (18), 8362-8363.
57. Bode, B. E.; Thamarath, S. S.; Gupta, K. B. S. S.; Alia, A.; Jeschke, G.; Matysik, J., The Solid-State Photo-CIDNP Effect and Its Analytical Application. In *Hyperpolarization Methods in NMR Spectroscopy*, Kuhn, L. T., Ed. Springer Berlin Heidelberg: Berlin, Heidelberg, 2013; pp 105-121.
58. Matysik, J.; Diller, A.; Roy, E.; Alia, A., The solid-state photo-CIDNP effect. *Photosynth. Res.* **2009**, *102* (2), 427.
59. Tanaka, S.; Liao, W.-C.; Ogawa, A.; Sato, K.; Copéret, C., DNP NMR spectroscopy of cross-linked organic polymers: rational guidelines towards optimal sample preparation. *Phys. Chem. Chem. Phys.* **2020**, *22* (6), 3184-3190.
60. Brownbill, N. J.; Sprick, R. S.; Bonillo, B.; Pawsey, S.; Aussenac, F.; Fielding, A. J.; Cooper, A. I.; Blanc, F., Structural Elucidation of Amorphous Photocatalytic Polymers from Dynamic Nuclear Polarization Enhanced Solid State NMR. *Macromolecules* **2018**, *51* (8), 3088-3096.
61. Chaudhari, S. R.; Griffin, J. M.; Broch, K.; Lesage, A.; Lemaire, V.; Dudenko, D.; Olivier, Y.; Sirringhaus, H.; Emsley, L.; Grey, C. P., Donor-acceptor stacking arrangements in bulk and thin-film high-mobility conjugated polymers characterized using molecular modelling and MAS and surface-enhanced solid-state NMR spectroscopy. *Chem. Sci.* **2017**, *8* (4), 3126-3136.
62. Blanc, F.; Chong, S. Y.; McDonald, T. O.; Adams, D. J.; Pawsey, S.; Caporini, M. A.; Cooper, A. I., Dynamic Nuclear Polarization NMR Spectroscopy Allows High-Throughput Characterization of Microporous Organic Polymers. *J. Am. Chem. Soc.* **2013**, *135* (41), 15290-15293.

63. Rankin, A. G. M.; Webb, P. B.; Dawson, D. M.; Viger-Gravel, J.; Walder, B. J.; Emsley, L.; Ashbrook, S. E., Determining the Surface Structure of Silicated Alumina Catalysts via Isotopic Enrichment and Dynamic Nuclear Polarization Surface-Enhanced NMR Spectroscopy. *J. Phys. Chem. C* **2017**, *121* (41), 22977-22984.
64. Sangodkar, R. P.; Smith, B. J.; Gajan, D.; Rossini, A. J.; Roberts, L. R.; Funkhouser, G. P.; Lesage, A.; Emsley, L.; Chmelka, B. F., Influences of Dilute Organic Adsorbates on the Hydration of Low-Surface-Area Silicates. *J. Am. Chem. Soc.* **2015**, *137* (25), 8096-8112.
65. Grüning, W. R.; Rossini, A. J.; Zagdoun, A.; Gajan, D.; Lesage, A.; Emsley, L.; Copéret, C., Molecular-level characterization of the structure and the surface chemistry of periodic mesoporous organosilicates using DNP-surface enhanced NMR spectroscopy. *Phys. Chem. Chem. Phys.* **2013**, *15* (32), 13270-13274.
66. Lafon, O.; Thankamony, A. S. L.; Kobayashi, T.; Carnevale, D.; Vitzthum, V.; Slowing, I. I.; Kandel, K.; Vezin, H.; Amoureux, J.-P.; Bodenhausen, G.; Pruski, M., Mesoporous Silica Nanoparticles Loaded with Surfactant: Low Temperature Magic Angle Spinning ¹³C and ²⁹Si NMR Enhanced by Dynamic Nuclear Polarization. *J. Phys. Chem. C* **2013**, *117* (3), 1375-1382.
67. Lafon, O.; Rosay, M.; Aussenac, F.; Lu, X.; Trébosc, J.; Cristini, O.; Kinowski, C.; Touati, N.; Vezin, H.; Amoureux, J.-P., Beyond the Silica Surface by Direct Silicon-29 Dynamic Nuclear Polarization. *Angew. Chem. Int. Ed.* **2011**, *50* (36), 8367-8370.
68. Lelli, M.; Gajan, D.; Lesage, A.; Caporini, M. A.; Vitzthum, V.; Miéville, P.; Héroguel, F.; Rascón, F.; Roussey, A.; Thieuleux, C.; Boualleg, M.; Veyre, L.; Bodenhausen, G.; Coperet, C.; Emsley, L., Fast Characterization of Functionalized Silica Materials by Silicon-29 Surface-Enhanced NMR Spectroscopy Using Dynamic Nuclear Polarization. *J. Am. Chem. Soc.* **2011**, *133* (7), 2104-2107.
69. Lesage, A.; Lelli, M.; Gajan, D.; Caporini, M. A.; Vitzthum, V.; Miéville, P.; Alauzun, J.; Roussey, A.; Thieuleux, C.; Mehdi, A.; Bodenhausen, G.; Coperet, C.; Emsley, L., Surface Enhanced NMR Spectroscopy by Dynamic Nuclear Polarization. *J. Am. Chem. Soc.* **2010**, *132* (44), 15459-15461.
70. Hanrahan, M. P.; Chen, Y.; Blome-Fernández, R.; Stein, J. L.; Pach, G. F.; Adamson, M. A. S.; Neale, N. R.; Cossairt, B. M.; Vela, J.; Rossini, A. J., Probing the Surface Structure of Semiconductor Nanoparticles by DNP SENS with Dielectric Support Materials. *J. Am. Chem. Soc.* **2019**, *141* (39), 15532-15546.
71. Protesescu, L.; Rossini, A. J.; Kriegner, D.; Valla, M.; de Kergommeaux, A.; Walter, M.; Kravchyk, K. V.; Nachttegaal, M.; Stangl, J.; Malaman, B.; Reiss, P.; Lesage, A.; Emsley, L.; Copéret, C.; Kovalenko, M. V., Unraveling the Core–Shell Structure of Ligand-Capped Sn/SnOx Nanoparticles by Surface-Enhanced Nuclear Magnetic Resonance, Mössbauer, and X-ray Absorption Spectroscopies. *ACS Nano* **2014**, *8* (3), 2639-2648.
72. Akbey, Ü.; Altin, B.; Linden, A.; Özçelik, S.; Gradzielski, M.; Oschkinat, H., Dynamic nuclear polarization of spherical nanoparticles. *Phys. Chem. Chem. Phys.* **2013**, *15* (47), 20706-20716.
73. Moroz, I. B.; Lund, A.; Kaushik, M.; Severy, L.; Gajan, D.; Fedorov, A.; Lesage, A.; Copéret, C., Specific Localization of Aluminum Sites Favors Ethene-to-Propene Conversion on (Al)MCM-41-Supported Ni(II) Single Sites. *ACS Catal.* **2019**, *9* (8), 7476-7485.

74. Perras, F. A.; Wang, Z.; Kobayashi, T.; Baiker, A.; Huang, J.; Pruski, M., Shedding light on the atomic-scale structure of amorphous silica–alumina and its Brønsted acid sites. *Phys. Chem. Chem. Phys.* **2019**, *21* (35), 19529-19537.
75. Kobayashi, T.; Pruski, M., Spatial Distribution of Silica-Bound Catalytic Organic Functional Groups Can Now Be Revealed by Conventional and DNP-Enhanced Solid-State NMR Methods. *ACS Catal.* **2019**, *9* (8), 7238-7249.
76. Moroz, I. B.; Larmier, K.; Liao, W.-C.; Copéret, C., Discerning γ -Alumina Surface Sites with Nitrogen-15 Dynamic Nuclear Polarization Surface Enhanced NMR Spectroscopy of Adsorbed Pyridine. *J. Phys. Chem. C* **2018**, *122* (20), 10871-10882.
77. Perras, F. A.; Boteju, K. C.; Slowing, I. I.; Sadow, A. D.; Pruski, M., Direct 17O dynamic nuclear polarization of single-site heterogeneous catalysts. *Chem. Commun.* **2018**, *54* (28), 3472-3475.
78. Perras, F. A.; Wang, Z.; Naik, P.; Slowing, I. I.; Pruski, M., Natural Abundance 17O DNP NMR Provides Precise O–H Distances and Insights into the Brønsted Acidity of Heterogeneous Catalysts. *Angew. Chem. Int. Ed.* **2017**, *56* (31), 9165-9169.
79. Berruyer, P.; Lelli, M.; Conley, M. P.; Silverio, D. L.; Widdifield, C. M.; Siddiqi, G.; Gajan, D.; Lesage, A.; Copéret, C.; Emsley, L., Three-Dimensional Structure Determination of Surface Sites. *J. Am. Chem. Soc.* **2017**, *139* (2), 849-855.
80. Wolf, P.; Liao, W.-C.; Ong, T.-C.; Valla, M.; Harris, J. W.; Gounder, R.; van der Graaff, W. N. P.; Pidko, E. A.; Hensen, E. J. M.; Ferrini, P.; Dijkmans, J.; Sels, B.; Hermans, I.; Copéret, C., Identifying Sn Site Heterogeneities Prevalent Among Sn-Beta Zeolites. *Helv. Chim. Acta* **2016**, *99* (12), 916-927.
81. Wolf, P.; Valla, M.; Rossini, A. J.; Comas-Vives, A.; Núñez-Zarur, F.; Malaman, B.; Lesage, A.; Emsley, L.; Copéret, C.; Hermans, I., NMR Signatures of the Active Sites in Sn- β Zeolite. *Angew. Chem. Int. Ed.* **2014**, *53* (38), 10179-10183.
82. Pinon, A. C.; Rossini, A. J.; Widdifield, C. M.; Gajan, D.; Emsley, L., Polymorphs of Theophylline Characterized by DNP Enhanced Solid-State NMR. *Mol. Pharm.* **2015**, *12* (11), 4146-4153.
83. Rossini, A. J.; Widdifield, C. M.; Zagdoun, A.; Lelli, M.; Schwarzwälder, M.; Copéret, C.; Lesage, A.; Emsley, L., Dynamic Nuclear Polarization Enhanced NMR Spectroscopy for Pharmaceutical Formulations. *J. Am. Chem. Soc.* **2014**, *136* (6), 2324-2334.
84. Rossini, A. J.; Zagdoun, A.; Hegner, F.; Schwarzwälder, M.; Gajan, D.; Copéret, C.; Lesage, A.; Emsley, L., Dynamic Nuclear Polarization NMR Spectroscopy of Microcrystalline Solids. *J. Am. Chem. Soc.* **2012**, *134* (40), 16899-16908.
85. Chakraborty, A.; Deligey, F.; Quach, J.; Mentink-Vigier, F.; Wang, P.; Wang, T., Biomolecular complex viewed by dynamic nuclear polarization solid-state NMR spectroscopy. *Biochem. Soc. Trans.* **2020**, *48* (3), 1089-1099.
86. Mandala, V. S.; Hong, M., High-sensitivity protein solid-state NMR spectroscopy. *Curr. Opin. Struct. Biol.* **2019**, *58*, 183-190.
87. Jaudzems, K.; Polenova, T.; Pintacuda, G.; Oschkinat, H.; Lesage, A., DNP NMR of biomolecular assemblies. *J. Struct. Biol.* **2019**, *206* (1), 90-98.
88. Jaudzems, K.; Bertarello, A.; Chaudhari, S. R.; Pica, A.; Cala-De Paepe, D.; Barbet-Massin, E.; Pell, A. J.; Akopjana, I.; Kotelovica, S.; Gajan, D.; Ouari, O.; Tars, K.; Pintacuda, G.; Lesage, A., Dynamic Nuclear Polarization-Enhanced Biomolecular NMR Spectroscopy at High Magnetic Field with Fast Magic-Angle Spinning. *Angew. Chem. Int. Ed.* **2018**, *57* (25), 7458-7462.

89. Sergeyev, I. V.; Itin, B.; Rogawski, R.; Day, L. A.; McDermott, A. E., Efficient assignment and NMR analysis of an intact virus using sequential side-chain correlations and DNP sensitization. *PNAS* **2017**, *114* (20), 5171-5176.
90. Akbey, Ü.; Oschkinat, H., Structural biology applications of solid state MAS DNP NMR. *J. Magn. Reson.* **2016**, *269*, 213-224.
91. van der Crujisen, E. A. W.; Koers, E. J.; Sauvée, C.; Hulse, R. E.; Weingarth, M.; Ouari, O.; Perozo, E.; Tordo, P.; Baldus, M., Biomolecular DNP-Supported NMR Spectroscopy using Site-Directed Spin Labeling. *Chem. Eur. J.* **2015**, *21* (37), 12971-12977.
92. Overhauser, A. W., Polarization of Nuclei in Metals. *Phys. Rev.* **1953**, *92* (2), 411-415.
93. Corzilius, B., Chapter 8 Dynamic Nuclear Polarization. In *Paramagnetism in Experimental Biomolecular NMR*, The Royal Society of Chemistry: 2018; pp 219-257.
94. Stevanato, G.; Casano, G.; Kubicki, D. J.; Rao, Y.; Esteban Hofer, L.; Menzildjian, G.; Karoui, H.; Siri, D.; Cordova, M.; Yulikov, M.; Jeschke, G.; Lelli, M.; Lesage, A.; Ouari, O.; Emsley, L., Open and Closed Radicals: Local Geometry around Unpaired Electrons Governs Magic-Angle Spinning Dynamic Nuclear Polarization Performance. *J. Am. Chem. Soc.* **2020**, *142* (39), 16587-16599.
95. Can, T. V.; Caporini, M. A.; Mentink-Vigier, F.; Corzilius, B.; Walsh, J. J.; Rosay, M.; Maas, W. E.; Baldus, M.; Vega, S.; Swager, T. M.; Griffin, R. G., Overhauser effects in insulating solids. *J. Chem. Phys.* **2014**, *141* (6), 064202.
96. Mentink-Vigier, F.; Vega, S.; De Paëpe, G., Fast and accurate MAS–DNP simulations of large spin ensembles. *Phys. Chem. Chem. Phys.* **2017**, *19* (5), 3506-3522.
97. Mentink-Vigier, F.; Akbey, Ü.; Hovav, Y.; Vega, S.; Oschkinat, H.; Feintuch, A., Fast passage dynamic nuclear polarization on rotating solids. *J. Magn. Reson.* **2012**, *224*, 13-21.
98. Thurber, K. R.; Tycko, R., Theory for cross effect dynamic nuclear polarization under magic-angle spinning in solid state nuclear magnetic resonance: The importance of level crossings. *J. Chem. Phys.* **2012**, *137* (8), 084508.
99. Mentink-Vigier, F.; Akbey, Ü.; Oschkinat, H.; Vega, S.; Feintuch, A., Theoretical aspects of Magic Angle Spinning - Dynamic Nuclear Polarization. *J. Magn. Reson.* **2015**, *258*, 102-120.
100. Hovav, Y.; Feintuch, A.; Vega, S., Theoretical aspects of dynamic nuclear polarization in the solid state – spin temperature and thermal mixing. *Phys. Chem. Chem. Phys.* **2013**, *15* (1), 188-203.
101. Atsarkin, V. A.; Kessenikh, A. V., Dynamic Nuclear Polarization in Solids: The Birth and Development of the Many-Particle Concept. *Appl. Magn. Reson.* **2012**, *43* (1), 7-19.
102. Wenckebach, W. T., Dynamic nuclear polarization via thermal mixing: Beyond the high temperature approximation. *J. Magn. Reson.* **2017**, *277*, 68-78.
103. Hu, K.-N.; Bajaj, V. S.; Rosay, M.; Griffin, R. G., High-frequency dynamic nuclear polarization using mixtures of TEMPO and trityl radicals. *J. Chem. Phys.* **2007**, *126* (4), 044512.
104. Carver, T. R.; Slichter, C. P., Polarization of Nuclear Spins in Metals. *Phys. Rev.* **1953**, *92* (1), 212-213.
105. Griesinger, C.; Bennati, M.; Vieth, H. M.; Luchinat, C.; Parigi, G.; Höfer, P.; Engelke, F.; Glaser, S. J.; Denysenkov, V.; Prisner, T. F., Dynamic nuclear

- polarization at high magnetic fields in liquids. *Prog. Nucl. Magn. Reson. Spectrosc.* **2012**, *64*, 4-28.
106. Cheng, C.-Y.; Han, S., Dynamic Nuclear Polarization Methods in Solids and Solutions to Explore Membrane Proteins and Membrane Systems. *Annu. Rev. Phys. Chem.* **2013**, *64* (1), 507-532.
 107. Chaudhari, S. R.; Wisser, D.; Pinon, A. C.; Berruyer, P.; Gajan, D.; Tordo, P.; Ouari, O.; Reiter, C.; Engelke, F.; Copéret, C.; Lelli, M.; Lesage, A.; Emsley, L., Dynamic Nuclear Polarization Efficiency Increased by Very Fast Magic Angle Spinning. *J. Am. Chem. Soc.* **2017**, *139* (31), 10609-10612.
 108. Björgvinsdóttir, S.; Walder, B. J.; Pinon, A. C.; Yarava, J. R.; Emsley, L., DNP enhanced NMR with flip-back recovery. *J. Magn. Reson.* **2018**, *288*, 69-75.
 109. Smith, A. A.; Corzilius, B.; Barnes, A. B.; Maly, T.; Griffin, R. G., Solid effect dynamic nuclear polarization and polarization pathways. *J. Chem. Phys.* **2012**, *136* (1), 015101.
 110. Haze, O.; Corzilius, B.; Smith, A. A.; Griffin, R. G.; Swager, T. M., Water-Soluble Narrow-Line Radicals for Dynamic Nuclear Polarization. *J. Am. Chem. Soc.* **2012**, *134* (35), 14287-14290.
 111. Corzilius, B.; Smith, A. A.; Barnes, A. B.; Luchinat, C.; Bertini, I.; Griffin, R. G., High-Field Dynamic Nuclear Polarization with High-Spin Transition Metal Ions. *J. Am. Chem. Soc.* **2011**, *133* (15), 5648-5651.
 112. Corzilius, B., Paramagnetic Metal Ions for Dynamic Nuclear Polarization. In *eMagRes*, Harris, R. K.; Wasylishen, R. L., Eds. 2018; pp 179-194.
 113. Mentink-Vigier, F.; Mathies, G.; Liu, Y.; Barra, A.-L.; Caporini, M. A.; Lee, D.; Hediger, S.; Griffin, R.; De Paëpe, G., Efficient cross-effect dynamic nuclear polarization without depolarization in high-resolution MAS NMR. *Chem. Sci.* **2017**, *8* (12), 8150-8163.
 114. Penzel, S.; Oss, A.; Org, M.-L.; Samoson, A.; Böckmann, A.; Ernst, M.; Meier, B. H., Spinning faster: protein NMR at MAS frequencies up to 126 kHz. *J. Biomol. NMR* **2019**, *73* (1), 19-29.
 115. Rosay, M.; Blank, M.; Engelke, F., Instrumentation for solid-state dynamic nuclear polarization with magic angle spinning NMR. *J. Magn. Reson.* **2016**, *264*, 88-98.
 116. Mak-Jurkauskas, M. L. a. G., R.G., High-Frequency Dynamic Nuclear Polarization. In *eMagRes*, 2010.
 117. Becerra, L. R.; Gerfen, G. J.; Bellew, B. F.; Bryant, J. A.; Hall, D. A.; Inati, S. J.; Weber, R. T.; Un, S.; Prisner, T. F.; McDermott, A. E.; Fishbein, K. W.; Kreisler, K. E.; Temkin, R. J.; Singel, D. J.; Griffin, R. G., A Spectrometer for Dynamic Nuclear Polarization and Electron Paramagnetic Resonance at High Frequencies. *J. Magn. Reson., Ser A* **1995**, *117* (1), 28-40.
 118. Gerfen, G. J.; Becerra, L. R.; Hall, D. A.; Griffin, R. G.; Temkin, R. J.; Singel, D. J., High frequency (140 GHz) dynamic nuclear polarization: Polarization transfer to a solute in frozen aqueous solution. *J. Chem. Phys.* **1995**, *102* (24), 9494-9497.
 119. Becerra, L. R.; Gerfen, G. J.; Temkin, R. J.; Singel, D. J.; Griffin, R. G., Dynamic nuclear polarization with a cyclotron resonance maser at 5 T. *Phys. Rev. Lett.* **1993**, *71* (21), 3561-3564.
 120. Wisser, D.; Karthikeyan, G.; Lund, A.; Casano, G.; Karoui, H.; Yulikov, M.; Menzildjian, G.; Pinon, A. C.; Pureau, A.; Engelke, F.; Chaudhari, S. R.; Kubicki, D.; Rossini, A. J.; Moroz, I. B.; Gajan, D.; Copéret, C.; Jeschke, G.; Lelli, M.; Emsley, L.; Lesage, A.; Ouari, O., BDPA-Nitroxide Biradicals Tailored for Efficient

- Dynamic Nuclear Polarization Enhanced Solid-State NMR at Magnetic Fields up to 21.1 T. *J. Am. Chem. Soc.* **2018**, *140* (41), 13340-13349.
121. Bernard, G. M.; Michaelis, V. K., Instrumentation for High-field Dynamic Nuclear Polarization NMR Spectroscopy. In *eMagRes*, Harris, R. K.; Wasylshen, R. L., Eds. 2019; Vol. 8, pp 77-86.
 122. Rosay, M.; Tometich, L.; Pawsey, S.; Bader, R.; Schauwecker, R.; Blank, M.; Borchard, P. M.; Cauffman, S. R.; Felch, K. L.; Weber, R. T.; Temkin, R. J.; Griffin, R. G.; Maas, W. E., Solid-state dynamic nuclear polarization at 263 GHz: spectrometer design and experimental results. *Phys. Chem. Chem. Phys.* **2010**, *12* (22), 5850-5860.
 123. Chaudhari, S. R.; Berruyer, P.; Gajan, D.; Reiter, C.; Engelke, F.; Silverio, D. L.; Copéret, C.; Lelli, M.; Lesage, A.; Emsley, L., Dynamic nuclear polarization at 40 kHz magic angle spinning. *Phys. Chem. Chem. Phys.* **2016**, *18* (15), 10616-10622.
 124. Berruyer, P.; Björgvinsdóttir, S.; Bertarello, A.; Stevanato, G.; Rao, Y.; Karthikeyan, G.; Casano, G.; Ouari, O.; Lelli, M.; Reiter, C.; Engelke, F.; Emsley, L., Dynamic Nuclear Polarization Enhancement of 200 at 21.15 T Enabled by 65 kHz Magic Angle Spinning. *J. Phys. Chem. Lett.* **2020**, *11* (19), 8386-8391.
 125. Ong, T.-C.; Mak-Jurkauskas, M. L.; Walish, J. J.; Michaelis, V. K.; Corzilius, B.; Smith, A. A.; Clausen, A. M.; Cheetham, J. C.; Swager, T. M.; Griffin, R. G., Solvent-Free Dynamic Nuclear Polarization of Amorphous and Crystalline ortho-Terphenyl. *J. Chem. Phys. B* **2013**, *117* (10), 3040-3046.
 126. Kurdzesau, F.; van den Brandt, B.; Comment, A.; Hautle, P.; Jannin, S.; van der Klink, J. J.; Konter, J. A., Dynamic nuclear polarization of small labelled molecules in frozen water–alcohol solutions. *J. Phys. D: Appl. Phys.* **2008**, *41* (15), 155506.
 127. Iijima, T., Thermal Analysis of Cryoprotective Solutions for Red Blood Cells. *Cryobiology* **1998**, *36* (3), 165-173.
 128. Zagdoun, A.; Casano, G.; Ouari, O.; Schwarzwälder, M.; Rossini, A. J.; Aussenac, F.; Yulikov, M.; Jeschke, G.; Copéret, C.; Lesage, A.; Tordo, P.; Emsley, L., Large Molecular Weight Nitroxide Biradicals Providing Efficient Dynamic Nuclear Polarization at Temperatures up to 200 K. *J. Am. Chem. Soc.* **2013**, *135* (34), 12790-12797.
 129. Lelli, M.; Chaudhari, S. R.; Gajan, D.; Casano, G.; Rossini, A. J.; Ouari, O.; Tordo, P.; Lesage, A.; Emsley, L., Solid-State Dynamic Nuclear Polarization at 9.4 and 18.8 T from 100 K to Room Temperature. *J. Am. Chem. Soc.* **2015**, *137* (46), 14558-14561.
 130. Hall, D. A.; Maus, D. C.; Gerfen, G. J.; Inati, S. J.; Becerra, L. R.; Dahlquist, F. W.; Griffin, R. G., Polarization-Enhanced NMR Spectroscopy of Biomolecules in Frozen Solution. *Science* **1997**, *276* (5314), 930-932.
 131. Hu, K.-N.; Yu, H.-h.; Swager, T. M.; Griffin, R. G., Dynamic Nuclear Polarization with Biradicals. *J. Am. Chem. Soc.* **2004**, *126* (35), 10844-10845.
 132. Song, C.; Hu, K.-N.; Joo, C.-G.; Swager, T. M.; Griffin, R. G., TOTAPOL: A Biradical Polarizing Agent for Dynamic Nuclear Polarization Experiments in Aqueous Media. *J. Am. Chem. Soc.* **2006**, *128* (35), 11385-11390.
 133. Sauvée, C.; Rosay, M.; Casano, G.; Aussenac, F.; Weber, R. T.; Ouari, O.; Tordo, P., Highly Efficient, Water-Soluble Polarizing Agents for Dynamic Nuclear Polarization at High Frequency. *Angew. Chem. Int. Ed.* **2013**, *52* (41), 10858-10861.
 134. Matsuki, Y.; Maly, T.; Ouari, O.; Karoui, H.; Le Moigne, F.; Rizzato, E.; Lyubenova, S.; Herzfeld, J.; Prisner, T.; Tordo, P.; Griffin, R. G., Dynamic Nuclear Polarization with a Rigid Biradical. *Angew. Chem. Int. Ed.* **2009**, *48* (27), 4996-5000.

135. Zagdoun, A.; Casano, G.; Ouari, O.; Lapadula, G.; Rossini, A. J.; Lelli, M.; Baffert, M.; Gajan, D.; Veyre, L.; Maas, W. E.; Rosay, M.; Weber, R. T.; Thieuleux, C.; Coperet, C.; Lesage, A.; Tordo, P.; Emsley, L., A Slowly Relaxing Rigid Biradical for Efficient Dynamic Nuclear Polarization Surface-Enhanced NMR Spectroscopy: Expedient Characterization of Functional Group Manipulation in Hybrid Materials. *J. Am. Chem. Soc.* **2012**, *134* (4), 2284-2291.
136. Sato, H.; Kathirvelu, V.; Fielding, A.; Blinco, J. P.; Micallef, A. S.; Bottle, S. E.; Eaton, S. S.; Eaton, G. R., Impact of molecular size on electron spin relaxation rates of nitroxyl radicals in glassy solvents between 100 and 300 K. *Mol. Phys.* **2007**, *105* (15-16), 2137-2151.
137. Jagtap, A. P.; Geiger, M.-A.; Stöppler, D.; Orwick-Rydmark, M.; Oschkinat, H.; Sigurdsson, S. T., bcTol: a highly water-soluble biradical for efficient dynamic nuclear polarization of biomolecules. *Chem. Commun.* **2016**, *52* (43), 7020-7023.
138. Geiger, M.-A.; Jagtap, A. P.; Kaushik, M.; Sun, H.; Stöppler, D.; Sigurdsson, S. T.; Corzilius, B.; Oschkinat, H., Efficiency of Water-Soluble Nitroxide Biradicals for Dynamic Nuclear Polarization in Rotating Solids at 9.4 T: bcTol-M and cyoly-TOTAPOL as New Polarizing Agents. *Chem. Eur. J.* **2018**, *24* (51), 13485-13494.
139. Thurber, K. R.; Tycko, R., Perturbation of nuclear spin polarizations in solid state NMR of nitroxide-doped samples by magic-angle spinning without microwaves. *J. Chem. Phys.* **2014**, *140* (18), 184201.
140. Mentink-Vigier, F.; Paul, S.; Lee, D.; Feintuch, A.; Hediger, S.; Vega, S.; De Paëpe, G., Nuclear depolarization and absolute sensitivity in magic-angle spinning cross effect dynamic nuclear polarization. *Phys. Chem. Chem. Phys.* **2015**, *17* (34), 21824-21836.
141. Mentink-Vigier, F.; Marin-Montesinos, I.; Jagtap, A. P.; Halbritter, T.; van Tol, J.; Hediger, S.; Lee, D.; Sigurdsson, S. T.; De Paëpe, G., Computationally Assisted Design of Polarizing Agents for Dynamic Nuclear Polarization Enhanced NMR: The AsymPol Family. *J. Am. Chem. Soc.* **2018**, *140* (35), 11013-11019.
142. Lund, A.; Casano, G.; Menzildjian, G.; Kaushik, M.; Stevanato, G.; Yulikov, M.; Jabbour, R.; Wisser, D.; Renom-Carrasco, M.; Thieuleux, C.; Bernada, F.; Karoui, H.; Siri, D.; Rosay, M.; Sergeyev, I. V.; Gajan, D.; Lelli, M.; Emsley, L.; Ouari, O.; Lesage, A., TinyPols: a family of water-soluble binitroxides tailored for dynamic nuclear polarization enhanced NMR spectroscopy at 18.8 and 21.1 T. *Chem. Sci.* **2020**, *11* (10), 2810-2818.
143. Mathies, G.; Caporini, M. A.; Michaelis, V. K.; Liu, Y.; Hu, K.-N.; Mance, D.; Zweier, J. L.; Rosay, M.; Baldus, M.; Griffin, R. G., Efficient Dynamic Nuclear Polarization at 800 MHz/527 GHz with Trityl-Nitroxide Biradicals. *Angew. Chem. Int. Ed.* **2015**, *54* (40), 11770-11774.
144. Reddy, T. J.; Iwama, T.; Halpern, H. J.; Rawal, V. H., General Synthesis of Persistent Trityl Radicals for EPR Imaging of Biological Systems. *J. Org. Chem.* **2002**, *67* (14), 4635-4639.
145. Koelsch, C. F., Syntheses with Triarylvinylmagnesium Bromides. α,γ -Bisdiphenylene- β -phenylallyl, a Stable Free Radical. *J. Am. Chem. Soc.* **1957**, *79* (16), 4439-4441.
146. Dane, E. L.; Maly, T.; Debelouchina, G. T.; Griffin, R. G.; Swager, T. M., Synthesis of a BDPA-TEMPO Biradical. *Org. Lett.* **2009**, *11* (9), 1871-1874.
147. Pinto, L. F.; Marín-Montesinos, I.; Lloveras, V.; Muñoz-Gómez, J. L.; Pons, M.; Veciana, J.; Vidal-Gancedo, J., NMR signal enhancement of >50 000 times in fast

- dissolution dynamic nuclear polarization. *Chem. Commun.* **2017**, 53 (26), 3757-3760.
148. Dane, E. L.; Swager, T. M., Synthesis of a Water-Soluble 1,3-Bis(diphenylene)-2-phenylallyl Radical. *J. Org. Chem.* **2010**, 75 (10), 3533-3536.
 149. Breslin, D. T.; Fox, M. A., Characterization of the excited-state reactivity of a persistent aryl-substituted allyl free radical. *J. Phys. Chem.* **1993**, 97 (50), 13341-13347.
 150. Muñoz-Gómez, J. L.; Monteagudo, E.; Lloveras, V.; Parella, T.; Veciana, J.; Vidal-Gancedo, J., A benzyl alcohol derivative of the BDPA radical for fast dissolution dynamic nuclear polarization NMR spectroscopy. *Org. Biomol. Chem.* **2015**, 13 (9), 2689-2693.
 151. Nishide, H.; Yoshioka, N.; Saitoh, Y.; Gotoh, R.; Miyakawa, T.; Tsuchida, E., Synthesis and Magnetic Property of Polyacetylene Bearing π Conjugated Bis(Diphenylene)Phenylallyl Radical. *J. Macromol. Sci., Pure Appl. Chem.* **1992**, 29 (9), 775-786.
 152. Mandal, S.; Sigurdsson, S. T., On the Limited Stability of BDPA Radicals. *Chem. Eur. J.* **2020**, 26 (33), 7486-7491.
 153. Gomberg, M., An Instance of Trivalent Carbon: Triphenylmethyl *J. Am. Chem. Soc.* **1900**, 22 (11), 757-771.
 154. Lankamp, H.; Nauta, W. T.; MacLean, C., A new interpretation of the monomer-dimer equilibrium of triphenylmethyl- and alkylsubstituted-diphenyl methyl-radicals in solution. *Tetrahedron Lett.* **1968**, 9 (2), 249-254.
 155. Nagao, A.; Takehiro, O.; Jun, Y., Molecular and Crystal Structures of Complexes of Stable Free Radical BDPA with Benzene and Acetone. *Bull. Chem. Soc. Jpn.* **1994**, 67 (1), 31-38.
 156. Henríquez, C. M. G.; Tagle, L. H.; Terraza, C. A.; González, A. B.; Cabrera, A. L.; Volkmann, U. G., Poly(ester)s and poly(amide)s with fluorene and diphenylsilane units in the main chain: Effects of iodine doping on the structure and electrical conductivity. *J. Appl. Polym. Sci.* **2012**, 125 (1), 477-487.
 157. Atkin, R.; Warr, G. G., The Smallest Amphiphiles: Nanostructure in Protic Room-Temperature Ionic Liquids with Short Alkyl Groups. *J. Chem. Phys. B* **2008**, 112 (14), 4164-4166.
 158. Singh, T.; Kumar, A., Aggregation Behavior of Ionic Liquids in Aqueous Solutions: Effect of Alkyl Chain Length, Cations, and Anions. *J. Chem. Phys. B* **2007**, 111 (27), 7843-7851.
 159. Dutta, R.; Kundu, S.; Sarkar, N., Ionic liquid-induced aggregate formation and their applications. *Biophys. Rev.* **2018**, 10 (3), 861-871.
 160. Cagnoli, R.; Caselli, M.; Libertini, E.; Mucci, A.; Parenti, F.; Ponterini, G.; Schenetti, L., Aggregation behaviour of a water-soluble ammonium-functionalized polythiophene: Luminescence enhancement induced by bile-acid anions. *Polymer* **2012**, 53 (2), 403-410.
 161. Liu, Y.; Villamena, F. A.; Rockenbauer, A.; Song, Y.; Zweier, J. L., Structural Factors Controlling the Spin-Spin Exchange Coupling: EPR Spectroscopic Studies of Highly Asymmetric Trityl-Nitroxide Biradicals. *J. Am. Chem. Soc.* **2013**, 135 (6), 2350-2356.
 162. Couet, W. R.; Brasch, R. C.; Sosnovsky, C.; Lukszo, J.; Prakash, I.; Gnewech, C. T.; Tozer, T. N., Influence of chemical structure of nitroxyl spin labels on their reduction by ascorbic acid. *Tetrahedron* **1985**, 41 (7), 1165-1172.

163. Forbes, M. D. E.; Dukes, K. E.; Avdievich, N. I.; Harbron, E. J.; DeSimone, J. M., Flexible Biradicals in Liquid and Supercritical Carbon Dioxide: The Exchange Interaction, the Chain Dynamics, and a Comparison with Conventional Solvents. *J. Chem. Phys. A* **2006**, *110* (5), 1767-1774.

Publications

- I. Mandal, S.; Sigurdsson, S. T., On the Limited Stability of BDPA Radicals. *Chem. Eur. J.* **2020**, *26* (33), 7486-7491. DOI: 10.1002/chem.202001084

- II. Mandal, S.; Sigurdsson, S. T., Water-soluble BDPA radicals with improved persistence. *Chem. Commun.* **2020**, *In press*. DOI: 10.1039/D0CC04920D

Paper I

Dynamic Nuclear Polarization

On the Limited Stability of BDPA Radicals

Sucharita Mandal and Snorri Th. Sigurdsson^{*[a]}

Abstract: 1,3-Bis(diphenylene)-2-phenylallyl (BDPA)-based radicals are of interest as polarizing agents for dynamic nuclear polarization (DNP). For this purpose, a BDPA-nitroxide biradical, employing a phosphodiester linkage, was synthesized. Contrary to what is commonly assumed, BDPA-derived radicals were observed to have limited stability. Hence, the effects of various factors on the stability of BDPA radicals were investigated. Solvent polarity was found to play a significant role on degradation; a polar BDPA radical was ob-

served to degrade faster in a non-polar solvent, whereas non-polar radicals were more unstable in polar solvents. The rate of decomposition was found to increase non-linearly with increasing radical concentration; a 2-fold increase in concentration led to a 3-fold increase in the rate of degradation. Collectively, these results indicate that the dimerization is a significant degradation pathway for BDPA radicals and indeed, a dimer of one BDPA radical was detected by mass spectrometry.


Introduction

NMR spectroscopy is a versatile technique for elucidating the structures of molecules by utilizing nuclear magnetic moments.^[1] However, a shortcoming of NMR spectroscopy is its inherently low sensitivity due to low nuclear spin polarization, i.e., the small difference between the numbers of nuclear spins that are aligned parallel or anti-parallel to an external magnetic field. This is especially a challenge when trying to measure analytes with natural isotopic abundance or at low concentrations.^[2] In contrast, electrons possess a much larger spin polarization. For example, at 100 K and 9.4 T, proton spin-polarization is about 0.01%, whereas the electron spin-polarization is approximately 10%.^[3] Spin polarization of electrons is transferable to nuclei of interest through a technique called dynamic nuclear polarization (DNP), which subsequently enhances the NMR signal-to-noise ratio.^[2b,3-4] In theory, 660- and 2600-fold enhancement can be achieved for ¹H and ¹³C, respectively with continuous-wave irradiation.^[3] In DNP experiments, stable organic radicals at mM concentration are generally included in the sample as the source of unpaired electrons and microwave irradiation is used to facilitate polarization transfer from the electrons to the nuclei.^[5]

There are three principal mechanisms through which polarization transfer can be accomplished in solid-state NMR using magic angle spinning (MAS), namely the Overhauser Effect (OE),^[6] the Solid Effect (SE),^[7] and the Cross Effect (CE).^[7-8] The CE is the most efficient mechanism for MAS-DNP, especially at

higher magnetic fields (> 5 T).^[9] The ideal polarizing agent for the CE should have an electron paramagnetic resonance (EPR) spectrum consisting of two sharp lines, separated by the Larmor frequency of the nucleus to be polarized.^[7c,10] However, there is no radical or radical pair known to possess such an EPR spectrum. Nitroxide biradicals are frequently used as polarizing agents in MAS-DNP as their EPR linewidth is approximately three-fold the proton Larmor frequency, and thus, fulfill the frequency condition for polarizing protons via the CE.^[7b,c,11] The ¹H-polarization can subsequently be transferred to ¹³C or ¹⁵N via cross-polarization.^[12] Carbon-centered radicals, such as the Finland trityl^[13] and 1,3-bis(diphenylene)-2-phenylallyl (BDPA)^[14] (Figure 1 A) possess a narrow EPR linewidth.^[15] Since their linewidths are narrower than the proton Larmor frequency, they cannot be used alone to polarize protons. However, when a carbon-centered radical is connected to a nitroxide, the EPR spectrum of such a heterobiradical consists of one sharp line and another much broader line, approximately separated by the proton Larmor frequency.^[9a,10] Thus, such biradicals are closer to an ideal polarizing agent for MAS-DNP experiments that utilize the CE. Another advantage is that lower microwave power can be used for efficient CE, due to presence of the narrow-line, slower relaxing radical.^[9b] Such heterobiradicals also lead to significantly lower depolarization under MAS-DNP conditions, compared to most bis-nitroxides.^[7c,16] Trityl-nitroxide or BDPA-nitroxide biradicals work especially well at magnetic fields higher than 10 T, where bis-nitroxides give lower enhancements.^[9a,c] A trityl-nitroxide biradical^[9a] and a BDPA-nitroxide biradical^[9c] have been shown to yield an enhancement of 65 and 64, respectively at 18.8 T using a 3.2 mm rotor. The enhancement of the latter was tripled using an 1.3 mm MAS-DNP rotor.^[9c] However, this enhancement is still far from the theoretical maximum and thus, there is still need for new polarizing agents with increased efficiency for DNP.

[a] S. Mandal, Prof. S. T. Sigurdsson
Department of Chemistry, Science Institute
University of Iceland, Dunhaga 3, 107 Reykjavik (Iceland)
E-mail: snorrisi@hi.is

 Supporting information and the ORCID identification number(s) for the author(s) of this article can be found under:
<https://doi.org/10.1002/chem.202001084>.

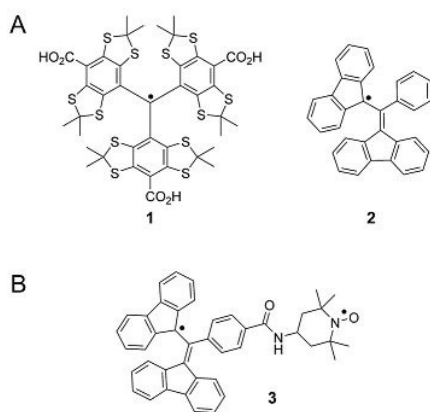


Figure 1. A. Narrow-line carbon-centered radicals, Finland trityl (**1**)^[13] and 1,3-bis(diphenylene)-2-phenylallyl (BDPA) (**2**).^[14] B. Previously reported BDPA-TEMPO biradical **3**.^[17]

In this paper, we describe synthesis of a new BDPA-nitroxide biradical using a phosphodiester linker. The biradical allowed us to readily quantify the amount of biradical relative to a nitroxide monoradical by EPR spectroscopy, as previously described for the BDPA-TEMPO biradical **3** (Figure 1B).^[17] While preparing and working with BDPA radicals, it became clear that they had limited stability. This was unexpected since BDPA radicals are usually referred to as stable radicals.^[14,18] However, as stated in the excellent review of Griller and Ingold on persistent carbon-centered radicals: “There is no doubt that the lax use of the word “stable” has introduced a freedom into discussion such that an author almost has the possibility, like Humpty Dumpty, to make “stable” mean just what he chooses.”^[19] IUPAC considers the stability of a radical to be a thermodynamic property and for a carbon-centered radical, it can be defined as the energy difference between the C–H bond strength of the radical and a suitable alkane (primary, secondary or tertiary). However, IUPAC recommends the use of “persistence”, which refers to a kinetic property, to describe a radical with a half-life greater than several minutes in diluted inert solvents. Keeping in mind that the notion of stable radicals

could be ambiguous, Griller and Ingold advised to use the term “stable” only for a radical which is highly unreactive to air, moisture etc., under ambient conditions and can be handled without further precautions similar to most organic compounds.^[19]

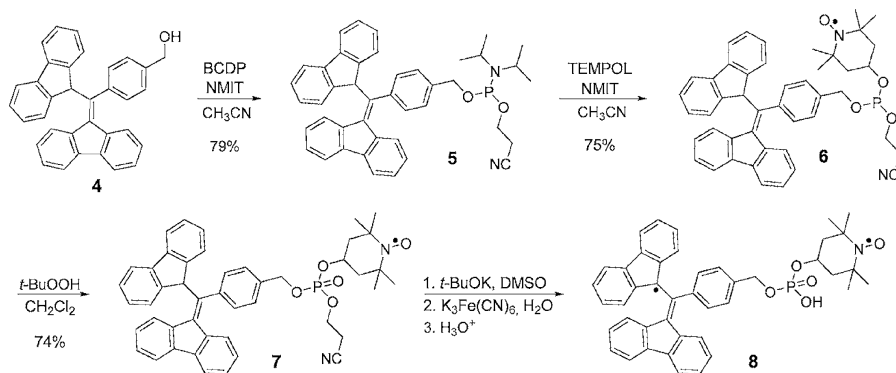
Understandably, many papers refer to the original report of the BDPA radical when discussing its persistence, where a footnote states that “A sample kept in air 23 years is unchanged in appearance and shows a high free-radical content.”^[14] More recent reports indicate that BDPA may not be as persistent as once thought. For example, in the supporting information of a paper from 2017, it states that “We realized that after being stored in the freezer for 6 months the EPR intensity signal of sample 5 decreases in 15%.”^[20] Another paper from 2018 on BDPA-derived biradicals reported that “The radicals are stable for 3 months as powders and stable in TCE solution for 2 weeks, when stored at -18°C in both cases”,^[9c] which also points to instability. Hence, we carried out a systematic investigation of the persistence of BDPA radicals under various conditions. The reaction conditions for generating BDPA radicals were also evaluated as their yields varied greatly with the methods that have been described in the literature.^[9c,21]

Results and Discussion

Synthesis of the BDPA-nitroxide biradical

The BDPA-nitroxide biradical was prepared utilizing a phosphodiester linker. First, BDPA alcohol **4**^[22] was phosphitylated to give phosphoramidite **5**, which was subsequently reacted with 4-hydroxy-2,2,6,6-tetramethylpiperidin-1-oxyl (TEMPOL), followed by an oxidation to give phosphodiester **7** (Scheme 1). The corresponding BDPA-nitroxide biradical (**8**) was generated by treating **7** sequentially with *t*BuOK and $\text{K}_3\text{Fe}(\text{CN})_6$.

Figure 2 shows EPR spectra of three different radicals. A single peak (Figure 2, top) was observed for the carbon-centered BDPA monoradical **2**, whereas nitroxide monoradical **7** shows the characteristic three peaks of nitroxides (Figure 2, middle). The spectrum of **8** (Figure 2, bottom) shows the presence of two components.^[17,20] Biradical **8** has three peaks in its



Scheme 1. Synthesis of BDPA-TEMPO biradical **8** containing a phosphodiester linker. BCDP: Bis(2-cyanoethyl)-*N,N*-diisopropylphosphoramidite. NMIT: *N*-Methylimidazolium triflate.

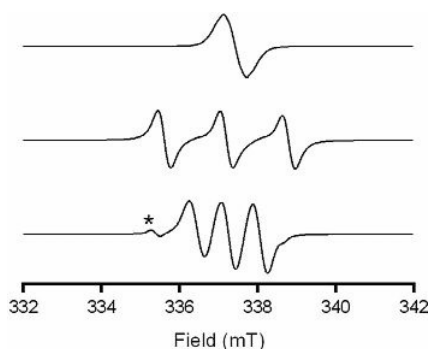


Figure 2. EPR spectra of BDPA radical **2** (top), nitroxide radical **7** (middle) and BDPA-nitroxide biradical **8** (bottom). The peak marked by asterisk in the biradical spectrum originated from a nitroxide monoradical that is present in the sample of the biradical. Experimental parameters: 9.43 GHz, microwave power 1 mW, sweep width 12 mT, modulation 0.2 mT, 23 °C.

spectrum, but the width of the spectrum is narrower than that of nitroxide **7**, due to strong *J*-coupling (≈ 100 MHz) between the TEMPO and the BDPA radical.^[17,20] The other component is a nitroxide monoradical derived from **8**, where one of its three peaks is well separated from the spectrum of **8** (Figure 2, bottom, asterisk). The ratio of these two spectral components representing the biradical and the nitroxide monoradical, can be quantified by double integration of the EPR spectrum (Supporting Information).^[17] The amount of biradical **8**, relative to the nitroxide monoradical, was determined to be 80–85%. This was slightly lower than the reported amount (92%) for BDPA-TEMPO biradical **3** (Figure 1 B).^[17] Hence, we decided to evaluate the different methods that have been reported for preparation of BDPA radicals.

Optimization of the conditions used to prepare BDPA radicals

To find the optimal conditions for the synthesis of BDPA radicals, precursor **7** was reacted with various bases in different solvents to give a carbanion, which was treated with an oxidizing agent to yield biradical **8**. A subsequent extraction of the biradical from the reaction mixture was carried out without any further purification and an EPR spectrum was immediately recorded. The spectrum was doubly integrated, as described above, to obtain the amount of the biradical relative to the nitroxide monoradical. Figure 3 shows the results obtained for DMSO:*t*BuOH (9:1), DMSO, DMF and CH₂Cl₂ as a function of the base used (*t*BuOK, DBU and aq. NaOH). Both AgNO₃^[17,21a,23] and K₃Fe(CN)₆^[18,21b,c] the oxidizing agents commonly used for the oxidation of the carbanion to the radical, yielded similar results (Figure 3 and Figure S4). Reaction in DMSO:*t*BuOH (9:1) with *t*BuOK followed by oxidation with AgNO₃, the conditions reported for the generation of biradical **3**,^[17] led to ca. 85% of biradical **8**. Reactions in the polar aprotic solvents, DMF^[21b,c] and DMSO^[17,23] gave ca. 90% of biradical (Figure 3). However, the amount of the biradical dropped drastically to ca. 30%, when the reaction was carried out in a non-polar solvent (CH₂Cl₂), which required using DBU as a base,^[9c,20,22] since

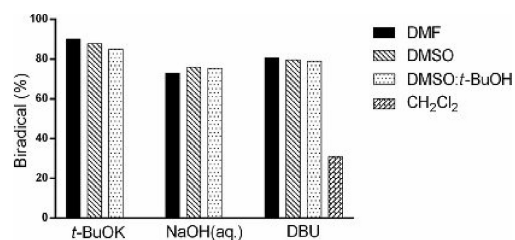


Figure 3. Optimization of the reaction conditions used to generate biradical **8**. Amount of the biradical is shown in different solvents (DMF, DMSO, DMSO:*t*BuOH 9:1, CH₂Cl₂) and for different bases (*t*BuOK, aq. NaOH, DBU), using AgNO₃ as the oxidizing agent.

*t*BuOK and aq. NaOH are not soluble in CH₂Cl₂. Use of DBU^[9c,20,22] and aq. NaOH^[21b] as the base instead of *t*BuOK in the polar solvents, gave biradical **8** in good yields (75–80%) (Figure 3). To conclude, the formation of the biradical was most efficient when the reaction was carried out in a polar aprotic solvent, using a strong base such as *t*BuOK. This was not unexpected, since a polar solvent should facilitate formation of the intermediate carbanion.

Persistence of BDPA radicals

The rapid decomposition of BDPA radicals that we unexpectedly observed prompted us to investigate the effect of various factors, such as solvents, temperature and oxygen, on the persistence of the BDPA radicals. As demonstrated above, EPR spectroscopy can be readily used to quantify the amount of biradical **8** relative to the nitroxide monoradical present in the sample. Hence, EPR was used to determine the rate of degradation of **8** under different conditions; this method was corroborated by UV-vis spectroscopy, following the absorption signal of the BDPA radical around 490 nm (Figure S7). Chromatographic purification of biradical **8** was carried out prior to these studies. However, the „purified“ samples contained only about 70% of the biradical, relative to the nitroxide monoradical, due to decomposition of the BDPA moiety during the purification process. Therefore, a pure sample of the biradical could not be obtained.

First, the solvent-dependent persistence of biradical **8** at 23 °C was investigated (Figure 4A). Solutions of **8** were prepared in 1,2-dichloroethane (DCE), MeOH and DMSO (5 mm) and their EPR spectra were recorded at various time intervals. These solvents were chosen to probe the effect of the solvent polarity. The initial rate of degradation of biradical **8** in different solvents was determined by plotting the amount of the biradical as a function of time (Supporting Information) and found to increase with decreasing polarity of the solvent (Figure 4A). The highest rate of decomposition was observed in DCE, with an initial rate of $(1.79 \pm 0.35) \cdot 10^{-7} \text{ Ms}^{-1}$. The degradation was significantly slower in MeOH and DMSO, $(1.79 \pm 0.03) \cdot 10^{-8} \text{ Ms}^{-1}$ and $(1.50 \pm 0.09) \cdot 10^{-8} \text{ Ms}^{-1}$, respectively.

The rate of degradation of biradical **8** in solution was also studied at different concentrations. Figure 5 shows the initial rates of degradation of **8** in DMSO for a series of solutions

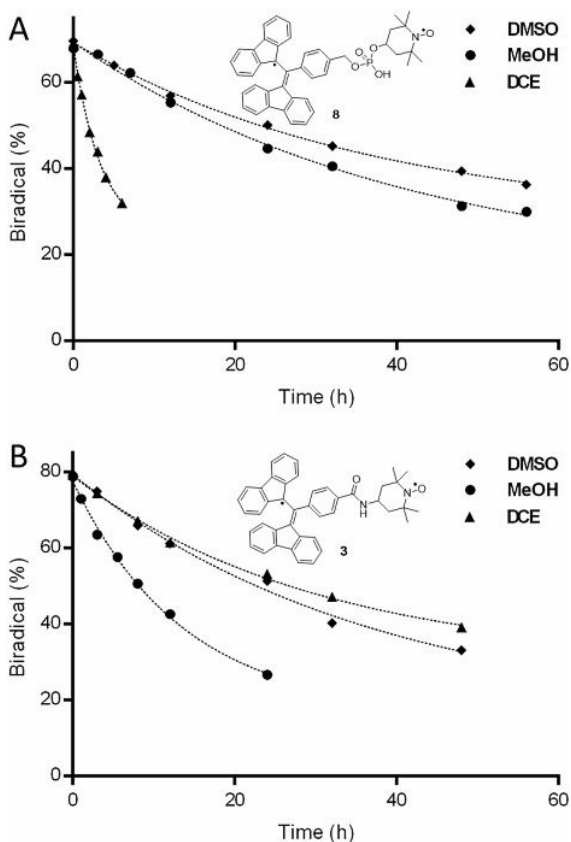


Figure 4. Rate of degradation of two different BDPA-nitroxide biradicals in various solvents (5 mM at 23 °C). The percentage of each biradical relative to a nitroxide monoradical, determined by double integration of its EPR spectrum, was plotted as a function of time and the initial rates of decomposition were calculated accordingly (see the Supporting Information). **A.** Biradical **8**; rates (Ms^{-1}): $(1.50 \pm 0.09) \cdot 10^{-8}$ (DMSO), $(1.79 \pm 0.03) \cdot 10^{-8}$ (MeOH), $(1.79 \pm 0.35) \cdot 10^{-7}$ (DCE). **B.** Biradical **3**; rates (Ms^{-1}): $(2.28 \pm 0.15) \cdot 10^{-8}$ (DMSO), $(7.18 \pm 0.64) \cdot 10^{-8}$ (MeOH), $(2.24 \pm 0.23) \cdot 10^{-8}$ (DCE). DCE is 1,2-dichloroethane.

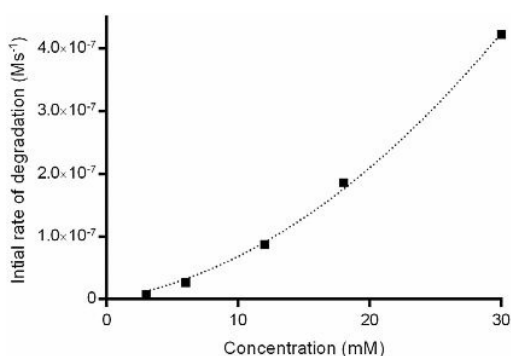


Figure 5. Concentration-dependent initial rates of biradical **8** in DMSO at 23 °C.

with varying concentration at 23 °C. The rate of degradation was found to increase non-linearly with increasing radical concentration. A 2-fold increase in the concentration led to a 3-

fold increase in the rate of degradation, which suggests a reaction order of ca. 1.6 with respect to biradical **8**. This result indicates that the well-known reaction with oxygen^[18] may not be the only degradation pathway since the oxidation is presumably a first/pseudo-first order reaction with respect to the biradical. One plausible explanation is that dimerization of BDPA radicals, which follows a second order kinetics, is also a pathway for degradation. Analysis of the decomposed products of biradical **8** by electrospray ionization (ESI) mass spectrometry indicated formation of multiple products, including the oxygenated products as previously described by Breslin and Fox,^[18] but the dimer of **8** was not found (Figure S12). Instead, masses approximately 1.8-fold the monomeric mass of **8** were observed which might be formed from a short-lived dimer. However, we were able to detect a BDPA dimer in the mass spectrum of decomposed products of BDPA radical **51**, obtained from compound **4** (Figure S13). This is, to our knowledge, the first reported indication that dimer formation is a significant pathway for decomposition of BDPA radicals. However, the fact that BDPA radicals dimerize is not surprising, since dimerization of the carbon-centered Gomberg's radical^[24] (triphenylmethyl/trityl) is well-known.^[25] In case of the trityl, introduction of substituents into the aromatic rings has been shown to prevent dimerization, with the Finland trityl being a good example.^[13]

To compare the persistence of biradical **8** with other BDPA radicals, the previously reported BDPA-TEMPO biradical **3**^[17] and unsubstituted BDPA radical **2** (Figure 1) were synthesized. These radicals are less polar than **8**. Figure 4B shows the solvent-dependent rate of degradation of biradical **3** in solution at 23 °C. It was found to be similar to that of **8**, although the solvent-dependence on the rates of decomposition was different. Both **3** and **8** have similar initial rate of degradation in DMSO ($(2.28 \pm 0.15) \cdot 10^{-8} \text{ Ms}^{-1}$) but different rates in DCE and MeOH. In DCE, biradical **3** was considerably more persistent than **8** with an initial rate of degradation $(2.24 \pm 0.23) \cdot 10^{-8} \text{ Ms}^{-1}$, whereas the opposite trend was observed in MeOH ($(7.18 \pm 0.64) \cdot 10^{-8} \text{ Ms}^{-1}$). The unsubstituted BDPA (**2**) showed a similar rate of degradation in solution (Figure S8) as the biradicals and the same solvent dependence as **3** ($(3.71 \pm 0.12) \cdot 10^{-8} \text{ Ms}^{-1}$ and $(4.64 \pm 0.18) \cdot 10^{-8} \text{ Ms}^{-1}$ for DCE and DMSO, respectively). In light of the concentration dependence of BDPA decomposition, a possible explanation for this compound-specific solvent effect is aggregation, since the polar biradical **8** degrades faster in a non-polar solvent and non-polar **2** and **3** are more unstable in a polar solvent. Aggregation would increase the rate of decomposition through dimer formation.

When the temperature was decreased, the degradation of **8** became slower, as expected. The rates decreased by ca. 6-fold for both DCE and MeOH by lowering the temperature from 23 °C to −18 °C (Figure S9A). On the other hand, the rate of degradation of **8** in DMSO at −18 °C was unexpectedly observed to be higher ($(3.86 \pm 0.62) \cdot 10^{-8} \text{ Ms}^{-1}$) than at 23 °C ($(1.50 \pm 0.09) \cdot 10^{-8} \text{ Ms}^{-1}$). One plausible explanation is that the radical aggregates due to accumulation of solutes at the crystal boundaries of the frozen DMSO. Quick-freezing in liquid nitrogen followed by incubation at −18 °C, in an attempt to pre-

vent possible aggregation, gave the same result. When the temperature of the DMSO solution was further lowered to -80°C , a significant increase in the persistence was observed; very little decomposition was observed after a month and after six months ca. 55% biradical remained (Figure S9B). Similar decomposition was observed in DCE after six months at -80°C but ca. 40% biradical remained in MeOH under the same condition. Biradical **8** was found to be stable in the solid state at -80°C , with no degradation for six months (Figure S9B). However, only ca. 38% biradical was intact after a month in the solid state at 23°C (Figure S10A). BDPA radical **2** was also observed to decompose in the solid state under exposure to air (Figure S10B), contrary to a previous report.^[14] This degradation was due to oxidation since no decomposition was observed when the solid samples were kept under vacuum for two weeks (Figure S10B). Hence, BDPA radicals cannot be termed 'stable', as once considered.^[14] However, the BDPA radicals showed no detectable decomposition when kept at -80°C in the solid state for longer periods of time (six months).

It is notable that exclusion of light, which has been reported to limit the reaction of BDPA radicals with oxygen,^[18] had no noticeable effects on the rate of decomposition. Formation of the same products was observed in presence and absence of light, both by ESI mass spectrometry and high-performance liquid chromatography (HPLC) (Figure S11B). Removal of oxygen by saturation with Ar and keeping the solution under a positive pressure of Ar, decreased the rate of degradation only by 1.5-2-fold (Figure S11A).

Conclusions

In conclusion, we have shed some light on the instability of BDPA radicals, both in solution and the solid state, which provides guidelines of how to handle BDPA radicals that are prepared for MAS-DNP NMR experiments. The strong electronic coupling between the BDPA and nitroxide radicals of biradical **8** enabled quantification of its rate of decomposition by EPR spectroscopy. The BDPA radicals reported here were found to be stable as solids at -80°C with no noticeable decomposition for six months, but under all other conditions we observed degradation in this time-frame. The radical concentration was found to significantly affect the rate of decomposition non-linearly; a 2-fold increase in the concentration resulted in a 3-fold increase in the rate of decomposition. A dimer of BDPA radical **S1** was detected by mass spectrometry, indicating that dimerization of BDPA radicals is one pathway of decomposition. The polarity of the solvent affected the rate of BDPA decomposition: a polar radical degraded faster in a non-polar solvent whereas a non-polar radical was less persistent in a polar solvent. In light of the concentration-dependent persistence of BDPA radicals, the solvent-dependent increase in the rate of decomposition is likely due to aggregation of the radicals, which would facilitate decomposition through dimer formation. When synthesizing new BDPA radicals that are more persistent as polarizing agents for DNP, it might be advisable to focus on structures that prevent dimer formation. Synthesis of

more stable BDPA radicals, keeping this design principle in mind, is underway in our laboratory and will be reported in due course.

Acknowledgements

This work is funded by Icelandic Research Fund (163393-052) from the Icelandic Centre for Research (Rannis). We thank Dr. S. Jonsdottir for assistance with collection of the NMR and HRMS (ESI) data; Dr. Frederic Mentink-Vigier for help with simulations and for valuable suggestions; and members of the Sigurdsson research group for helpful discussions.

Conflict of interest

The authors declare no conflict of interest.

Keywords: BDPA • dynamic nuclear polarization • EPR spectroscopy • radical stability • radicals

- [1] Q. Teng, *Structural Biology—Practical NMR Applications*, Springer US, 2013.
- [2] a) A. N. Smith, K. Märker, S. Hediger, G. De Paëpe, *J. Phys. Chem. Lett.* **2019**, *10*, 4652–4662; b) A. J. Rossini, A. Zagdoun, M. Lelli, A. Lesage, C. Copéret, L. Emsley, *Acc. Chem. Res.* **2013**, *46*, 1942–1951; c) A. G. M. Rankin, J. Trébosc, F. Pourpoint, J.-P. Amoureux, O. Lafon, *Solid State Nucl. Magn. Reson.* **2019**, *101*, 116–143.
- [3] A. S. Lilly Thankamony, J. J. Wittmann, M. Kaushik, B. Corzilius, *Prog. Nucl. Magn. Reson. Spectrosc.* **2017**, *102–103*, 120–195.
- [4] a) A. W. Overhauser, *Phys. Rev.* **1953**, *92*, 411–415; b) T. R. Carver, C. P. Slichter, *Phys. Rev.* **1953**, *92*, 212–213; c) T. V. Can, Q. Z. Ni, R. G. Griffin, *J. Magn. Reson.* **2015**, *253*, 23–35; d) T. Maly, G. T. Debelouchina, V. S. Bajaj, K.-N. Hu, C.-G. Joo, M. L. Mak-Jurkauskas, J. R. Sirigiri, P. C. A. v. d. Wel, J. Herzfeld, R. J. Temkin, R. G. Griffin, *J. Chem. Phys.* **2008**, *128*, 052211; e) B. Corzilius, *Paramagnetism in Experimental Biomolecular NMR*, The Royal Society of Chemistry, **2018**, pp. 219–257; f) D. Lee, S. Hediger, G. De Paëpe, *Solid State Nucl. Magn. Reson.* **2015**, *66–67*, 6–20; g) B. Corzilius, *Annu. Rev. Phys. Chem.* **2020**, *71*, 7.1–7.28.
- [5] K.-N. Hu, *Solid State Nucl. Magn. Reson.* **2011**, *40*, 31–41.
- [6] T. V. Can, M. A. Caporini, F. Mentink-Vigier, B. Corzilius, J. J. Walsh, M. Rosay, W. E. Maas, M. Baldus, S. Vega, T. M. Swager, R. G. Griffin, *J. Chem. Phys.* **2014**, *141*, 064202.
- [7] a) F. J. Mentink-Vigier, S. Vega, G. De Paëpe, *Phys. Chem. Chem. Phys.* **2017**, *19*, 3506–3522; b) F. Mentink-Vigier, Ü. Akbey, Y. Hovav, S. Vega, H. Oschkinat, A. Feintuch, *J. Magn. Reson.* **2012**, *224*, 13–21; c) K. R. Thurber, R. Tycko, *J. Chem. Phys.* **2012**, *137*, 084508.
- [8] F. Mentink-Vigier, Ü. Akbey, H. Oschkinat, S. Vega, A. Feintuch, *J. Magn. Reson.* **2015**, *258*, 102–120.
- [9] a) G. Mathies, M. A. Caporini, V. K. Michaelis, Y. Liu, K.-N. Hu, D. Mance, J. L. Zweier, M. Rosay, M. Baldus, R. G. Griffin, *Angew. Chem. Int. Ed.* **2015**, *54*, 11770–11774; *Angew. Chem.* **2015**, *127*, 11936–11940; b) F. Mentink-Vigier, G. Mathies, Y. Liu, A.-L. Barra, M. A. Caporini, D. Lee, S. Hediger, R. G. Griffin, G. De Paëpe, *Chem. Sci.* **2017**, *8*, 8150–8163; c) D. Wissler, G. Karthikeyan, A. Lund, G. Casano, H. Karoui, M. Yulikov, G. Menzildjian, A. C. Pinon, A. Porea, F. Engelke, S. R. Chaudhari, D. Kubicki, A. J. Rossini, I. B. Moroz, D. Gajan, C. Copéret, G. Jeschke, M. Lelli, L. Emsley, A. Lesage, O. Ouari, *J. Am. Chem. Soc.* **2018**, *140*, 13340–13349.
- [10] K.-N. Hu, V. S. Bajaj, M. Rosay, R. G. Griffin, *J. Chem. Phys.* **2007**, *126*, 044512.
- [11] K.-N. Hu, H.-h. Yu, T. M. Swager, R. G. Griffin, *J. Am. Chem. Soc.* **2004**, *126*, 10844–10845.
- [12] J. Schaefer, *eMagRes* (Eds.: R. K. Harris, R. L. Wasylishen), **2007**.
- [13] T. J. Reddy, T. Iwama, H. J. Halpern, V. H. Rawal, *J. Org. Chem.* **2002**, *67*, 4635–4639.

- [14] C. F. Koelsch, *J. Am. Chem. Soc.* **1957**, *79*, 4439–4441.
- [15] a) W. de Boer, *J. Low Temp. Phys.* **1976**, *22*, 185–212; b) J. Heckmann, W. Meyer, E. Radtke, G. Reicherz, S. Goertz, *Phys. Rev. B* **2006**, *74*, 134418.
- [16] a) F. Mentink-Vigier, S. Paul, D. Lee, A. Feintuch, S. Hediger, S. Vega, G. De Paëpe, *Phys. Chem. Chem. Phys.* **2015**, *17*, 21824–21836; b) F. Mentink-Vigier, I. Marín-Montesinos, A. P. Jagtap, T. Halbritter, J. van Tol, S. Hediger, D. Lee, S. T. Sigurdsson, G. De Paëpe, *J. Am. Chem. Soc.* **2018**, *140*, 11013–11019.
- [17] E. L. Dane, T. Maly, G. T. Debelouchina, R. G. Griffin, T. M. Swager, *Org. Lett.* **2009**, *11*, 1871–1874.
- [18] D. T. Breslin, M. A. Fox, *J. Phys. Chem.* **1993**, *97*, 13341–13347.
- [19] D. Griller, K. U. Ingold, *Acc. Chem. Res.* **1976**, *9*, 13–19.
- [20] L. F. Pinto, I. Marín-Montesinos, V. Lloveras, J. L. Muñoz-Gómez, M. Pons, J. Veciana, J. Vidal-Gancedo, *Chem. Commun.* **2017**, *53*, 3757–3760.
- [21] a) O. Haze, B. Corzilius, A. A. Smith, R. G. Griffin, T. M. Swager, *J. Am. Chem. Soc.* **2012**, *134*, 14287–14290; b) H. Nishide, N. Yoshioka, Y. Saitoh, R. Gotoh, T. Miyakawa, E. Tsuchida, *J. Macromol. Sci. Pure Appl. Chem.* **1992**, *29*, 775–786; c) R. Kuhn, A. Neugebauer, *Monatsh. Chem.* **1964**, *95*, 3–23.
- [22] J. L. Muñoz-Gómez, E. Monteagudo, V. Lloveras, T. Parella, J. Veciana, J. Vidal-Gancedo, *Org. Biomol. Chem.* **2015**, *13*, 2689–2693.
- [23] E. L. Dane, T. M. Swager, *J. Org. Chem.* **2010**, *75*, 3533–3536.
- [24] M. Gomberg, *J. Am. Chem. Soc.* **1900**, *22*, 757–771.
- [25] H. Lankamp, W. T. Nauta, C. MacLean, *Tetrahedron Lett.* **1968**, *9*, 249–254.

Manuscript received: March 1, 2020

Version of record online: May 12, 2020

Chemistry–A European Journal

Supporting Information

On the Limited Stability of BDPA Radicals

Sucharita Mandal and Snorri Th. Sigurdsson^{*[a]}

Supporting Information

Table of Contents

1. List of abbreviations.....	2
2. Synthetic procedures.....	2
General materials and methods	2
BDPA phosphoramidite 5	3
BDPA-nitroxide 6	6
BDPA-nitroxide 7	6
BDPA-nitroxide biradical 8	7
3. Optimization of reaction conditions to prepare BDPA radicals.....	8
4. Quantification of the amount of biradical vs. nitroxide monoradical	8
5. Persistence of BDPA radicals.....	9
6. MS analyses of BDPA-decomposition products	13
References	14

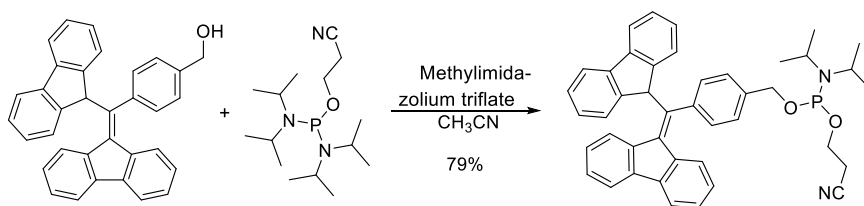
1. List of abbreviations

Aq.	Aqueous
BDPA	1,3-Bisdiphenylene-2-phenylallyl
Calcd	Calculated
DCE	1,2-Dichloroethane
DMSO	Dimethyl sulfoxide
EPR	Electron paramagnetic resonance
ESI	Electrospray ionization
HRMS	High resolution mass spectrometry
NMR	Nuclear magnetic resonance
Pet ether	Petroleum ether
Satd.	Saturated
TEMPO	2,2,6,6-Tetramethylpiperidine-1-oxyl
TFA	Trifluoroacetic acid
TLC	Thin layer chromatography

2. Synthetic procedures

General materials and methods

Chemicals were purchased from Sigma-Aldrich Co. or ChemGenes and were used without further purification. All moisture sensitive reactions were carried out in oven-dried glassware under an inert atmosphere of Ar. Thin layer chromatography (TLC) was carried out using glass plates pre-coated with silica gel (Kieselgel 60 F₂₅₄, 0.2 mm, Silicycle), using UV light for visualization. Silica gel for flash chromatography (230-400 mesh, 60 Å) was purchased from Silicycle. ¹H-, ¹³C- and ³¹P-NMR spectra were recorded at the frequencies stated, using deuterated solvents as internal standards on a Bruker Avance 400 spectrometer. ³¹P-NMR chemical shifts are reported relative to 85% H₃PO₄ as an external standard. Radicals show broadening and loss of NMR signals due to their paramagnetic nature and therefore, those NMR spectra are not shown. Mass spectrometric analyses of all organic compounds were performed on an ESI-HRMS (Bruker, MicrOTOF-Q). HPLC chromatograms were recorded on a Beckman Coulter Gold HPLC system using a NUCLEOSIL C18 4.6 x 150 mm analytical column with UV detection at 254 nm. Solvent gradients for analytical RP-HPLC were run at 1.0 mL/min using the following gradient program: solvent A, 0.1% TFA in H₂O; solvent B, CH₃CN; 0-2 min isocratic 50% B, 2-12 min linear gradient 50-100% B, 12-14 min isocratic 100% B, 14-16 min linear gradient 100-50% B, 16-17 min isocratic 50% B.



BDPA phosphoramidite 5. To a solution of alcohol **4** (100 mg, 0.22 mmol) in anhydrous CH₃CN (2 mL) were added *N*-methylimidazolium triflate (58 mg, 0.24 mmol) and 2-cyanoethyl-*N,N,N,N*-tetraisopropylphosphane (0.15 mL, 0.45 mmol) and the resulting solution stirred for 2 h. H₂O (10 mL) was added and the mixture extracted with CH₂Cl₂ (3 x 10 mL). The combined organic layers were washed with brine (3 x 10 mL), dried over Na₂SO₄ and concentrated *in vacuo*. The residue was purified by flash-column chromatography using a gradient elution (pet ether:EtOAc:Et₃N; 93:5:2 to 88:10:2) to give **5** (114 mg, 79%) as a reddish-brown solid.

TLC (Silica gel, pet ether:EtOAc, 70:30 + 2-3 drops of Et₃N): *R_f* (**4**) = 0.3, *R_f* (**5**) = 0.7

¹H NMR (400 MHz, CDCl₃): δ = 8.43 (d, *J* = 7.9 Hz, 1H), 7.89 (d, *J* = 7.6 Hz, 1H), 7.75 (d, *J* = 7.6 Hz, 1H), 7.66 (d, *J* = 7.6 Hz, 2H), 7.61 (d, *J* = 7.5 Hz, 2H), 7.47 (td, *J* = 7.5, 0.9 Hz, 1H), 7.40 – 7.31 (m, 3H), 7.30 – 7.20 (m, 3H), 7.00 (d, *J* = 7.7 Hz, 2H), 6.82 (td, *J* = 7.4, 1.2 Hz, 1H), 6.67 (d, *J* = 7.9 Hz, 2H), 6.50 (s, 1H), 5.94 (d, *J* = 8.0 Hz, 1H), 4.68 – 4.49 (m, 2H), 3.84 – 3.70 (m, 2H), 3.68 – 3.52 (m, 2H), 2.55 (td, *J* = 6.4, 3.1 Hz, 2H), 1.20 (d, *J* = 6.8 Hz, 6H), 1.12 (d, *J* = 6.8 Hz, 6H) ppm.

¹³C NMR (101 MHz, CDCl₃): δ = 144.97, 144.25, 142.07, 141.41, 139.89, 139.02, 138.81, 138.13, 138.06, 137.89, 136.31, 128.52, 128.28, 127.57, 127.54, 127.39, 127.05, 126.65, 126.08, 125.61, 125.20, 120.10, 120.03, 119.17, 117.72, 65.49, 65.30, 58.66, 58.47, 52.88, 43.35, 43.23, 24.80, 24.72, 24.68, 24.61, 20.47, 20.40 ppm.

³¹P NMR (162 MHz, CDCl₃): δ = 148.84 ppm.

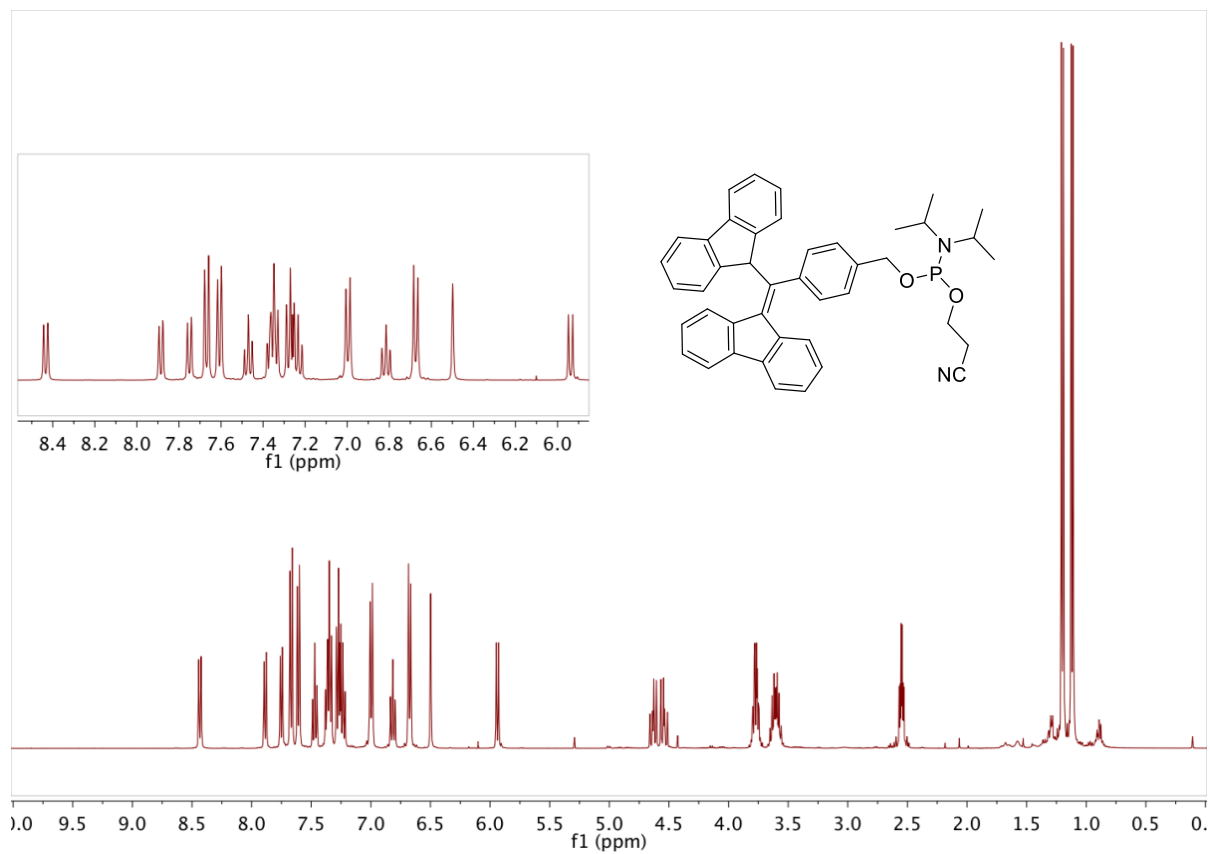


Figure S1. ¹H-NMR spectrum of compound 5.

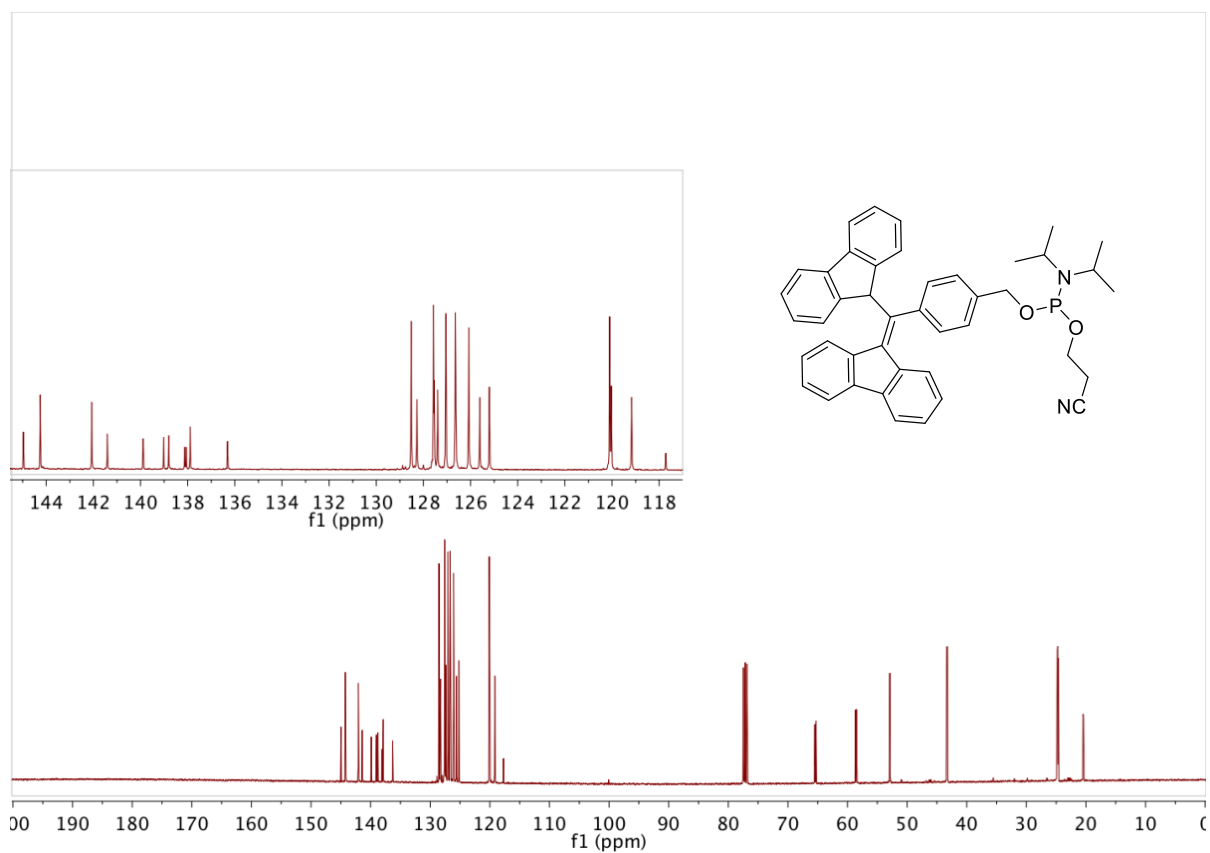


Figure S2. ¹³C-NMR spectrum of compound 5.

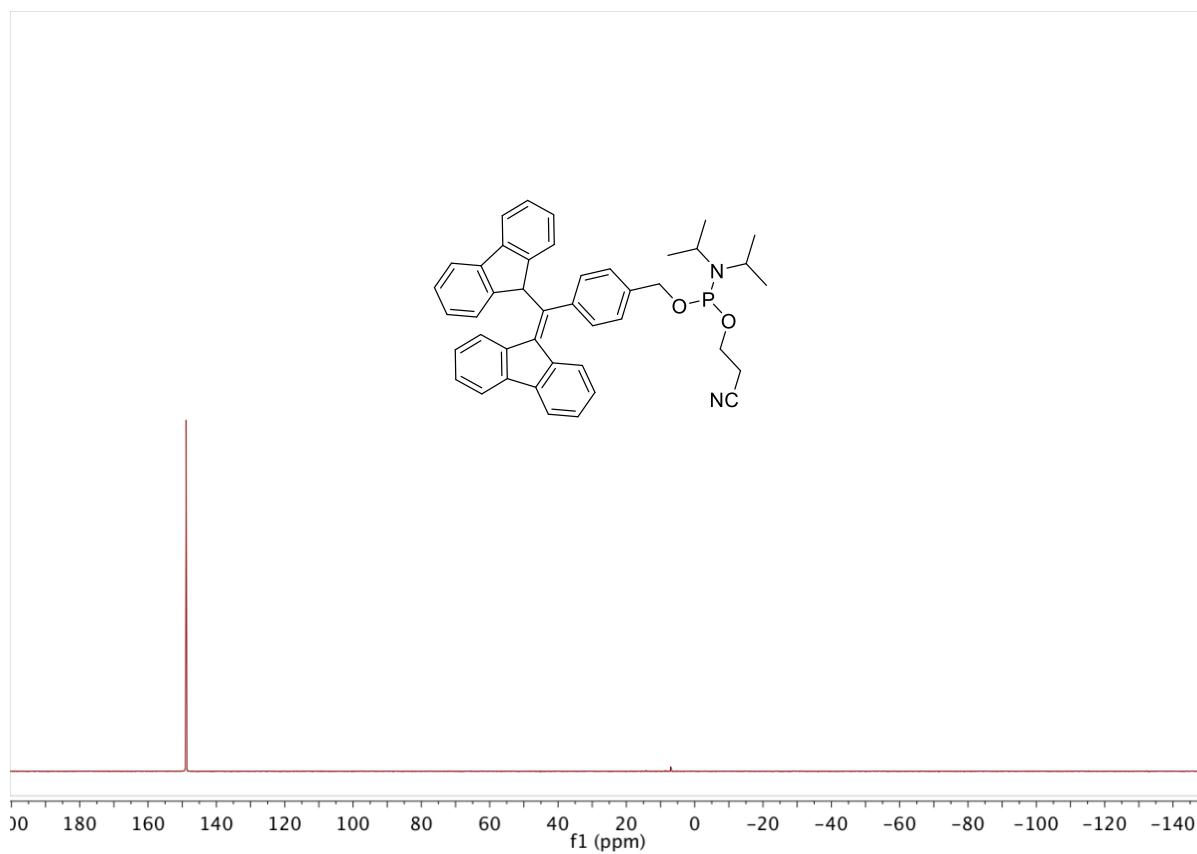
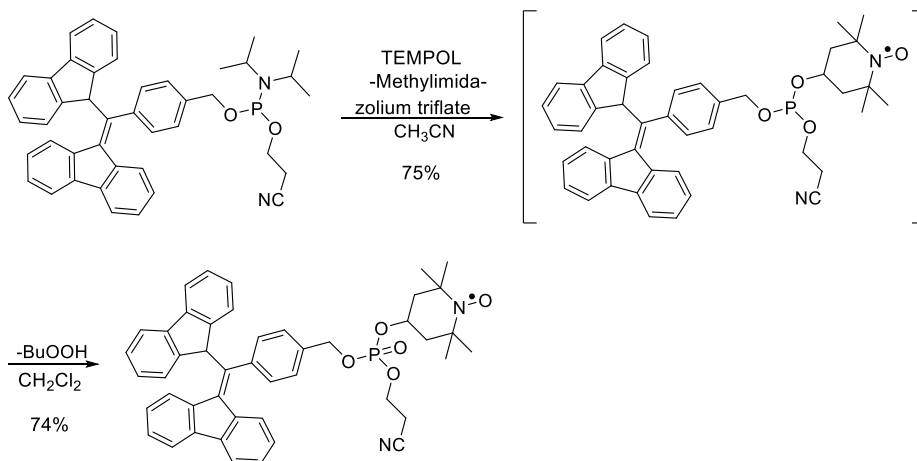


Figure S3. ^{31}P -NMR spectrum of compound 5.



BDPA-nitroxide 6. To a solution of **5** (200 mg, 0.31 mmol) in anhydrous CH₃CN (3 mL) were added 4-hydroxy-TEMPO (80 mg, 0.46 mmol) and *N*-methylimidazolium triflate (72 mg, 0.31 mmol) and the resulting solution stirred for 2 h. H₂O (10 mL) was added and the mixture extracted with CH₂Cl₂ (3 x 10 mL). The combined organic layers were washed with brine (3 x 10 mL), dried over Na₂SO₄ and concentrated *in vacuo*. The product was purified by flash-column chromatography using a gradient elution (pet ether:EtOAc:Et₃N; 73:25:2 to 68:30:2) to give **6** (166 mg, 75%) as a reddish-brown solid. This compound was used directly in the next step without further analysis.

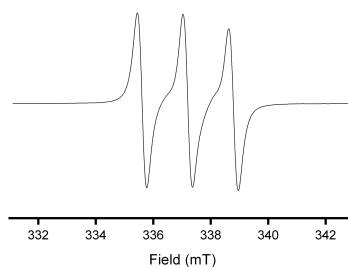
TLC (Silica gel, pet ether:EtOAc, 70:30 + 2-3 drops of Et₃N): R_f (**5**) = 0.7, R_f (**6**) = 0.3

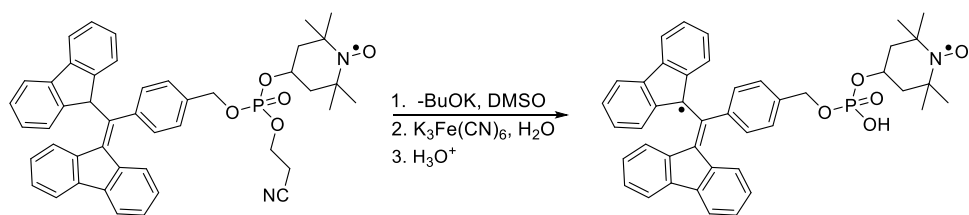
BDPA-nitroxide 7. To a solution of **6** (200 mg, 0.28 mmol) in CH₂Cl₂ (1 mL) was added *t*-BuOOH (0.13 mL, 1.39 mmol, 70% in H₂O) and the resulting solution stirred for 30 min. H₂O (5 mL) was added and the mixture extracted with CH₂Cl₂ (3 x 5 mL). The combined organic layers were washed with brine (3 x 5 mL), dried over Na₂SO₄ and concentrated *in vacuo*. The product was purified by flash-column chromatography using a gradient elution (pet ether:EtOAc; 25:75 to 0:100) to give **7** (150 mg, 74%) as a reddish-brown solid.

TLC (Silica gel, pet ether:EtOAc, 25:75): R_f (**6**) = 0.8, R_f (**7**) = 0.2

HRMS (ESI): m/z calcd for C₄₆H₄₄N₂O₅P+Na⁺: 758.2880 [M+Na]⁺; found 758.2864.

EPR:





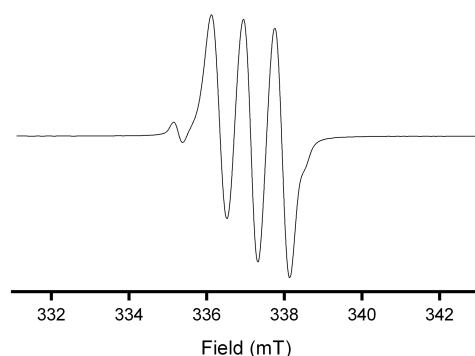
BDPA-nitroxide biradical 8. To a solution of **7** (15 mg, 0.02 mmol) in DMSO (3 mL) was added $t\text{-BuOK}$ (12 mg, 0.10 mmol) and the resulting solution stirred at 21 °C for 1 h. A solution of $\text{K}_3\text{Fe}(\text{CN})_6$ (34 mg, 0.10 mmol) in H_2O (1 mL) was added and the brown solution stirred for 1 min, followed by another addition of H_2O (10 mL) and extraction with EtOAc (2 x 20 mL). The combined organic layers were washed with satd. aq. NH_4Cl (50 mL), dried over Na_2SO_4 and concentrated *in vacuo*. The crude product was purified by TLC using 0.1% acetic acid in $\text{CH}_2\text{Cl}_2:\text{MeOH}$ (85:15) to give **8** (7.5 mg, 55%) as a reddish-brown solid.

TLC (Silica gel, $\text{CH}_2\text{Cl}_2:\text{MeOH}$, 95:5): R_f (**7**) = 0.6, R_f (**8**) = 0.0

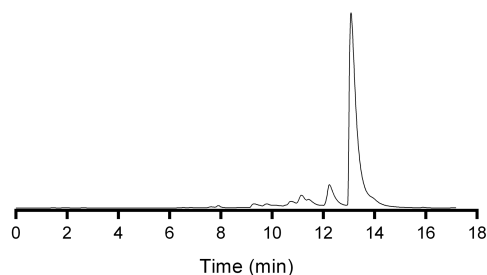
(Silica gel, $\text{CH}_2\text{Cl}_2:\text{MeOH}:\text{AcOH}$, 85:15:0.1): R_f (**8**) = 0.3

HRMS (ESI): m/z calcd for $\text{C}_{43}\text{H}_{39}\text{NO}_5\text{P-H}^-$: 680.2571 $[\text{M-H}]^-$; found: 680.2561.

EPR:



HPLC:



3. Optimization of reaction conditions to prepare BDPA radicals

To find the optimal conditions for preparation of BDPA radicals, a similar protocol was used as described above for the synthesis of biradical **8**. Compound **7** (1 mg, 0.0014 mmol) was first treated with a base (*t*-BuOK, aq. NaOH or DBU; 0.007 mmol) in DMSO, DMSO:*t*-BuOH (9:1), DMF or CH₂Cl₂ (0.5 mL). The resulting carbanion was oxidized to the radical by either aq. K₃Fe(CN)₆ or AgNO₃ (100 mM, 70 μL) except for the reaction in CH₂Cl₂ where the oxidation was carried out using a solution of AgNO₃ in CH₃CN (1 M, 3 μL).^[1] The solution was rapidly extracted in EtOAc, a few drops of MeOH were added and an EPR spectrum was recorded after bubbling Ar through the solution for one minute. The amount of biradical **8** was quantified as described in the next section.

The results obtained for DMSO:*t*-BuOH (9:1), DMSO, DMF and CH₂Cl₂ as a function of the base (*t*-BuOK, DBU and aq. NaOH), using AgNO₃ as the oxidant are described in the main text (**Figure 3**). Similar results were obtained when K₃Fe(CN)₆ was used as the oxidant instead of AgNO₃ (**Figure S4**).

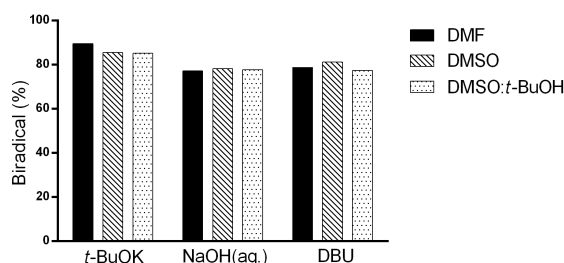


Figure S4. Optimization of the reaction conditions used to generate biradical **8**. Amount of the biradical is shown in different solvents (DMF, DMSO, DMSO:*t*-BuOH 9:1) and for different bases (*t*-BuOK, aq. NaOH, DBU), using K₃Fe(CN)₆ as the oxidizing agent.

4. Quantification of the amount of biradical vs. nitroxide monoradical

The amount of the biradical **8**, relative to the nitroxide monoradical resulting from degradation of the BDPA radical of **8**, can be quantified by double integration of the EPR spectrum.^[2] **Figure S5A** shows an EPR spectrum of biradical **8** and the first integration of this spectrum is shown in **Figure S5B**. The small peak between 335-336 mT in the first integrated spectrum, which is one of the three peaks of the nitroxide-derived monoradical, was fitted to a Gaussian and two more Gaussians with same parameters were added as shown in **Figure S5B**. These three Gaussians were then subtracted from the whole spectrum and the subtracted spectrum was assigned to the biradical. Area of the gaussians (g) and the biradical (b) was then determined by integration.

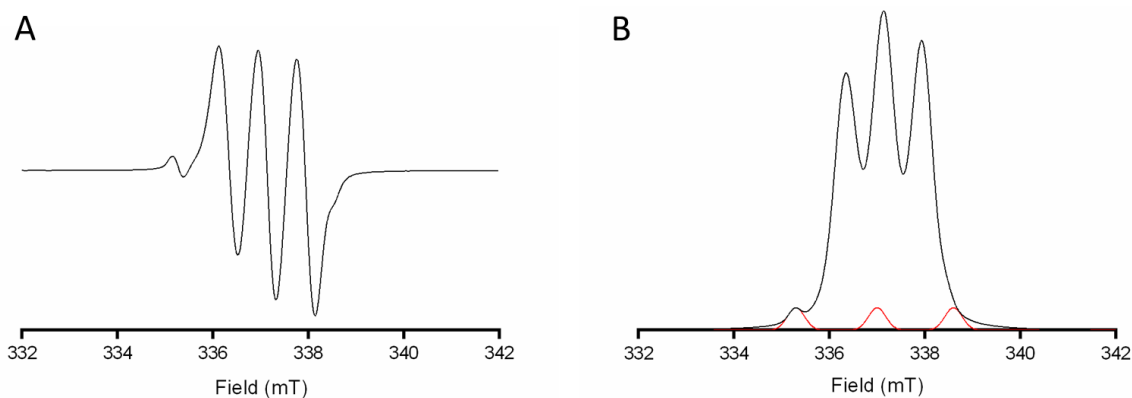


Figure S5. **A.** EPR spectrum of biradical **8**. **B.** First integration of the EPR spectrum (black). The red curve shows the fitted gaussians for the three peaks of the nitroxide monoradical.

Since the biradical signal originates from two electrons, the area of the biradical was divided by 2 to get the molar ratio for the biradical relative to the nitroxide monoradical: $b_{1/2} = \frac{b}{2}$. Hence, percentage of the biradical vs the monoradical was determined by: $\frac{b_{1/2}}{b_{1/2} + g} \cdot 100$.

5. Persistence of BDPA radicals

The persistence of BDPA radicals was investigated under several different conditions. The rate of degradation was primarily determined by recording EPR spectra at various time intervals. The biradical samples for the stability experiments were prepared in the following manner: A stock solution (10 mM) of the radicals were prepared either in MeOH (biradical **8**) or CH₂Cl₂ (biradical **3** and BDPA radical **2**). Aliquots (10 μL) were removed and distributed into microfuge tubes. The solvent was removed in a vacuum concentrator and the solid was redissolved in MeOH, DMSO or DCE (20 μL). Commercially purchased solvents were used for investigation of biradicals **8** and **3** without additional drying and purification. However, solvents were dried using molecular sieves (3 Å) prior to their use for the stability studies of BDPA radical **2**. A number of solid samples were not dissolved in order to explore the persistence in the solid state. The solid and dissolved samples were kept at 23 °C, -18 °C and -80 °C, in the presence of air. At various time intervals, one sample vial was removed and analysed by EPR spectroscopy. Samples in the solid state were dissolved in DMSO (20 μL) before recording the EPR spectra. Ar was bubbled through the solutions for 3-4 sec prior to the EPR measurements.

The effect of oxygen on the persistence of **8** was also investigated. Instead of using a glovebox, a flask was evacuated under vacuum and refilled with argon three times. The flask was charged with a solution of the radical that had previously been deoxygenated by bubbling with argon. Aliquots were removed under a positive pressure of Ar for analysis by EPR spectroscopy.

After the EPR measurements, the spectra were doubly integrated and the percentage of the biradical present in the sample was determined as discussed earlier (see **Section 4**, SI). The amount of the biradical was plotted as a function of time and the data points were fitted to an exponential one-phase decay with the model, $y = (y_0 - a)exp(-k \cdot x)$. The model was found to be in excellent agreement with the data points, with a $R^2 > 0.99$. From the fitting curve, the initial rate of degradation was calculated by drawing a tangent at time = 0, as shown in **Figure S6**. All the experiments were repeated a minimum three times and the standard deviation was calculated from different sets.

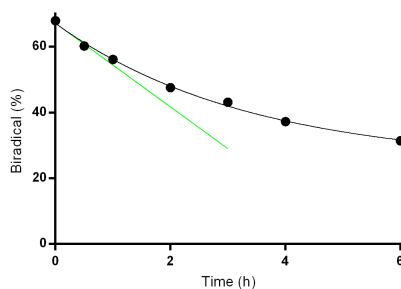


Figure S6. The decomposition of the biradical **8** in DCE (5 mM, 23 °C) (black). The data points were fitted to an exponential one-phase decay. A tangent line of the fitting curve was drawn at $t = 0$ (green), to calculate the initial rate of degradation.

The persistence of BDPA radicals can also be investigated by UV-vis spectroscopy, as they absorb strongly in the visible region.^[3] A solution of biradical **8** (5 mM) was prepared in DCE and UV-vis spectra were recorded at different time intervals after diluting the aliquots 125-fold. **Figure S7A** shows the UV-vis spectra of **8** at various times. The peak between 400 – 550 nm arises from the absorption of the BDPA radical and was observed to decrease with time. The rate of degradation was determined by plotting the absorbance of **8** at 490 nm (λ_{max}) as a function of time (**Figure S7B**, left y-axis). The results obtained by EPR spectroscopy under the same condition (5 mM solution of **8** in DCE at 23 °C) were also included in the same plot (**Figure S7B**, right y-axis); the rates of degradation obtained by UV-vis and EPR spectroscopy are very similar.

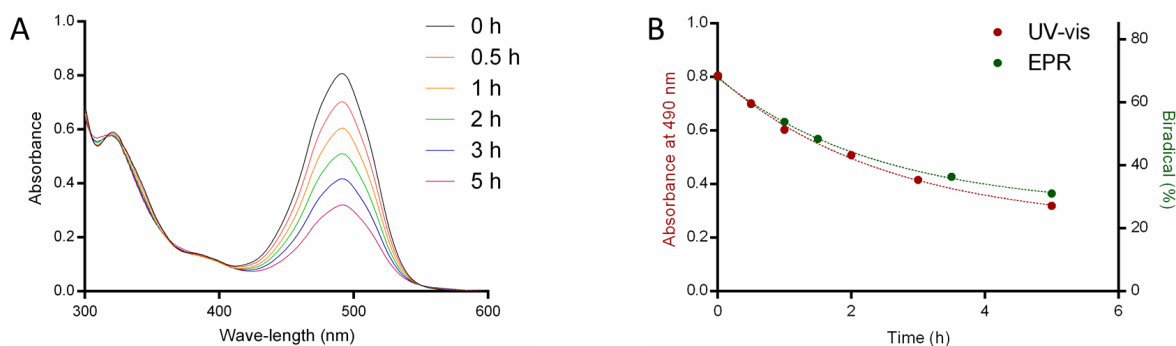


Figure S7. The rate of degradation of biradical **8** in DCE (5 mM) at 23 °C determined by UV-vis spectroscopy. **A.** The UV-vis absorbance spectra of biradical **8** at different times. **B.** The absorbance of the BDPA radical at 490 nm (left y-axis) and the percentage of the biradical relative to the nitroxide monoradical as determined by EPR spectroscopy (right y-axis), were plotted as a function of time.

The rate of the decomposition in solution at 23 °C for both biradical **8** and **3** is shown in **Figure 4**. **Figure S8** shows the results for the unsubstituted BDPA (**2**) at 23 °C in solution which was found to have an initial rate of degradation $(4.64 \pm 0.18) \cdot 10^{-8} \text{ Ms}^{-1}$ in DMSO and $(3.71 \pm 0.12) \cdot 10^{-8} \text{ Ms}^{-1}$ in DCE.

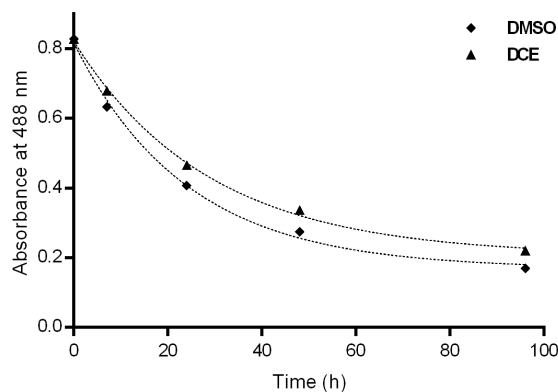


Figure S8. Rate of degradation of BDPA radical (**2**) in solution monitored by UV-vis spectroscopy (5 mM at 23 °C). The initial rates are as follows: $(4.64 \pm 0.18) \cdot 10^{-8} \text{ Ms}^{-1}$ in DMSO and $(3.71 \pm 0.12) \cdot 10^{-8} \text{ Ms}^{-1}$ in DCE.

The degradation of **8** in MeOH, DMSO and DCE at -18 °C is shown in **Figure S9A**. Ca. 6-fold decrease in the rate of degradation was observed for MeOH and DCE compared to 23 °C. However, the rate in DMSO at -18 °C was found to be higher $((3.86 \pm 0.62) \cdot 10^{-8} \text{ Ms}^{-1})$ than at 23 °C $((1.50 \pm 0.09) \cdot 10^{-8} \text{ Ms}^{-1})$, presumably due to aggregation (see discussion in the main text). The **Figure S9B** shows the degradation at -80 °C, over a month.

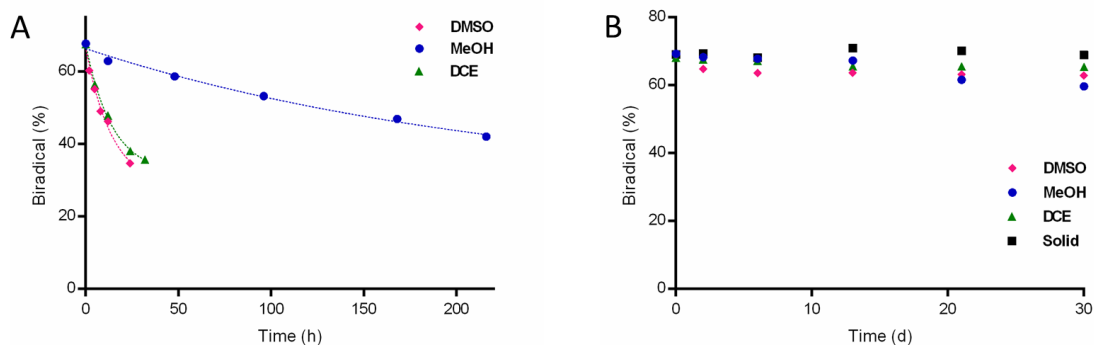


Figure S9. A. The rate of decomposition of biradical **8** at -18 °C in different solvents (5 mM). The initial rates are as follows: $(3.86 \pm 0.62) \cdot 10^{-8} \text{ Ms}^{-1}$ in DMSO, $(3.75 \pm 0.45) \cdot 10^{-8} \text{ Ms}^{-1}$ in DCE and $(2.46 \pm 0.6) \cdot 10^{-9} \text{ Ms}^{-1}$ in MeOH. **B.** The degradation of biradical **8** at -80 °C as a solid and after dissolution in different solvents (5 mM). After six months, ~40% biradical was present in MeOH and ~55% in DCE and DMSO. Negligible decomposition was observed for the solid samples.

The persistence of biradical **8** was also determined in the solid state at 23 °C where it was considerably more stable, although only ca. 38% biradical remained after a month (**Figure S10A**). The unsubstituted BDPA (**2**) also shows decomposition in the solid-state (**Figure S10B**) which was found to be due to oxidation, since no decomposition was observed when kept under vacuum for 2 weeks (**Figure S10B**).

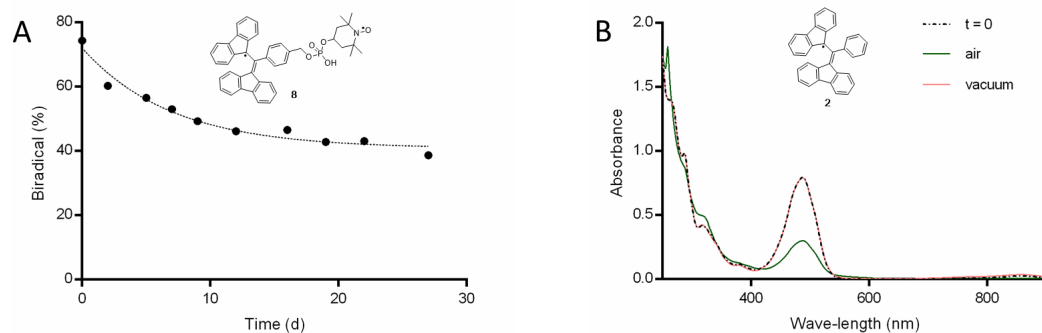


Figure S10. The decomposition of BDPA radicals at 23 °C in the solid state. **A.** The degradation for biradical **8** for a month. **B.** The UV-vis spectra of solid samples of the unsubstituted BDPA (**2**), kept under air and vacuum after 14 days.

In solution, deoxygenation with Ar led to a minor improvement in results with 1.5-2-fold decrease in rate of degradation as shown for biradical **8** in **Figure S11A**. Exclusion of light had no visible effects on the decomposition, neither the rate nor the profile of the degradation products (**Figure S11B**).

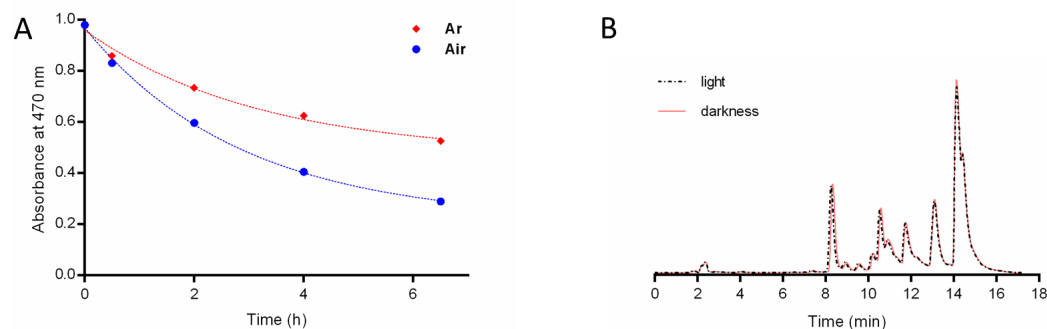


Figure S11. A. The degradation of the biradical **8** (5 mM) at 23 °C in DCE monitored by UV-vis spectroscopy under air vs argon. **B.** HPLC chromatograms of solutions of biradical **8** in MeOH kept in presence and absence of light for 24 h.

6. MS analyses of BDPA-decomposition products

In an attempt to provide evidence for dimer formation, the decomposition products of BDPA radicals were analysed by ESI mass spectrometry. **Figure S12** shows the mass spectrum of the decomposition products of biradical **8** in the negative-ion mode. Formation of multiple products was observed, including the oxygenated compounds (masses 695.2378 and 697.2533) as described by Breslin and Fox,^[3] but the mass corresponding to the dimer was not found. However, masses ca. 1.8 -fold the mass of **8** (between m/z 1100-1300) can be observed that might arise from a short-lived dimer.

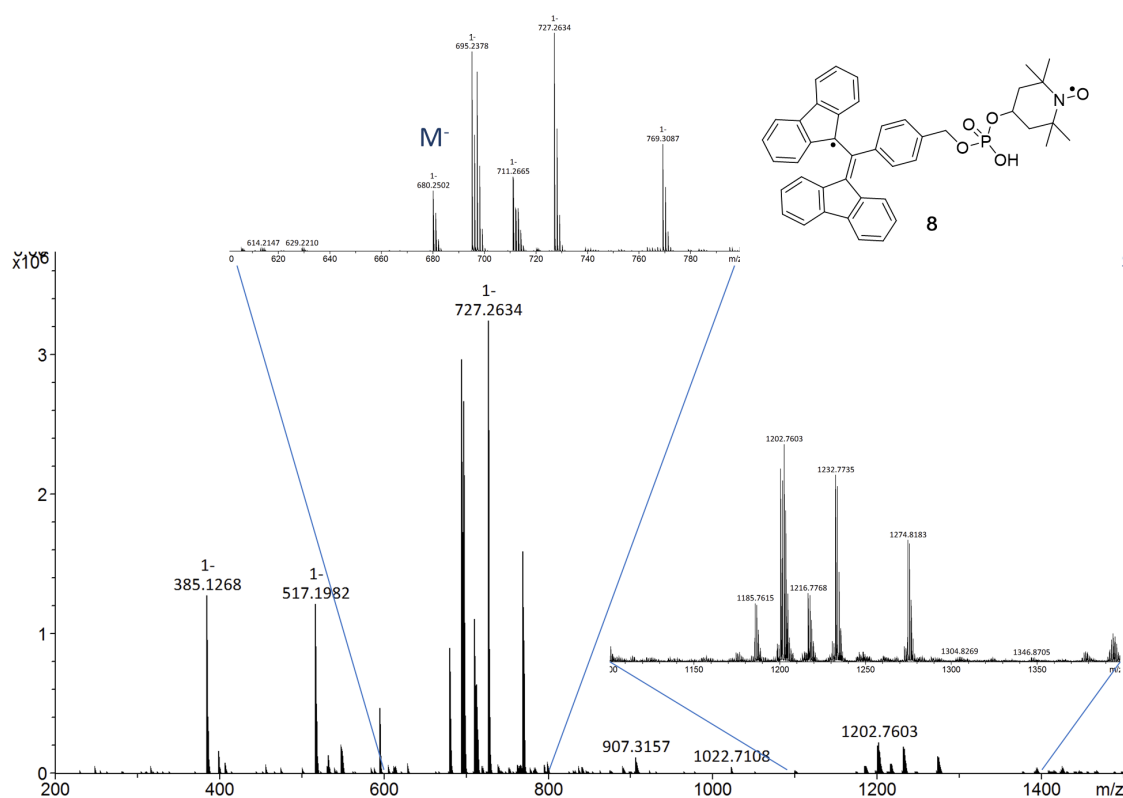


Figure S12. The HRMS (ESI) spectrum of the decomposition products of biradical **8** in MeOH (30 mM) at 23 °C, recorded in a negative-ion mode. All the masses shown in the spectrum come from the sample.

Figure S13 shows the mass spectrum of the decomposition products of BDPA radical **S1** in the positive ion mode. The similar oxygenated products as described for biradical **8** can be seen as well. Here, the mass of the dimer (917.3384) could be detected.

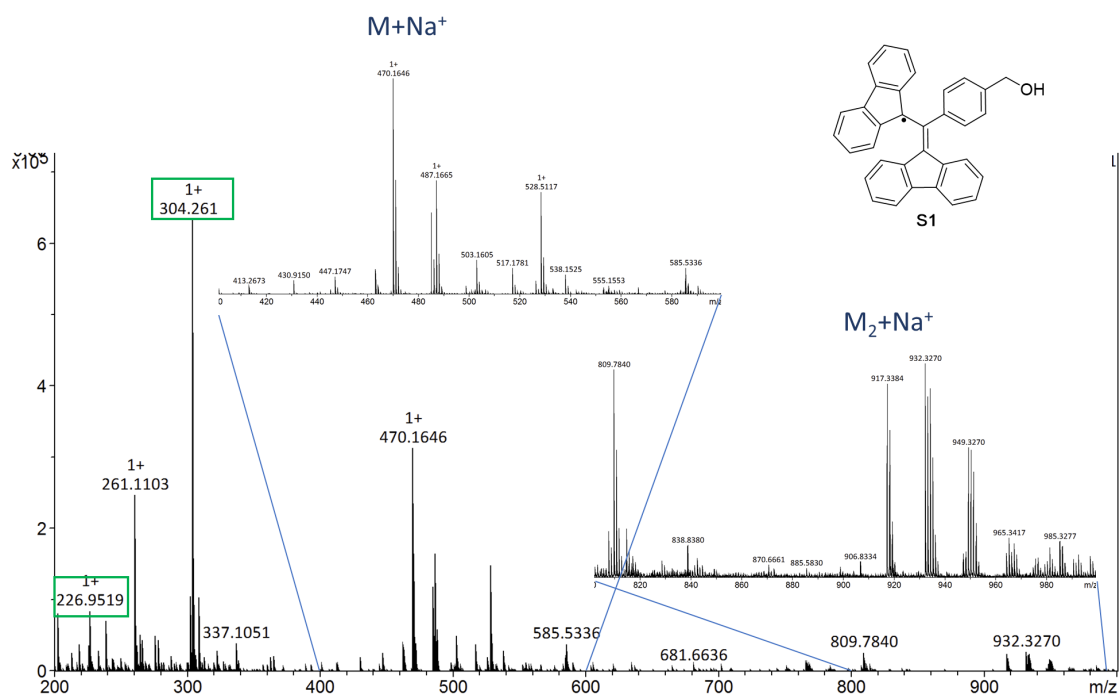


Figure S13. The HRMS (ESI) spectrum of the decomposition products of the BDPA radical **S1** in MeOH (5 mM) at 23 °C, recorded in a positive-ion mode. The green boxes indicate the peaks of the reference compounds.

References

- [1] D. Wisser, G. Karthikeyan, A. Lund, G. Casano, H. Karoui, M. Yulikov, G. Menzildjian, A. C. Pinon, A. Porea, F. Engelke, S. R. Chaudhari, D. Kubicki, A. J. Rossini, I. B. Moroz, D. Gajan, C. Copéret, G. Jeschke, M. Lelli, L. Emsley, A. Lesage, O. Ouari, *J. Am. Chem. Soc.* **2018**, *140*, 13340-13349.
- [2] E. L. Dane, T. Maly, G. T. Debelouchina, R. G. Griffin, T. M. Swager, *Org. Lett.* **2009**, *11*, 1871-1874.
- [3] D. T. Breslin, M. A. Fox, *J. Phys. Chem.* **1993**, *97*, 13341-13347.

Paper II


 Cite this: *Chem. Commun.*, 2020, 56, 13121

 Received 17th July 2020,
Accepted 21st September 2020

DOI: 10.1039/d0cc04920d

rsc.li/chemcomm

Water-soluble BDPA radicals with improved persistence†

 Sucharita Mandal and Snorri Th. Sigurdsson *

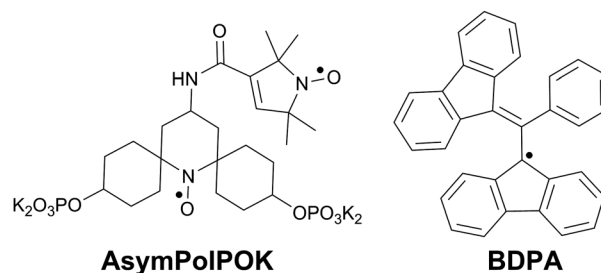
1,3-Bis(diphenylene)-2-phenylallyl (BDPA) radicals are promising polarizing agents for increasing the sensitivity of NMR spectroscopy through dynamic nuclear polarization (DNP), but have low persistence and solubility in aqueous media. New tetraalkyl/aryl-ammonium derivatives of BDPA are soluble in polar solvents and are highly persistent, with 5–20-fold lower initial rates of degradation than BDPA.

Solid-state nuclear magnetic resonance (ssNMR) spectroscopy with magic angle spinning (MAS), is a valuable technique to acquire high-resolution structural information of heterogeneous systems, such as amyloid fibrils,¹ membrane proteins² and heterogeneous catalysts.³ However, a major challenge of NMR spectroscopy is its low sensitivity due to the small population difference of nuclear spins in the ground state *vs.* the excited state under an applied magnetic field. For instance, this difference is only $\sim 0.01\%$ for protons at 9.4 T (400 MHz) and 100 K. This low nuclear polarization can, however, be significantly increased using dynamic nuclear polarization (DNP), leading to enhanced NMR signals. DNP enables the transfer of polarization to nuclei from unpaired electrons, for which the polarization in a magnetic field is more than two to three orders of magnitude higher than that of the nuclear spins, using microwave irradiation.⁵ Persistent organic radicals are commonly introduced into samples during DNP experiments as the source of unpaired electrons.

Nitroxides are the most common choice of radicals for use as polarizing agents, due to their high persistence, relative ease of synthesis and electron paramagnetic resonance (EPR) properties. In particular, the broad EPR linewidth of the nitroxides makes them highly effective for the cross-effect (CE), which is the most efficient polarization transfer mechanism for MAS–DNP NMR.⁶ CE is a three-spin mechanism involving two electrons and a nucleus, and requires a polarizing agent that

has an EPR linewidth broader than the nuclear Larmor frequency.⁶ Therefore, biradicals that have two strongly coupled electron spins are more effective than monoradicals.⁸ Nitroxide biradicals with improved DNP performance have been prepared in years past, mostly by trial and error.⁹ More recently, advanced simulations have been applied for the design of more efficient polarizing agents.⁴ An example is **AsymPolPOK** (Fig. 1), which is currently one of the most efficient nitroxide biradicals for DNP; the two nitroxides are linked by a short tether and have an orthogonal orientation relative to each other, resulting in large *J*-coupling and dipolar interactions between the two electron spins.⁴

Recent technological advancements have enabled DNP NMR at high magnetic fields (≥ 18.8 T).¹⁰ However, the efficiency of nitroxides, as polarizing agents, decreases substantially with increasing magnetic field, due to a considerable broadening of their EPR spectra.^{6b} In contrast, the carbon-centered Finland trityl¹¹ and 1,3-bis(diphenylene)-2-phenylallyl (**BDPA**)⁷ (Fig. 1) radicals have significantly narrower EPR linewidths than nitroxides¹² and longer electron relaxation rates,¹³ making them promising polarizing agents at high magnetic fields. When connected to a nitroxide, they give significantly higher signal enhancements than nitroxide biradicals,¹⁴ because the EPR transition of the narrow-line, slow-relaxing carbon radical can be efficiently saturated while the dipolar-coupled fast-relaxing nitroxide ensures multiple polarization transfers to the nuclei.^{14b,15} Another advantage of these carbon-based heteromeric biradicals


 Fig. 1 Structures of **AsymPolPOK**⁴ and **BDPA**⁷ radicals.

University of Iceland, Department of Chemistry, Science Institute, Dunhaga 3, Reykjavik 107, Iceland. E-mail: snorrisi@hi.is

† Electronic supplementary information (ESI) available. See DOI: 10.1039/d0cc04920d

over most nitroxide biradicals is that they produce lower nuclear depolarization, a process that decreases the effective gain in sensitivity.^{4,16}

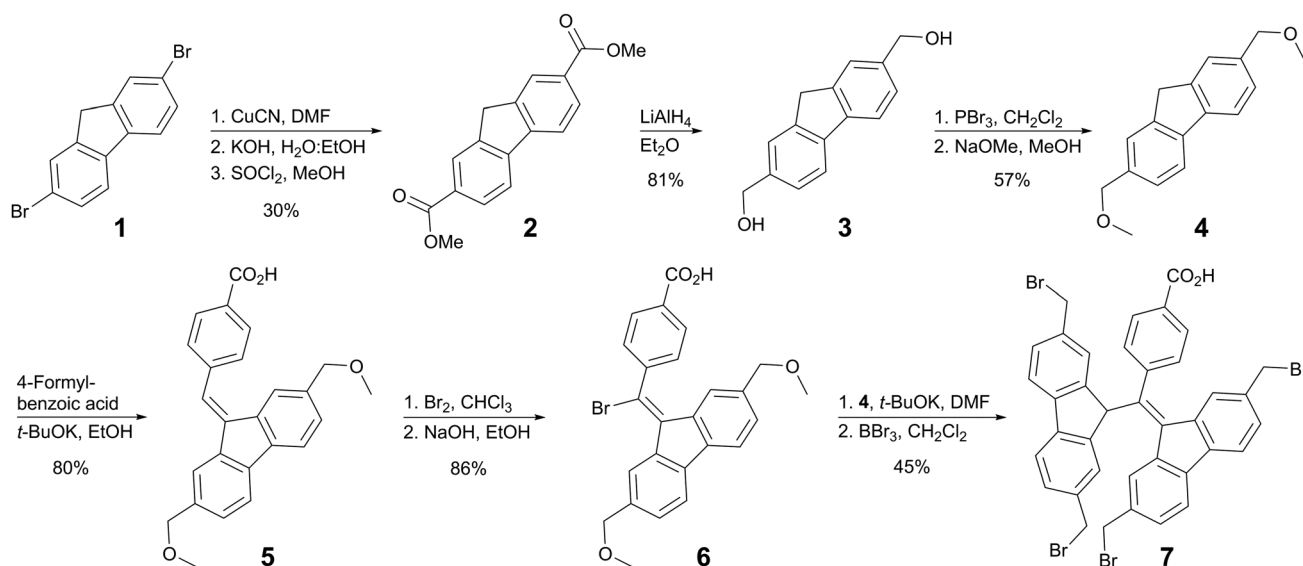
An advantage of the BDPA over the Finland trityl radical is its relative ease of synthesis.^{11,17} However, BDPA radicals have seen limited use for DNP,^{14c,18} due to two major obstacles. First, the lack of solubility of BDPA radicals in aqueous media limits their applications for biomolecules. A BDPA derivative that contains two carboxylates has been prepared but still has insufficient solubility in aqueous media for DNP applications,¹⁹ while persulfonated BDPA, a mixture of radicals with different degrees of substitution, cannot be readily conjugated to nitroxides.²⁰ Second, BDPA radicals have limited persistence in solution, primarily due to dimerization, as we have recently reported.²¹ Here we describe a new class of BDPA radicals that addresses these two shortcomings of BDPA radicals for DNP. These BDPA radicals contain four positively charged ammonium groups that enhance solubility in aqueous solutions, in addition to increasing their persistence. We also demonstrate that these new BDPA radicals can be used to prepare water-soluble BDPA-nitroxide biradicals.

The strategy for the preparation of water-soluble BDPA-based radicals was to attach charged functional groups to BDPA that should also enhance their persistence by preventing decomposition through dimerization.²¹ The 2,7-positions of fluorene were selected for incorporation of tetraalkyl/aryl-ammonium groups. These positions can be readily functionalized and enable incorporation of four charged groups into the BDPA radical. We chose to incorporate an isolating methylene linker between the fluorene ring and these functional groups to prevent their interaction with the BDPA radical, which is delocalized in the fluorene rings.²²

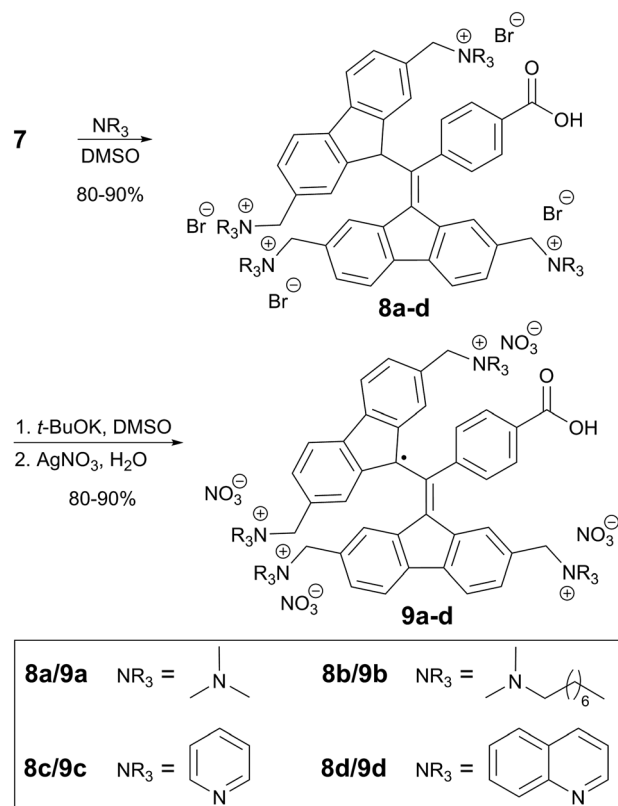
The synthesis started with the incorporation of cyano groups by the Sandmeyer reaction of 2,7-dibromofluorene (**1**), followed by their hydrolysis (Scheme 1).²³ Purification of the resulting

fluorene-2,7-dicarboxylic acid was not feasible due to its extremely limited solubility. Consequently, the carboxylates were converted to esters to yield fluorene derivative **2** and subsequently reduced to afford diol **3** in good yields. The hydroxyl groups were protected as methoxy ethers to provide **4**, since the presence of the unprotected hydroxyl groups led to very low yields in the following steps. Condensation of **4** with 4-formylbenzoic acid afforded **5** and bromination, followed by elimination gave **6** in excellent yields. Compound **6** was further coupled with another unit of 2,7-dimethoxymethylfluorene (**4**) with subsequent conversion of the methoxy ethers to bromides to yield tetra-(bromomethyl)-BDPA derivative **7**.

The benzylic bromides of **7** could be readily substituted with nucleophiles. Hence, compound **7** was used as a building block to synthesize a series of BDPA radicals with different tetraalkylammonium groups, to demonstrate the generality of this approach for the preparation of derivatives with custom-made physical properties (Scheme 2). In addition to trimethylamine, the more lipophilic *N,N*-dimethyloctylamine was selected, along with the aromatic amines pyridine and quinoline. Reaction of these amines with **7** afforded compounds **8a-d** in good yields. It is noteworthy that the products could be easily isolated from the reaction mixture by precipitation. These compounds had good solubility in “DNP juice”²⁴ (glycerol: water, 6:4), a solvent commonly used for DNP-NMR, and their relative variance in solubility reflected the nature of the substituents on the tetraalkylammonium groups; **8a** had the highest solubility (>150 mM) and the more lipophilic **8b** the lowest (20 mM), while the pyridinium and the quinolinium derivatives had intermediate solubility (**8c**, 65 mM; **8d**, 45 mM). Sequential treatment of compounds **8a-d** with *t*-BuOK and AgNO₃ yielded BDPA radicals **9a-d**; again the products were isolated from the reaction mixture by precipitation. As is common for such reactions,²¹ ca. 85% of the products were radicals, as determined by spin-counting using EPR spectroscopy (ESI[†]).



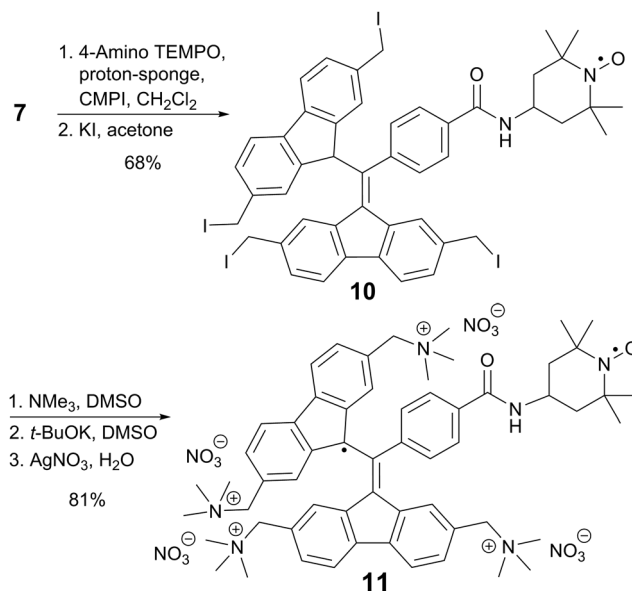
Scheme 1 Synthesis of tetra-(bromomethyl)-BDPA carboxylic acid **7**.



Scheme 2 Synthesis of tetraalkyl/aryl-ammonium BDPA derivatives **9a-d**.

The carboxylic acid group present in the *para*-position on the benzene ring of BDPA derivative **7** was included for the conjugation of other radicals to BDPA, for the purpose of preparing water-soluble BDPA-based biradicals. To demonstrate the synthesis of a BDPA-nitroxide biradical, compound **7** was coupled with 4-amino TEMPO and the resulting compound **10** was treated sequentially with trimethylamine, *t*-BuOK and AgNO₃ to give **11** (Scheme 3). This is, to our knowledge, the first reported example of a water-soluble BDPA-nitroxide biradical. The EPR spectrum of **11** shows three sharp lines due to a strong interaction between the BDPA and the nitroxide radical (ESI[†]); a *J*-coupling of 140 MHz between the two paramagnetic centers has been determined for a BDPA-TEMPO biradical with the same core structure.¹⁷

Having demonstrated the improved solubility of the BDPA radicals in a polar solvent, we investigated their persistence by monitoring their absorbance²⁵ at 503 nm. Fig. 2 shows a plot of the persistence of **9a** as a function of time in four different solvents: DMSO, DNP juice, MeOH and water. Radical **9a** could also be quantified by EPR spectroscopy;²¹ the data for DNP juice are shown in Fig. S25B (ESI[†]). The persistence was remarkably high in DMSO (Fig. 2), with an initial rate of degradation *ca.* 20-fold less than what we had previously observed for BDPA radicals.²¹ After two weeks in DMSO at 23 °C, only *ca.* 10% of the radical had degraded; this is an unprecedented degree of persistence for BDPA radicals.



Scheme 3 Synthesis of the water-soluble BDPA-TEMPO biradical **11**.

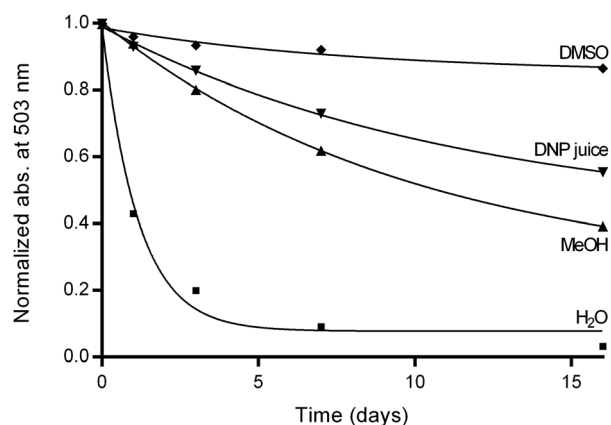


Fig. 2 Persistence of the water-soluble BDPA radical **9a** in solution (10 mM) at 23 °C, monitored by UV-vis spectroscopy at 503 nm. The initial rates of degradation are as follows: $\sim 2.0 \times 10^{-9} \text{ M s}^{-1}$ (DMSO, ♦), $\sim 5.8 \times 10^{-9} \text{ M s}^{-1}$ (DNP juice, ▼), $\sim 8.9 \times 10^{-9} \text{ M s}^{-1}$ (MeOH, ▲), $\sim 92.1 \times 10^{-9} \text{ M s}^{-1}$ (H₂O, ■).

A large variation in solvent-dependent persistence was observed for **9a** (Fig. 2), **9b**, **9d** and **11** (ESI[†]). The persistence of **9a** was markedly lower in polar protic solvents than it was in DMSO; *ca.* 40% and 50% of the radicals had degraded in DNP juice and MeOH, respectively after two weeks. However, the rate of degradation in MeOH was still at least 5-fold lower than what has been previously observed with BDPA radicals.²¹ The data shown in Fig. 2 were collected at 23 °C, negligible degradation was observed in DNP juice at -80 °C after one month (Fig. S28, ESI[†]).

The persistence of **9a** was much lower in water than in other solvents (Fig. 2), with *ca.* 50% decomposition within 48 h. Since dimerization is a major decomposition pathway for BDPA radicals in solution,²¹ we determined the concentration dependence of the initial rate of degradation for a series of aqueous solutions of **9a**.

Indeed, we observed a non-linear concentration-dependence,²¹ with a reaction order of *ca.* 1.6 with respect to the radical (Fig. S29, ESI[†]). Moreover, we observed a major peak in the mass spectrum of **9a** in water after 48 h corresponding to the dimer of **9a** (Fig. S31, ESI[†]).

It may seem counterintuitive that **9a** would aggregate in water. However, there have been reports of aggregation of tetraalkylammonium salts in water.²⁶ It has been postulated that this may be due to the electrostatic attraction between the positively charged nitrogen and the counter anion, as well as hydrophobic interactions between the alkyl substituents.²⁶ An attempt to reduce aggregation of **9a** in water by increasing the ionic strength resulted in a decrease of its persistence; the initial rate of degradation increased *ca.* 2-fold in the presence of 100 mM NaCl (Fig. S30, ESI[†]). DMSO has been shown to reduce the aggregation of ammonium-functionalized polythiophene relative to water,²⁷ which is consistent with our results.

In summary, we have described the synthesis and characterization of a series of water-soluble tetraalkyl/aryl-ammonium BDPA radicals, including a BDPA-nitroxide biradical. These BDPA radicals can be readily used to prepare heterobiradicals as polarizing agents for investigation of biomolecules by MAS-DNP NMR spectroscopy at high magnetic fields. The radicals show significantly improved persistence in solution,²¹ presumably due to a reduced tendency to aggregate. Although the persistence of these radicals in water was substantially less than in DMSO, the tetrabromo intermediate **7** can be used to prepare a wide variety of derivatives with tailor-made properties, including limited aggregation in water.

The authors acknowledge the financial support from the Icelandic Research Fund (163393-052) and the University of Iceland Research Fund. We thank Dr S. Jonsdottir for assistance with collection of the NMR and HRMS (ESI) data and members of the Sigurdsson research group for helpful discussions.

Conflicts of interest

There are no conflicts to declare.

References

- (a) R. Tycko, *Annu. Rev. Phys. Chem.*, 2011, **62**, 279–299; (b) B. H. Meier, R. Riek and A. Böckmann, *Trends Biochem. Sci.*, 2017, **42**, 777–787.
- (a) Q. Z. Ni, E. Daviso, T. V. Can, E. Markhasin, S. K. Jawla, T. M. Swager, R. J. Temkin, J. Herzfeld and R. G. Griffin, *Acc. Chem. Res.*, 2013, **46**, 1933–1941; (b) M. Hong, Y. Zhang and F. Hu, *Annu. Rev. Phys. Chem.*, 2012, **63**, 1–24; (c) M. R. Elkins and M. Hong, *Curr. Opin. Struct. Biol.*, 2019, **57**, 103–109; (d) L. A. Baker and M. Baldus, *Curr. Opin. Struct. Biol.*, 2014, **27**, 48–55; (e) V. S. Mandala, J. K. Williams and M. Hong, *Annu. Rev. Biophys.*, 2018, **47**, 201–222.
- (a) W. Zhang, S. Xu, X. Han and X. Bao, *Chem. Soc. Rev.*, 2012, **41**, 192–210; (b) J. Xu, Q. Wang and F. Deng, *Acc. Chem. Res.*, 2019, **52**, 2179–2189.
- F. Mentink-Vigier, I. Marin-Montesinos, A. P. Jagtap, T. Halbritter, J. van Tol, S. Hediger, D. Lee, S. T. Sigurdsson and G. De Paëpe, *J. Am. Chem. Soc.*, 2018, **140**, 11013–11019.
- (a) A. S. Lilly Thankamony, J. J. Wittmann, M. Kaushik and B. Corzilius, *Prog. Nucl. Magn. Reson. Spectrosc.*, 2017, **102–103**, 120–195; (b) B. Corzilius, *Annu. Rev. Phys. Chem.*, 2020, **71**, 7.1–7.28.
- (a) F. Mentink-Vigier, Ü. Akbey, Y. Hovav, S. Vega, H. Oschkinat and A. Feintuch, *J. Magn. Reson.*, 2012, **224**, 13–21; (b) K. R. Thurber and R. Tycko, *J. Chem. Phys.*, 2012, **137**, 084508; (c) F. Mentink-Vigier, S. Vega and G. De Paëpe, *Phys. Chem. Chem. Phys.*, 2017, **19**, 3506–3522; (d) F. Mentink-Vigier, Ü. Akbey, H. Oschkinat, S. Vega and A. Feintuch, *J. Magn. Reson.*, 2015, **258**, 102–120.
- C. F. Koelsch, *J. Am. Chem. Soc.*, 1957, **79**, 4439–4441.
- K.-N. Hu, H.-h. Yu, T. M. Swager and R. G. Griffin, *J. Am. Chem. Soc.*, 2004, **126**, 10844–10845.
- (a) A. Zagdoun, G. Casano, O. Ouari, M. Schwarzwälder, A. J. Rossini, F. Aussenac, M. Yulikov, G. Jeschke, C. Copéret, A. Lesage, P. Tordo and L. Emsley, *J. Am. Chem. Soc.*, 2013, **135**, 12790–12797; (b) C. Sauvée, M. Rosay, G. Casano, F. Aussenac, R. T. Weber, O. Ouari and P. Tordo, *Angew. Chem., Int. Ed.*, 2013, **52**, 10858–10861; (c) A. P. Jagtap, M.-A. Geiger, D. Stöppler, M. Orwick-Rydmark, H. Oschkinat and S. T. Sigurdsson, *Chem. Commun.*, 2016, **52**, 7020–7023; (d) A. Lund, G. Casano, G. Menzildjian, M. Kaushik, G. Stevanato, M. Yulikov, R. Jabbour, D. Wisser, M. Renom-Carrasco, C. Thieuleux, F. Bernada, H. Karoui, D. Siri, M. Rosay, I. V. Sergeev, D. Gajan, M. Lelli, L. Emsley, O. Ouari and A. Lesage, *Chem. Sci.*, 2020, **11**, 2810–2818.
- M. Rosay, M. Blank and F. Engelke, *J. Magn. Reson.*, 2016, **264**, 88–98.
- T. J. Reddy, T. Iwama, H. J. Halpern and V. H. Rawal, *J. Org. Chem.*, 2002, **67**, 4635–4639.
- (a) J. H. Ardenkjær-Larsen, I. Laursen, I. Leunbach, G. Ehnholm, L. G. Wistrand, J. S. Petersson and K. Golman, *J. Magn. Reson.*, 1998, **133**, 1–12; (b) W. de Boer, *J. Low Temp. Phys.*, 1976, **22**, 185–212.
- V. Meyer, S. S. Eaton and G. R. Eaton, *Appl. Magn. Reson.*, 2014, **45**, 993–1007.
- (a) G. Mathies, M. A. Caporini, V. K. Michaelis, Y. Liu, K.-N. Hu, D. Mance, J. L. Zweier, M. Rosay, M. Baldus and R. G. Griffin, *Angew. Chem., Int. Ed.*, 2015, **54**, 11770–11774; (b) K.-N. Hu, V. S. Bajaj, M. Rosay and R. G. Griffin, *J. Chem. Phys.*, 2007, **126**, 044512; (c) D. Wisser, G. Karthikeyan, A. Lund, G. Casano, H. Karoui, M. Yulikov, G. Menzildjian, A. C. Pinon, A. Pura, F. Engelke, S. R. Chaudhari, D. Kubicki, A. J. Rossini, I. B. Moroz, D. Gajan, C. Copéret, G. Jeschke, M. Lelli, L. Emsley, A. Lesage and O. Ouari, *J. Am. Chem. Soc.*, 2018, **140**, 13340–13349.
- K.-N. Hu, *Solid State Nucl. Magn. Reson.*, 2011, **40**, 31–41.
- (a) F. Mentink-Vigier, S. Paul, D. Lee, A. Feintuch, S. Hediger, S. Vega and G. De Paëpe, *Phys. Chem. Chem. Phys.*, 2015, **17**, 21824–21836; (b) K. R. Thurber and R. Tycko, *J. Chem. Phys.*, 2014, **140**, 184201.
- E. L. Dane, T. Maly, G. T. Debelouchina, R. G. Griffin and T. M. Swager, *Org. Lett.*, 2009, **11**, 1871–1874.
- L. F. Pinto, I. Marín-Montesinos, V. Lloveras, J. L. Muñoz-Gómez, M. Pons, J. Veciana and J. Vidal-Gancedo, *Chem. Commun.*, 2017, **53**, 3757–3760.
- E. L. Dane and T. M. Swager, *J. Org. Chem.*, 2010, **75**, 3533–3536.
- O. Haze, B. Corzilius, A. A. Smith, R. G. Griffin and T. M. Swager, *J. Am. Chem. Soc.*, 2012, **134**, 14287–14290.
- S. Mandal and S. T. Sigurdsson, *Chem. – Eur. J.*, 2020, **26**, 7486–7491.
- A. Nagao, O. Takehiro and Y. Jun, *Bull. Chem. Soc. Jpn.*, 1994, **67**, 31–38.
- C. M. G. Henríquez, L. H. Tagle, C. A. Terraza, A. B. González, A. L. Cabrera and U. G. Volkmann, *J. Appl. Polym. Sci.*, 2012, **125**, 477–487.
- G. J. Gerfen, L. R. Becerra, D. A. Hall, R. G. Griffin, R. J. Temkin and D. J. Singel, *J. Chem. Phys.*, 1995, **102**, 9494–9497.
- D. T. Breslin and M. A. Fox, *J. Phys. Chem.*, 1993, **97**, 13341–13347.
- (a) R. Atkin and G. G. Warr, *J. Phys. Chem. C*, 2008, **112**, 4164–4166; (b) T. Singh and A. Kumar, *J. Phys. Chem. C*, 2007, **111**, 7843–7851; (c) R. Dutta, S. Kundu and N. Sarkar, *Biophys. Rev.*, 2018, **10**, 861–871.
- R. Cagnoli, M. Caselli, E. Libertini, A. Mucci, F. Parenti, G. Ponterini and L. Schenetti, *Polymer*, 2012, **53**, 403–410.

Supporting Information

Water-soluble BDPA radicals with improved persistence

Sucharita Mandal and Snorri Th. Sigurdsson*

University of Iceland, Department of Chemistry, Science Institute, Dunhaga 3,
107 Reykjavik, Iceland. E-mail: snorrиси@hi.is

Table of Contents

List of abbreviations.....	2
Synthetic procedures.....	2
General materials and methods.....	2
Dimethyl-9 <i>H</i> -fluorene-2,7-dicarboxylate (2).....	3
(9 <i>H</i> -Fluorene-2,7-diyl)dimethanol (3).....	5
2,7-Bis(methoxymethyl)-9 <i>H</i> -fluorene (4).....	7
Compound 5	9
Compound 12	11
Compound 6	13
Tetra-(methoxymethyl)-BDPA 13	15
Tetra-(bromomethyl)-BDPA 7	17
Tetraalkylammonium BDPA 8a	19
BDPA radical 9a	21
Tetraalkylammonium BDPA 8b	22
BDPA radical 9b	24
Tetrapyridinium BDPA 8c	25
BDPA radical 9c	27
Tetraquinolinium BDPA 8d	28
BDPA radical 9d	30
Tetra-(iodomethyl)-BDPA-TEMPO 10	31
BDPA-TEMPO biradical 11	32
Solubility in DNP juice.....	33
Quantification of BDPA radicals.....	33
Persistence of BDPA radicals.....	33
Analysis of BDPA-decomposition products.....	36
References:.....	37

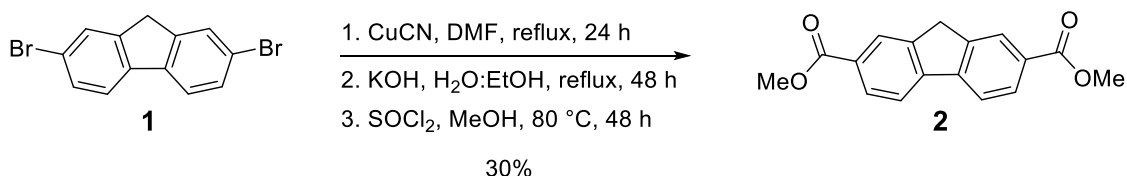
List of abbreviations

BDPA	1,3- Bisdiphenylene-2- phenylallyl
Calcd	Calculated
CMPI	2-Chloro-1-methylpyridinium iodide
DMF	Dimethylformamide
DMSO	Dimethyl sulfoxide
EPR	Electron paramagnetic resonance
ESI	Electrospray ionization
HPLC	High-performance liquid chromatography
HRMS	High resolution mass spectrometry
NMR	Nuclear magnetic resonance
Pet ether	Petroleum ether
RP	Reverse phase
Satd.	Saturated
TEMPO	2,2,6,6-Tetramethylpiperidine 1-oxyl
TFA	Trifluoroacetic acid
TLC	Thin layer chromatography

Synthetic procedures

General materials and methods

Chemicals were purchased from Sigma-Aldrich Co. or ChemGenes and were used without further purification. All moisture sensitive reactions were carried out in oven-dried glassware under an inert atmosphere of Ar. CH₂Cl₂ was dried over calcium hydride and freshly distilled before use. DMSO and DMF were dried over molecular sieves (3 Å). Thin layer chromatography (TLC) was carried out using glass plates pre-coated with silica gel (Kieselgel 60 F₂₅₄, 0.2 mm, Silicycle), using UV light for visualization. Silica gel for flash chromatography (230-400 mesh, 60 Å) was purchased from Silicycle. ¹H- and ¹³C-NMR spectra were recorded at the frequencies stated, using deuterated solvents as internal standards on a Bruker Avance 400 spectrometer. Radicals show broadening and loss of NMR signals due to their paramagnetic nature and therefore, those NMR spectra are not shown. Mass spectrometric analyses of all organic compounds were performed on an ESI-HRMS (Bruker, MicrOTOF-Q). EPR spectra were recorded on a MiniScope MS200 with following experimental parameters: 9.43 GHz, microwave power 1 mW, sweep width 12 mT, modulation 0.2 mT, 23 °C. HPLC chromatograms were recorded on a Beckman Coulter Gold HPLC system using a NUCLEODUR C18 Pyramid 4.6 x 150 mm analytical column with UV detection at 254 nm. Solvent gradients for analytical RP-HPLC were run at 1.0 mL/min using the following gradient: solvent A, 0.1% TFA in H₂O; solvent B, CH₃CN; 0-2 min isocratic 0% B, 2-12 min linear gradient 0-100% B, 12-14 min linear gradient 100-0% B, 14-16 min isocratic 0% B.



Dimethyl-9H-fluorene-2,7-dicarboxylate (2). To a solution of 2,7-dibromo-9H-fluorene (**1**) (6 g, 18.52 mmol) in DMF (50 mL) was added CuCN (3.7 g, 40.74) and the resulting solution heated at 160 °C for 24 h under Ar atmosphere.¹ The reaction mixture was cooled to 60 °C and poured into aq. solution of FeCl₃·6H₂O (11 g, 40.74 mmol) containing HCl (6 mL). The yellow precipitate formed was filtered, washed with H₂O and dried. The precipitate was redissolved in H₂O:EtOH (50:50, 200 mL), KOH (10.4 g, 185.2 mmol) added and the resulting solution refluxed for 48 h. The reaction mixture was cooled to 23 °C, filtered and the filtrate was acidified with HCl (15 mL). The precipitate formed was filtered, washed with H₂O and dried.¹ The precipitate was redissolved in MeOH (50 mL), SOCl₂ (1.7 mL, 40.74 mmol) was added drop-wise and the resulting solution heated at 80 °C for 48 h. The reaction mixture was cooled and poured into H₂O (300 mL). The precipitate formed was filtered and purified by flash-column chromatography using a gradient elution (pet ether:EtOAc; 85:15 to 80:20) to give **2** (1.6 g, 30%) as a yellowish solid.

TLC (Silica gel, pet ether:EtOAc, 80:20): R_f (**2**) = 0.5

¹H NMR (400 MHz, CDCl₃): δ 8.26 (s, 2H), 8.12 (dd, J = 8.1, 1.5 Hz, 2H), 7.89 (d, J = 8.0 Hz, 2H), 4.01 (s, 2H), 3.96 (s, 6H) ppm.

¹³C NMR (101 MHz, CDCl₃): δ 167.26, 145.07, 144.26, 129.49, 128.93, 126.51, 120.57, 52.31, 36.90 ppm.

HRMS (ESI): m/z calcd for C₁₇H₁₄O₄+Na⁺: 305.0784 [M +Na]⁺; found 305.0781.

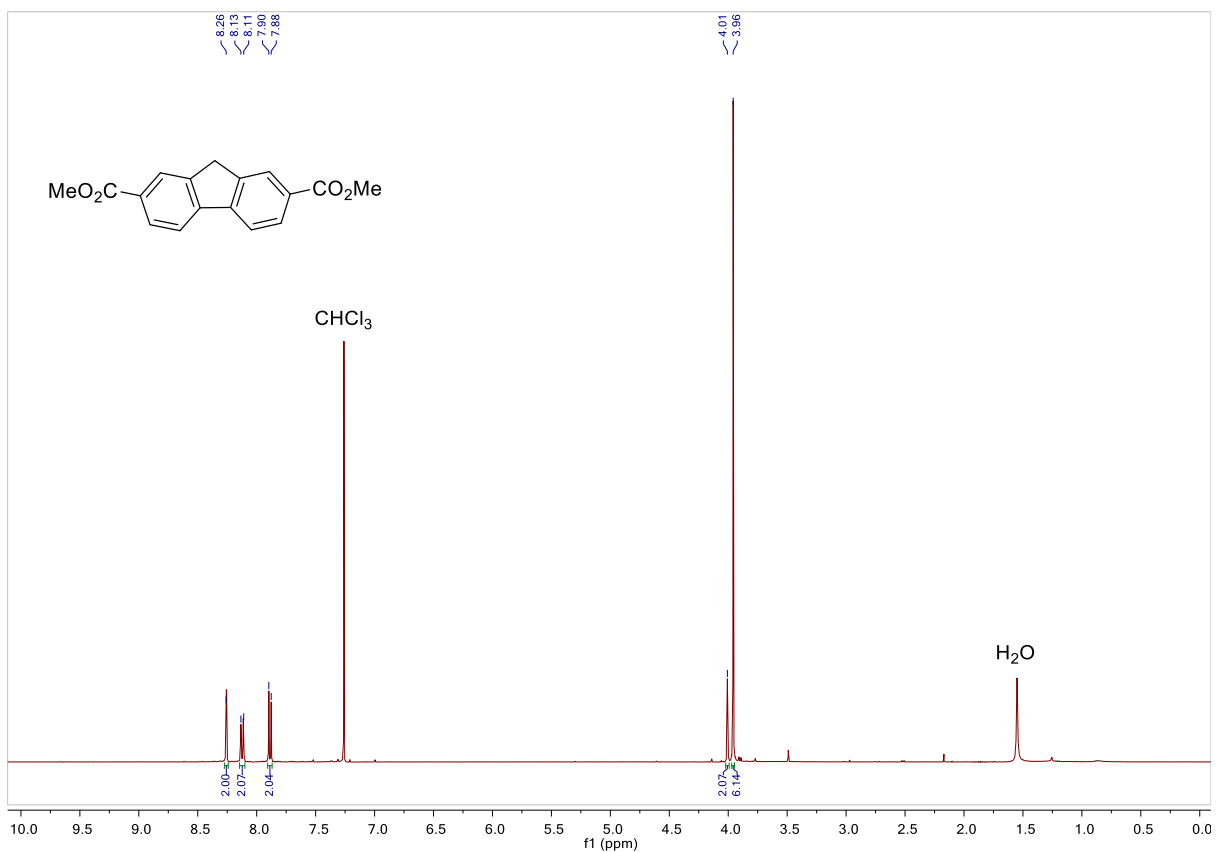


Figure S1. ¹H-NMR spectrum of compound 2.

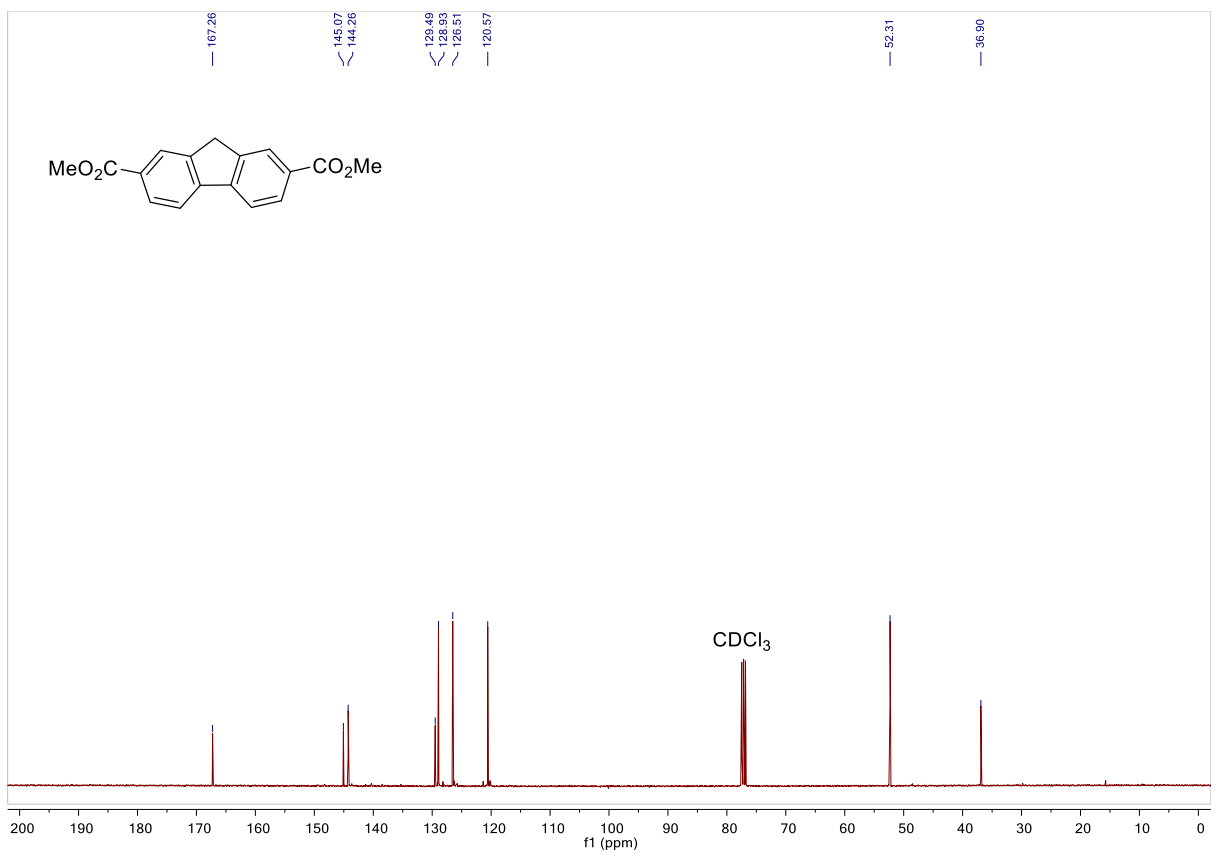
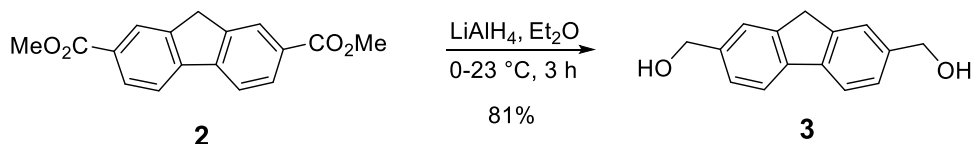


Figure S2. ¹³C-NMR spectrum of compound 2.



(9H-Fluorene-2,7-diyl)dimethanol (3). To a solution of dimethyl-9H-fluorene-2,7-dicarboxylate (**2**) (2.0 g, 7.08 mmol) in Et₂O (50 mL) at 0 °C, LiAlH₄ solution (14.2 mL, 14.17 mmol, 1 M in THF) was added and the resulting solution stirred at 23 °C for 3 h. The reaction was quenched by drop-wise addition of EtOH until the effervescence ceased and satd. aq. NH₄Cl (10 mL) added. The mixture was filtered through celite and concentrated *in vacuo*. The crude product was purified by flash-column chromatography using a gradient elution (CH₂Cl₂:MeOH; 97:03 to 95:05) to give **3** (1.3 g, 81%) as a yellowish solid.

TLC (Silica gel, CH₂Cl₂:MeOH; 97:03): *R_f* (**2**) = 0.9, *R_f* (**3**) = 0.3

¹H NMR (400 MHz, DMSO-*d*₆): δ 7.80 (d, *J* = 7.8 Hz, 2H), 7.52 (s, 2H), 7.31 (d, *J* = 7.6 Hz, 2H), 5.18 (t, *J* = 5.7 Hz, 2H), 4.56 (d, *J* = 5.7 Hz, 4H), 3.88 (s, 2H) ppm.

¹³C NMR (101 MHz, DMSO-*d*₆): δ 143.03, 141.07, 139.75, 125.21, 123.37, 119.39, 63.17, 36.27 ppm.

HRMS (ESI): *m/z* calcd for C₁₅H₁₄O₂+Na⁺: 249.0886 [*M*+Na]⁺; found 249.0885.

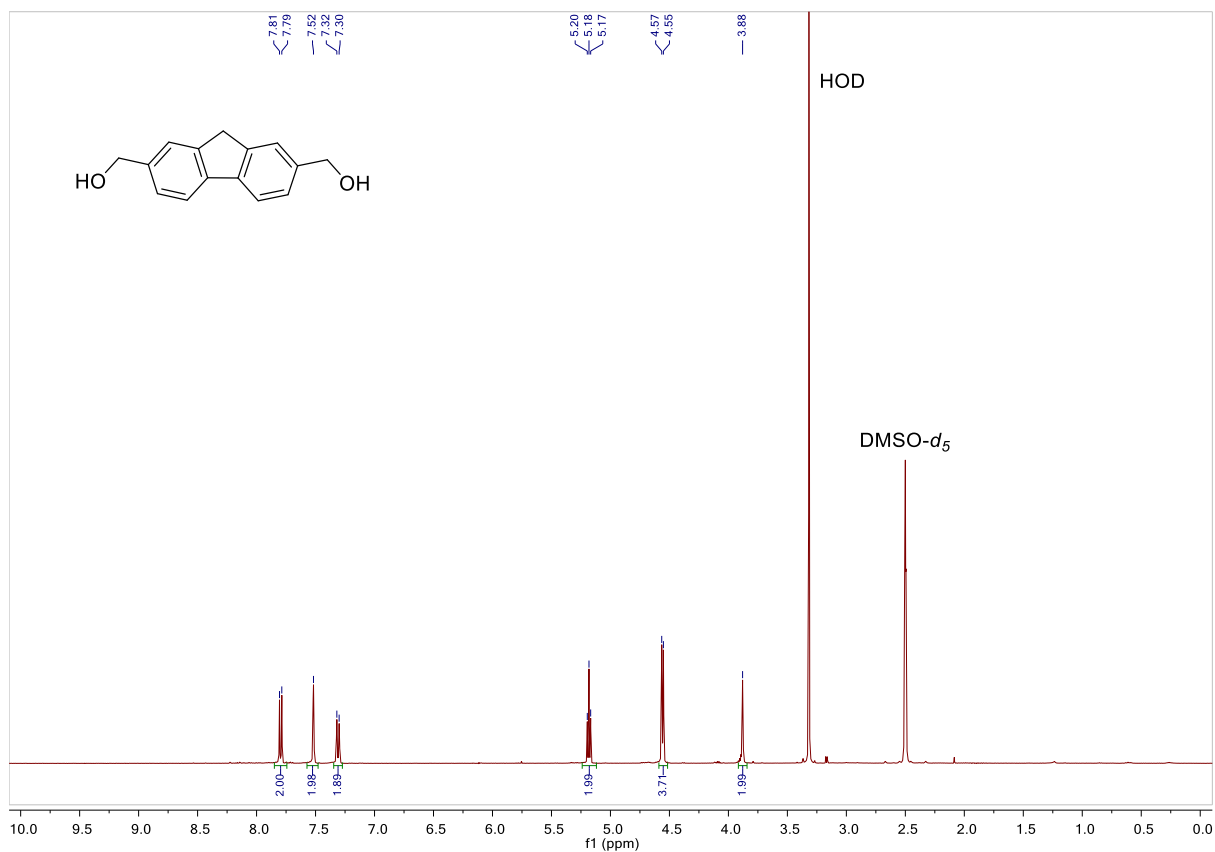


Figure S3. ¹H-NMR spectrum of compound 3.

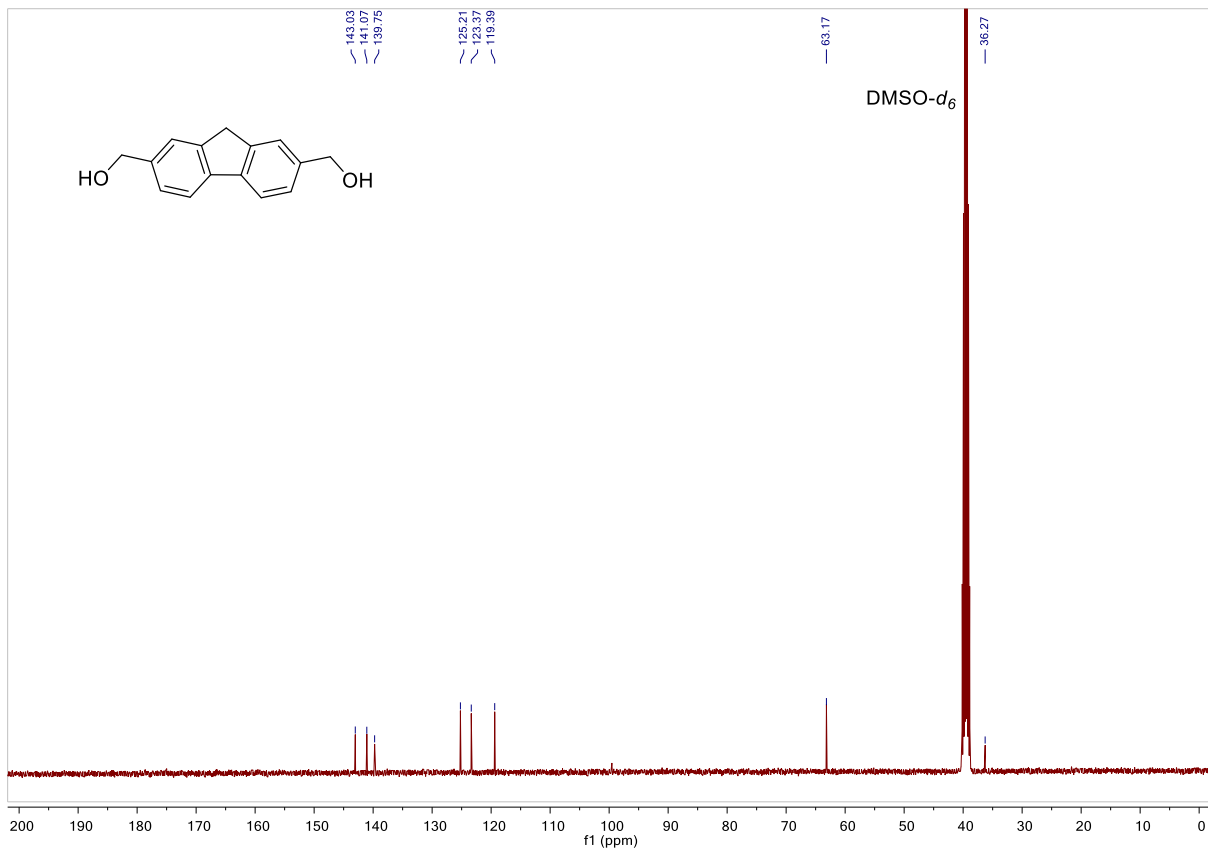
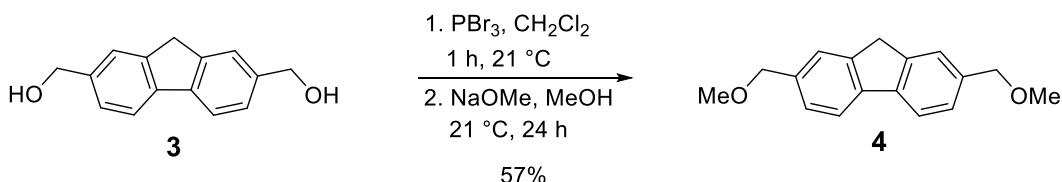


Figure S4. ¹³C-NMR spectrum of compound 3.



2,7-Bis(methoxymethyl)-9H-fluorene (4). To a solution of (9H-fluorene-2,7-diyl)dimethanol (**3**) (1.32 g, 5.83 mmol) in CH₂Cl₂ (50 mL), PBr₃ (0.6 mL, 5.83 mmol) was added and the resulting solution stirred at 21 °C for 1 h. The solvent was removed *in vacuo* and the residue treated with a freshly made NaOMe solution, prepared by slowly dissolving Na metal (1.34 g, 58.30 mmol) in MeOH (50 mL). The resulting mixture was stirred at 21 °C for 24 h and extracted with EtOAc (3 x 50 mL). The combined organic layers were washed with brine (2 x 100 mL), dried over Na₂SO₄ and concentrated *in vacuo*. The crude product was purified by flash-column chromatography using a gradient elution (pet ether:EtOAc; 90:10 to 85:15) to give **4** (0.85 g, 57%) as a white solid.

TLC (Silica gel, pet ether:EtOAc; 70:30): R_f (**3**) = 0.1, R_f (**4**) = 0.6

¹H NMR (400 MHz, CDCl₃): δ 7.75 (d, J = 7.8 Hz, 2H), 7.53 (s, 2H), 7.34 (d, J = 7.8, 2H), 4.53 (s, 4H), 3.89 (s, 2H), 3.42 (s, 6H) ppm.

¹³C NMR (101 MHz, CDCl₃): δ 143.85, 141.23, 136.93, 126.75, 124.74, 119.88, 75.14, 58.26, 36.90 ppm.

HRMS (ESI): m/z calcd for C₁₇H₁₈O₂+Na⁺: 277.1199 [M +Na]⁺; found 277.1191.

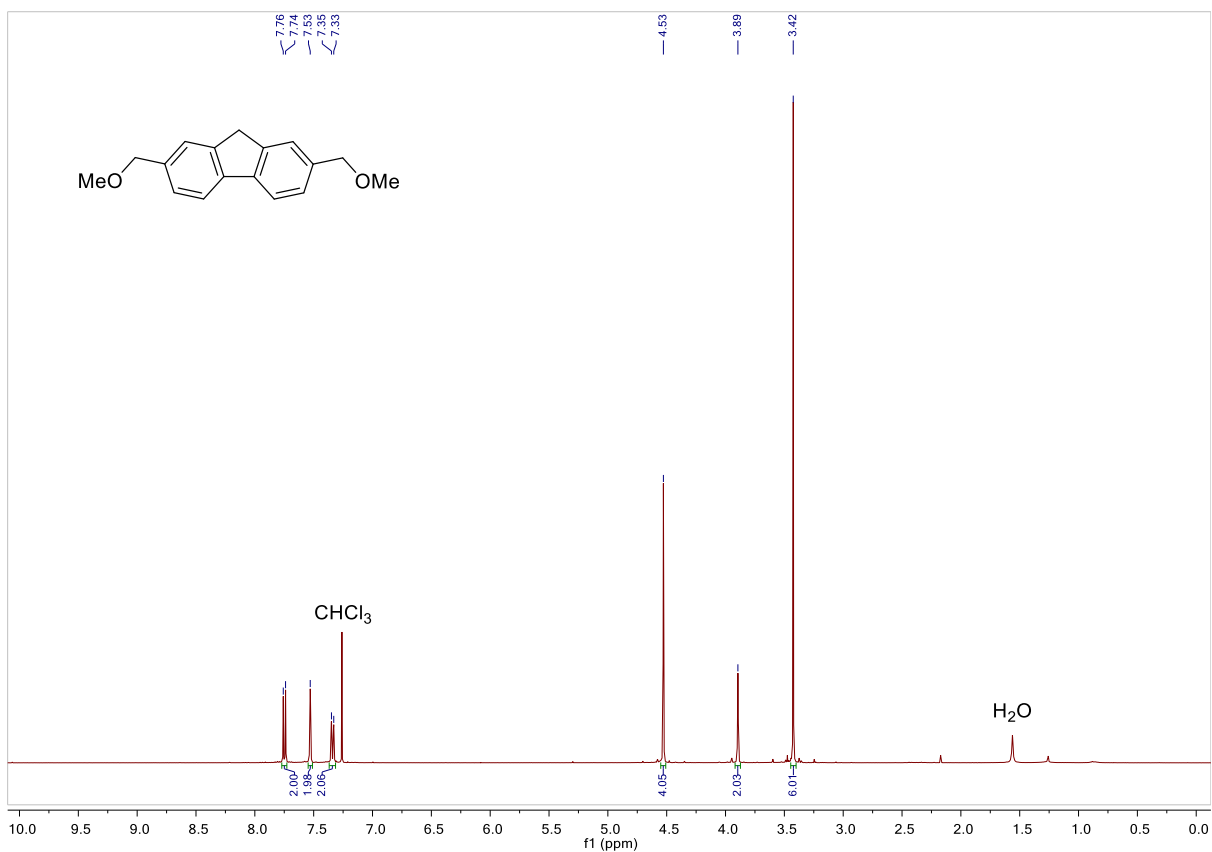


Figure S5. ¹H-NMR spectrum of compound 4.

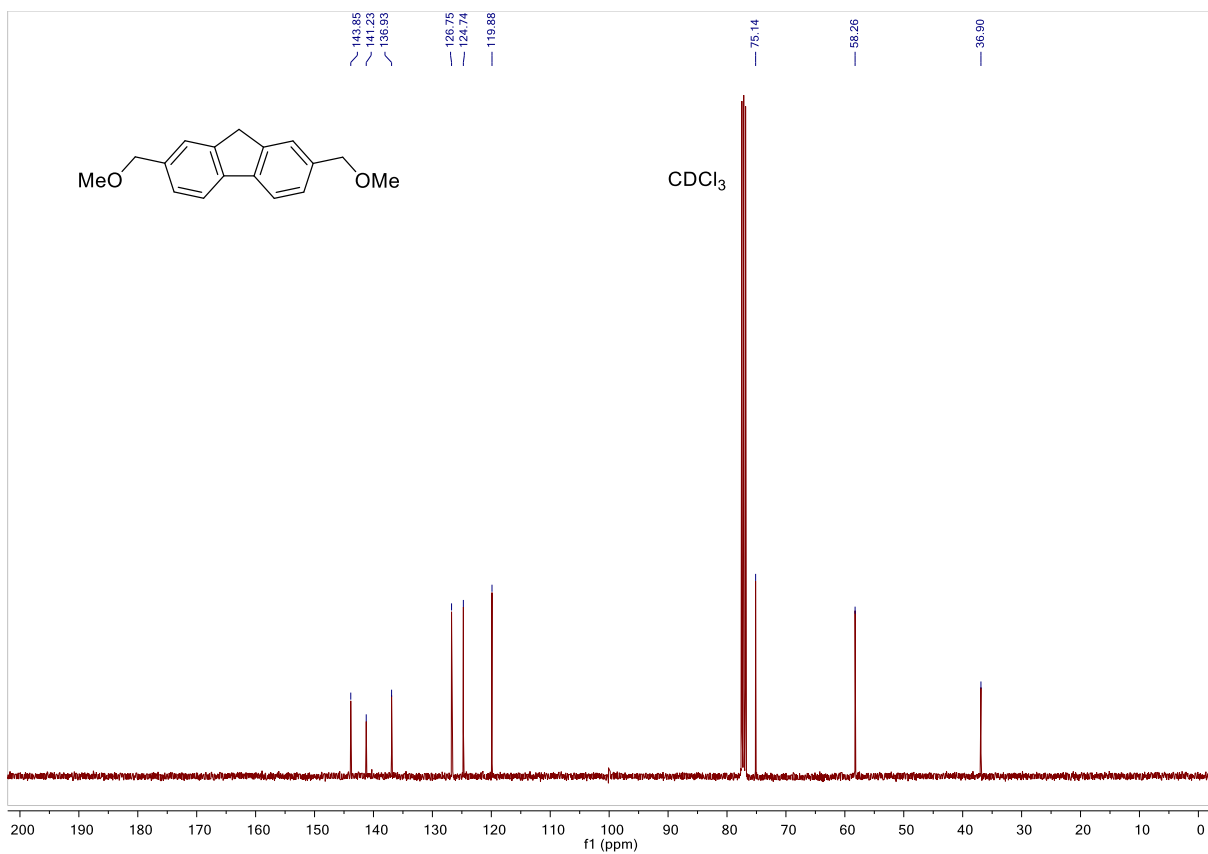
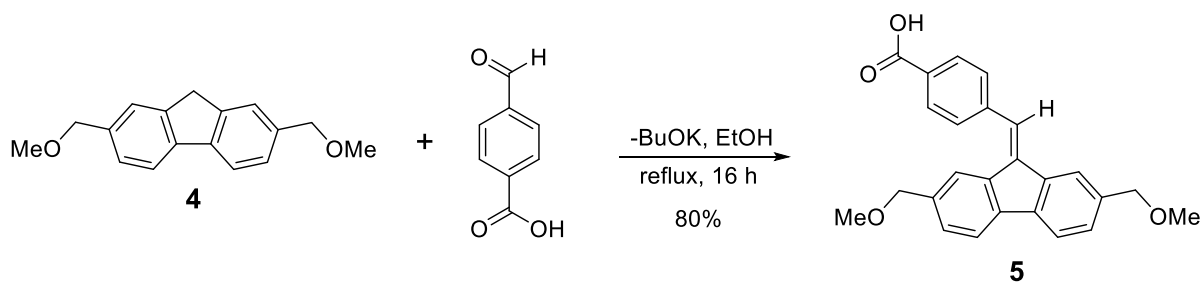


Figure S6. ¹³C-NMR spectrum of compound 4.



Compound 5. To a solution of 2,7-bis(methoxymethyl)-9H-fluorene (**4**) (400 mg, 7.08 mmol) in EtOH (25 mL), 4-formylbenzoic acid (354 mg, 2.36 mmol) and *t*-BuOK (528 mg, 4.71 mmol) were added and the resulting solution refluxed for 16 h. The solution was cooled, acidified with aq. HCl (1 M, 25 mL) and extracted with EtOAc (3 x 30 mL). The combined organic layers were washed with brine (3 x 50 mL), dried over Na₂SO₄ and concentrated *in vacuo*. The crude product was purified by flash-column chromatography using a gradient elution (CH₂Cl₂:MeOH; 100:0 to 97:03) to give **5** (490 mg, 80%) as a yellow solid.

TLC (Silica gel, CH₂Cl₂:MeOH; 97:03): *R_f* (**4**) = 0.9, *R_f* (**5**) = 0.3

¹H NMR (400 MHz, DMSO-*d*₆): δ 8.06 (d, *J* = 8.3 Hz, 2H), 7.95 (s, 1H), 7.93 (s, 1H), 7.84 (d, *J* = 5.0 Hz, 1H), 7.82 (d, *J* = 4.9 Hz, 1H), 7.73 (d, *J* = 8.3 Hz, 2H), 7.46 (s, 1H), 7.37 (dd, *J* = 7.7, 1.3 Hz, 1H), 7.31 (dd, *J* = 7.8, 1.4 Hz, 1H), 4.51 (s, 2H), 4.28 (s, 2H), 3.34 (s, 3H), 3.20 (s, 3H) ppm.

¹³C NMR (101 MHz, DMSO-*d*₆): δ 167.04, 140.62, 140.05, 139.11, 137.73, 137.53, 137.06, 136.22, 135.76, 130.70, 129.50, 129.36, 128.54, 128.27, 127.44, 122.93, 120.33, 120.03, 119.66, 73.84, 73.53, 57.49, 57.33 ppm.

HRMS (ESI): *m/z* calcd for C₂₅H₂₁O₄-H: 385.1445 [*M*-H]⁻; found 385.1447.

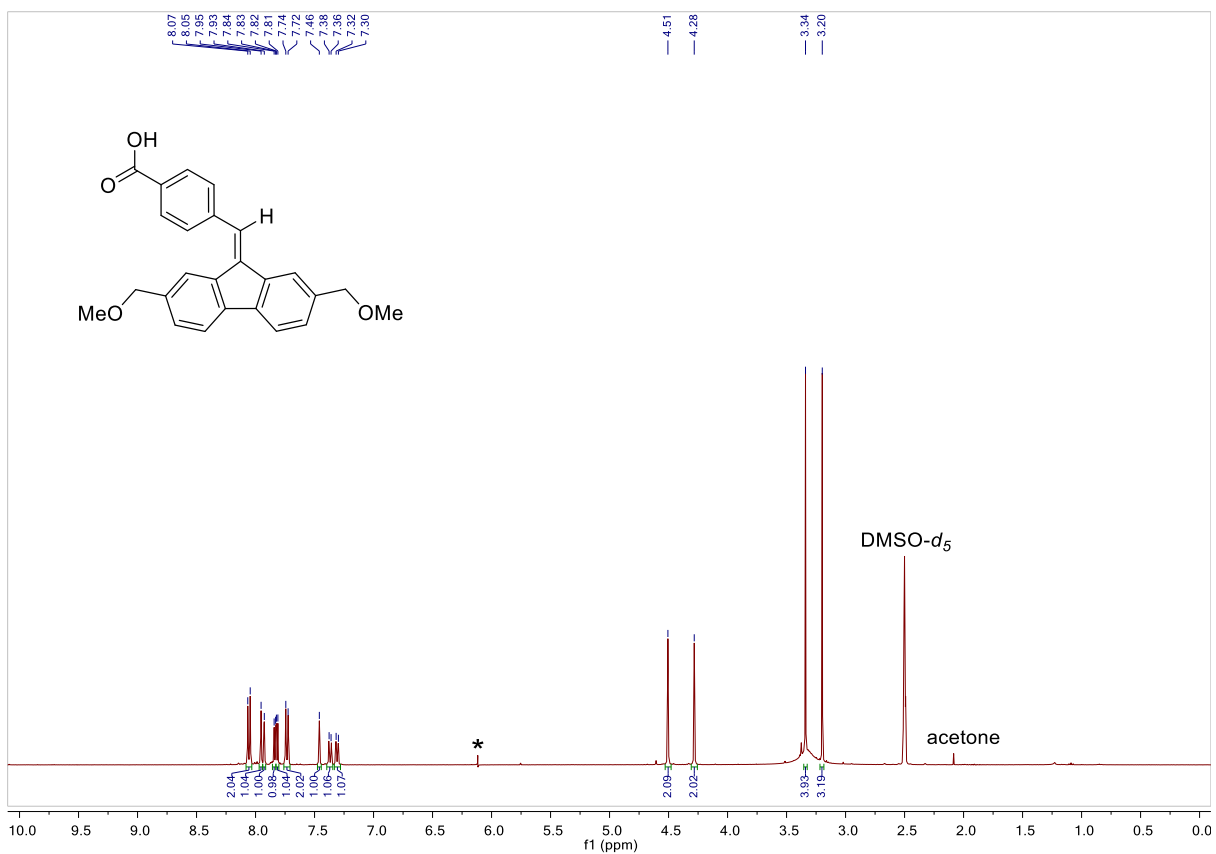


Figure S7. ¹H-NMR spectrum of compound 5. The asterisk indicates an instrumental glitch.

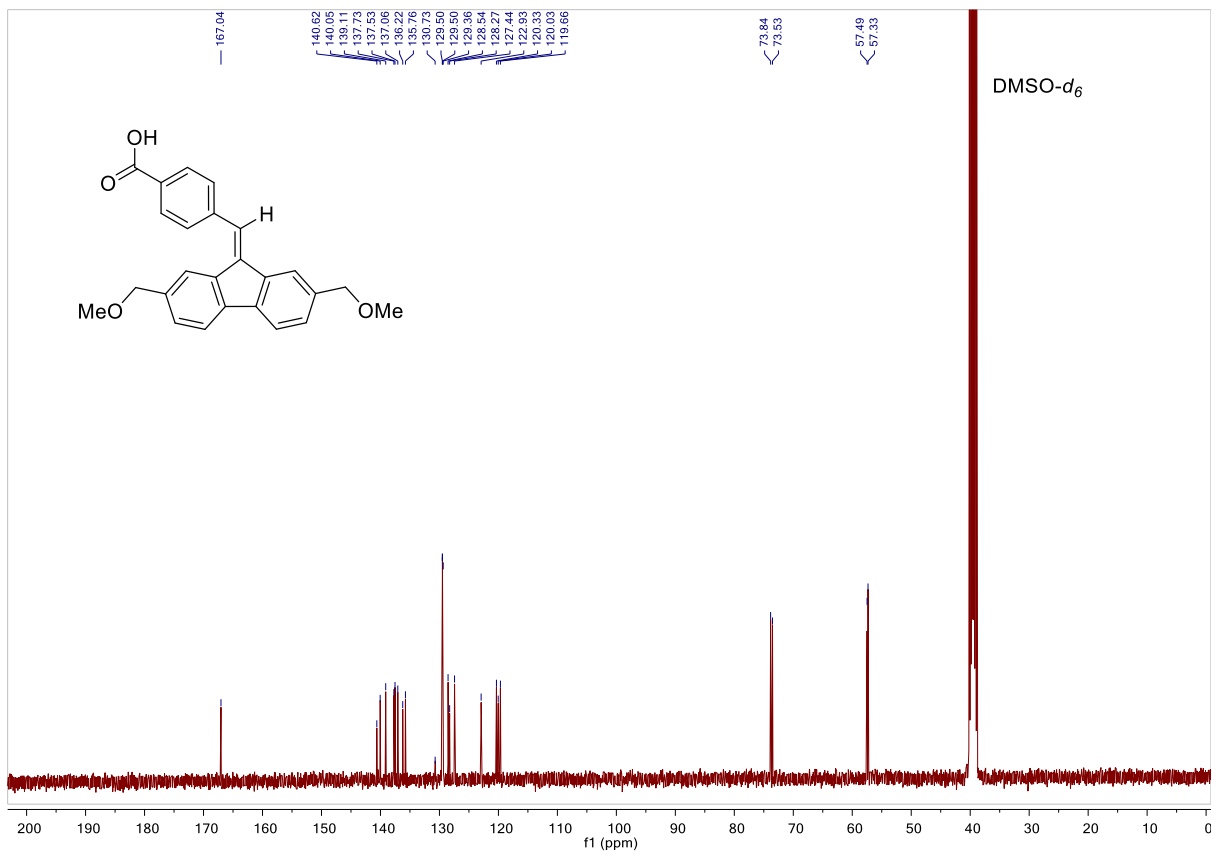
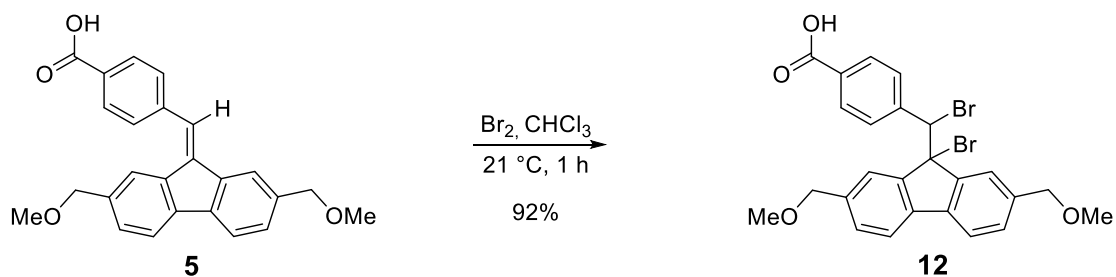


Figure S8. ¹³C-NMR spectrum of compound 5.



Compound 12. To a solution of compound **5** (500 mg, 1.29 mmol) in CHCl_3 (5 mL), Br_2 (66 μL , 1.29 mmol) was added and the resulting solution was stirred at 21 $^\circ\text{C}$ for 1 h. Satd. aq. $\text{Na}_2\text{S}_2\text{O}_3$ (10 mL) was added and the mixture extracted with CH_2Cl_2 (3 x 10 mL). The combined organic layers were washed with brine (2 x 30 mL), dried over Na_2SO_4 and concentrated *in vacuo*. The crude product was purified by flash-column chromatography using a gradient elution (CH_2Cl_2 :MeOH; 100:0 to 97:03) to give **12** (645 mg, 92%) as a yellow solid.

TLC (Silica gel, CH_2Cl_2 :MeOH; 97:03): R_f (**5**) = 0.3, R_f (**12**) = 0.3

^1H NMR (400 MHz, CDCl_3): δ 8.05 (s, 1H), 7.70 (d, J = 8.3 Hz, 2H), 7.53 (s, 1H), 7.49 (d, J = 7.8 Hz, 1H), 7.42 (dd, J = 7.8, 1.5 Hz, 1H), 7.38 (d, J = 7.7 Hz, 1H), 7.22 (dd, J = 7.8, 1.4 Hz, 1H), 7.01 (d, J = 8.1 Hz, 2H), 5.81 (s, 1H), 4.60 (d, J = 2.5 Hz, 2H), 4.56 – 4.42 (m, 2H), 3.48 (s, 3H), 3.41 (s, 3H) ppm.

^{13}C NMR (101 MHz, CDCl_3): δ 170.56, 145.34, 145.02, 142.12, 138.78, 138.36, 138.29, 138.24, 129.63, 129.54, 129.26, 129.11, 129.09, 125.89, 125.08, 120.07, 74.57, 74.34, 65.15, 61.05, 58.22, 58.10 ppm.

HRMS (ESI): m/z calcd for $\text{C}_{25}\text{H}_{21}\text{Br}_2\text{O}_4\text{-H}^-$: 542.9812 [$M\text{-H}$] $^-$; found 542.9834.

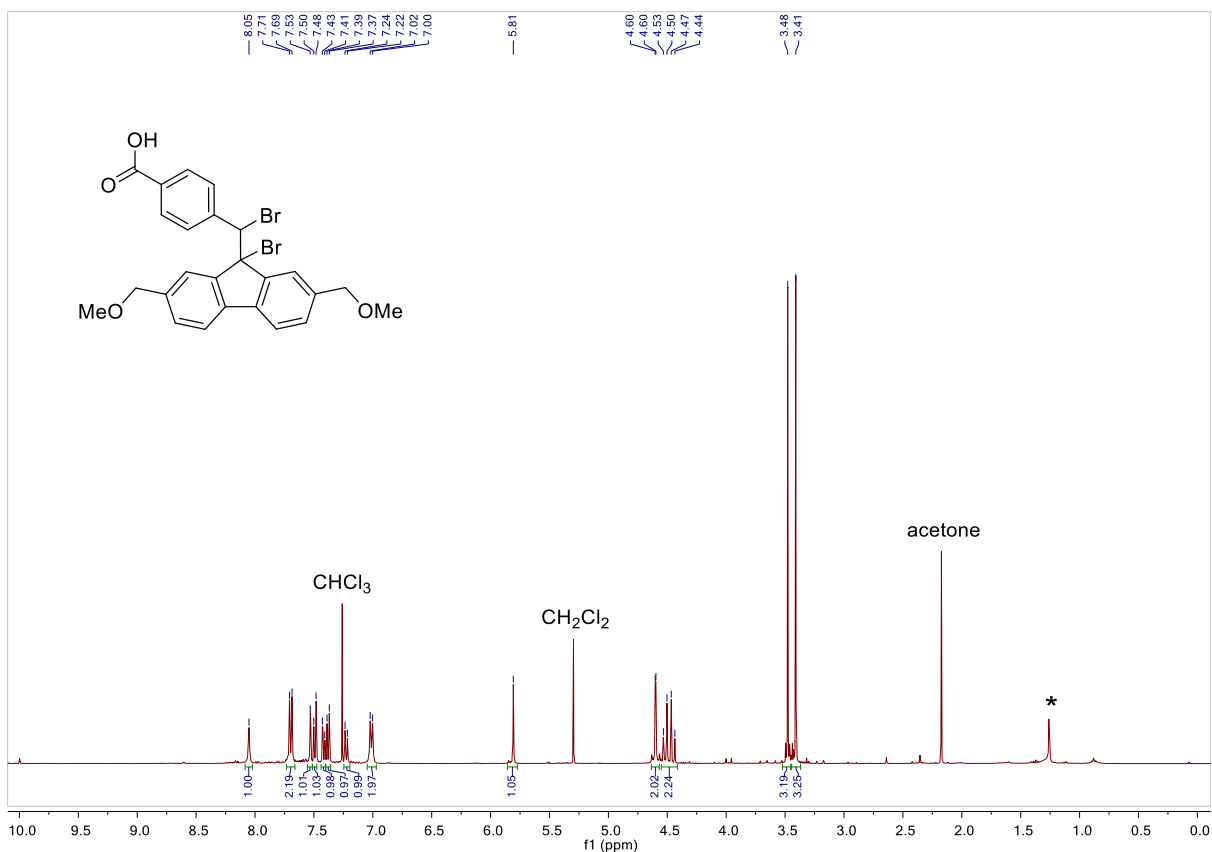


Figure S9. ¹H-NMR spectrum of compound 12. The asterisk indicates an impurity from a preparatory TLC.

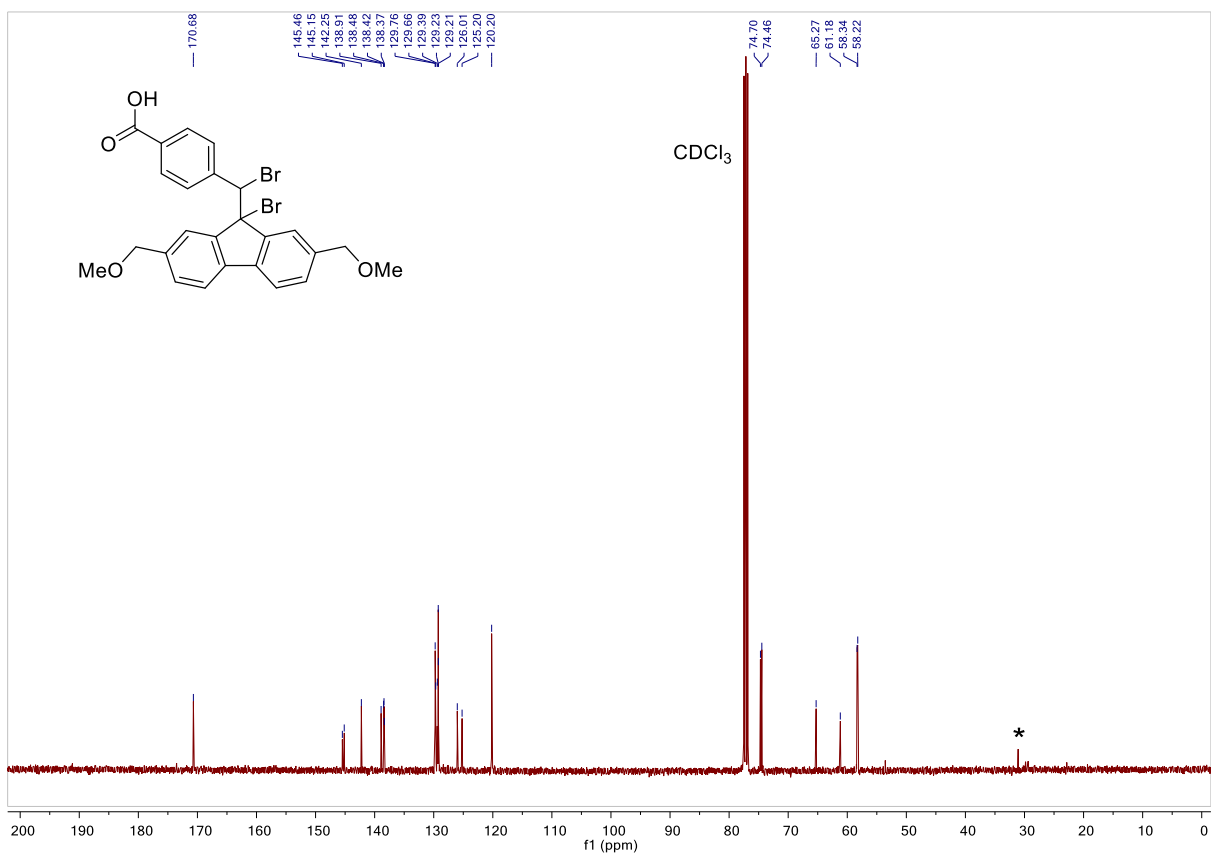
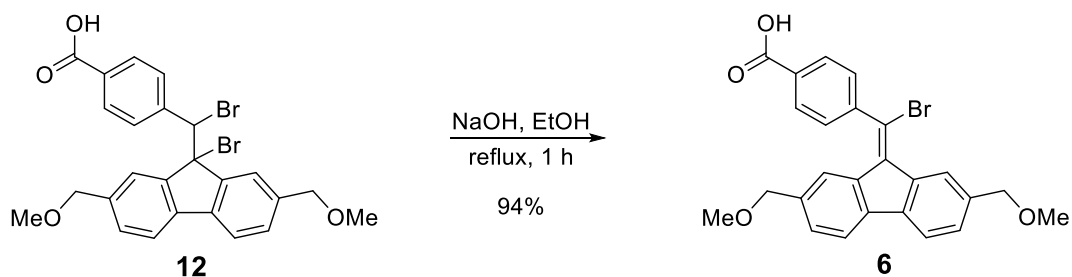


Figure S10. ¹³C-NMR spectrum of compound 12. The asterisk indicates an impurity from a preparatory TLC.



Compound 6. To a solution of compound **12** (645 mg, 1.18 mmol) in EtOH (30 mL), NaOH (189 mg, 4.72 mmol) was added and the resulting solution refluxed for 1 h. The solution was cooled to 23 °C, acidified with aq. HCl (1 N, 50 mL) and extracted with EtOAc (3 x 50 mL). The combined organic layers were washed with brine (2 x 100 mL), dried over Na₂SO₄ and concentrated *in vacuo*. The crude product was purified by flash-column chromatography using a gradient elution (CH₂Cl₂:MeOH; 100:0 to 97:03) to give **6** (520 mg, 94%) as an orange solid.

TLC (Silica gel, CH₂Cl₂:MeOH; 97:03): *R_f* (**12**) = 0.3, *R_f* (**6**) = 0.3

¹H NMR (400 MHz, DMSO-*d*₆): δ 8.73 (s, 1H), 8.13 (d, *J* = 8.4 Hz, 2H), 7.88 (d, *J* = 7.7 Hz, 1H), 7.79 (d, *J* = 7.7 Hz, 1H), 7.61 (d, *J* = 8.3 Hz, 2H), 7.47 (dd, *J* = 7.7, 1.4 Hz, 1H), 7.19 (dd, *J* = 7.8, 1.4 Hz, 1H), 6.00 (s, 1H), 4.54 (s, 2H), 4.06 (s, 2H), 3.35 (s, 3H), 3.02 (s, 3H) ppm.

¹³C NMR (101 MHz, DMSO-*d*₆): δ 166.68, 145.93, 139.95, 138.33, 137.59, 137.33, 137.23, 137.14, 135.39, 131.50, 130.44, 129.25, 128.54, 127.83, 124.76, 123.15, 123.10, 119.98, 119.71, 73.92, 73.19, 57.55, 57.30 ppm.

HRMS (ESI): *m/z* calcd for C₂₅H₂₁BrO₄-H⁻: 463.0550 [*M*-H]⁻; found 463.0541.

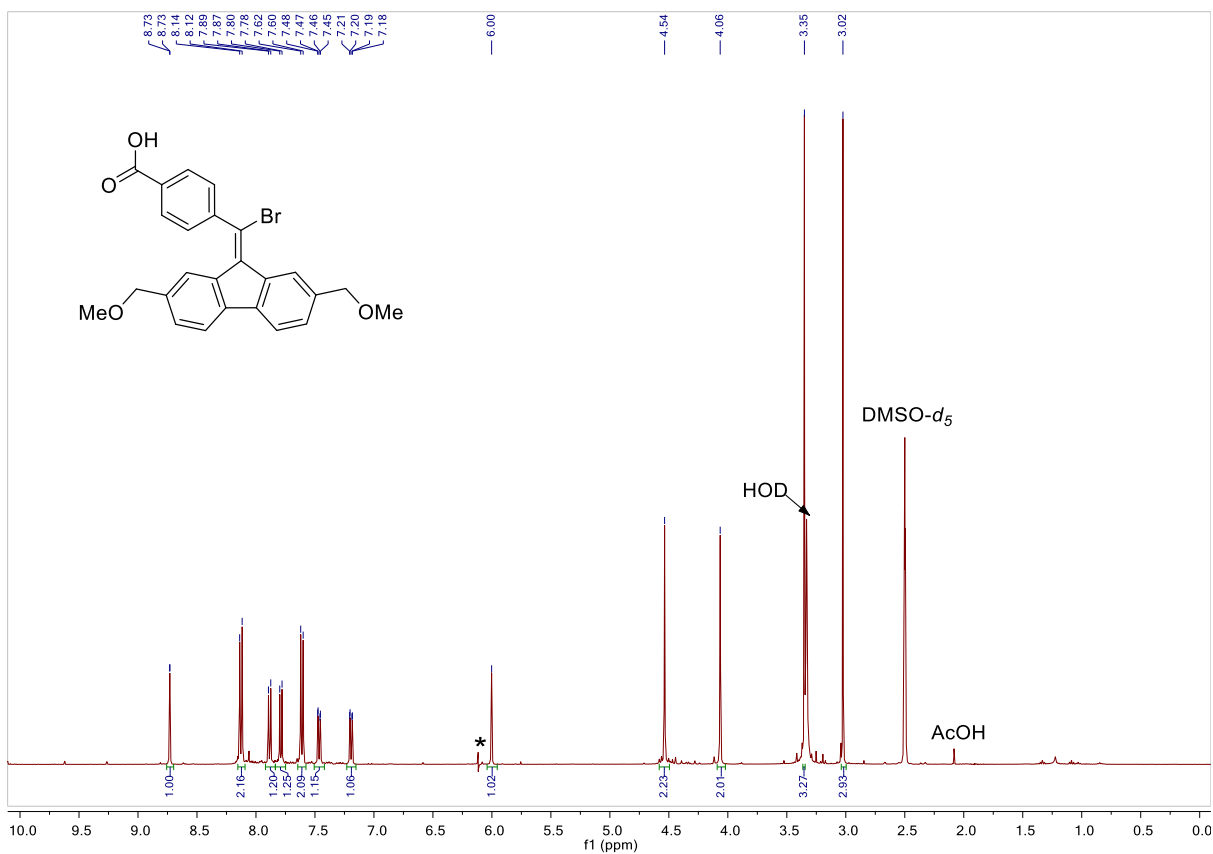


Figure S11. ¹H-NMR spectrum of compound 6. The asterisk indicates an instrumental glitch.

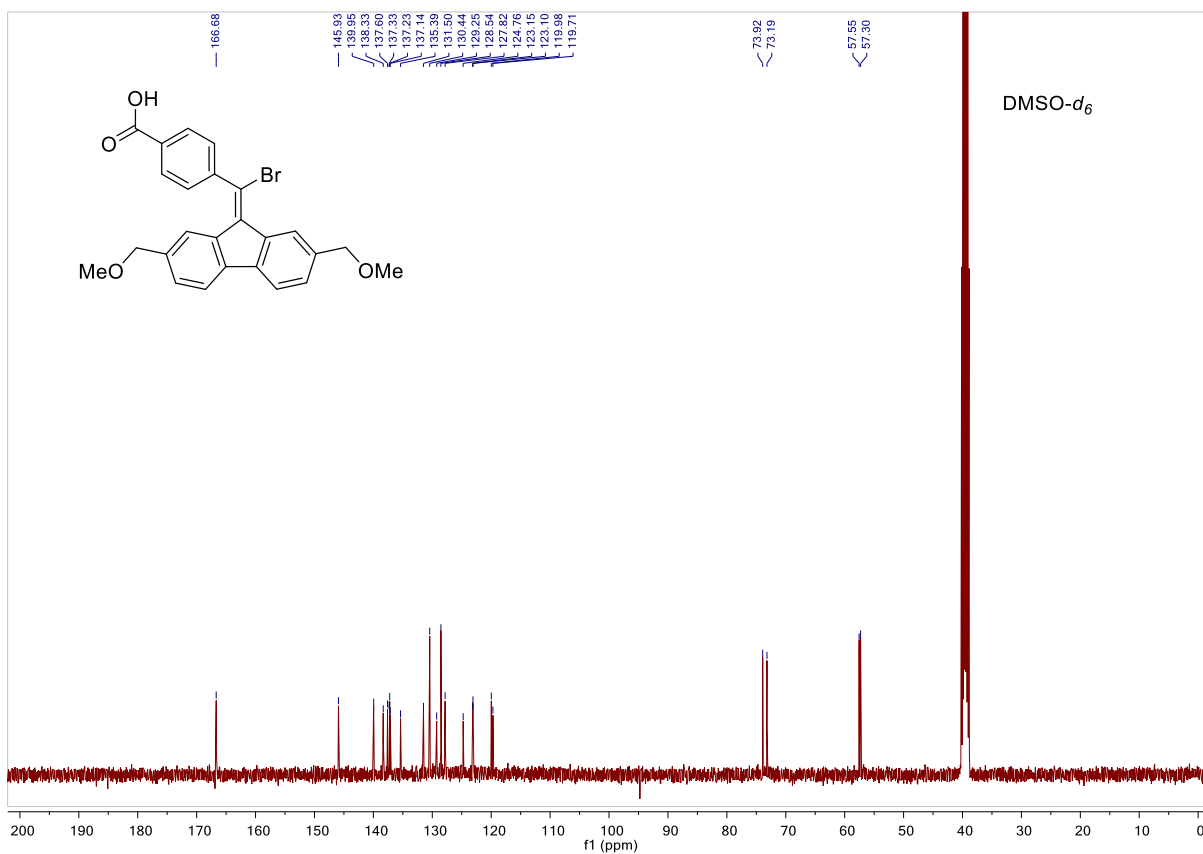
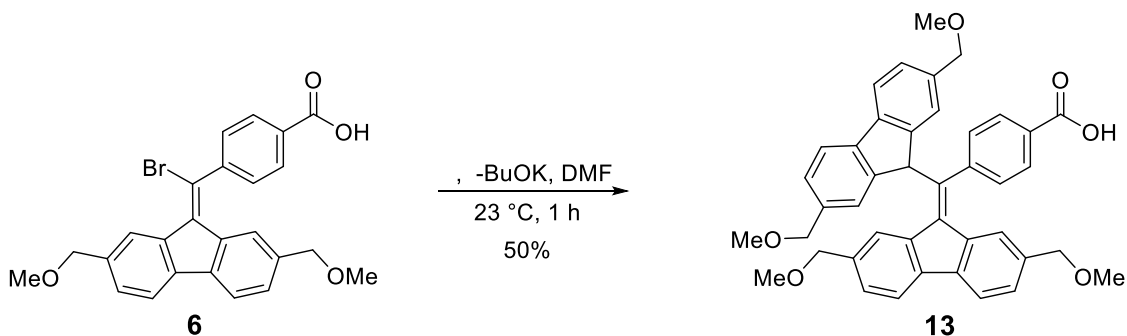


Figure S12. ¹³C-NMR spectrum of compound 6.



Tetra-(methoxymethyl)-BDPA 13. Compound **6** (1.4 g, 3.01 mmol), 2,7-bis(methoxymethyl)-9*H*-fluorene (**4**) (918 mg, 3.61 mmol) and *t*-BuOK (1.69 g, 15.04 mmol) were weighed into a round-bottom flask and DMF (50 mL) was added. The resulting solution was stirred at 23 °C for 1 h, acidified with aq. HCl (1 N, 100 mL) and extracted with EtOAc (3 x 100 mL). The combined organic layers were washed with brine (2 x 200 mL), dried over Na₂SO₄ and concentrated *in vacuo*. The crude product was purified by flash-column chromatography using a gradient elution (CH₂Cl₂:MeOH; 100:0 to 98:02) to give **13** (960 mg, 50%) as a yellow solid.

TLC (Silica gel, CH₂Cl₂:MeOH; 97:03): *R_f* (**6**) = 0.3, *R_f* (**13**) = 0.35

¹H NMR (400 MHz, CDCl₃): δ 8.35 (s, 1H), 7.84 (d, *J* = 7.8 Hz, 1H), 7.75 – 7.66 (m, 3H), 7.61 (d, *J* = 7.8 Hz, 2H), 7.57 (s, 2H), 7.48 (dd, *J* = 8.0, 1.2 Hz, 1H), 7.32 (dd, *J* = 7.9, 1.4 Hz, 2H), 7.20 (dd, *J* = 7.7, 1.4 Hz, 1H), 6.77 (d, *J* = 8.4 Hz, 2H), 6.51 (s, 1H), 5.76 (s, 1H), 4.53 (s, 2H), 4.47 (s, 4H), 4.03 (s, 2H), 3.39 (s, 3H), 3.34 (s, 6H), 3.11 (s, 3H) ppm.

¹³C NMR (101 MHz, CDCl₃): δ 170.91, 144.37, 144.34, 143.50, 141.49, 140.98, 139.38, 139.00, 138.90, 137.54, 137.46, 136.63, 136.19, 129.67, 129.11, 128.55, 128.15, 127.76, 127.48, 125.52, 125.21, 124.78, 120.21, 120.10, 119.35, 75.21, 74.81, 74.77, 58.20, 58.02, 57.95, 52.24 ppm.

HRMS (ESI): *m/z* calcd for C₄₂H₃₇O₆-H⁻: 637.2596 [*M*-H]⁻; found 637.2589.

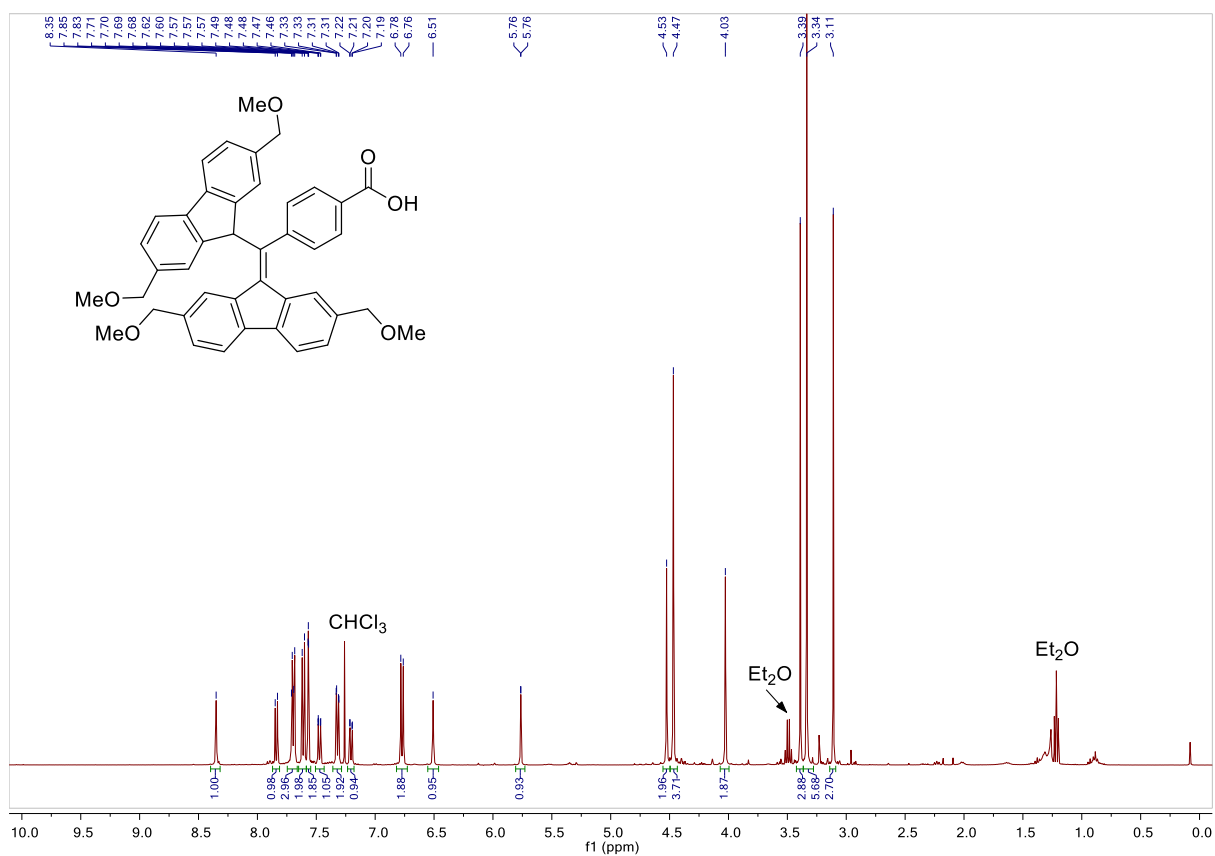


Figure S13. ¹H-NMR spectrum of compound 13.

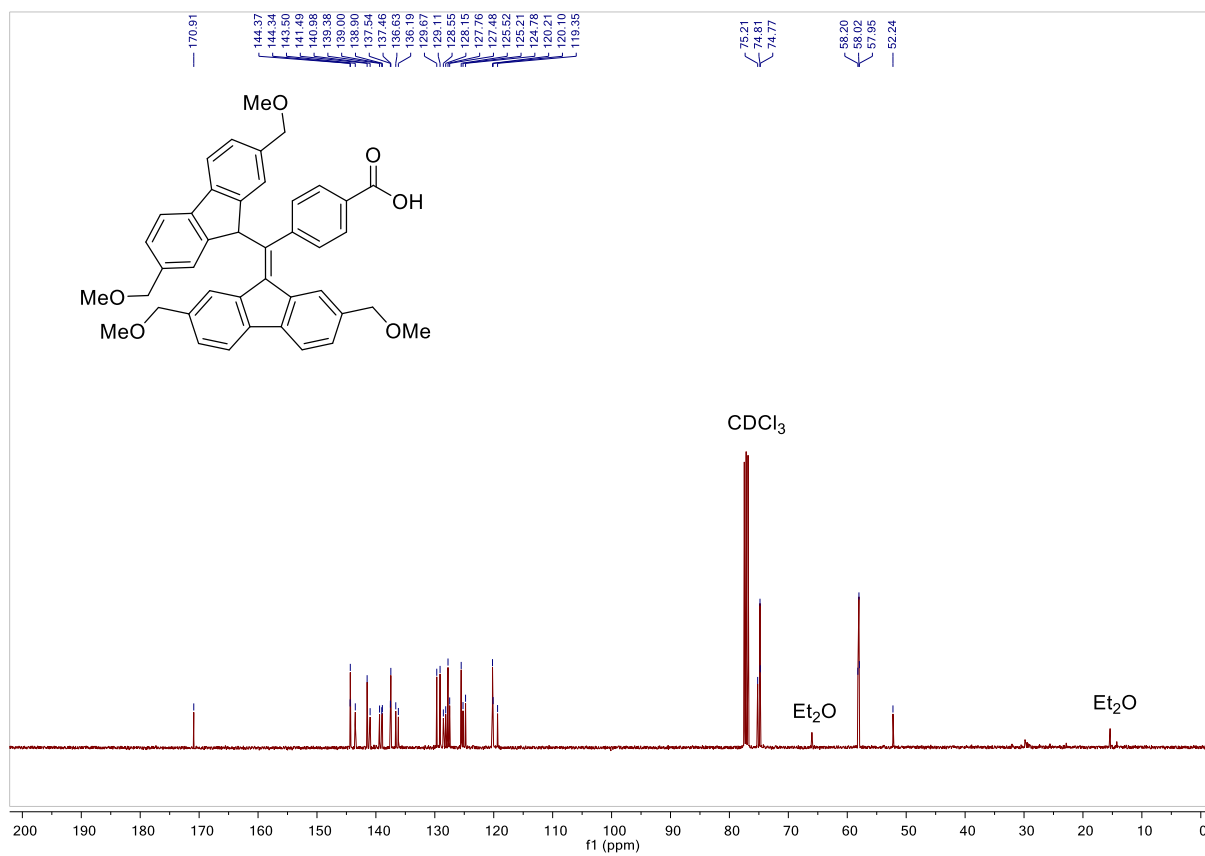
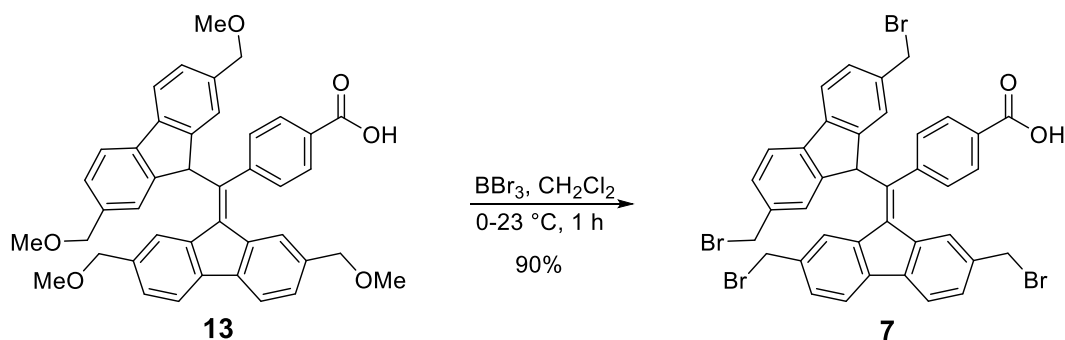


Figure S14. ¹³C-NMR spectrum of compound 13.



Tetra-(bromomethyl)-BDPA 7. To a solution of compound **13** (930 mg, 1.45 mmol) in CH_2Cl_2 (30 mL) at 0 °C, BBr_3 (0.6 mL, 5.82 mmol) was added and the resulting solution stirred at 23 °C for 1 h. The reaction was quenched with satd. aq. NaHCO_3 (30 mL) and extracted with CH_2Cl_2 (3 x 50 mL). The combined organic layers were dried over Na_2SO_4 and concentrated *in vacuo*. The crude product was purified by flash-column chromatography using a gradient elution (CH_2Cl_2 :MeOH; 100:0 to 98:02) to give **7** (1.08 g, 90%) as an orange solid.

TLC (Silica gel, CH_2Cl_2 :MeOH; 97:03): R_f (**13**) = 0.35, R_f (**7**) = 0.5

$^1\text{H NMR}$ (400 MHz, CDCl_3): δ 8.40 (s, 1H), 7.84 (d, $J = 7.8$ Hz, 1H), 7.76 (d, $J = 8.4$ Hz, 2H), 7.69 (d, $J = 7.8$ Hz, 1H), 7.63 (s, 2H), 7.60 (d, $J = 7.9$ Hz, 2H), 7.55 (dd, $J = 7.8, 1.4$ Hz, 1H), 7.38 (dd, $J = 7.9, 1.6$ Hz, 2H), 7.28 (dd, $J = 7.6, 1.4$ Hz, 1H), 6.77 (d, $J = 8.4$ Hz, 2H), 6.43 (s, 1H), 5.87 (s, 1H), 4.61 (s, 2H), 4.53 (q, $J = 7.7$ Hz, 4H), 4.08 (s, 2H) ppm.

$^{13}\text{C NMR}$ (101 MHz, CDCl_3): δ 170.91, 144.56, 144.06, 143.59, 141.73, 141.15, 139.56, 139.29, 139.20, 137.55, 137.48, 136.59, 135.74, 130.06, 129.94, 129.26, 128.97, 128.91, 128.46, 126.85, 126.61, 125.94, 120.84, 120.76, 119.83, 52.28, 34.36, 34.14, 33.91 ppm.

HRMS (ESI): m/z calcd for $\text{C}_{38}\text{H}_{25}\text{Br}_4\text{O}_2\text{-H}^-$: 828.8594 [$M\text{-H}$] $^-$; found 828.8621.

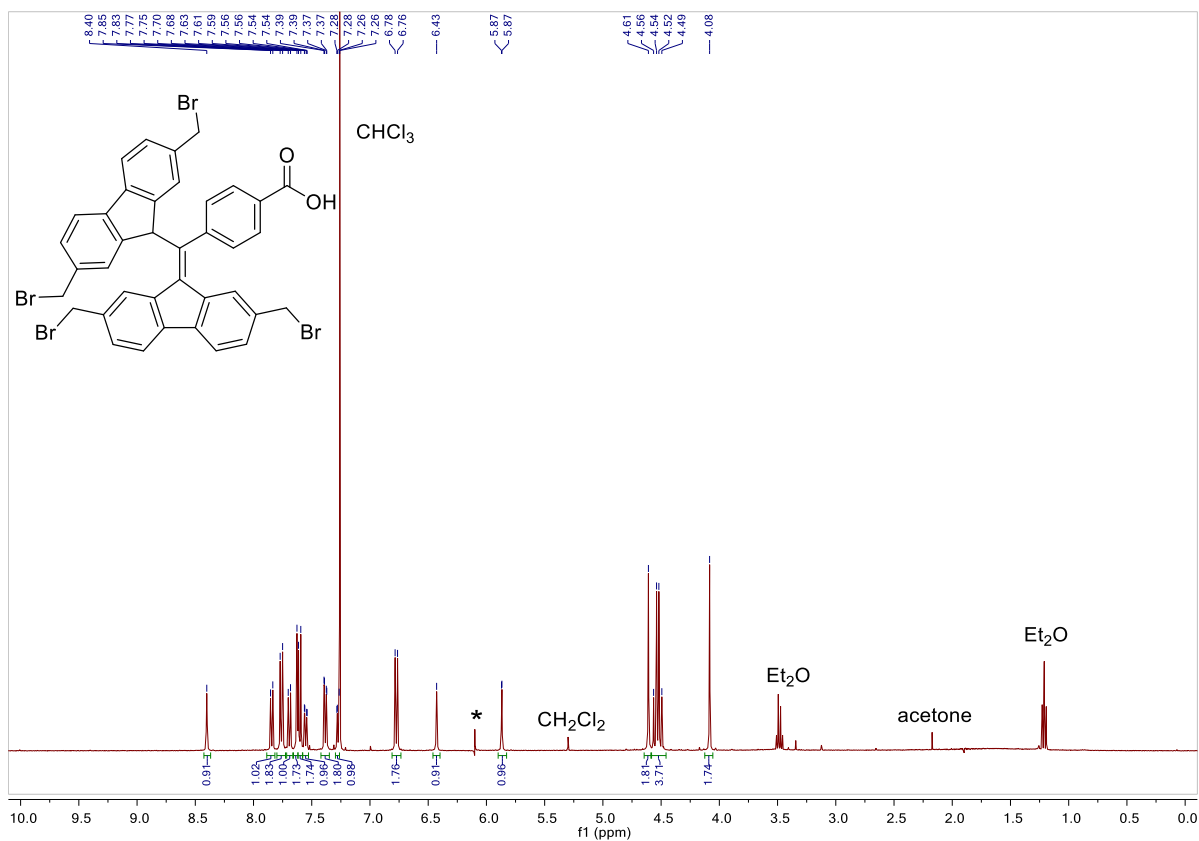


Figure S15. ¹H-NMR spectrum of compound 7. The asterisk indicates an instrumental glitch.

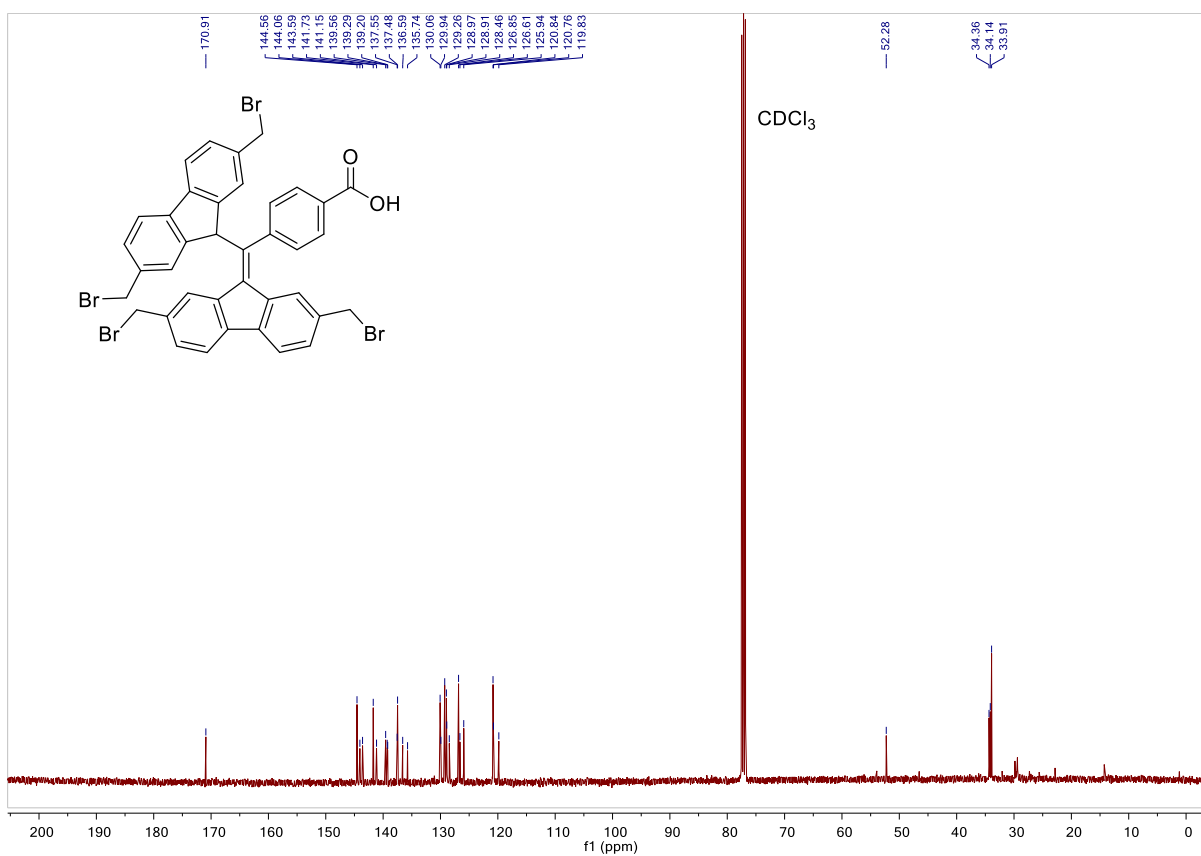
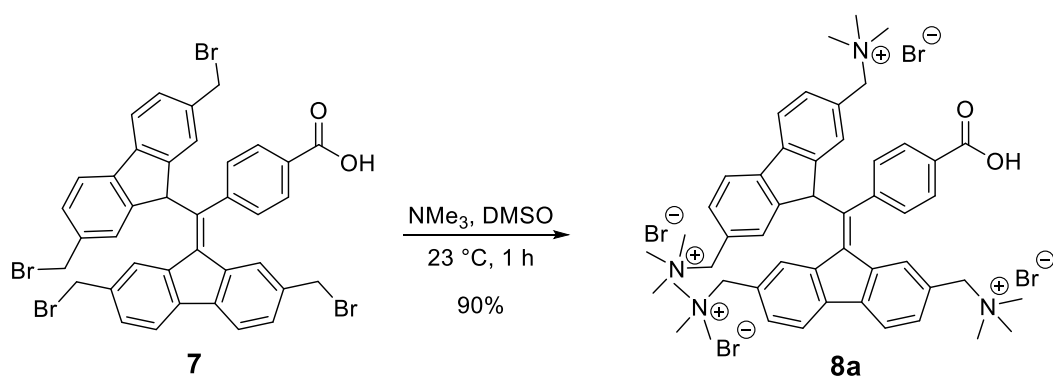


Figure S16. ¹³C-NMR spectrum of compound 7.

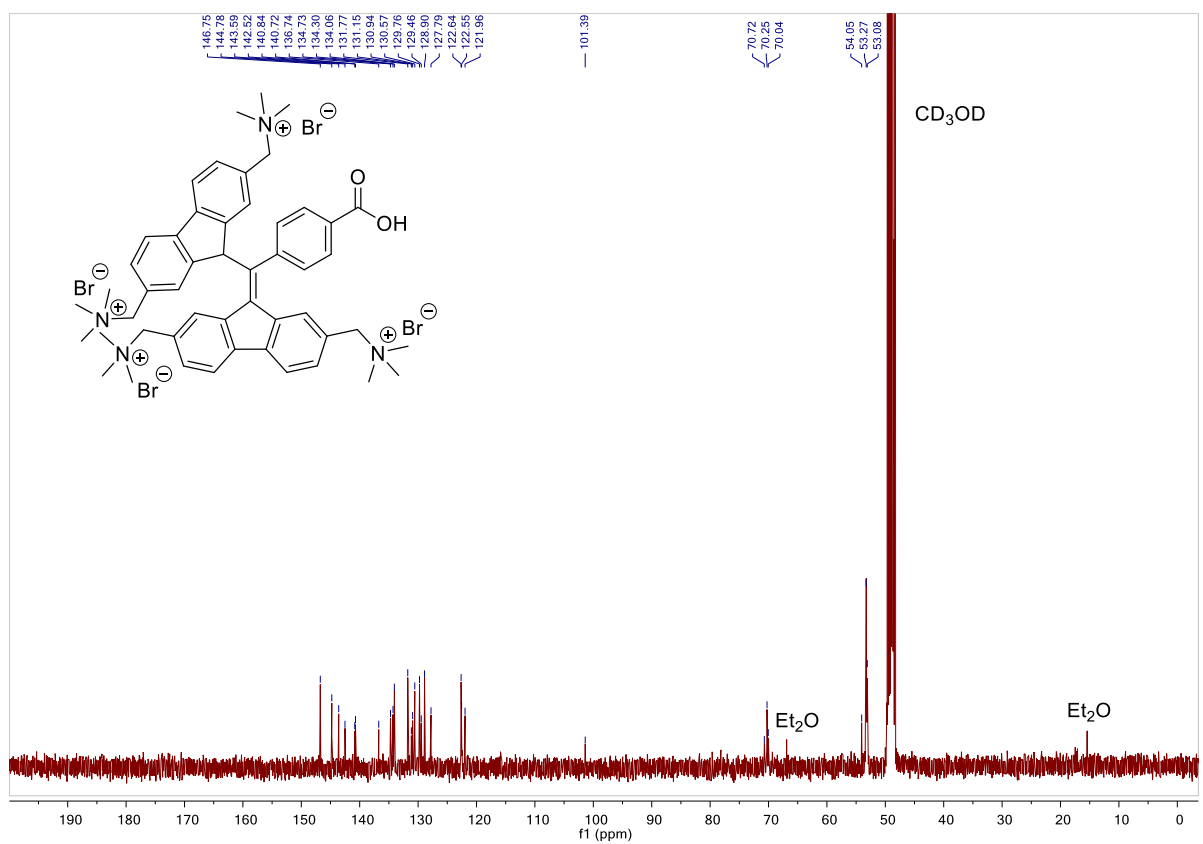
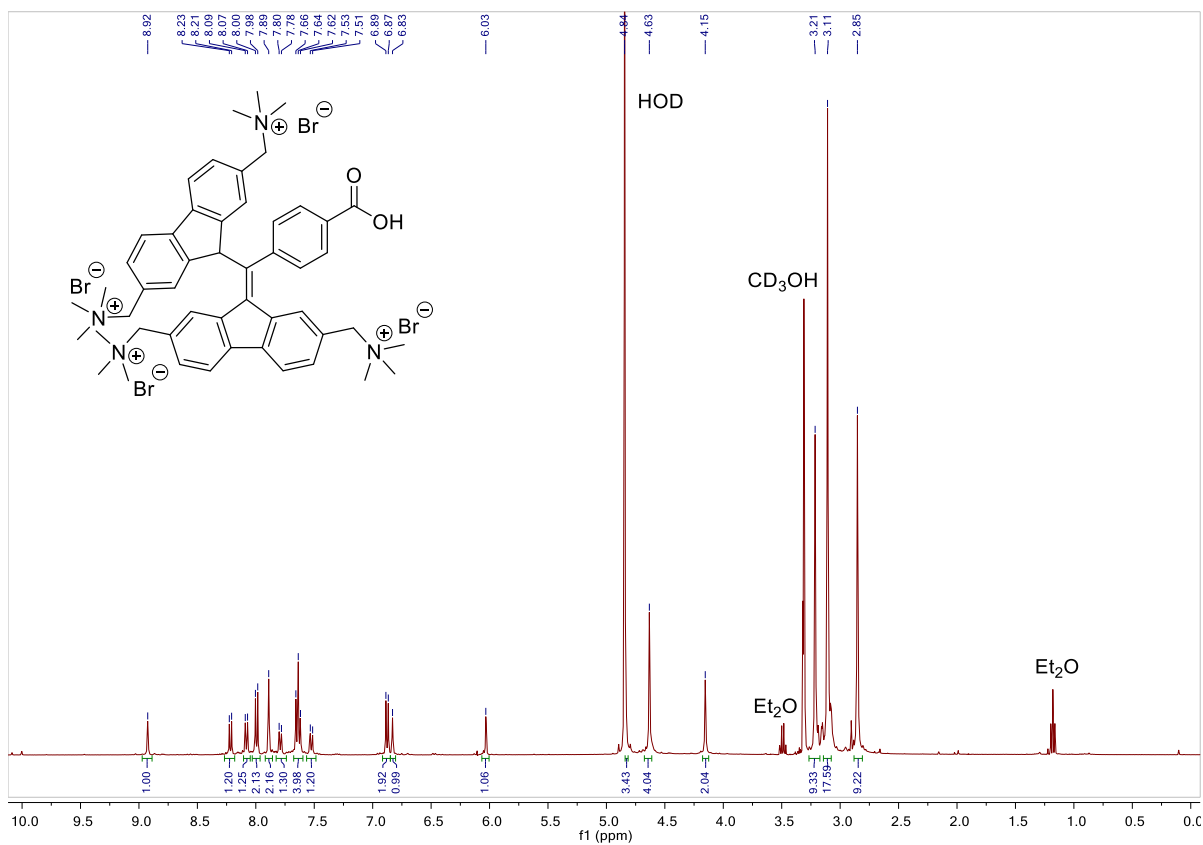


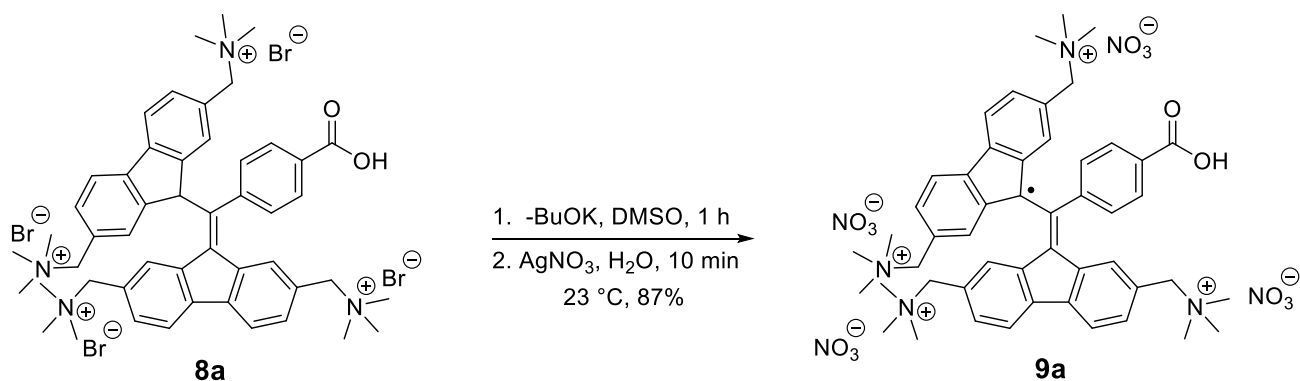
Tetraalkylammonium BDPA 8a. To a solution of tetra-bromo BDPA derivative **7** (20 mg, 0.024 mmol) in DMSO (2 mL), NMe₃ (60 μL, 0.24 mmol, 4 M) was added and the resulting solution stirred at 23 °C for 1 h. The reaction mixture was poured into Et₂O (10 mL), the precipitate collected by centrifugation followed by decantation of the solvent. The precipitate was redissolved in MeOH (2 mL) and reprecipitated by addition of Et₂O (10 mL). This precipitation was repeated to yield **8a** (23 mg, 90%) as a reddish brown solid.

¹H NMR (400 MHz, Methanol-*d*₄) δ 8.92 (s, 1H), 8.22 (d, *J* = 7.8 Hz, 1H), 8.08 (d, *J* = 7.8 Hz, 1H), 7.99 (d, *J* = 7.9 Hz, 2H), 7.89 (d, *J* = 1.4 Hz, 2H), 7.79 (dd, *J* = 7.9, 1.2 Hz, 1H), 7.70 – 7.58 (m, 4H), 7.53 (dd, *J* = 7.8, 1.6 Hz, 1H), 6.88 (d, *J* = 8.3 Hz, 2H), 6.83 (s, 1H), 6.03 (d, *J* = 1.5 Hz, 1H), 4.84 (s, 2H), 4.63 (s, 4H), 4.15 (s, 2H), 3.21 (s, 9H), 3.11 (s, 18H), 2.85 (s, 9H) ppm.

¹³C NMR (101 MHz, Methanol-*d*₄) δ 146.75, 144.78, 143.59, 142.52, 140.84, 140.72, 136.74, 134.73, 134.30, 134.06, 131.77, 131.15, 130.94, 130.57, 129.76, 129.46, 128.90, 127.79, 122.64, 122.55, 121.96, 101.39, 70.72, 70.25, 70.04, 54.05, 53.27, 53.08 ppm.

HRMS (ESI): *m/z* calcd for C₅₀H₆₂N₄O₂-H³⁺: 249.8259 [*M*-H]³⁺; found 249.8252.

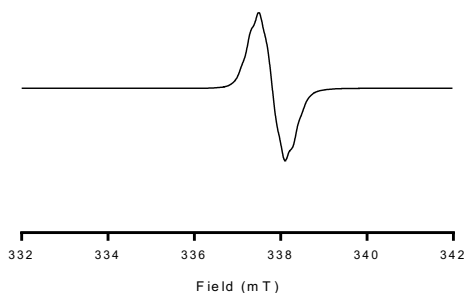




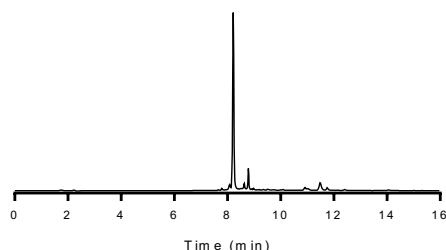
BDPA radical 9a. To a solution of **8a** (13 mg, 0.012 mmol) in DMSO (1 mL) was added a freshly prepared $t\text{-BuOK}$ solution (96 μL , 0.024 mmol, 0.25 M in DMSO) and the resulting solution stirred at 23 °C for 1 h. A solution of AgNO_3 (10 mg, 0.06 mmol) in H_2O (0.2 mL) was added and the brown solution stirred for 10 min. The mixture was centrifuged, the solution was decanted and poured into Et_2O (10 mL). The precipitate formed was collected by centrifugation followed by decantation of the solvent. The precipitate was redissolved in MeOH (2 mL) and reprecipitated by addition of Et_2O (10 mL) twice. The precipitate was redissolved in MeOH (2 mL), filtered through celite and dried to give **9a** (10.5 mg, 87%) as a reddish brown solid.

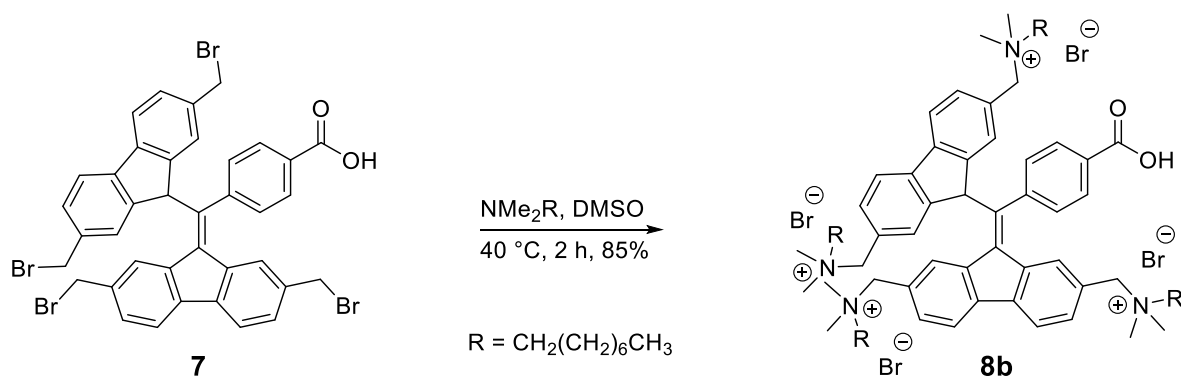
HRMS (ESI): m/z calcd for $\text{C}_{50}\text{H}_{61}\text{N}_4\text{O}_2+\text{NO}_3^{3+}$: 270.4885 $[\text{M}+\text{NO}_3]^{3+}$; found: 270.4854.

EPR (H_2O):



HPLC:



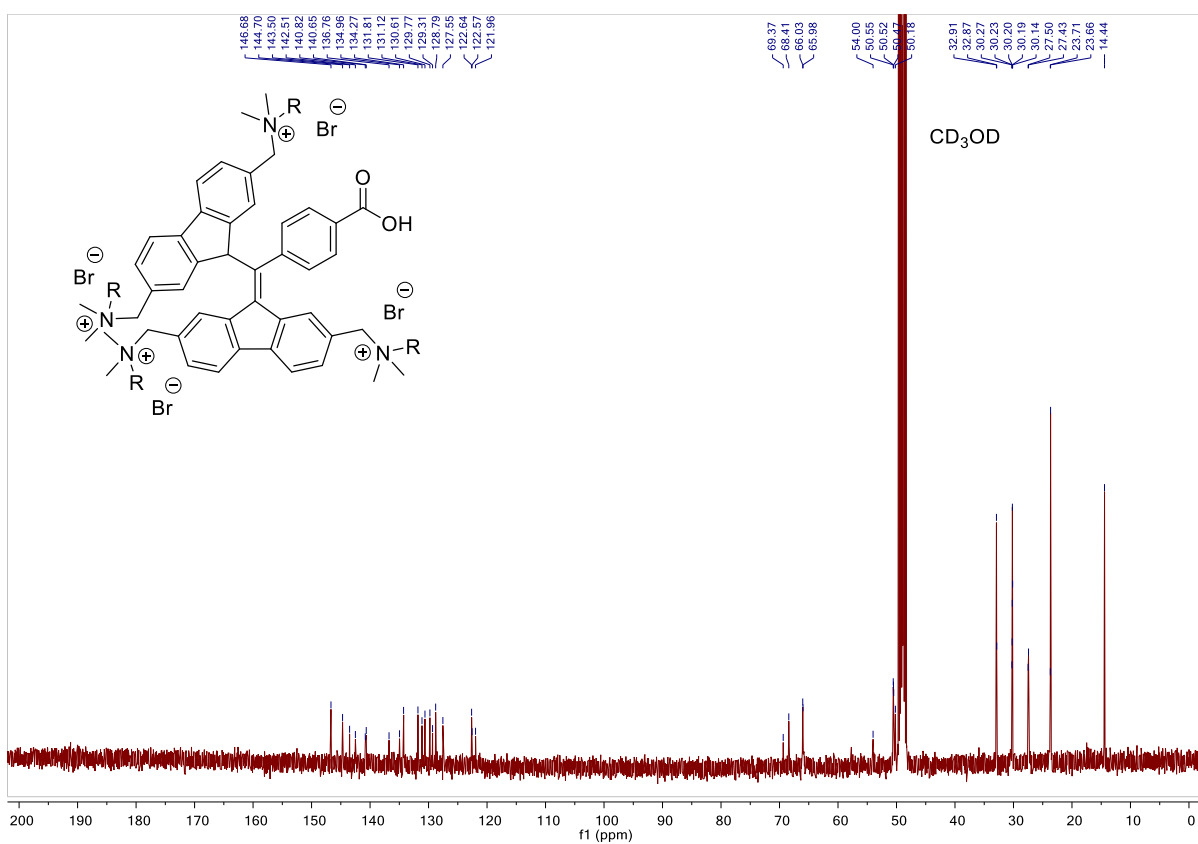
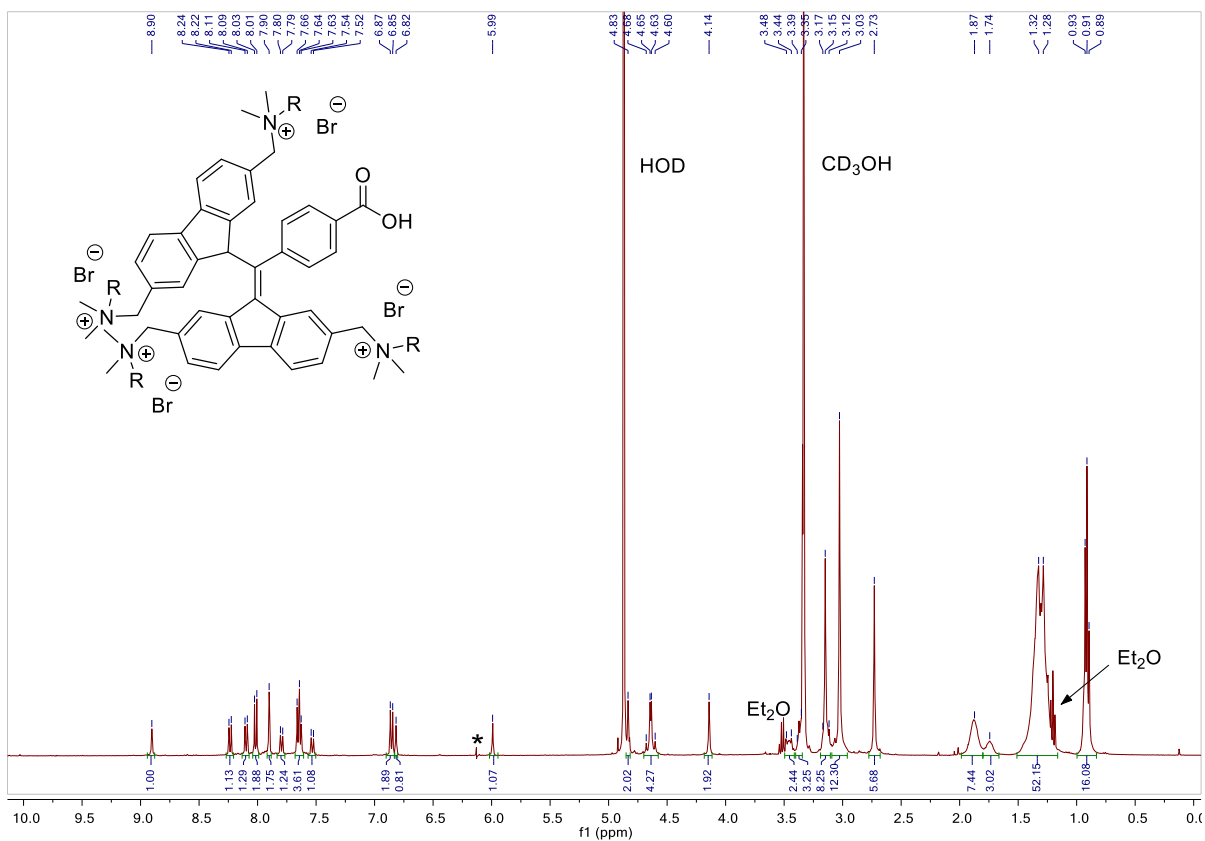


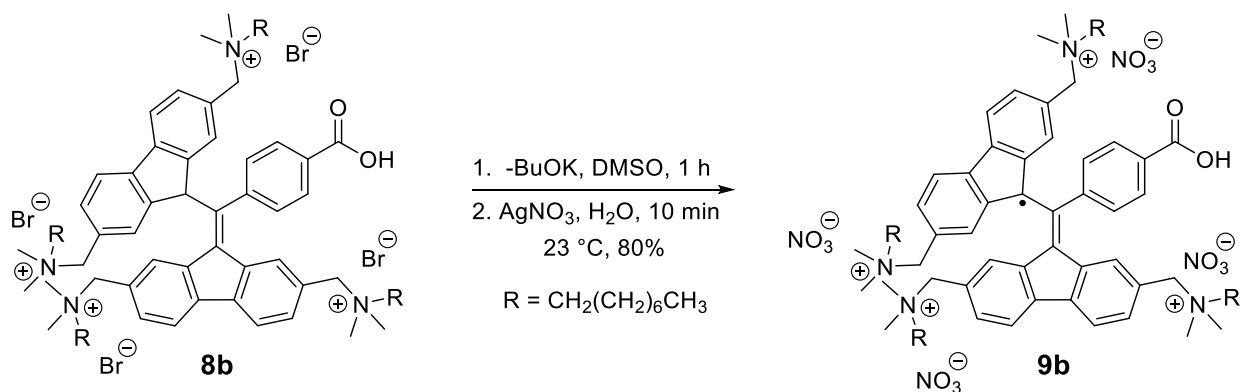
Tetraalkylammonium BDPA 8b. To a solution of tetra-bromo BDPA derivative **7** (10 mg, 0.012 mmol) in DMSO (1 mL), *N,N*-dimethyloctylamine (25 μ L, 0.12 mmol) was added and the resulting solution stirred at 40 $^\circ$ C for 2 h. The reaction mixture was poured into Et₂O (10 mL), the precipitate collected by centrifugation followed by decantation of the solvent. The precipitate was redissolved in MeOH (2 mL) and reprecipitated by addition of Et₂O (10 mL). This precipitation was repeated to yield **8b** (15 mg, 85%) as a reddish brown solid.

¹H NMR (400 MHz, MeOD) δ 8.88 (s, 1H), 8.21 (d, *J* = 7.9 Hz, 1H), 8.07 (d, *J* = 7.8 Hz, 1H), 7.99 (d, *J* = 7.9 Hz, 2H), 7.88 (s, 2H), 7.77 (dd, *J* = 7.9, 1.2 Hz, 1H), 7.66 – 7.59 (m, 4H), 7.51 (dd, *J* = 8.0, 1.5 Hz, 1H), 6.83 (d, *J* = 8.3 Hz, 2H), 6.79 (s, 1H), 5.97 (s, 1H), 4.81 (s, 2H), 4.67 – 4.55 (m, 4H), 4.12 (s, 2H), 3.47 – 3.40 (m, 2H), 3.40 – 3.32 (m, 4H), 3.15 – 3.12 (m, 8H), 3.00 (s, 12H), 2.71 (s, 6H), 1.85 (bs, 6H), 1.72 (bs, 2H), 1.48 – 1.13 (m, 40H), 0.89 (t, *J* = 6.7 Hz, 12H) ppm.

¹³C NMR (101 MHz, MeOD) δ 146.68, 144.70, 143.50, 142.51, 140.82, 140.65, 136.76, 134.96, 134.27, 131.81, 131.12, 130.61, 129.77, 129.31, 128.79, 127.55, 122.64, 122.57, 121.96, 69.37, 68.41, 66.03, 65.98, 54.00, 50.55, 50.52, 50.47, 50.18, 32.91, 32.87, 30.27, 30.23, 30.20, 30.19, 30.14, 27.50, 27.43, 23.71, 23.66, 14.44 ppm.

HRMS (ESI): *m/z* calcd for C₇₈H₁₁₇N₄O₂-H³⁺: 380.6387 [*M*-H]³⁺; found 380.6396.

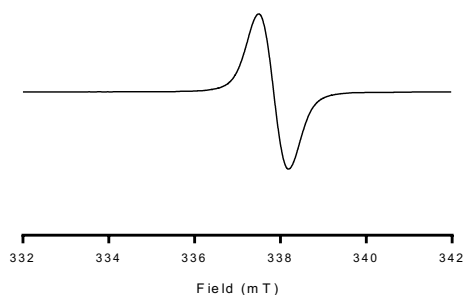




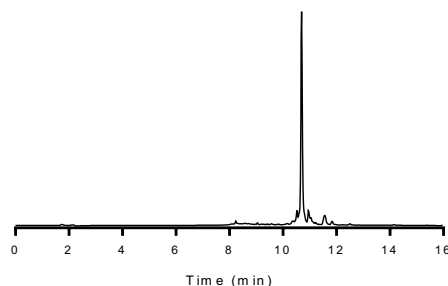
BDPA radical 9b. To a solution of **8b** (8 mg, 0.005 mmol) in DMSO (1 mL) was added a freshly prepared $t\text{-BuOK}$ solution (40 μL , 0.01 mmol, 0.25 M in DMSO) and the resulting solution stirred at 23 °C for 1 h. A solution of AgNO_3 (4 mg, 0.025 mmol) in H_2O (0.2 mL) was added and the brown solution stirred for 10 min. The mixture was centrifuged, the solution was decanted and poured into Et_2O (10 mL). The precipitate formed was collected by centrifugation followed by decantation of the solvent. The precipitate was redissolved in MeOH (2 mL) and reprecipitated by addition of Et_2O (10 mL) twice. The precipitate was redissolved in MeOH (2 mL), filtered through celite and dried to give **9b** (6 mg, 80%) as a reddish brown solid.

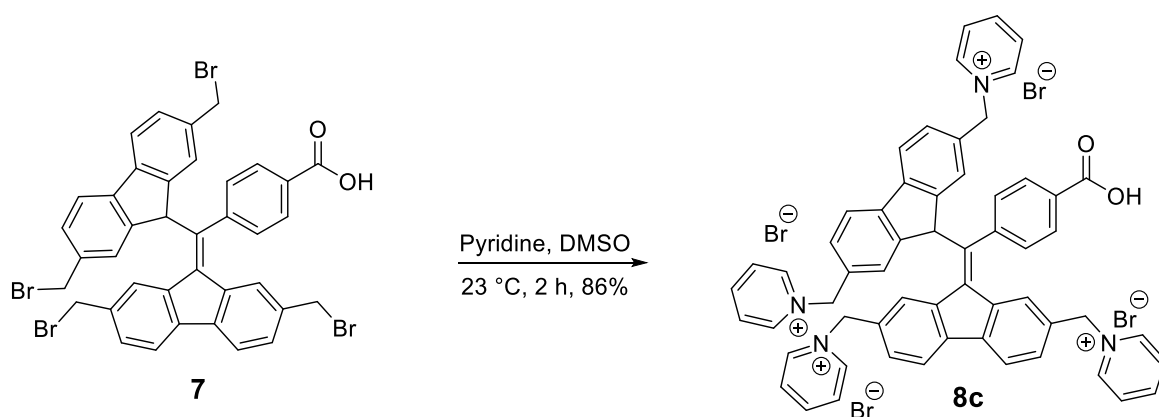
HRMS (ESI): m/z calcd for $\text{C}_{78}\text{H}_{117}\text{N}_4\text{O}_2^{4+}$: 285.4789 [M] $^{4+}$; found 285.4788.

EPR (MeOH):



HPLC:





Tetrapyridinium BDPA 8c. To a solution of tetra-bromo BDPA derivative **7** (10 mg, 0.012 mmol) in DMSO (1 mL), pyridine (10 μL , 0.12 mmol) was added and the resulting solution stirred at 23 $^\circ\text{C}$ for 2 h. The reaction mixture was poured into Et₂O (10 mL), the precipitate collected by centrifugation followed by decantation of the solvent. The precipitate was redissolved in MeOH (2 mL) and reprecipitated by addition of Et₂O (10 mL). This precipitation was repeated to yield **8c** (12 mg, 86%) as a reddish brown solid.

¹H NMR (400 MHz, MeOD) δ 9.25 – 9.16 (m, 2H), 9.14 – 9.04 (m, 4H), 8.77 (s, 1H), 8.71 – 8.53 (m, 6H), 8.15 – 8.11 (m, 7H), 8.07 – 8.02 (m, 2H), 8.00 (d, J = 7.8 Hz, 1H), 7.87 (d, J = 7.9 Hz, 2H), 7.76 (s, 2H), 7.67 (dd, J = 8.0, 1.3 Hz, 1H), 7.53 (dt, J = 7.8, 1.9 Hz, 3H), 7.39 (d, J = 8.3 Hz, 2H), 6.70 (s, 1H), 6.64 (d, J = 8.3 Hz, 2H), 6.05 (s, 2H), 5.92 (s, 4H), 5.75 (s, 1H), 5.55 (s, 2H) ppm.

¹³C NMR (101 MHz, MeOD) δ 168.79, 147.51, 147.36, 147.32, 146.80, 146.33, 146.16, 146.02, 145.78, 144.23, 143.93, 142.92, 141.70, 141.12, 140.67, 136.57, 134.45, 134.20, 133.46, 131.19, 131.12, 130.61, 130.53, 130.33, 129.73, 129.71, 129.55, 128.25, 127.95, 126.22, 122.83, 121.98, 65.65, 65.60, 65.53, 53.81 ppm.

HRMS (ESI): m/z calcd for C₅₈H₄₆N₄O₂⁴⁺: 207.5900 [M]⁴⁺; found 207.5898.

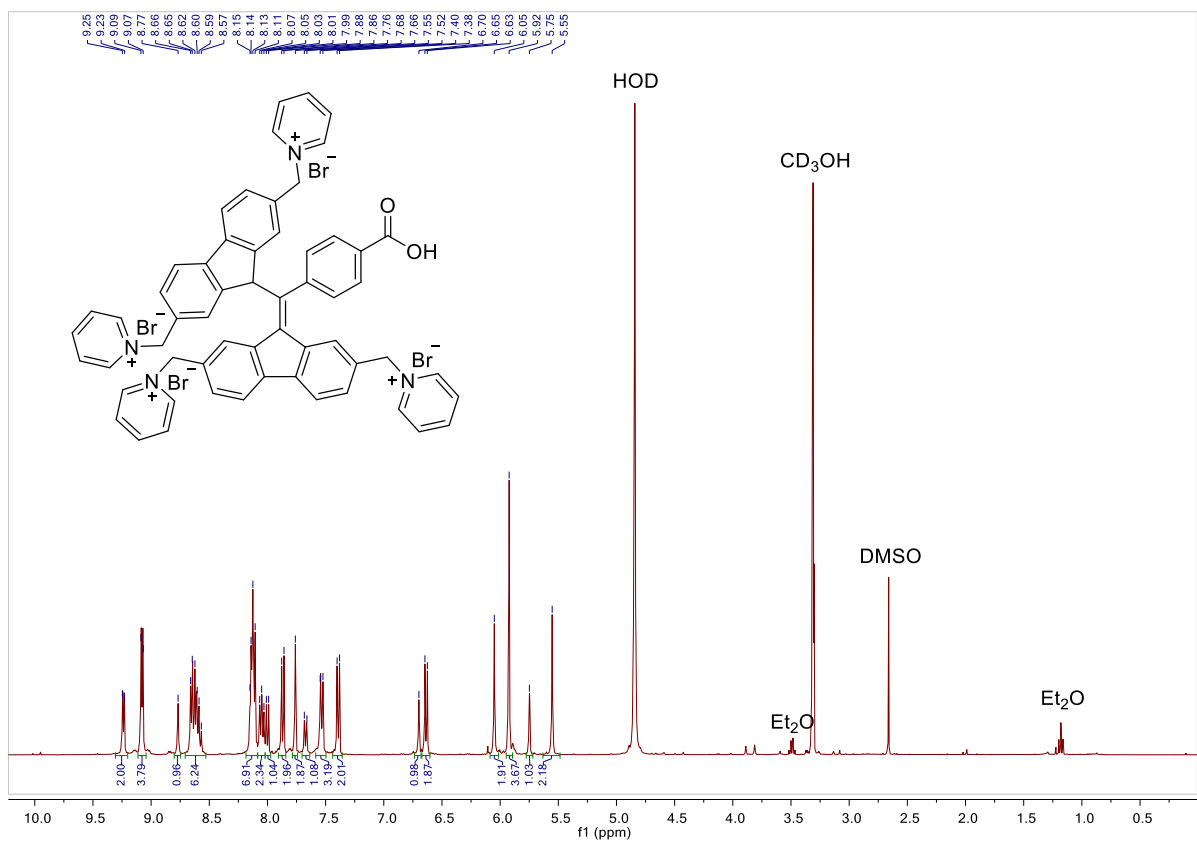


Figure S21. ¹H-NMR spectrum of compound **8c**.

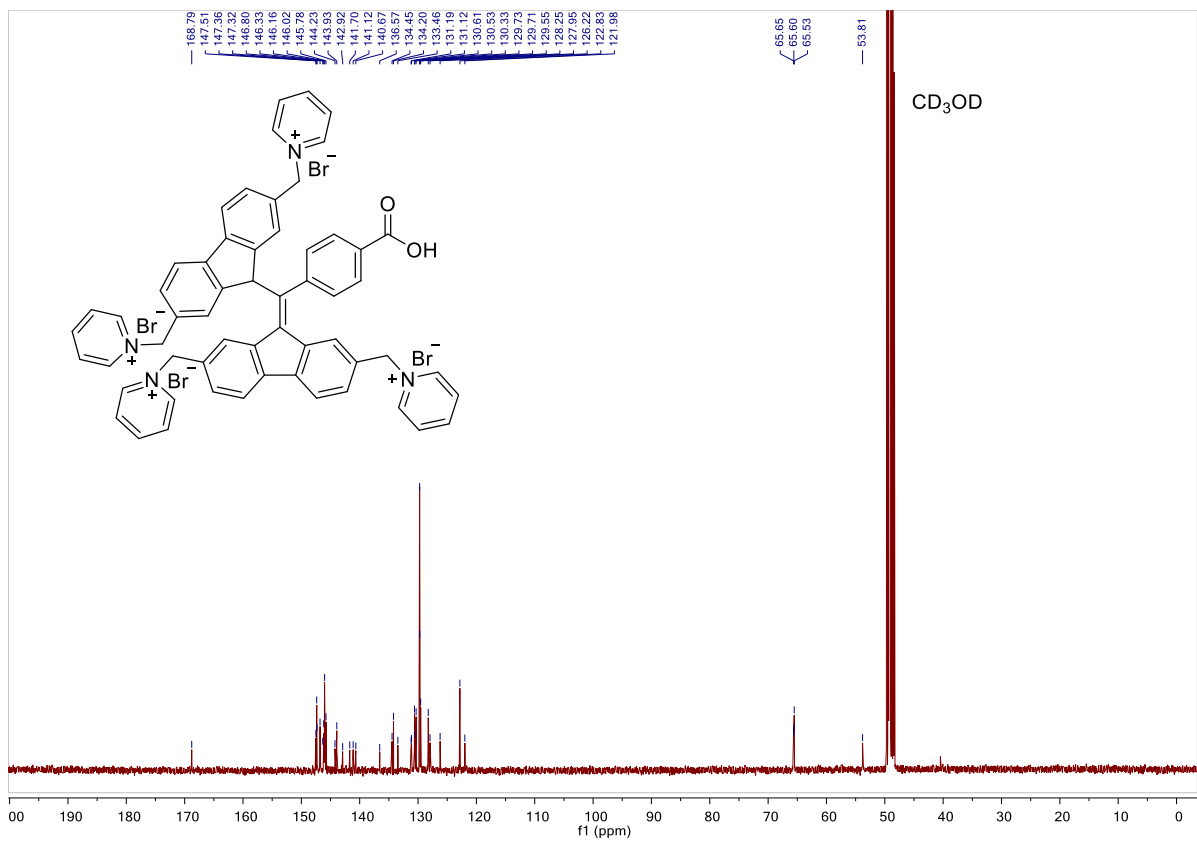
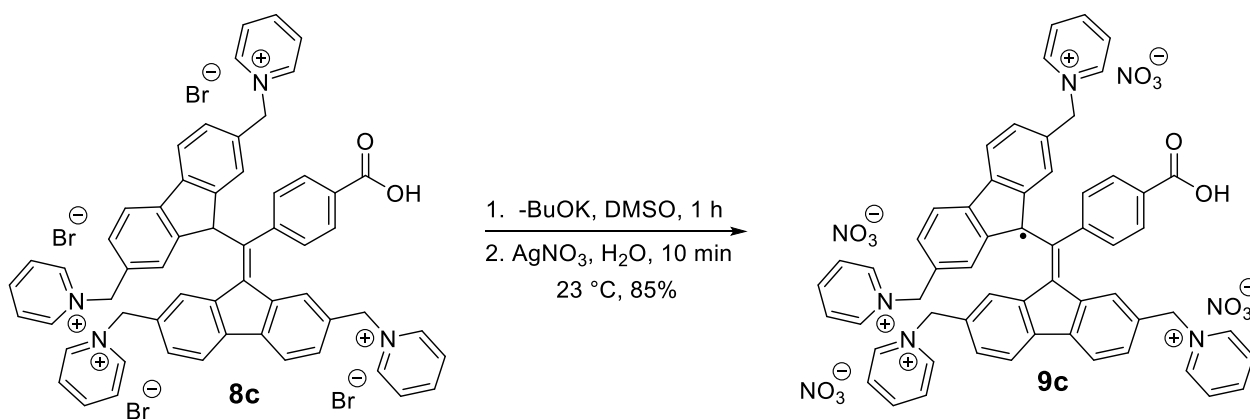


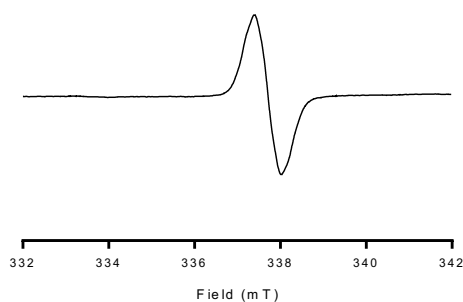
Figure S22. ¹³C-NMR spectrum of compound **8c**.



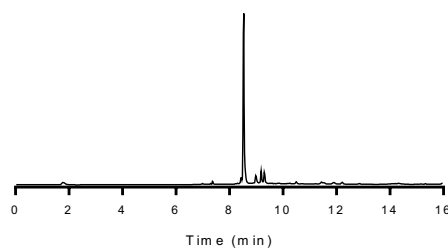
BDPA radical 9c. To a solution of **8c** (12 mg, 0.01 mmol) in DMSO (1 mL) was added a freshly prepared $t\text{-BuOK}$ solution (80 μL , 0.02 mmol, 0.25 M in DMSO) and the resulting solution stirred at 23 °C for 1 h. A solution of AgNO_3 (9 mg, 0.05 mmol) in H_2O (0.2 mL) was added and the brown solution stirred for 10 min. The mixture was centrifuged, the solution was decanted and poured into Et_2O (10 mL). The precipitate formed was collected by centrifugation followed by decantation of the solvent. The precipitate was redissolved in MeOH (2 mL) and reprecipitated by addition of Et_2O (10 mL) twice. The precipitate was redissolved in MeOH (2 mL), filtered through celite and dried to give **9c** (9.5 mg, 85%) as a reddish brown solid.

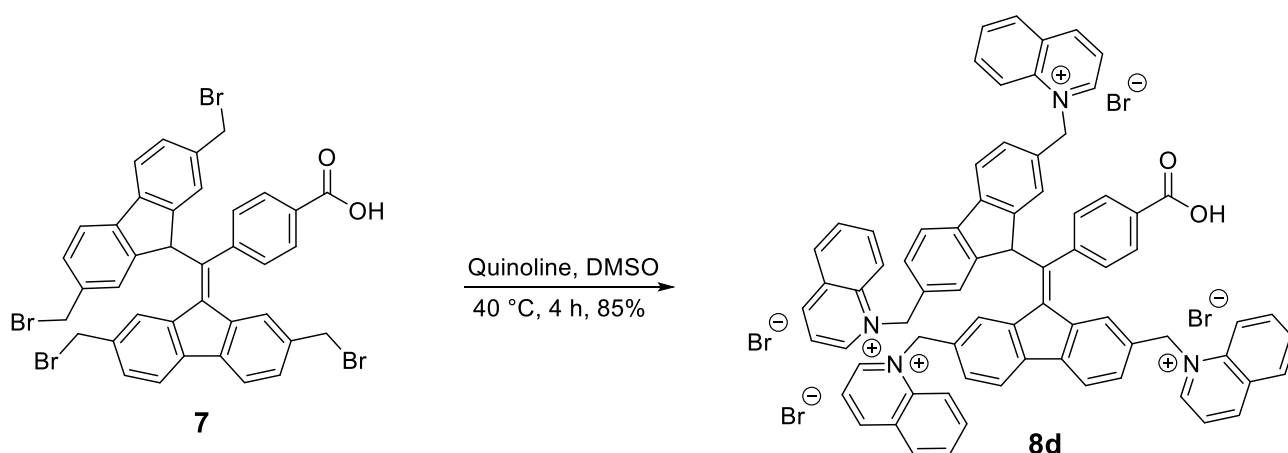
HRMS (ESI): m/z calcd for $\text{C}_{58}\text{H}_{45}\text{N}_4\text{O}_2+\text{NO}_3^{3+}$: 297.1135 $[\text{M}+\text{NO}_3]^{3+}$; found: 297.1151.

EPR (H_2O):



HPLC:



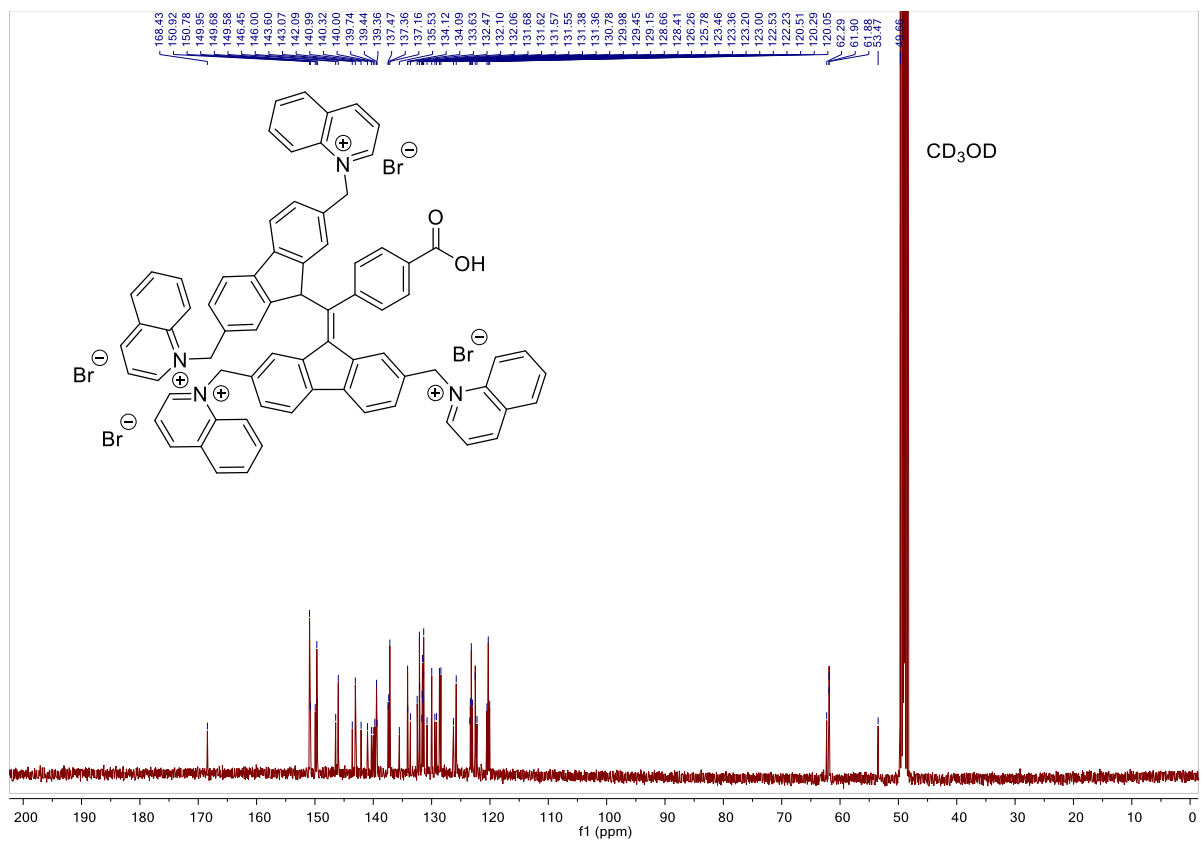
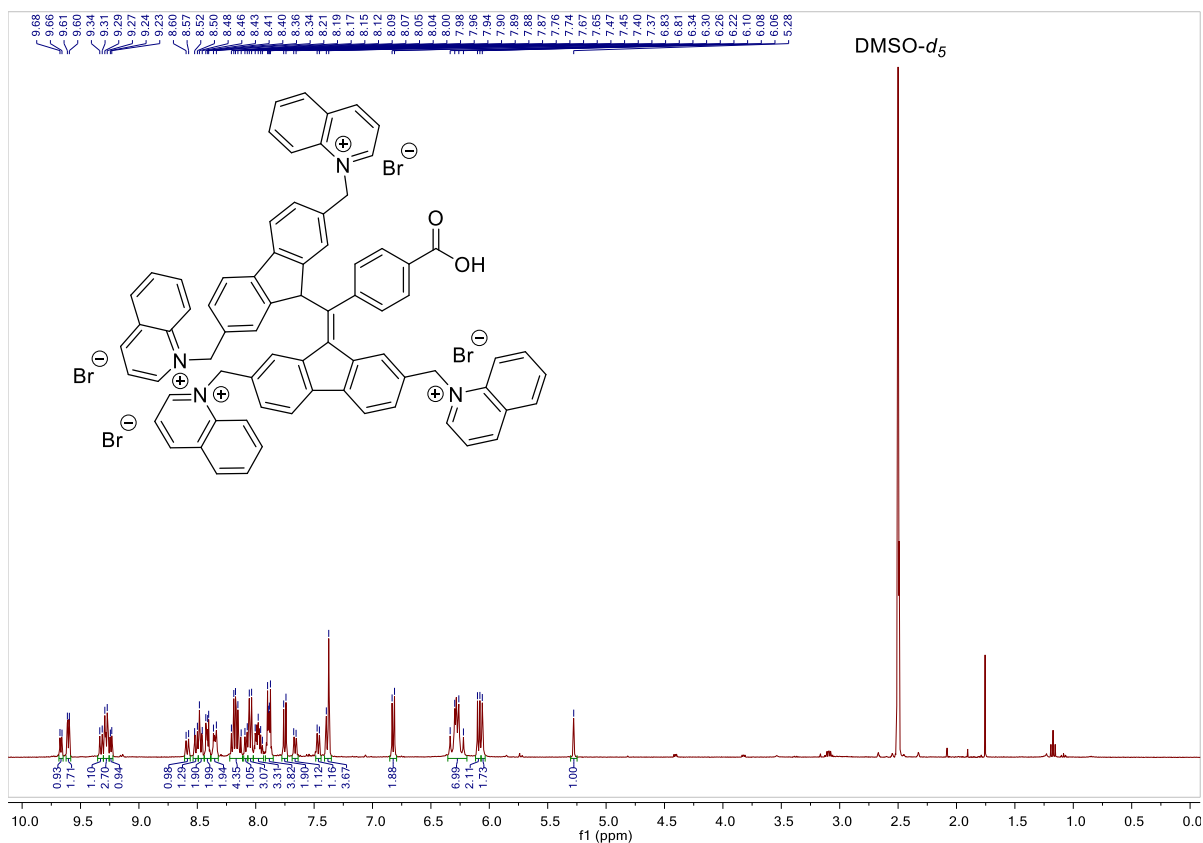


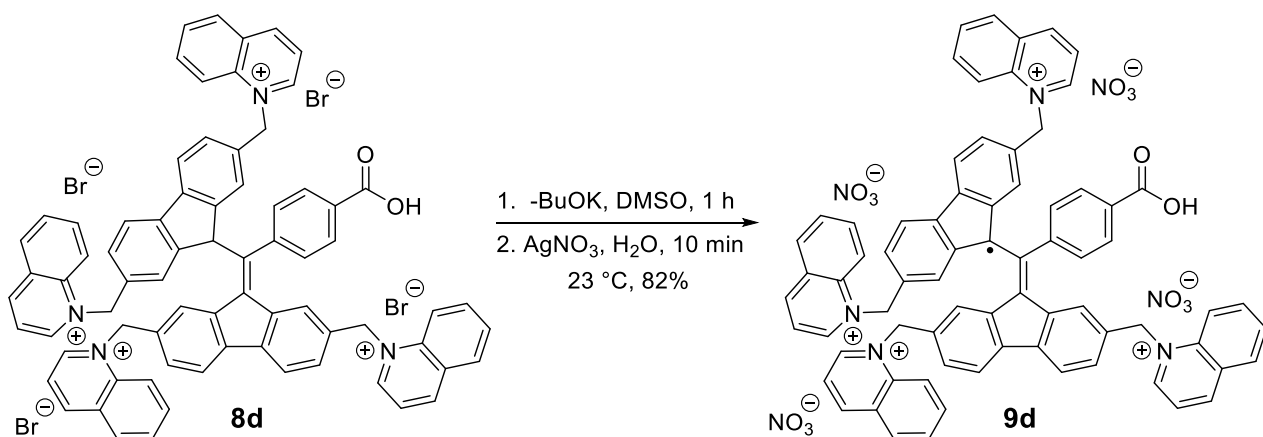
Tetraquinolinium BDPA 8d. To a solution of tetra-bromo BDPA derivative **7** (10 mg, 0.012 mmol) in DMSO (1 mL), quinoline (14 μL , 0.12 mmol) was added and the resulting solution stirred at 40 $^{\circ}\text{C}$ for 4 h. The reaction mixture was poured into Et_2O (10 mL), the precipitate collected by centrifugation followed by decantation of the solvent. The precipitate was redissolved in MeOH (2 mL) and reprecipitated by addition of Et_2O (10 mL). This precipitation was repeated to yield **8d** (13.5 mg, 85%) as a reddish brown solid.

$^1\text{H NMR}$ (400 MHz, $\text{DMSO}-d_6$) δ 9.67 (dd, $J = 6.0, 1.4$ Hz, 1H), 9.60 (dd, $J = 5.9, 1.4$ Hz, 2H), 9.32 (d, $J = 8.6$ Hz, 1H), 9.28 (dd, $J = 8.5, 3.7$ Hz, 3H), 9.24 (dd, $J = 6.0, 1.4$ Hz, 1H), 8.59 (d, $J = 8.4$ Hz, 1H), 8.51 (dd, $J = 8.2, 1.6$ Hz, 1H), 8.49 – 8.45 (m, 2H), 8.44 – 8.39 (m, 2H), 8.38 – 8.32 (m, 2H), 8.22 – 8.11 (m, 4H), 8.11 – 8.07 (m, 1H), 8.07 – 8.03 (m, 3H), 8.00 – 7.97 (m, 2H), 7.95 (dd, $J = 7.1, 1.2$ Hz, 1H), 7.93 – 7.84 (m, 4H), 7.75 (d, $J = 7.5$ Hz, 2H), 7.66 (dd, $J = 8.0, 1.5$ Hz, 1H), 7.47 (dd, $J = 8.1, 1.2$ Hz, 1H), 7.40 – 7.37 (m, 4H), 6.82 (d, $J = 8.4$ Hz, 2H), 6.38 – 6.18 (m, 7H), 6.09 (d, $J = 8.3$ Hz, 2H), 6.06 (s, 2H), 5.28 (d, $J = 1.4$ Hz, 1H) ppm.

$^{13}\text{C NMR}$ (101 MHz, MeOD) δ 168.43, 150.92, 150.78, 149.95, 149.68, 149.58, 146.45, 146.00, 143.60, 143.07, 142.09, 140.99, 140.32, 140.00, 139.74, 139.44, 139.36, 137.47, 137.36, 137.16, 135.53, 134.12, 134.09, 133.63, 132.47, 132.10, 132.06, 131.68, 131.62, 131.57, 131.55, 131.38, 131.36, 130.78, 129.98, 129.45, 129.15, 128.66, 128.41, 126.26, 125.78, 123.46, 123.36, 123.20, 123.00, 122.53, 122.23, 120.51, 120.29, 120.05, 62.29, 61.90, 61.88, 53.47 ppm.

HRMS (ESI): m/z calcd for $\text{C}_{74}\text{H}_{54}\text{N}_4\text{O}_2^{4+}$: 257.6056 $[M]^{4+}$; found 257.6031.

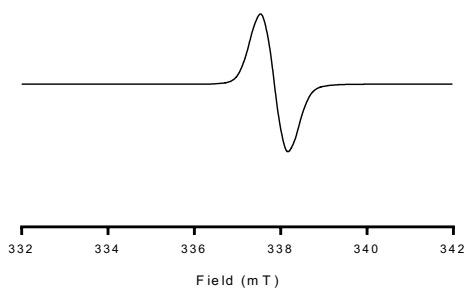




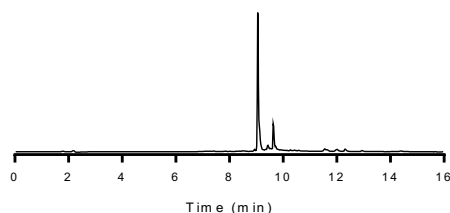
BDPA radical 9d. To a solution of **8d** (13 mg, 0.01 mmol) in DMSO (1 mL) was added a freshly prepared $t\text{-BuOK}$ solution (80 μL , 0.02 mmol, 0.25 M in DMSO) and the resulting solution stirred at 23 °C for 1 h. A solution of AgNO_3 (9 mg, 0.05 mmol) in H_2O (0.2 mL) was added and the brown solution stirred for 10 min. The mixture was centrifuged, the solution was decanted and poured into Et_2O (10 mL). The precipitate formed was collected by centrifugation followed by decantation of the solvent. The precipitate was redissolved in MeOH (2 mL) and reprecipitated by addition of Et_2O (10 mL) twice. The precipitate was redissolved in MeOH (2 mL), filtered through celite and dried to give **9d** (10 mg, 82%) as a reddish brown solid.

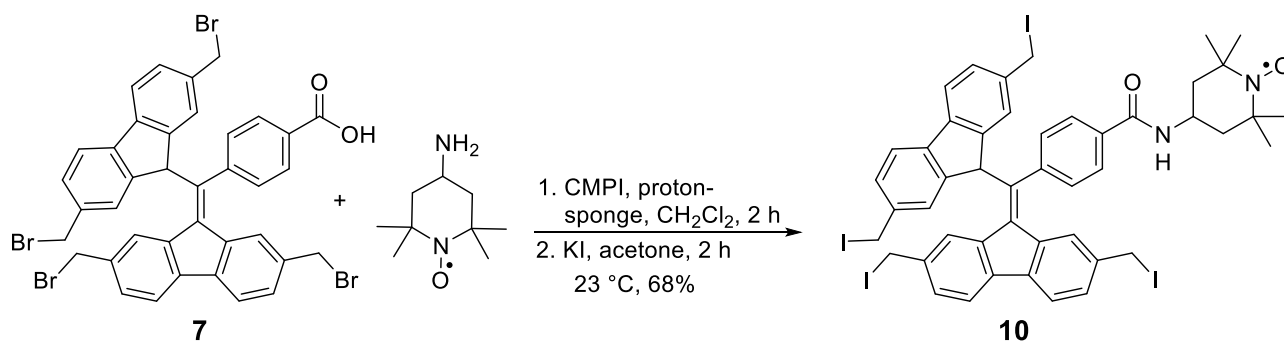
HRMS (ESI): m/z calcd for $\text{C}_{74}\text{H}_{53}\text{N}_4\text{O}_2^{4+}$: 257.3537 [M] $^{4+}$; found 257.3599.

EPR (H_2O):



HPLC:



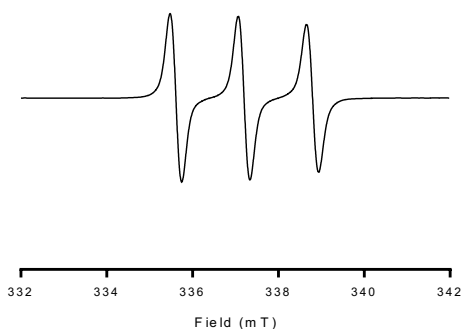


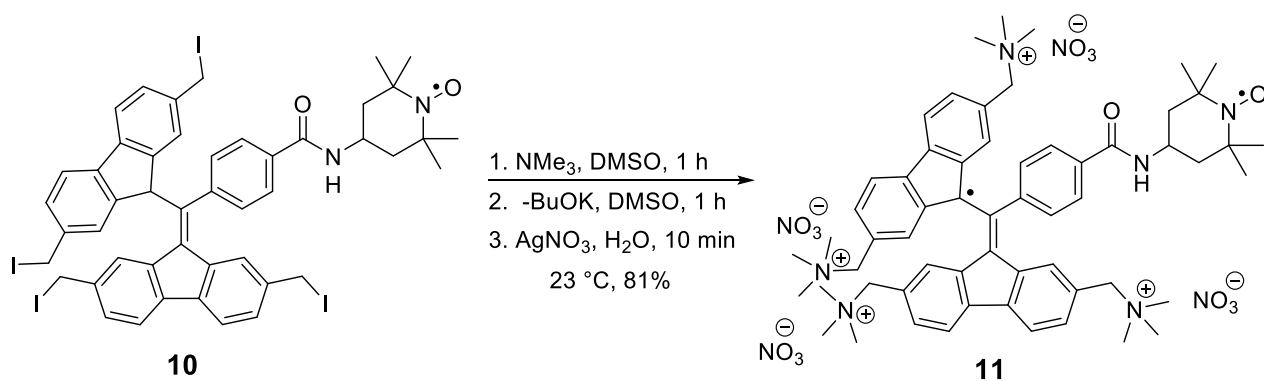
Tetra-(iodomethyl)-BDPA-TEMPO 10. To a solution of BDPA **7** (200 mg, 0.24 mmol) and 2-chloro-1-methylpyridinium iodide (CMPI) (67 mg, 0.26 mmol) in CH_2Cl_2 (10 mL), 4-amino TEMPO (45 mg, 0.26 mmol) and 1,8-bis(dimethylamino)naphthalene (proton-sponge) (103 mg, 0.48 mmol) were added. The resulting solution was stirred at 23 °C for 2 h, aq. HCl (1 N, 20 mL) added and extracted with CH_2Cl_2 (2 x 30 mL). The combined organic layers were dried over Na_2SO_4 and concentrated *in vacuo*. The residue was redissolved in acetone (10 mL), KI (398 mg, 2.40 mmol) added and the resulting solution stirred at 23 °C for 2 h. H_2O (20 mL) was added and the mixture extracted with CH_2Cl_2 (2 x 30 mL). The combined organic layers were dried over Na_2SO_4 and concentrated *in vacuo*. The product was purified by flash-column chromatography using a gradient elution (pet ether:EtOAc; 80:20 to 70:30) to give **10** (193 mg, 68%) as a reddish solid.

TLC (Silica gel, pet ether:EtOAc, 70:30): R_f (**7**) = 0.2, R_f (**10**) = 0.3

HRMS (ESI): m/z calcd for $\text{C}_{47}\text{H}_{43}\text{I}_4\text{N}_2\text{O}_2 + \text{Na}^+$: 1197.9396 [$M + \text{Na}$] $^+$; found 1197.9402

EPR (CH_2Cl_2):

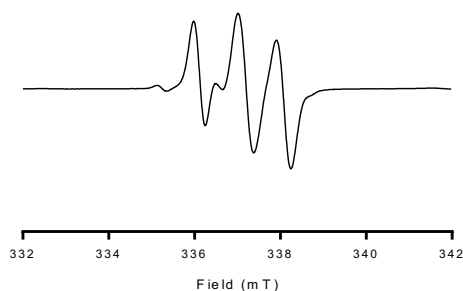




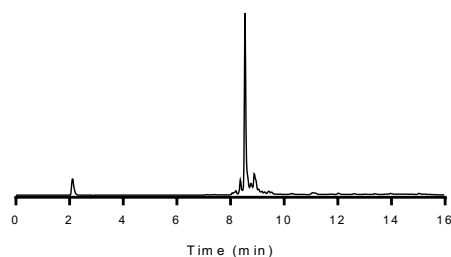
BDPA-TEMPO biradical 11. To a solution of BDPA derivative **10** (10 mg, 0.0085 mmol) in DMSO (1 mL), NMe_3 (21 μL , 0.085 mmol, 4 M) was added and the resulting solution stirred at 23 °C for 1 h. The reaction mixture was poured into Et_2O (10 mL), the precipitate collected by centrifugation followed by decantation of the solvent. The precipitate was redissolved in MeOH (2 mL) and reprecipitated by addition of Et_2O (10 mL) twice and dried. The precipitate was dissolved in DMSO (1 mL), freshly prepared $t\text{-BuOK}$ solution (70 μL , 0.017 mmol, 0.25 M in DMSO) added and the resulting solution stirred at 23 °C for 1 h. A solution of AgNO_3 (7 mg, 0.043 mmol) in H_2O (0.2 mL) was added and the brown solution stirred for 10 min. The mixture was centrifuged, the solution was decanted and poured into Et_2O (10 mL). The precipitate formed was collected by centrifugation followed by decantation of the solvent. The precipitate was redissolved in MeOH (2 mL) and reprecipitated by addition of Et_2O (10 mL) twice. The precipitate was redissolved in MeOH (2 mL), filtered through celite and dried to give **11** (8 mg, 81%) as a reddish brown solid.

HRMS (ESI): m/z calcd for $\text{C}_{59}\text{H}_{78}\text{N}_4\text{O}_2+\text{NO}_3^{3+}$: 321.5349 $[\text{M}+\text{NO}_3]^{3+}$; found: 321.5420.

EPR (DMSO):



HPLC:



Solubility in DNP juice

The solubility of the tetraalkyl/aryl-ammonium BDPA derivatives **8a-d** in DNP juice (glycerol: H₂O, 6:4) was determined by UV-vis spectroscopy. For each of compounds **8a-d**, solutions were prepared in the glycerol-H₂O mixture at different concentrations. A calibration curve was prepared by recording the UV-vis spectra of these solutions and plotting the absorbance at the wavelength stated, 342 nm (**8a**), 290 nm (**8b**), 324 nm (**8c**) and 336 nm (**8d**) as a function of the concentration. The maximum solubility of compounds **8a-d** was determined from the calibration curve by recording the absorbance of a saturated solution. The values were as follows: >150 mM (**8a**), 20 mM (**8b**), 65 mM (**8c**) and 45 mM (**8d**).

Quantification of BDPA radicals

EPR spectroscopy was used to quantify the amount of tetraalkyl/aryl-ammonium BDPA radicals present in each sample. The EPR spectra of a solution of 4-hydroxy TEMPO (1 mM) and BDPA radicals **9a-d** (1 mM) in DMSO were recorded and double-integrated to obtain the area under the peaks. The percentage of BDPA radicals **9a-d** was determined by comparing these two areas, which was found to be approximately 92% (**9a**), 82% (**9b**), 85% (**9c**) and 80% (**9d**). The amount of the biradical **11** was determined with respect to a nitroxide monoradical impurity present in the sample² and found to be ca. 90%.

Persistence of BDPA radicals

Solvent-dependent persistence. The persistence of BDPA radicals was investigated under different conditions by monitoring the absorption of BDPA radicals at 503 nm using UV-vis spectroscopy. The samples were prepared in the following manner: A stock solution of the radicals (10 mM for radical **9a**, 5 mM for biradical **11**, 1 mM for radical **9b** and **9d**) were prepared in MeOH. Aliquots were removed from the stock solutions (200 μ L), distributed into microfuge tubes, dried in a vacuum concentrator and the solid was redissolved in the chosen solvent (200 μ L). The solutions were kept at 23 °C in the presence of air and UV-vis spectra were recorded at different time intervals by taking out aliquots (2-20 μ L) followed by dilution with H₂O (0.5 mL). Commercially purchased solvents were used without further drying and purification for these experiments, except for DMSO which was dried over molecular sieves (3 Å).

Figure S25A shows the UV-vis spectra of BDPA radical **9a** in DNP juice at various times. The peak between 400 – 550 nm arises from the absorption of the BDPA radical and decreases when the radical decomposes. **Figure S25B** shows the persistence of **9a**, as investigated by both UV-vis (left y-axis) and EPR spectroscopy (right y-axis).² Both techniques give similar results.

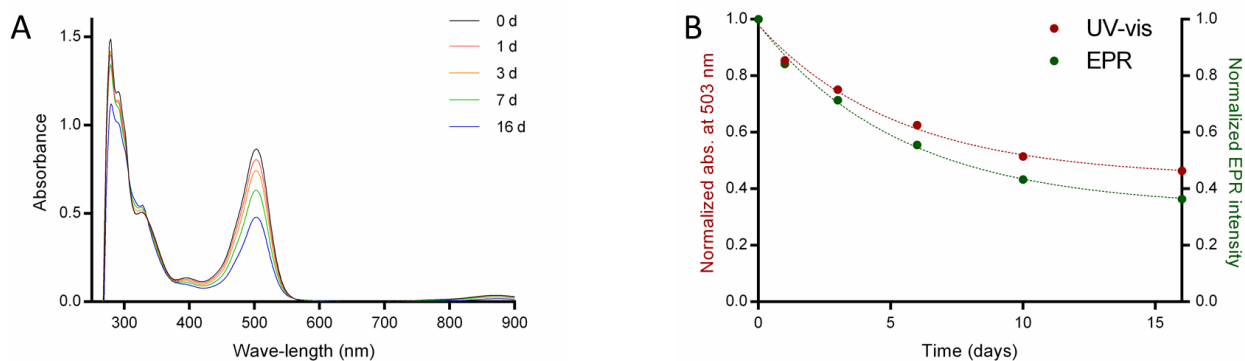


Figure S25. Persistence of BDPA radical **9a** in DNP juice (10 mM) at 23 °C. **A.** The UV-vis absorbance spectra of BDPA radical **9a** at different times. **B.** The normalized absorbance of **9a** at 503 nm (left y-axis) and the normalized EPR intensity of the radical (right y-axis) plotted as a function of time.

The solvent-dependent persistence of radical **9a** at 23 °C is shown in **Figure 2**. The tetraalkylammonium BDPA-TEMPO biradical **11**, which has the same tetraalkylammonium group as radical **9a**, shows a similar solvent-dependency as **9a** (**Figure S26**). The highest persistence of **11** was observed in DMSO, with a decomposition of ca. 10% of the radical after 2 weeks. Ca. 40-50% of the radical was decomposed in DNP juice and MeOH under the same condition. However, similar to what was found for **9a**, a significantly higher degradation was observed in water.

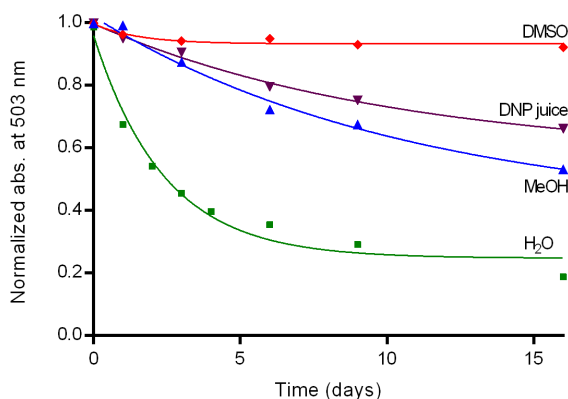


Figure S26. Persistence of BDPA-TEMPO biradical **11** in solution (5 mM) at 23 °C monitored by UV-vis spectroscopy at 503 nm.

Figure S27 shows the persistence of radicals **9b** and **9d** in solution at 23 °C. Due to the limited solubility of these radicals in MeOH in which the stock solutions were prepared for the experiments, persistence for a 1 mM solution is reported. A similar solvent-dependency was observed for these radicals as well.

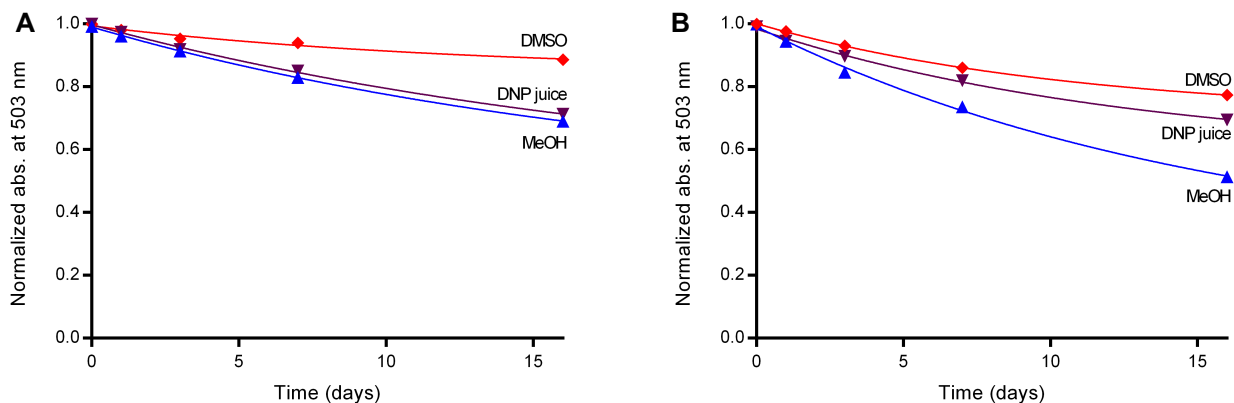


Figure S27. Persistence of radicals **9b** (A) and **9d** (B) in solution (1 mM) at 23 °C.

Temperature-dependent persistence. We investigated the persistence of radical **9a** at -80 °C in DNP juice by UV-vis spectroscopy (**Figure S28**). Negligible degradation was detected after 30 days, as has been observed with other BDPA radicals.²

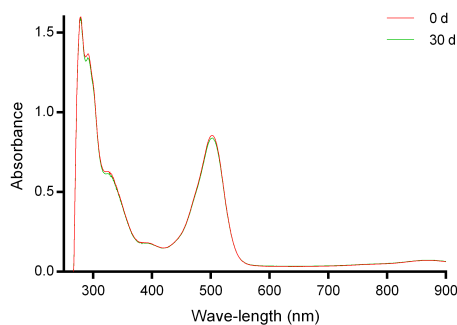


Figure S28. The persistence of radical **9a** at -80 °C in DNP juice (10 mM) investigated by UV-vis spectroscopy.

Concentration-dependent persistence. To determine if dimerization was a major pathway of degradation of the BDPA radicals in water, the rate of decomposition of radical **9a** in water was investigated for solutions of different concentration. The initial rates of degradation were determined² and plotted as a function of concentration (**Figure S29**). The rate was found to increase 3-fold with a 2-fold increase in the concentration, with a reaction order of ca. 1.6 with respect to the radical suggesting dimerization in water. A similar result was also obtained for biradical **11** (data not shown).

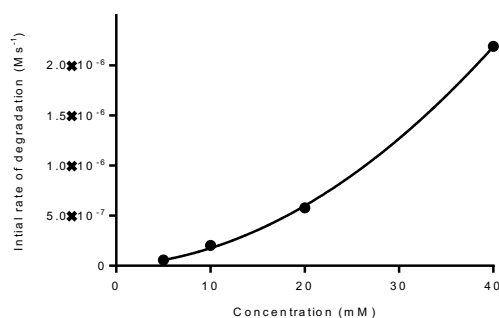


Figure S29. Concentration-dependent initial rates of BDPA radical **9a** in water at 23 °C.

Ionic strength-dependent persistence. In an attempt to reduce aggregation in water by increasing the ionic strength, the persistence of **9a** was determined in presence of varying concentration of NaCl (aq.) (**Figure S30**). However, this data shows that the presence of NaCl is detrimental to the persistence of **9a**.

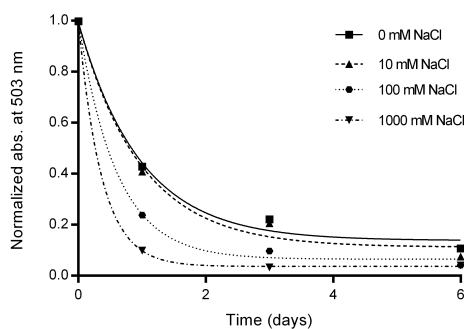


Figure S30. Persistence of BDPA radical **9a** at different concentration of NaCl (aq.) as a function of time.

Analysis of BDPA-decomposition products

To detect dimerization, we investigated the decomposition of **9a** in water by HRMS (ESI). **Figure S31** shows a mass spectrum of **9a** in water at 23 °C after 48 h. Formation of a major peak (m/z 560.6397) was observed which can only originate through dimerization of **9a**. The mass is triply charged, possibly due to the presence of eight ammonium cations and two carboxylate anions in the dimeric structure along with three counter anions (NO_3^-). We speculate that the dimer is formed in a similar fashion as the Gomberg radical through a σ -bond formation between two radicals,³ followed by oxidation/ H_2 elimination. A putative structure of the dimer ($\text{C}_{100}\text{H}_{118}\text{N}_{11}\text{O}_{13}^{3+}$; m/z 560.6309) is shown in **Figure S31**.

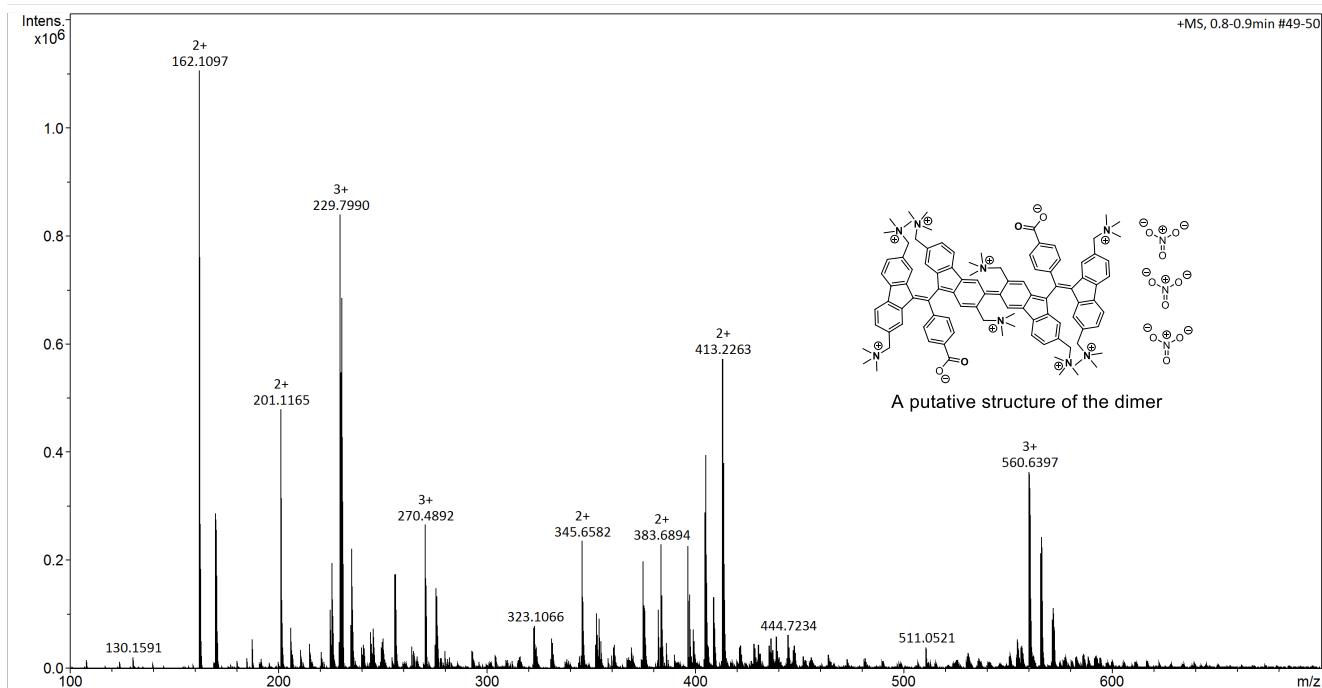


Figure S31. The HRMS (ESI) spectrum of radical **9a** in water (5 mM) kept for 48 h at 23 °C, recorded in a positive-ion mode. All the masses in the spectrum originate from the sample.

References:

1. C. M. G. Henríquez, L. H. Tagle, C. A. Terraza, A. B. González, A. L. Cabrera and U. G. Volkman, *J. Appl. Polym. Sci.*, 2012, **125**, 477-487.
2. S. Mandal and S. T. Sigurdsson, *Chem. Eur. J.*, 2020, **26**, 7486-7491.
3. H. Lankamp, W. T. Nauta and C. MacLean, *Tetrahedron Lett.*, 1968, **9**, 249-254.